

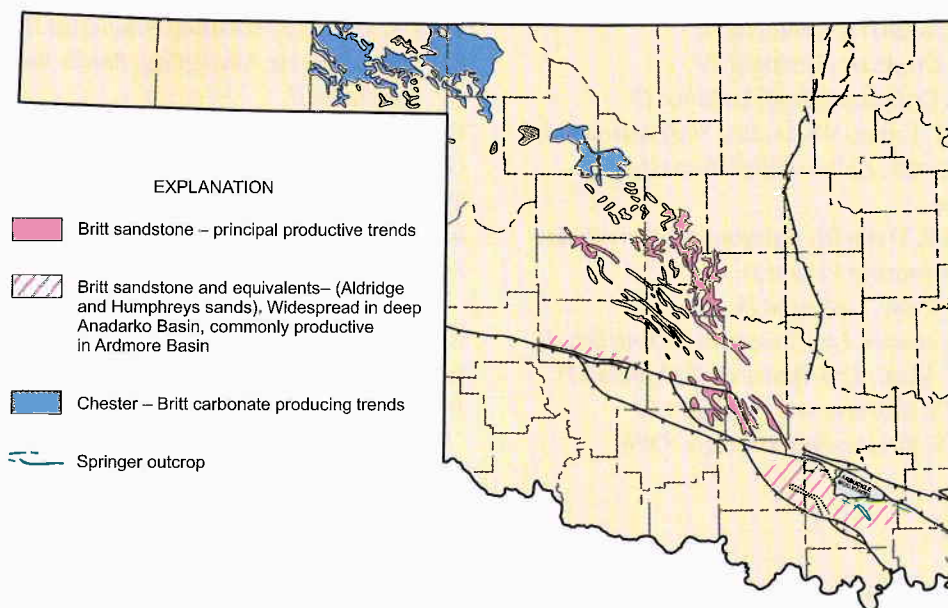


Oklahoma Geological Survey
G. Randy Keller, Interim Director

Circular 111
ISSN 0078-4397

Morrow and Springer in the Southern Midcontinent, 2005 Symposium

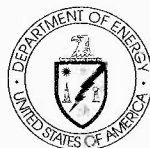
Richard D. Andrews, *Editor*



Proceedings of a symposium held May 10–11, 2005, in Oklahoma City, Oklahoma.

Co-sponsored by:

Oklahoma Geological Survey
and
National Energy Technology Office,
U.S. Department of Energy



The University of Oklahoma
Norman
2008

OKLAHOMA GEOLOGICAL SURVEY

G. RANDY KELLER, Interim Director

SURVEY STAFF

JAMES H. ANDERSON, <i>Manager of Cartography</i>	JAMES E. LAWSON, JR., <i>Chief Geophysicist</i>
RICHARD D. ANDREWS, <i>Geologist IV</i>	LAURIE A. LOLLIS, <i>Graphics Presentations Technician</i>
BETTY D. BELLIS, <i>Staff Assistant III</i>	KENNETH V. LUZA, <i>Engineering Geologist IV</i>
SHANIKA L. BIVINES, <i>Financial Administrator and Office Manager</i>	RICHARD G. MURRAY, <i>Copy Center Operator</i>
MITZI G. BLACKMON, <i>Staff Assistant II</i>	SUE M. PALMER, <i>Staff Assistant I</i>
DAN T. BOYD, <i>Geologist IV</i>	DAVID O. PENNINGTON, <i>Facilities Attendant II</i>
RAYMON L. BROWN, <i>Geophysicist III</i>	W. LLOYD REED, <i>Lab/Research Technician IV</i>
BRIAN J. CARDOTT, <i>Geologist IV</i>	TOM H. SANDERS, <i>Facilities Attendant II</i>
JAMES R. CHAPLIN, <i>Geologist IV</i>	CONNIE G. SMITH, <i>Marketing, Public Relations Specialist II</i>
JANISE L. COLEMAN, <i>Staff Assistant II</i>	PAUL E. SMITH, <i>Supervisor, Copy Center</i>
TAMMIE K. CREEL-WILLIAMS, <i>Staff Assistant III</i>	G. RUSSELL STANDRIDGE, <i>GIS Specialist</i>
SUE B. CRITES, <i>Editor, Oklahoma Geology Notes</i>	THOMAS M. STANLEY, <i>Geologist IV</i>
CHARLES R. DYER III, <i>Equipment Operations Maintenance Person IV</i>	JOYCE A. STIEHLER, <i>Staff Assistant II</i>
ROBERT O. FAY, <i>Geologist IV</i>	MICHELLE J. SUMMERS, <i>Technical Project Coordinator</i>
AMIE R. GIBSON, <i>Lab/Research Technician III</i>	NEIL H. SUNESON, <i>Geologist IV</i>
JAMES W. KING, <i>Lab/Research Technician IV</i>	JENNIFER L. VEAL, <i>Staff Assistant II</i>
STANLEY T. KRUKOWSKI, <i>Geologist IV</i>	JANE L. WEBER, <i>Database Coordinator</i>
EUGENE V. KULLMANN, <i>Manager, OPIC</i>	

On The Cover

The Springer Britt reservoir occurs throughout much of the Anadarko Basin and Shelf areas in western Oklahoma. Shown here is the distribution of productive sandstone trends (pink) and correlative carbonate facies (blue). Areal distribution patterns of the Britt sandstone are usually oriented northwest to southeast except along the eastern part of the subsurface trend map where they are predominantly north to south. During Britt time, sand was transported into the basin via deeply incised south-trending river channels. This sand was then reworked by marine processes forming off-shore bars that parallel ancient shorelines. Farther to the northwest, Britt interval changes facies from sandstone to shale and finally to carbonate strata. In the Oklahoma Panhandle, the Britt carbonate forms one of the most prolific gas reservoirs of the region. Regionally persistent shale marker beds permit this correlation. In the past, Britt and Boatwright carbonates were informally identified as the Chester limestone.

Richard D. Andrews
Oklahoma Geological Survey

This publication, printed by the Oklahoma Geological Survey, is issued by the Oklahoma Geological Survey as authorized by Title 70, Oklahoma Statutes, 1981, Sections 231–238. 1,050 copies have been prepared for distribution at a cost of \$16,254.69 to the taxpayers of the State of Oklahoma. Copies have been deposited with the Publications Clearinghouse of the Oklahoma Department of Libraries.

PREFACE

This volume contains proceedings of the 17th annual two-day theme symposium “Morrow and Springer in the Southern Midcontinent.” Because these traditional sandstone reservoirs are some of the most prolific in the southern Midcontinent, their hydrocarbon resources have been, and currently are, the premier exploration and development targets for recovery of oil and gas economically. Information critical in delineating production trends, subsurface mapping, stratigraphic nomenclature, trapping mechanisms, logging and well stimulation, seismic imaging, and secondary recovery is important to facilitate exploitation of these resources. To aid in disseminating this information and technology, the Oklahoma Geological Survey (OGS) and the U.S. Department of Energy, National Energy Technology Laboratory (DOE-NETL) in Tulsa cosponsored this event. It was held May 10–11, 2005, at the Clarion Hotel Meridian Convention Center in Oklahoma City. About 250 attendees were present making it one of the most popular workshops in this series. Twenty-one speakers made presentations, and four individuals contributed poster sessions. From this pool, 10 speakers submitted manuscripts that are printed here as full papers. The remaining 11 talks are represented by abstracts.

Topics presented at this symposium are extremely varied and include a mixture of studies completed by consulting geologists, geoscientists in the local petroleum industry, and geoscientists from prominent universities and state geological surveys. Research concepts and conclusions, stratigraphic nomenclature and correlations, and age determinations used by the various authors in this volume do not necessarily agree with those of the OGS.

Persons involved in the organization and planning of the symposium include Richard Andrews, general chair and poster chair; Michelle Summers, meeting coordinator; Bill Lawson of DOE-NETL; and Charles Mankin, director of the OGS. Other OGS personnel who contributed greatly include Tammie Creel, registration chair; and Connie Smith, publicity chair. Appreciation is expressed to each of them and to the many authors who helped achieve this successful symposium.

RICHARD D. ANDREWS
General Chairman

CONTENTS

Papers

- 1 Morrow and Springer Strata in the Southern Midcontinent**
Richard D. Andrews
- 13 Secondary Oil Recovery from the Upper Morrow Purdy Sandstone in Rice NE Field, Texas County, Oklahoma**
Richard D. Andrews
- 27 Fighting the Tide: Morrow-Springer Gas in Oklahoma**
Dan T. Boyd
- 39 Iodine Production from Morrowan Sandstones, Anadarko Basin, Northwestern Oklahoma**
Stanley T. Krukowski
- 49 Trends in Composition of Morrowan Gases in Southwestern Kansas**
K. David Newell
- 63 Depositional and Diagenetic Controls of Compartmentalization in Springer Reservoirs, Southeastern Anadarko Basin, Oklahoma**
James Puckette and Aaron Rice
- 81 Sequence Stratigraphy, Lithofacies, and Reservoir Quality, Upper Morrow Sandstones, Northwestern Shelf, Anadarko Basin**
James Puckette, Zuhair Al-Shaieb (deceased) and Erin Van Evera
- 97 Potential Stratigraphic Reservoirs in the Morrowan Jackfork Group, Southeastern Oklahoma**
R. M. Slatt, B. Omatsola, A. M. Garich-Faust, and G. A. Romero
- 111 Imaging Thin Morrow and Springer Sandstones with High-Frequency Three-Dimensional Seismic Techniques in the Anadarko Basin**
Bob Springman
- 121 Geo-Engineering Modeling of Morrow/Atoka Incised-Valley-Fill Deposits Using Web-Based Freeware**
W. Lynn Watney, Saibal Bhattacharya, Alan Byrnes, John Doveton, and John Victorine

CONTENTS

Abstracts

- 137 Springer Gas-Play Development—Anadarko Basin**
Tim O. Brown and Robert A. Northcutt
- 139 Controls on Porosity Origin, Preservation, Reduction, and Restoration in Two Types of Morrow Reservoirs in Western Oklahoma**
Bruce N. Carpenter
- 141 Morrowan to Early Atokan Structural Evolution of the Frontal Ouachitas and Arkoma Basin, Southeastern Oklahoma**
Ibrahim Çemen, James Puckette, Rodney Feller, Steve Hadaway, and Ata Sagnak
- 143 Logging-Tool-Deployment Methods that Ensure Acquisition of Accurate Log Data through Morrow and Springer Strata**
Mark W. Houpe
- 145 Cromwell Sandstone Sequence Stratigraphy and Porosity Development in Kinta Field, Haskell County, Oklahoma**
Bryant Reasnor and Dennis Kerr
- 147 The Concept of Intermittent Structure and its Influence on Morrow–Springer Deposition**
Kurt Rottmann
- 149 Regional Sequence Stratigraphy and Depositional Environments of the Lower Pennsylvanian in Southwest Kansas**
Galo A. Salcedo and Timothy R. Carr
- 151 Overview of Postle Field, a Morrow CO₂ Flood, Texas County, Oklahoma**
John Southwell
- 153 Examples of Trapping Mechanisms in the Cromwell Sandstone (Morrowan), Hughes County, Oklahoma**
Maxwell J. Tilford
- 155 Deep-Gas-Well Stimulation of the Springer in the Anadarko Basin**
Steve Wolhart

Morrow and Springer Strata in the Southern Midcontinent

Richard D. Andrews

Oklahoma Geological Survey
Norman, Oklahoma

ABSTRACT.—The Late Mississippian and Early Pennsylvanian mark a period of time when prolific sandstone reservoirs in the Southern Midcontinent region were deposited. Formal names of these reservoirs include the Springer and Morrow Groups, whereas industry personnel use numerous informal subsurface names to identify specific sandstone intervals throughout the region (Fig. 1).

The Springer Group is Late Mississippian to Early Pennsylvanian in age and contains multiple sandstone units primarily within the Anadarko and Ardmore Basins. Cumulative production from these reservoirs is ~5.3 trillion cubic ft of gas (TCFG) and ~902 million barrels of oil (MMBO) from ~2,600 wells (IHS Energy, 2005). Sandstone occurs mostly in the form of marine bars, although incised channel deposits that trend southward into the Anadarko Basin are also recognized. In the deepest part of the Anadarko Basin, and throughout most of the Ardmore Basin, the lowermost sandstone unit in the Springer Fm. is interpreted to consist of north-trending turbidites. The Springer changes facies in a northwesterly direction, where it grades from sandstone to shale and then to limestone. In northwestern Oklahoma, and in the Oklahoma and Texas Panhandles, this carbonate is most often referred to simply as the “Chester,” although this specific rock unit actually lies beneath the Mississippian Springer. Cumulative production from the Springer carbonate is ~3 TCFG and ~24 MMBO from ~3,500 wells (IHS Energy, 2005).

The Morrow Group is Early Pennsylvanian in age and includes sandstone reservoirs primarily in the Arkoma and Anadarko Shelf and Basin areas. In the former, the lower Morrow produces from the Cromwell Sandstone. Cumulative production from this reservoir is 884 BCFG and 123 MMBO (IHS Energy, 2005). The Cromwell Sandstone, noteworthy for its excellent porosity and permeability, was deposited in a very shallow marine (shelf) environment. In contrast, the Anadarko Basin and Shelf areas contain widespread sandstone in both upper and lower Morrow intervals. Cumulative production of the Morrow from ~14,000 wells in Oklahoma and the Texas Panhandle is 23 TCFG and 550 MMBO (IHS Energy, 2005). Like the Springer, most Morrow sediments were derived from fluvial corridors that extended into the basin from the north. Therefore, depositional environments were dynamic, resulting in intermingled sandstone facies of fluvial, tidal, and marine deposits. One component of the upper Morrow along the southern margin of the Anadarko Basin is chert. This mineral is believed to have been derived from erosion of the Ordovician Viola during the Wichita orogeny. The coarse clasts of chert are a conspicuous component of sandstone and conglomerate wash that prograded northward into the basin. Because of diagnostic chert inclusions within these strata, the upper Morrow defines the relative age of pre-Pennsylvanian erosion. Therefore, by late Morrowan time the Wichita Mountains were already an eroded positive province such that the very first movements probably were early Morrowan or slightly earlier.

Also Early Pennsylvanian in age, the Jackfork Group represents deep-marine facies of the Morrow in the Ouachita Uplift of southeastern Oklahoma. Strata associated with this rock assemblage include turbidites that formed the main gas reservoir in the Potato Hills Field. There is considerable exploration interest in this rock sequence in adjacent areas of the Ouachitas, because this province is largely underexplored and the gas-reserve potential is high.

SPRINGER

During Late Mississippian and Early Pennsylvanian time, much of southern and western Oklahoma was covered by seas. Deposition during the first part of this period (early Springer) was almost entirely of open-marine origin, and sediments consisted mostly of clay with occasional pulses of (deep-water?) sand. Several thousand feet of black shale is recorded in the deep Anadarko Basin, whereas this shale thins to only a few hundred feet eastward into the Arkoma Basin of Oklahoma. This shale interval is the Goddard Shale.

Strata in the upper part of the Springer Group are much different, because sandstone is a major component. In the subsurface Anadarko Basin, three main sandstone intervals are present, each composed of one or more distinct sandstone units. From oldest to youngest, these members include the Boatwright, Britt, and Cunningham (Figs. 2–4). Roughly equivalent subsurface sandstones occur in the Ardmore Basin: the Sims, Humphreys, Aldridge, and Markham. The surface equivalents are the Rod Club, Overbrook, and Lake Ardmore Members. Springer-age sandstone also occurs in the Arkoma Basin of eastern Oklahoma, where it is informally

known as the Jefferson sandstone. This sandstone interval is entirely of marine origin and is correlative with the Cunningham sandstone of the Anadarko Basin.

Sand comprising the Britt and Cunningham intervals was transported into the Anadarko Basin from the north via incised fluvial systems. It was later reworked in the form of detached and/or distributary-mouth bars that trend to the northwest. Only marine facies are recognized in the Boatwright and its equivalent member, the Rod Club. Throughout most of the Anadarko Basin, these marine facies occur in the form of shelf bars, although in the Ardmore Basin and the deep Anadarko Basin, turbidites are common. Sedimentary structures (bottom marks) of turbidites on outcrop in the Ardmore Basin indicate north-trending current and transportation directions. This is the opposite of the upper and middle Springer sandstone members, whose source was to the north with sediment transport to the south.

The Boatwright and Britt sandstone intervals gradually change facies to the northwest, first becoming shaly and then calcareous. In far northwestern Oklahoma and in the Oklahoma and Texas Panhandles, these two members consist mostly of limestone that is locally oolitic and of a shallow, restricted-marine (ramp or carbonate bank/shoreline) origin. These deposits are often incorrectly referred to as the Chester limestone, but the real Chester is much lower in the section. Depositional and facies changes as previously described are indicated in the trend maps of Figures 2 and 3. Additionally, these facies changes are shown in Andrews (2001, pl. 7, cross section B-B'). The Cunningham sandstone shales out to the northwest and has no carbonate facies.

MORROW

The regional distribution of Morrow sediments in Oklahoma and parts of Texas and Arkansas is shown in Figure 5. Various depositional facies are indicated, which extend across much of southern and northwestern Oklahoma, northwestern Arkansas, and the Texas Panhandle. The Morrow is eroded over much of south-central Oklahoma for several miles (or even tens of miles) on either side of the Nemaha Fault Zone. It is likely that the Morrow was not deposited in north-central or far southwestern Oklahoma because of the rising structural provinces of the Nemaha and Wichita Uplifts, respectively. Farther south, in the Ardmore Basin, Morrow sandstone probably did not extend much farther south than the city of Ardmore. Evidence for this comes from the Primrose Member, which at outcrop has no obvious textural profiles or sedimentary structures typical of shelf bar deposits. Rather, the Primrose near Ardmore is more typical of deeper water de-

posits: very fine-grained to silty sandstone with predominately thin, parallel bedding; abundant glauconite; beds containing plentiful sponge spicules; and the absences of shallow-water invertebrates. Farther east in the Arkoma Basin (Fig. 5), the Morrow contains thick accumulations of marine bar sandstone that shale out north of the Choctaw Fault. In the Ouachita Mountain Uplift in far southeastern Oklahoma, deep-water turbidites of the Morrowan Jackfork Group comprise the principal reservoir in the Potato Hills area.

Morrow in Southeastern Oklahoma

Morrow sandstone occurs throughout much of the Arkoma Basin and is widespread in parts of the Ouachita Uplift. In the former, the sandstone is formally called the Cromwell Sandstone Member of the Union Valley Formation. In the latter, the sandstone occurs as turbidites within the Jackfork Group.



SYSTEM	SERIES	GROUP	FORMAL SURFACE NAMES (FORMATION)	INFORMAL SUBSURFACE NAMES
	Atokan		Atoka (surface name where exposed in eastern Oklahoma)	"Granite wash"  Thirteen Finger lime
PENNSYLVANIAN	Morrowan	Morrow	Wapanucka Formation (Arkansas Basin) McCully Formation (Oklahoma Ozark Uplift) Bloyd Formation (Arkansas Ozark Uplift)	Upper Morrow Purdy } Sturgis } Sandstones in the Bowles } Oklahoma Kelly } Panhandle Lips } Purvis } Pury ar } Deep Anadarko Pierce } Basin sandstone Bradstreet } and conglomerate
			Union Valley Limestone (Ardmore Basin) Sausbee Formation (Oklahoma Ozark Uplift) Hale Formation (Arkansas Ozark Uplift) Cromwell Sandstone Mbr. of the Union Valley Fm. in the Arkoma Basin	Lower Morrow "Squaw Belly" (limy sediments and limestone, sometimes called middle Morrow) Lower Morrow sandstone Mocane-Laverne } Sandstone in Keyes } OK Panhandle Primrose Sandstone
MISSISSIPPIAN	Chesterian	Springer	Jefferson sandstone Springer Formation (surface name where exposed in Carter Co., south-central Oklahoma)	Cunningham sandstone Britt sandstone Britt carbonate Boatwright sandstone Boatwright carbonate
			Goddard Formation	Goddard shale Goddard sandstone } Flattop Goodwin Goddard
	Meramecian		Pitkin Ls. (Ozark Uplift) Fayetteville sh. (Ozark Up.)	"False" Caney  "Chester" limestone Caney shale
			Mayes-Sycamore Ls.	Sycamore Limestone

Figure 1. Stratigraphic-nomenclature chart of the Springer and Morrow Groups and bounding strata relevant primarily to western Oklahoma. Modified from Andrews (1995, 1999, 2001, 2003).

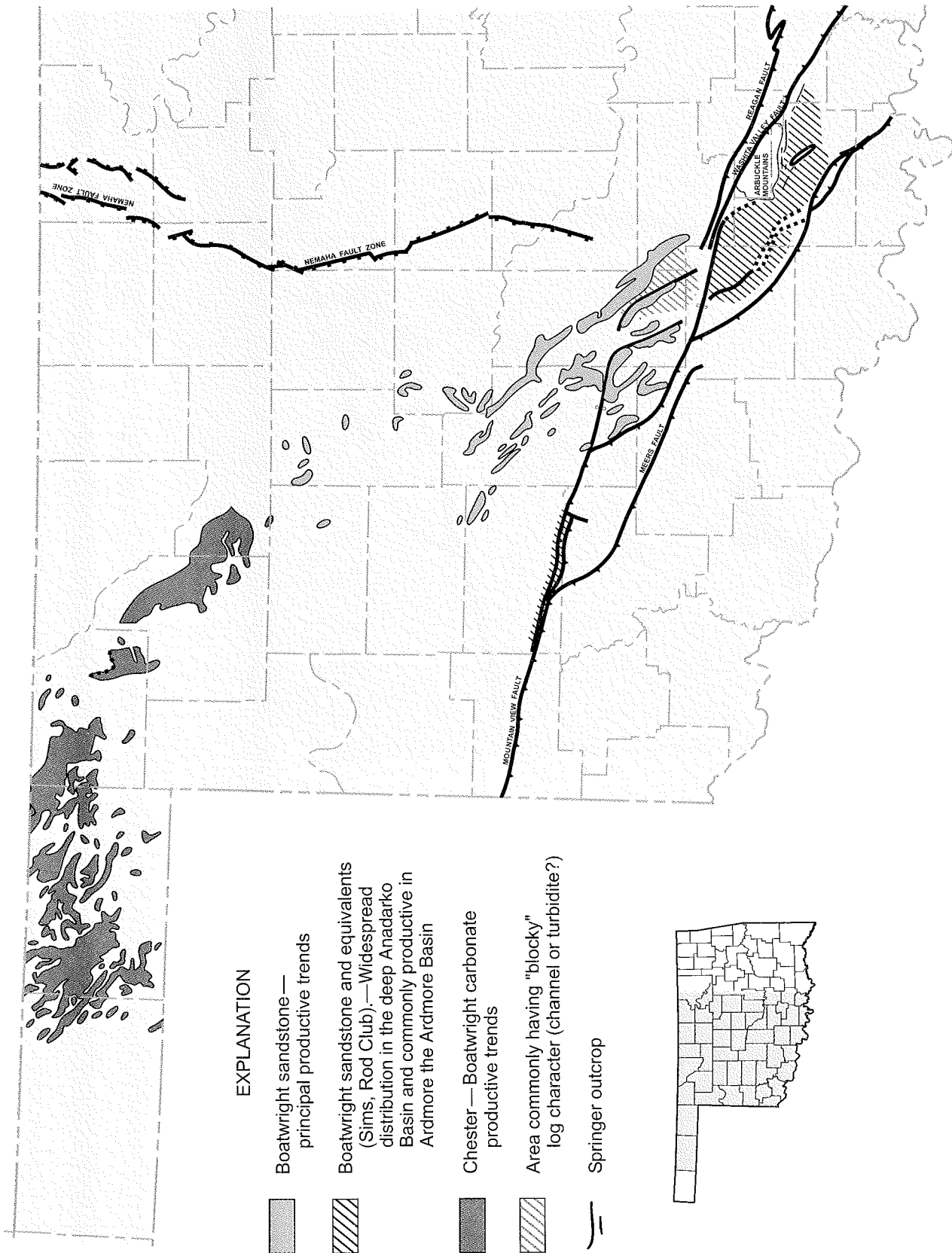


Figure 2. Boatwright sandstone and carbonate map, showing principal productive trends in the Anadarko and Ardmore Basins, Oklahoma. Modified from Andrews (2001).

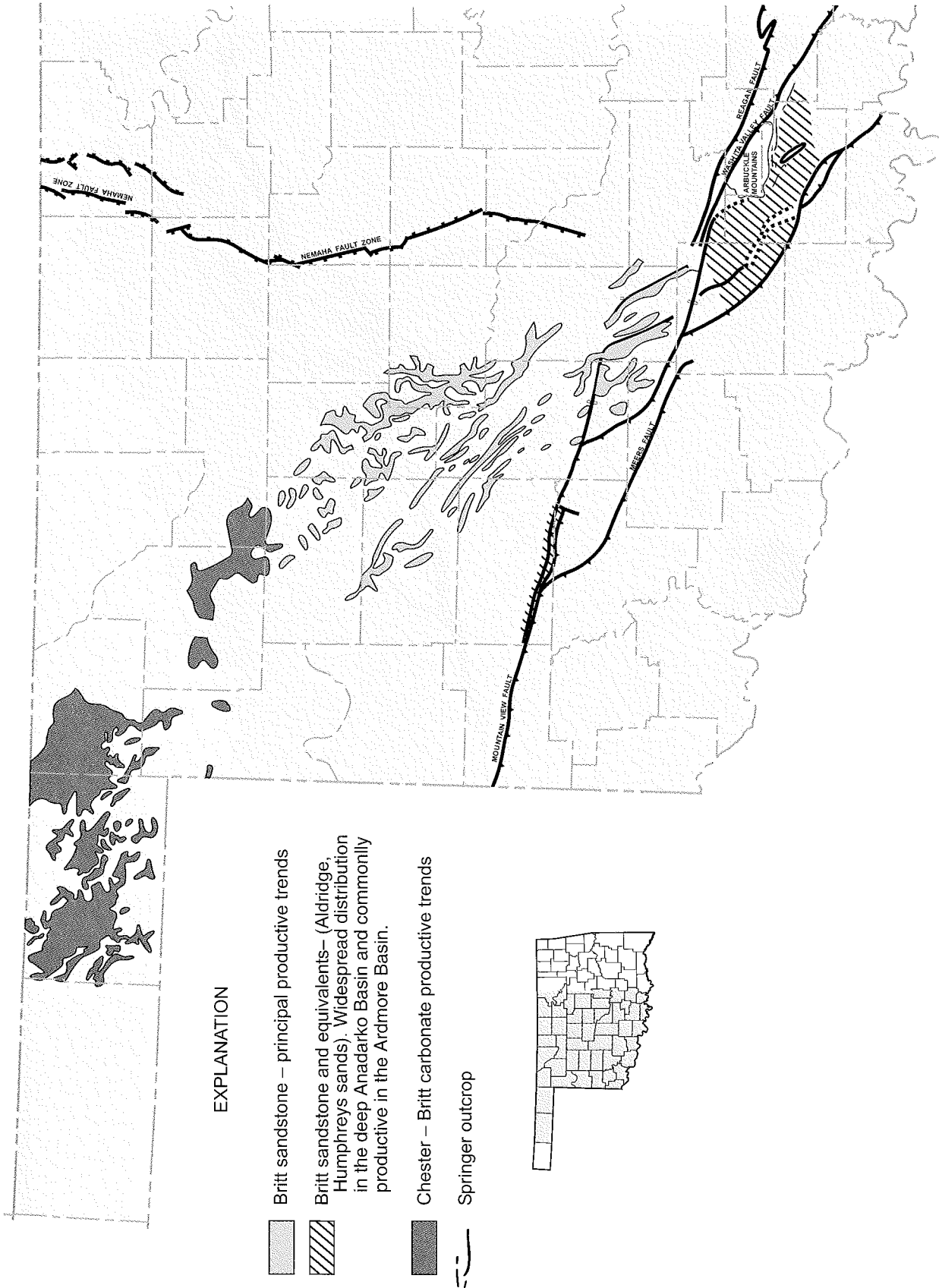


Figure 3. Britt sandstone and carbonate map, showing principal productive trends in the Anadarko and Ardmore Basins, Oklahoma. Modified from Andrews (2001).

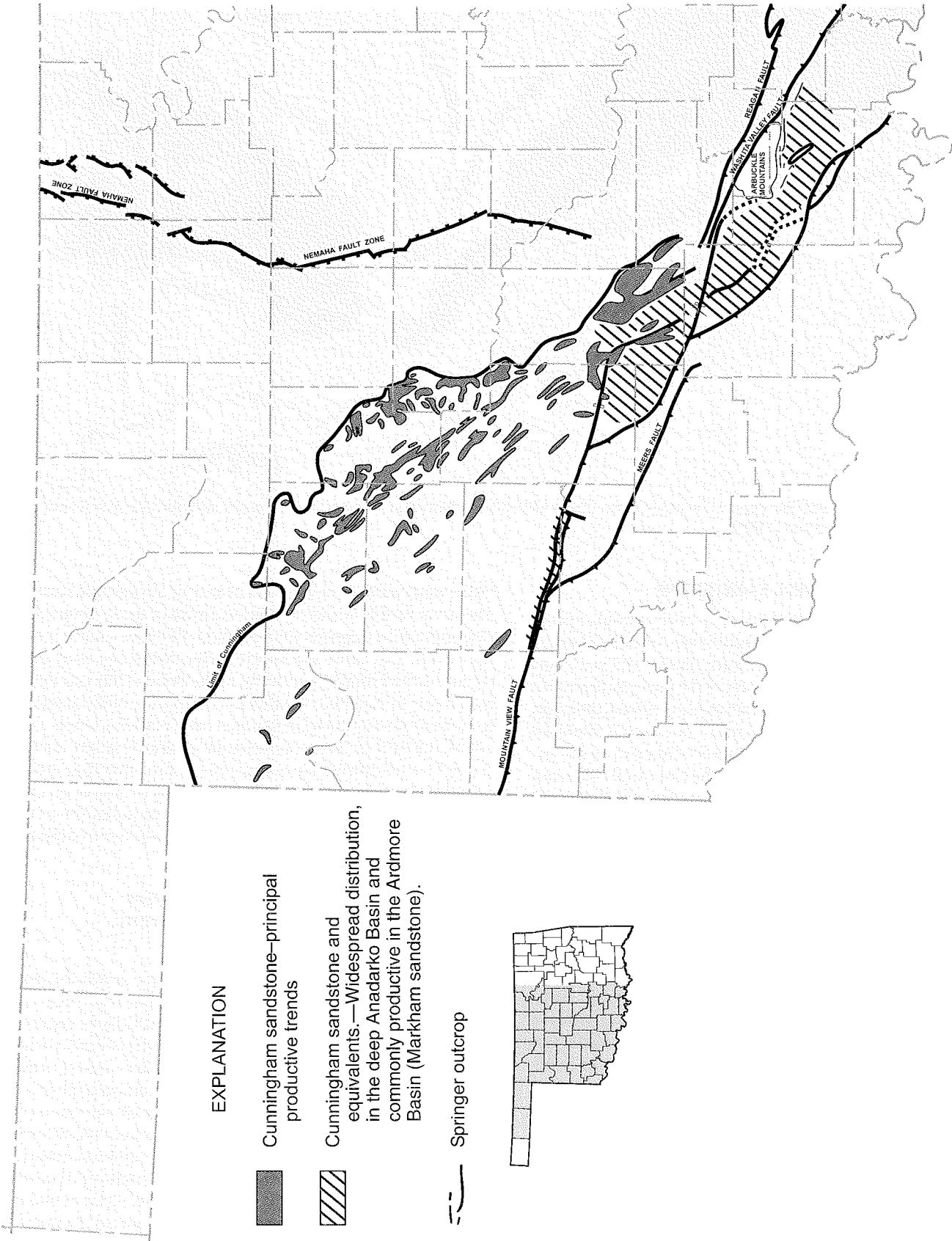


Figure 4. Cunningham sandstone map, showing principal productive trends in the Anadarko and Ardmore Basins, Oklahoma. Modified from Andrews (2001).

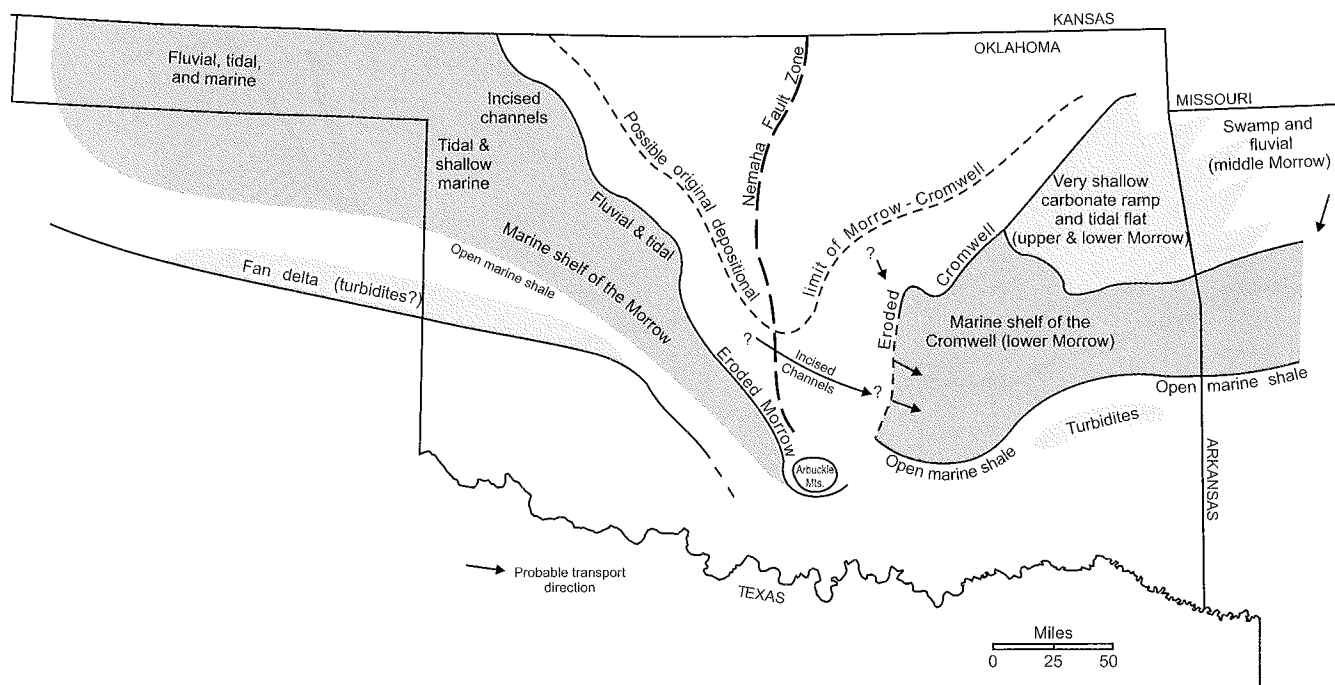


Figure 5. Map showing paleogeographic reconstruction of the Morrow in Oklahoma and western Arkansas. Interpretations in Arkansas are modified from Sutherland (1988).

CROMWELL SANDSTONE

Most of the Cromwell Sandstone occurs in thick, north-south-trending marine bars just east of the Arbuckle Uplift in the western half of the Arkoma Basin (Fig. 6). The proximity and sandstone thickness in this part of the basin indicate that the source of the sand was from the west-northwest, although any evidence of this presumption is lost by erosion. There are no known sediment-supply corridors extending from the immediate north and east; additionally, the Cromwell shales out southward into the basin. On a regional scale, the Cromwell interval gradually thins and contains increasingly less sandstone to the east and north. In the shallow subsurface flanking the southwestern edge of the Ozark Uplift, the unit contains mostly shale. On outcrop in the Oklahoma Ozarks, the Morrowan is composed mostly of bioclastic limestone with subordinate amounts of marine sandstone and shale. The emergence of limestone in this interval typifies a shallowing depositional tendency to the east that is gradational from a carbonate ramp to tidal-flat (subaerial) deposits. In northwestern Arkansas, sandstone in the Morrow is dominantly of fluvial origin, but these river systems trend to the south and are sediment-supply corridors for the Morrow mostly in Arkansas; they do not provide much coarse clastics for the Cromwell in Oklahoma.

Jackfork Group

Directly south of the Choctaw Fault, which is the southern boundary of the Arkoma Basin, the Morrow consists mostly of calcareous shale. This "shale corridor" defines the open-marine facies of the Morrowan sea that persisted throughout the region. However, south of the Morrow shale corridor are tur-

bidite sandstone sequences that belong to the Jackfork Group. The most widely known surface location of these deep-marine sandstone deposits is in southern Le Flore County near Big Cedar. The same sandstone facies continues west into the subsurface and is productive in the Potato Hills Gas Field (southwest of Talihina). Another good exposure of the Jackfork is ~6 mi south-southeast of Rattan (east of Antlers), where it is ~200 ft thick (N. H. Suneson, personal communication, 2005). It would seem intuitively reasonable to presume that these turbidites were transported off the shelf by means of southwest-trending feeder channels. However, no subsurface- or surface-mapping evidence is known by this author to support this assumption.

Morrow in the Western Part of the Southern Midcontinent

Upper Morrow (Fig. 7)

In the Oklahoma and Texas Panhandles, southwestern Kansas, and southeastern Colorado, the upper Morrow contains coarse-grained sandstones and conglomerates consistent with incised channel deposits. These fluvial systems trend to the southeast, and their source was from igneous terranes in Colorado. The clastics contain significant amounts of feldspar and are classified as feldspathic or arkosic sandstones. At the opposite end of the Anadarko Basin, both in Oklahoma and Texas, chert washes were deposited along the northern flanks of the rising Wichita Mountains. These deposits spread northward up to 20 mi into the deep Anadarko Basin as lobes of fan deltas. In between, in restricted areas within the deep, southeastern part of the Anadarko Basin, the upper Morrow

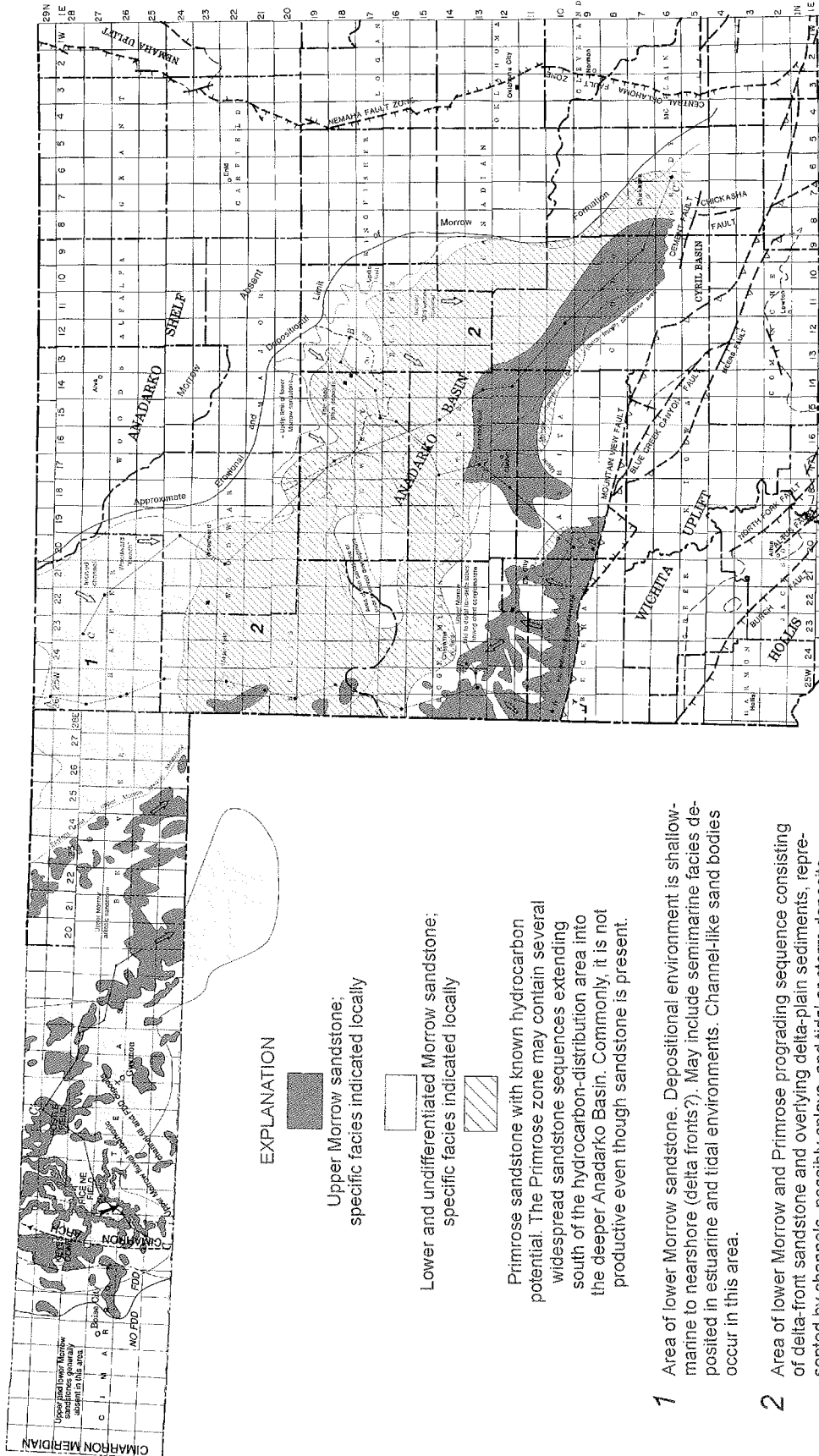


Figure 7. Map showing Morrow sandstone distribution patterns in the Anadarko Shelf and Basin areas of Oklahoma. Modified from Andrews (1995, 1999).

produces from fine-grained clastics that typify most Morrow sandstones.

Lower Morrow

The lower Morrow is generally defined as that sequence within the Morrow Group that underlies the Squaw Belly: limy strata roughly in the middle of the group that are widespread throughout much of the Southern Midcontinent. Sandstone is common within the lower Morrow, forming some of the most prolific reservoirs of gas and condensate. This sandstone occurs in two main intervals. Figure 7 shows the upper part has no commonly accepted name, whereas the lower part is known as the Primrose. In the Ardmore Basin the latter is a formal surface name. The areal-distribution pattern of lower Morrow sandstone in the Anadarko Basin and Shelf areas having known hydrocarbon potential. These sandstones also extend deeper into the basin, where cementation significantly reduces porosity and permeability. Nevertheless, these deeper

areas remain good exploration targets because overpressuring commonly compensates for poorer reservoir quality.

MORROW SIMILARITIES

Morrow strata have remarkable similarities throughout much of the Southern Midcontinent (Fig. 8). The section that is referred to as upper Morrow is composed largely of marine shale with local bursts of coarse clastics. The middle part of the Morrow is defined by a limy zone called the Squaw Belly (Anadarko Basin) or the Union Valley Limestone (Arkoma Basin; Figs. 1, 8). Beneath this marker zone is the lower Morrow, which is usually dominated by sandstone. In the Anadarko Basin the upper part of the lower Morrow has no commonly accepted or formal name; in eastern Oklahoma, where it occurs in the Arkoma Basin, it is designated the Upper Cromwell Sandstone. A second main sandstone interval occurs beneath this one and is designated the Lower Cromwell Sandstone or Primrose Sandstone (Anadarko and Ardmore Basins). Un-

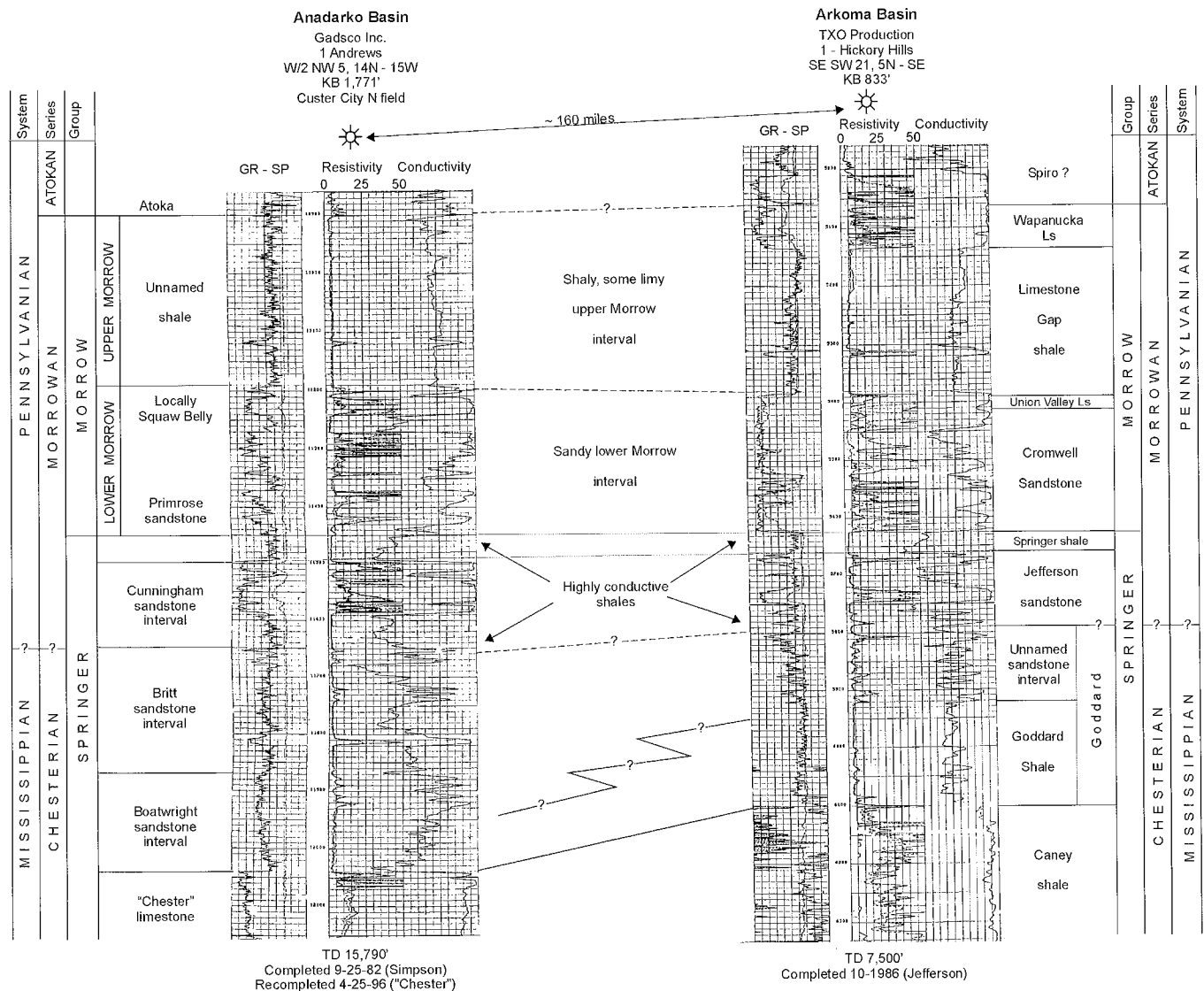


Figure 8. Geophysical logs showing comparison of Morrow stratigraphy in the Anadarko Basin of southwestern Oklahoma and the Arkoma Basin of southeastern Oklahoma. From Andrews (2003).

derlying the Primrose or Cromwell Sandstone is a relatively thin shale unit (about 20–40 ft thick) that has unusually high conductivity (low resistivity). This marker bed separates the Morrow from the underlying Pennsylvanian upper Springer, and hence it is informally called the Springer shale. It is not the Mississippian System's upper boundary, however. The sandstone directly beneath this conductive shale is either the Cunningham (Anadarko Basin) or the Jefferson (Arkoma Basin). The Pennsylvanian–Mississippian boundary likely occurs within this sandstone interval, or slightly beneath.

An interesting feature is the character of the shale in the Morrow interval versus the shale in the Springer interval. Most shale in the Morrow is very calcareous (it effervesces in dilute hydrochloric acid) and is light gray, whereas most shale in the Springer is much less calcareous (it usually does not effervesce) and is darker gray or black.

PRODUCTION Springer

Cumulative oil and gas production from ~6,100 Springer wells in Oklahoma and the Texas Panhandle is 922 MMBO and ~8.4 TCFG, respectively (IHS Energy, 2005) (Fig. 9). Most of the oil production is attributed to Springer correlatives in the Ardmore Basin, whereas that in the Anadarko Basin is largely condensate associated with gas production. Springer sandstones account for ~63% of total gas production or ~5.3 TCF (IHS Energy, 2005) (Fig. 10). The remainder (~3 TCF) is attributed to Springer carbonates (IHS Energy, 2005) (Fig. 11). On a per-well basis, the Springer produces an average of 151 MBO and 1,377 MMCFG.

Annual Springer oil production (Fig. 9) follows a remarkable straight-line decline as plotted on a log-normal graph. The last 2 years of data (2003 and 2004) indicate that oil production has dropped below 5 MMBO per year. Gas production appears to be relatively steady since 1992 at ~200 BCF per year. Many exceptionally good wells deeper in the basin have actually increased this trend over the past few years.

Morrow

Morrow in Anadarko Basin

Cumulative oil and gas production from ~14,000 Morrow (excluding the Cromwell) wells in Oklahoma and the Texas Panhandle is ~550 MMBO and ~23 TCFG (IHS Energy, 2005) (Fig. 12). This is almost 3 times the gas volume and 60% of the oil volume as compared to the entire Springer. Much of the oil production comes from the upper Morrow arkosic sandstone in the Panhandle area, although a significant volume is also attributed to gas-well condensate production. Gas production comes largely from the lower Morrow sandstone interval, including the Primrose. On a per-well basis, the Morrow produces an average of 39 MBO and 1,643 MMCFG.

Cromwell in Arkoma Basin

Cumulative oil and gas production from ~2,000 Cromwell wells in Oklahoma is ~123 MMBO and ~884 BCFG (IHS Energy, 2005) (Fig. 13). This is considerably less than that of the Morrow or Springer in the Anadarko Basin. Nevertheless, on

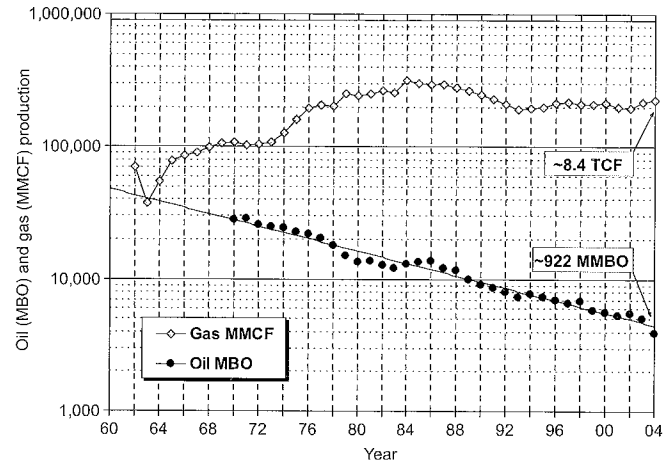


Figure 9. Graph showing annual oil and gas production from the Springer Group (sandstone and carbonate) in Oklahoma and the Texas Panhandle. Data tabulated through 2004 from IHS Energy (2005).

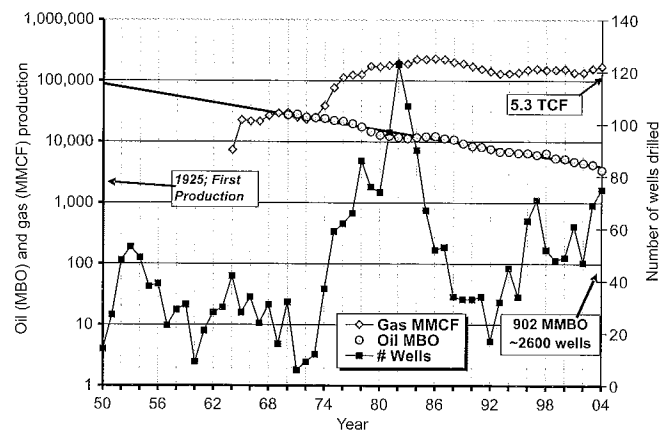


Figure 10. Graph showing annual oil and gas production from the Springer Group (sandstone only) in Oklahoma. Data tabulated through 2004 from IHS Energy (2005).

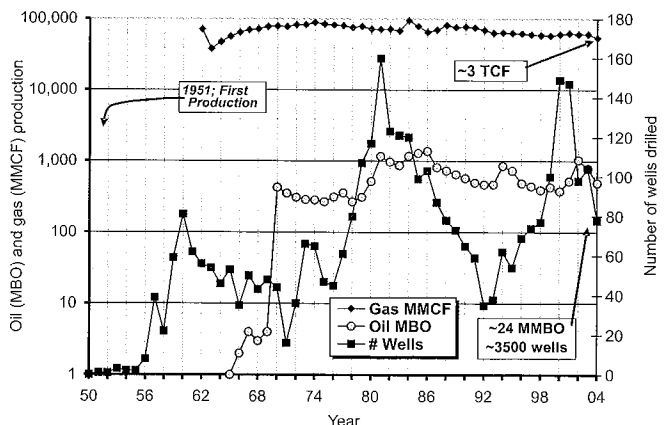


Figure 11. Graph showing annual oil and gas production from the Springer Group (carbonate only) in Oklahoma and the Texas Panhandle. Data tabulated through 2004 from IHS Energy (2005).

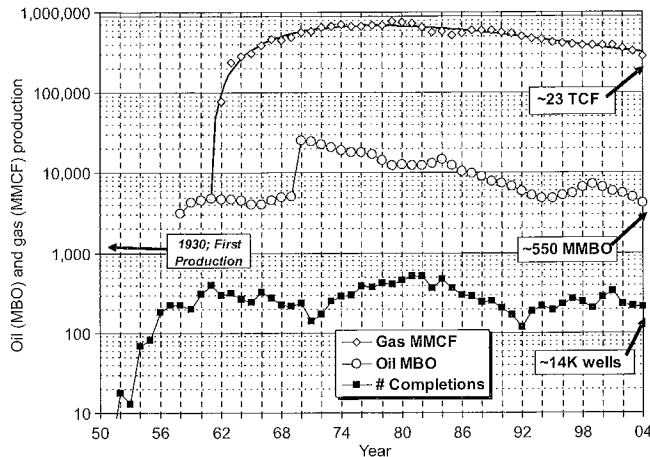


Figure 12. Graph showing annual oil and gas production from the Morrow Group (excluding the Cromwell) in Oklahoma and the Texas Panhandle. Data tabulated through 2004 from IHS Energy (2005).

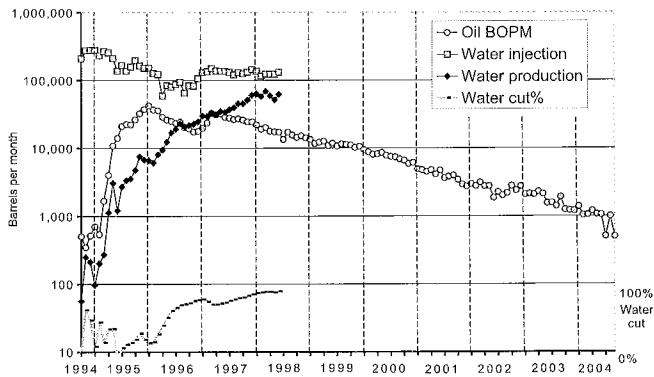


Figure 13. Graph showing annual oil and gas production from the Cromwell Sandstone in southeastern Oklahoma. Data tabulated through 2004 from IHS Energy (2005).

a per-well basis, the Cromwell ranks high in oil production (~61 MBO/well) but relatively low in average gas production (~439 MMCF per well). Importantly, production depths of the Cromwell are considerably less than those of the Morrow and Springer in the Anadarko Basin, so the economic value of Cromwell gas, when considering drilling, completion, and operating costs, should still be high.

REFERENCES CITED

- Andrews, R. D., 1995, Fluvial-dominated deltaic (FDD) oil reservoirs in Oklahoma: the Morrow play: Oklahoma Geological Survey Special Publication 95-1, 67 p.
- 1999, Morrow gas play in the Anadarko basin and shelf of Oklahoma: Oklahoma Geological Survey Special Publication 99-4, 133 p.
- 2001, Springer gas play in western Oklahoma: Oklahoma Geological Survey Special Publication 2001-1, 123 p.
- 2003, Cromwell play in southeastern Oklahoma: Oklahoma Geological Survey Special Publication 2003-2, 87 p.
- IHS Energy (Petroleum Information/Dwights LLC), 2005, Annual Morrow production data.
- Sutherland, P. K., 1988, Late Mississippian and Pennsylvanian depositional history in the Arkoma Basin area, Oklahoma and Arkansas: Geological Society of America Bulletin, v. 100, p. 1787–1802.

Secondary Oil Recovery from the Upper Morrow Purdy Sandstone in Rice NE Field, Texas County, Oklahoma

Richard D. Andrews

Oklahoma Geological Survey
Norman, Oklahoma

ABSTRACT.—Rice NE Field is primarily an oil reservoir in western Texas County in the Oklahoma Panhandle (Fig. 1). It was discovered in 1963 by Apache Corporation, and production comes from two upper Morrow sandstone units. The reservoir consists of coarse to very coarse grained arkosic sandstone of fluvial origin deposited within incised valleys.

This study summarizes the results of a waterflood that began in 1994. Until that time, primary oil recovery from the Purdy “C” sandstone was only ~650,000 barrels of oil (650 MBO) or <7% of the original oil in place (OOIP). Modeling indicated a potential incremental oil recovery of up to 3.2 million barrels of oil (MMBO). The inception of waterflooding encountered numerous problems with old production tubing, but the project nevertheless was very successful. To date, cumulative secondary oil production is ~1.2 MMBO (IHS Energy, 2005), which is almost twice primary production but only about one-third of expected recovery. Recovery efficiency for both primary and secondary oil is ~19%.

The less-than-expected waterflood oil production is probably attributable to permeability and porosity variations that permitted water breakthrough and nonuniform fluid movement within the reservoir. Also, a contributing factor may be lower-than-expected oil saturation.

STRATIGRAPHY

Within the study area the Morrow Group is 500–600 ft thick and contains two main sandstone intervals: the upper Morrow Purdy and the lower Morrow Keyes (Fig. 2). These two intervals are separated by a limy zone informally called the Squaw Belly. The upper Morrow contact is with the Atoka Thirteen Finger limestone, which is distinguished by thin, high resistivity limestone beds. The lower Morrow boundary is the top of the Mississippian “Chester” limestone, which is probably correlative with one of the Springer carbonates.

The principal reservoirs in the immediate study area include the upper Morrow sandstones. These are informally identified as the Purdy “B” and “C.” Although both sandstones produce within the field, only the lower sandstone, the Purdy “C,” was waterflooded. Some additional secondary oil remains in the upper sandstone, although potential recovery from this reservoir is aggravated by limited areal extent and small-scale compartmentalization.

Both upper Morrow Purdy sandstone units have fluvial origins within an incised-valley depositional setting. These channels extend to the south-southeast from terrigenous source provinces in Colorado and western Kansas. They eventually end in a shallow-marine embayment in northwestern Oklahoma and northern Texas (Fig. 3).

Upper Morrow Purdy “B” Sandstone

The upper Morrow Purdy “B” sandstone occurs primarily in the northern part of the field and was exploited soon after discovery. Within the field, this sandstone unit reaches thick-

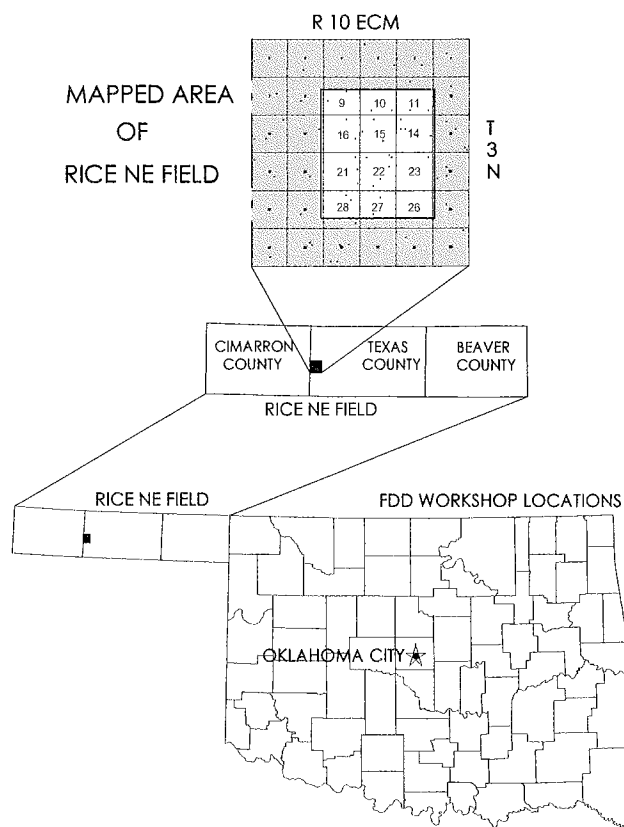


Figure 1. Generalized location map of Rice NE Field in western Texas County, Oklahoma.

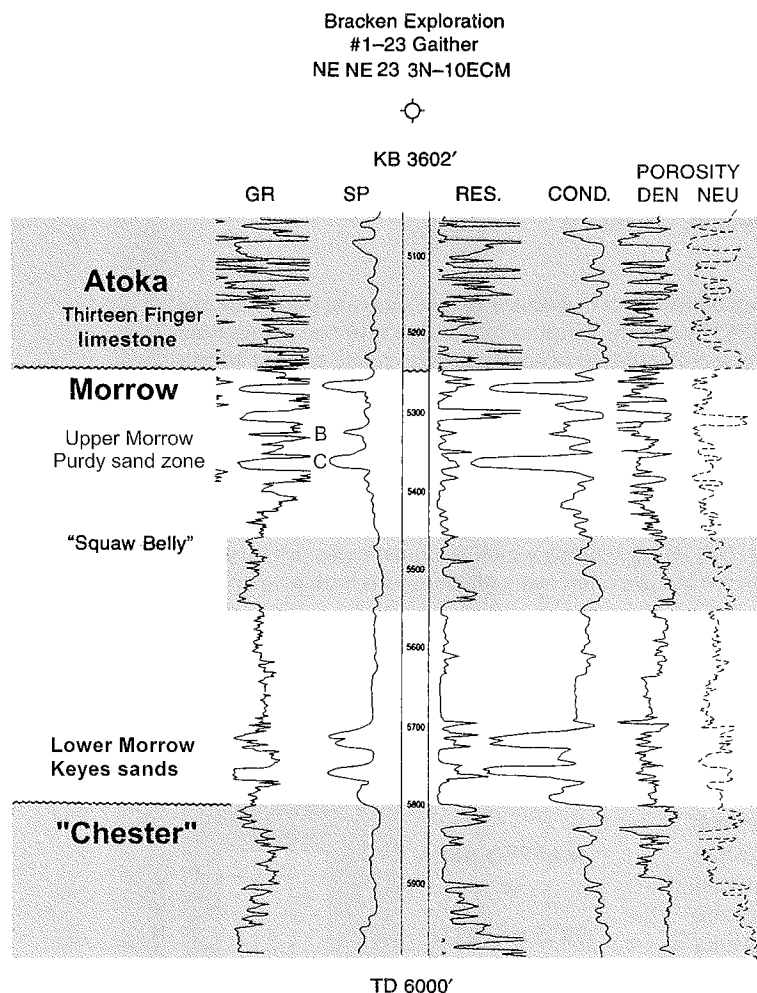


Figure 2. Type log for Rice NE Field, showing subsurface nomenclature of the Morrowan in the area. GR = gamma ray; SP = spontaneous potential; RES. = resistivity; COND. = conductivity; DEN = density; NEU = neutron.

nesses of 22 ft but is usually much thinner and probably averages <10 ft thick. Typically, the Purdy "B" thickens and thins, or becomes discontinuous over relatively short distances of a third of a mile (see Fig. 4, cross section A-A'). Porosity and permeability reductions further restrict the areal extent and thickness of net sandstone such that compartmentalization occurs in three separate pools (Fig. 5). Each of these contains separate gas-oil and oil-water contacts. Although the "B" sandstone continues farther to the northwest, it is displaced upward by a major north-south-trending fault, and the sandstone directly west of this fault is wet.

Upper Morrow Purdy "C" Sandstone

This interval is the principal reservoir in the field and is the interval subject to secondary-recovery efforts. The net Purdy "C" sandstone reaches almost 40 ft in thickness but averages less than half this throughout the field. Consequently, sandstone thickness, areal distribution, and reservoir properties

are highly variable, as shown in cross section B-B' (Fig. 6). Sandstone deposition is most significant directly down-flow of a meander bend from where the river was redirected southward (Fig. 7). This event may have occurred in response to initial uplift of the north-south-bounding fault to the west.

As shown in Table 1, the upper Morrow Purdy sandstone is composed largely of quartz (~70%), plagioclase (~15-18%), and clays (~12%). Trace amounts of potassium feldspar and ankerite are also present (Harpham, 1996). Therefore, the rock is technically a feldspathic or arkosic sandstone. Of importance is the clay content, because most of this constituent consists of kaolinite (~70-80% of the clay content) and chlorite (16-22%). The kaolinite is particularly troublesome during production or pressure surges that dislodge clay platelets, causing them to plug pores. In a similar manner, chlorite reacts with hydrochloric acid (routinely used in acid cleanup of wells), forming an insoluble residue that also plugs pores.

Routine porosity of the upper Morrow in the southern part of Rice NE Field shows a good relationship to permeability (Fig. 8). These data indicate that sandstone with a net porosity of $\geq 10\%$ has permeability in the range of 1-100 millidarcies (md). Actual values are provided in the inset table of this graph.

STRUCTURE

Although trapping in Rice NE Field is purely stratigraphic, structural displacement probably had a significant role in sandstone distribution and ultimately in hydrocarbon emplacement. As shown in Figure 9, two prominent northeast-trending faults bracket this field. The western fault has a displacement of ~600 ft (up to the west), and initial movement probably redirected fluvial patterns southward.

The southwest part of Rice NE Field is the structurally highest part of the field. Most of the field lies within a trough that extends to the northeast. The hydrocarbon column is ~250 ft, with the upper 50 ft or so constituting the gas cap. The oil-water contact partially circumscribes the field to the north and northeast.

HYDROCARBON PRODUCTION

Total gas production of ~3.4 BCF is largely reflected by recovery from one well drilled to the gas cap of the Purdy "C" reservoir. Primary oil production totals almost 1 MMBO, with 333 MBO attributed to the Purdy "B" and 651 MBO to the Purdy "C" (which was waterflooded). Production started in 1963, primarily along the northern part of the field, and declined steadily during the next 18 years. It was not until 1981 that the main part of the field was discovered directly south of the initial producing area. This field extension constitutes the bulk of the Purdy "C" reserves, both primary and secondary.

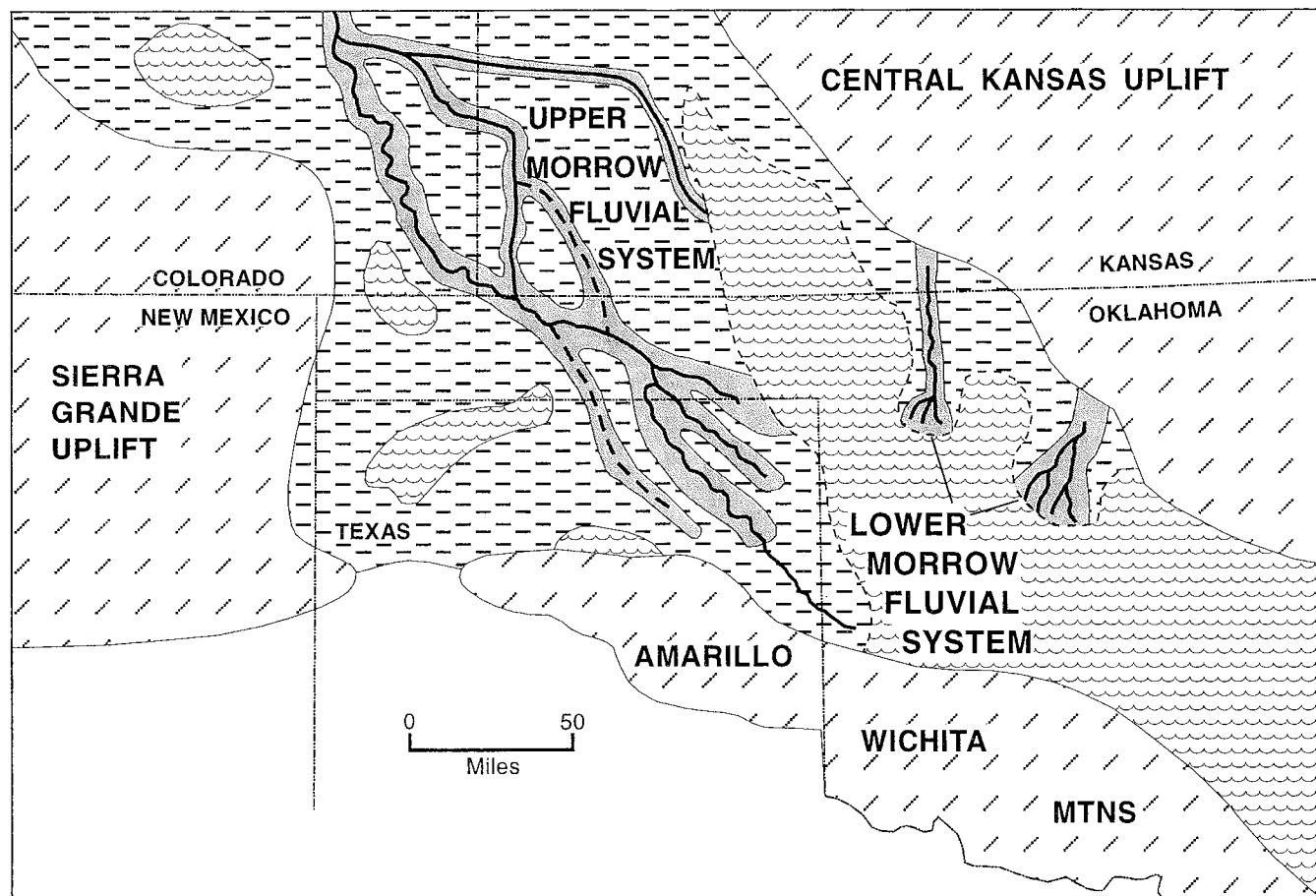


Figure 3. Map showing Morrow fluvial systems in the Midcontinent.

The jump in production, starting in 1982 (see graph, Fig. 10), reflects this development. In subsequent years, extending into 1994, production again declined to just over 10 barrels of oil per day (BOPD) for the entire field. At this time, Ensign Operating Company of Denver began secondary waterflooding. Within about a year, production spiked to several hundred BOPD, which is a larger volume than during any of the primary recovery periods. Nevertheless, secondary production started to decline rapidly, beginning in 2000, nearly 6 years after the flood began. To date, secondary recovery is 1.19 MMBO. Production data are tabulated in Table 2.

THE WATERFLOOD

Beginning in early 1994, Ensign started injecting water into the reservoir at the rate of ~200,000 barrels of water per month or about 600–700 barrels of water per day (BWPD) per well. About 10 wells were designated as injection wells, and 9 wells for production. Figure 11 shows the fillup bubble map after 1 year. (Harpham, 1996). At this stage of injection the reservoir had a rapid response in oil production. Wells directly down-dip from the gas cap in a band extending northeast to southwest across sec. 22 began producing large volumes of oil, banked by the advancing water (Fig. 12). This is the area

of primary response, which eventually spread to producers farther north in sec. 15.

Now, >10 years later, the period of secondary recovery has matured to a rate of only ~20 BOPD, down from a high of almost 900 BOPD. Cumulative incremental oil production is almost 1.2 MMBO, which is almost twice the primary production. The total recovery is ~19% of the OOIP. The response of this waterflood is graphed in Figure 13. Oil production is current through 2004; however, water-injection and production data were available only through the first half of 1998. Nevertheless, the trends can be easily inferred during subsequent years.

Modeling of the Rice NE reservoir resulted in the prediction of an additional recoverable 3.2 MMBO. This is almost 3 times the volume actually recovered. Errors in this prediction probably are attributed to unaccountable fluid movement from variations in porosity and permeability. Oil sweep was particularly effective, although not nearly as good as predicted. Presumably, oil was flushed from selective zones having preferred paths of fluid mobility. This reservoir attribute is typical of fluvial deposits, and some element of "reality" should have been factored into this prediction. In light of many waterflood studies, a recovery factor of 1:1 (secondary

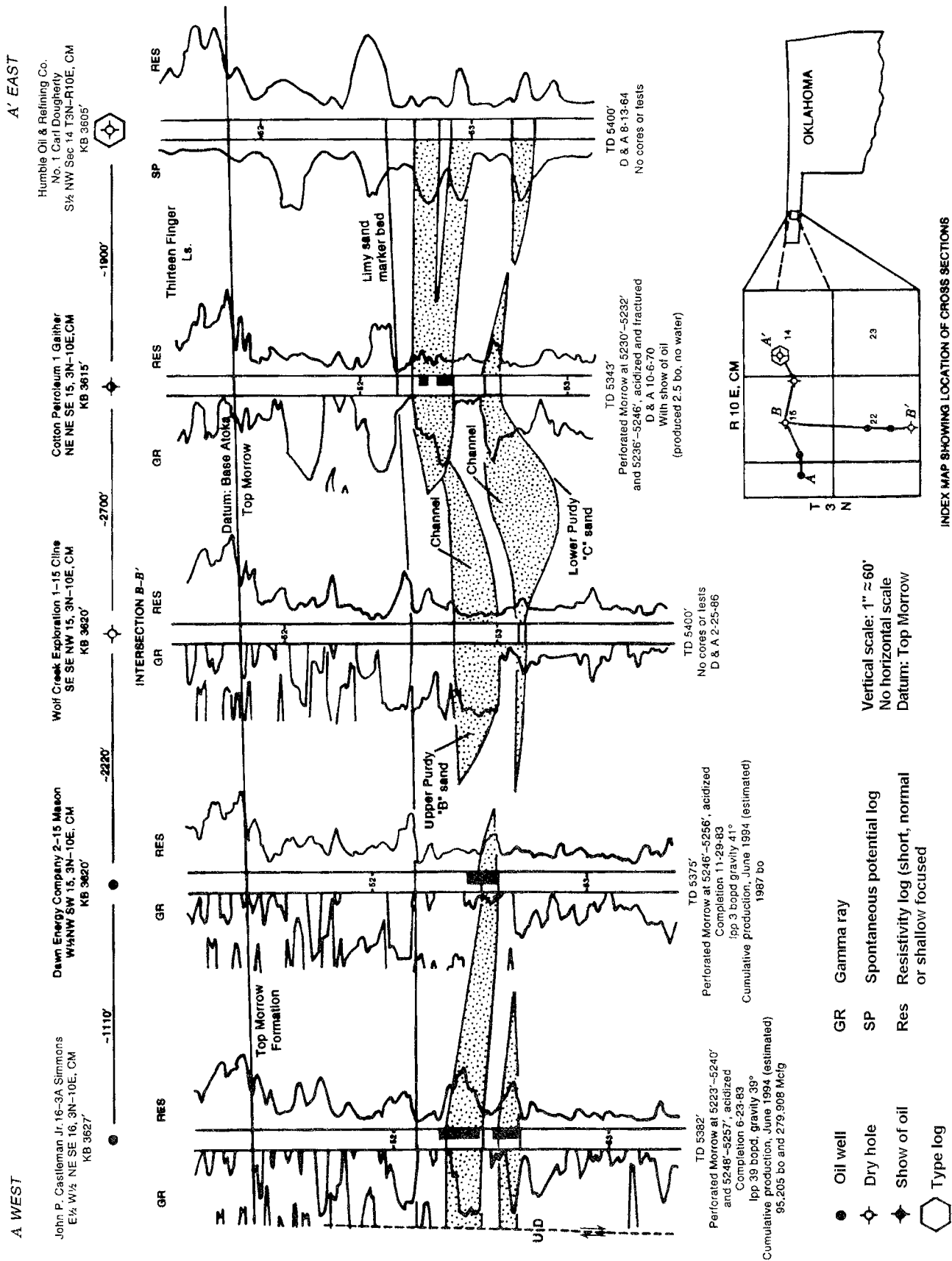


Figure 4. Stratigraphic cross section A-A' (west-east) across the northern part of Rice NE Field. (Cross section B-B' is shown in Figure 6.)

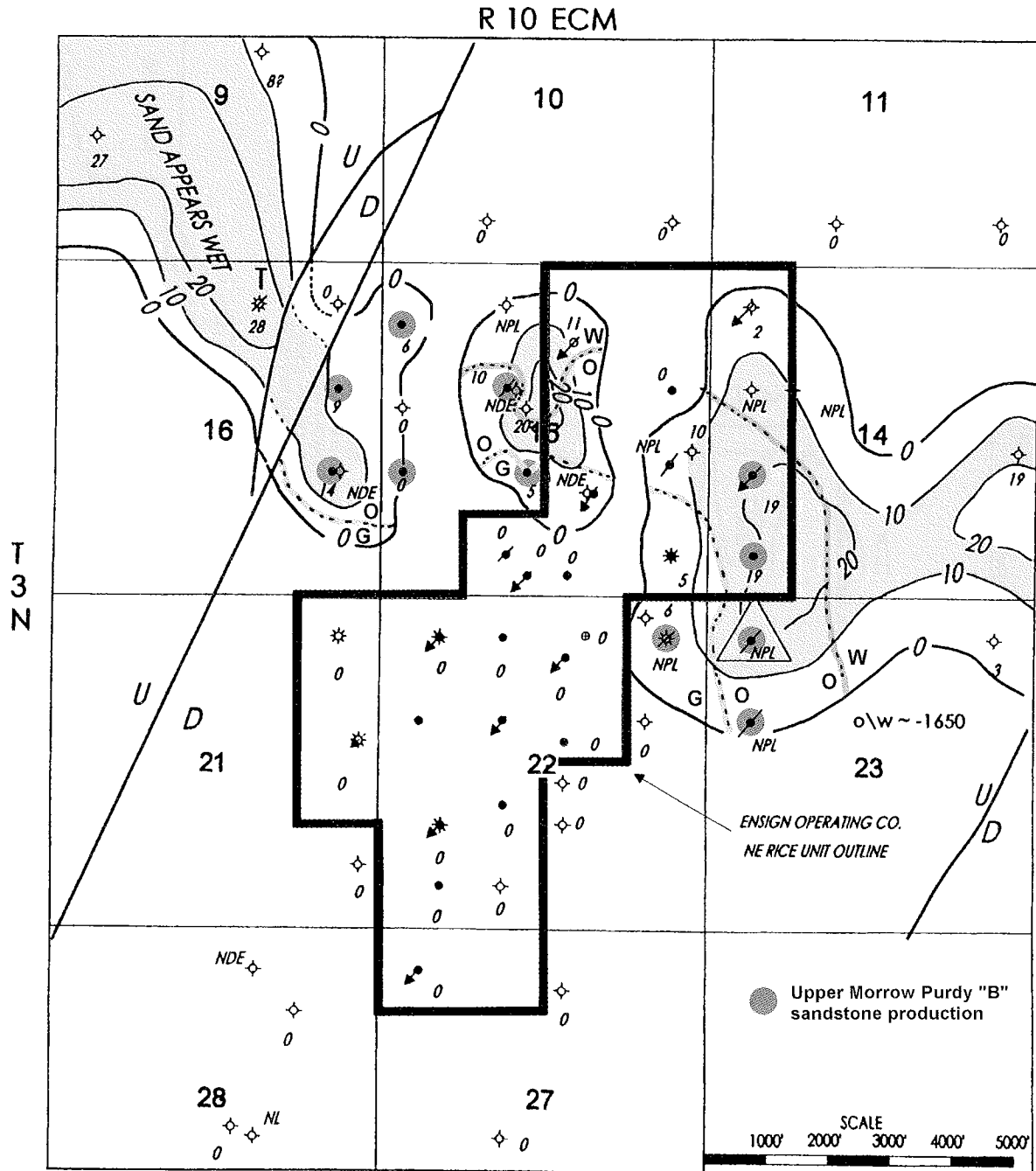


Figure 5. Isopach map showing net upper Purdy "B" sandstone having porosity of $\geq 10\%$. Contour interval, 10 ft. Oil-water and gas-oil contacts are shown.

vs. primary) is always hoped for but often not attained. A 2:1 ratio, as shown by this flood, is exceptional.

A summary of engineering and reservoir properties of this field and reservoir is provided in Table 3.

REFERENCES CITED

- Harpham, S. T., 1996, Waterflood implementation and preliminary results: Northeast Rice Morrow Unit, Texas County, Oklahoma, in DOE-Industry sponsored projects "Traveling Technology Workshops," Spring 1996 (sponsored by BDM Oklahoma and the Petroleum Technology Transfer Council [PTTC]).
- IHS Energy (Petroleum Information/Dwights LLC), 2005, Annual Morrow production data.

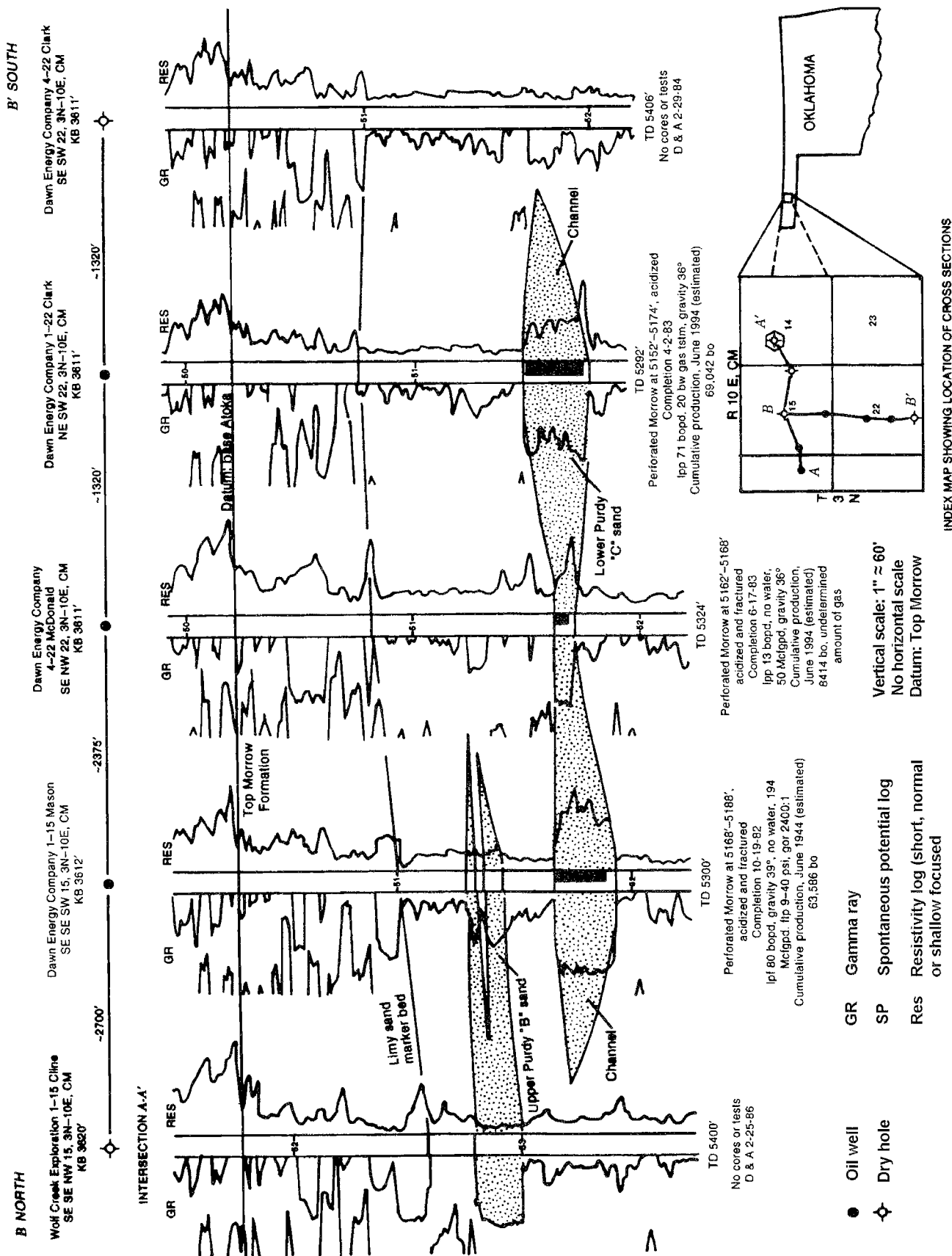


Figure 6. Stratigraphic cross section B-B' (north-south) across the central part of Rice NE Field. (Cross section A-A' is shown in Figure 4.)

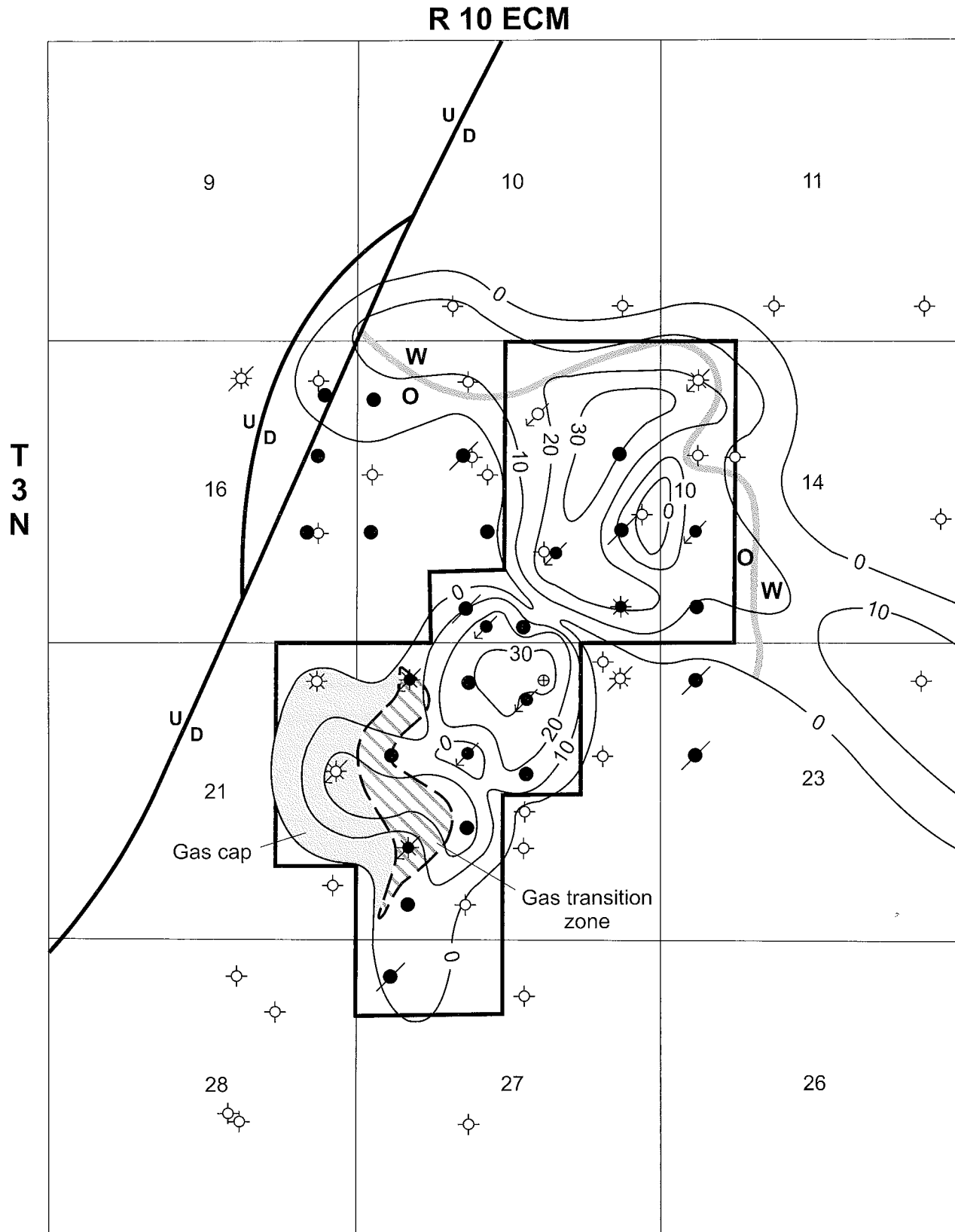


Figure 7. Isopach map showing net lower Purdy "C" sandstone having porosity of $\geq 10\%$. Contour interval, 10 ft. Waterflood unit outline and oil-water and gas-oil contacts are shown.

TABLE 1.—X-Ray Diffraction Analysis of Two Sandstone Intervals Within Ensign's NERMSU^a Salt Water Supply Well No. 1, NW¼NE¼ sec. 22, T. 3 N., R. 10 ECM, Texas County, Oklahoma

	Sample depth 5,177 ft	Sample depth 5,210 ft
Whole-Rock Mineralogy		
Quartz	70%	71%
Potassium feldspar	—	trace
Plagioclase	18%	15%
Ankerite (Fe-Mg carbonate)	—	1%
Illite-smectite	trace	trace
Illite + mica	1%	1%
Kaolinite	8%	10%
Chlorite	3%	2%
Relative Clay Abundance		
Illite-smectite	3%	1%
Illite + mica	6%	4%
Kaolinite	69%	79%
Chlorite	22%	16%
% smectite in mixed-layer illite-smectite	10%	10%

^aNortheast Rice Morrow Sand Unit.

Source: Harpham (1996).

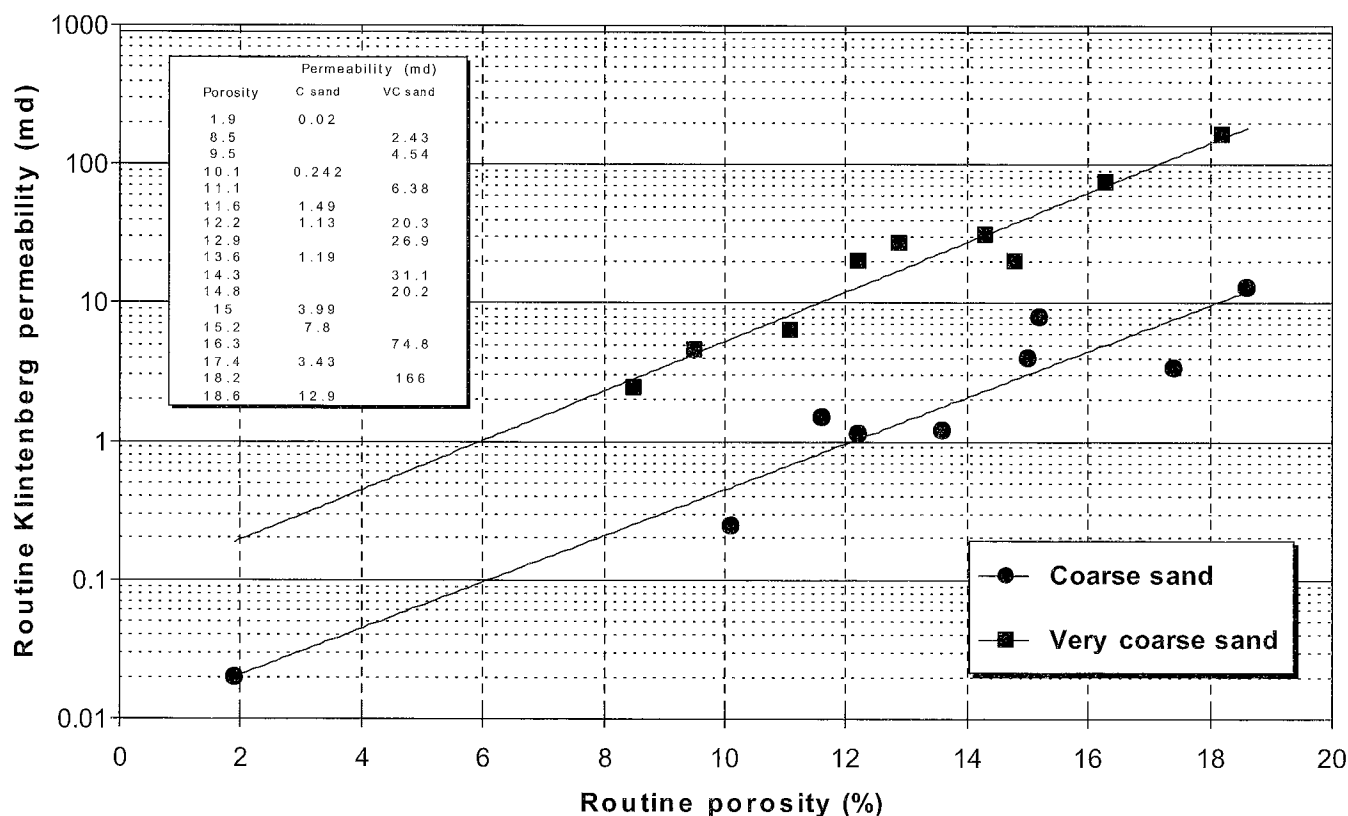


Figure 8. Porosity-versus-permeability plot of sandstone in Rice NE Field. Data from Harpham (1996).

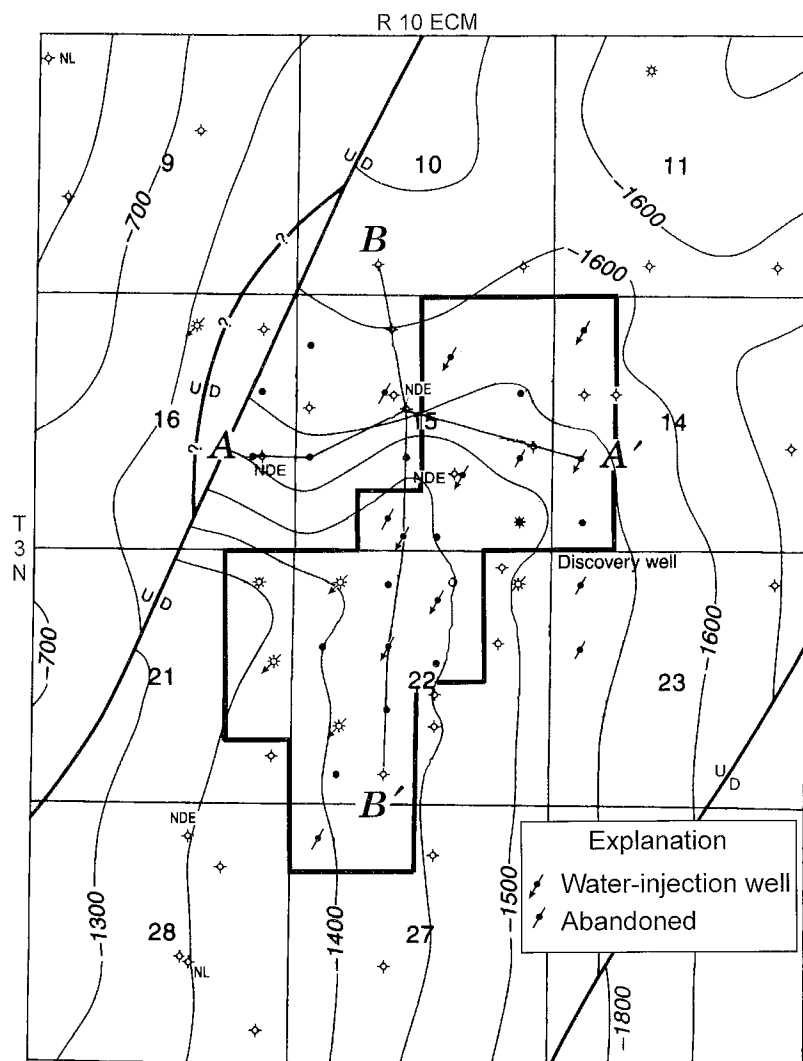


Figure 9. Structure map depicting the top of the Morrow in Rice NE Field. Contour interval, 50 ft. Waterflood unit outline and major faults are shown, as are lines of cross sections A-A' and B-B'.

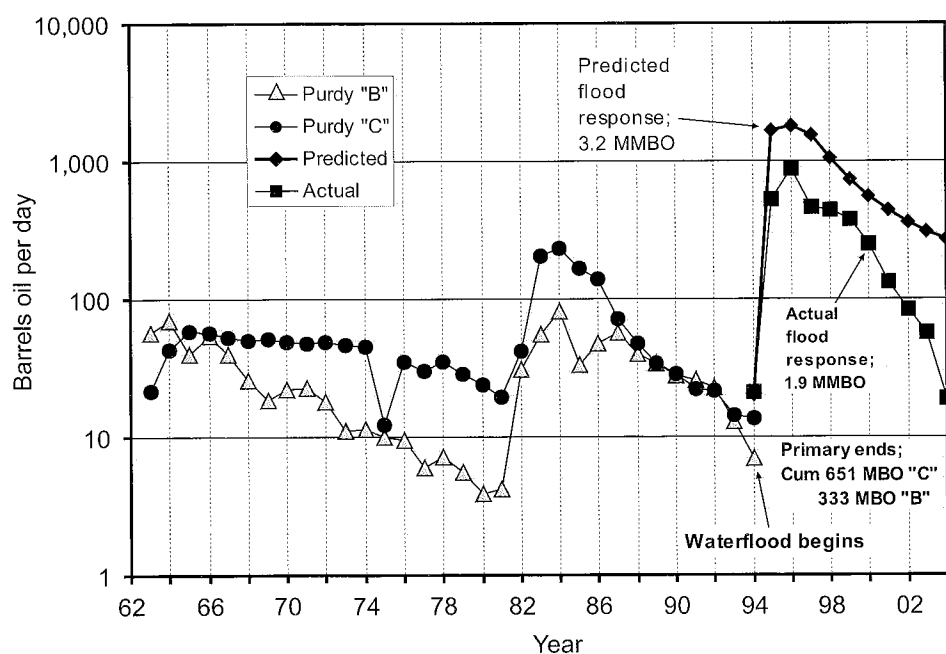


Figure 10. Graph showing annual oil production, including predicted and actual enhanced recovery, for Rice NE Field. Data from Harpham (1996) and IHS Energy (2005).

TABLE 2.—Production Data for Rice NE Field

Upper Morrow Purdy "B" Sandstone Production						Upper Morrow Purdy "C" Sandstone Production						Purdy "B" & "C" Combined			
Year	No. of wells	Annual oil (bbl)	Average daily field (bbl)	Average per well (bbl)	Cumulative oil production (bbl)	No. of wells	Annual oil (bbl)	Average daily field (bbl)	Average per well (bbl)	Cumulative oil production (bbl)	Annual oil production (bbl)	Average daily production field (bbl)	Cumulative oil production (bbl)		
1962	0	0	0.0	0.0	0	0	0	0.0	0.0	0	0	0	0		
1963	3	20,780	56.9	19.0	20,780	1	7,970	21.8	21.8	7,970	28,750	79	28,750		
1964	3	25,796	70.7	23.6	46,576	2	15,832	43.4	21.7	23,802	41,628	114	70,378		
1965	2	14,576	39.9	20.0	61,152	2	21,145	57.9	29.0	44,947	35,721	98	106,099		
1966	2	19,781	54.2	27.1	80,933	2	20,677	56.6	28.3	65,624	40,458	111	146,557		
1967	2	14,506	39.7	19.9	95,439	2	19,111	52.4	26.2	84,735	33,617	92	180,174		
1968	2	9,529	26.1	13.1	104,968	2	18,345	50.3	25.1	103,080	27,874	76	208,048		
1969	2	6,705	18.4	9.2	111,673	2	18,016	51.3	25.6	121,787	25,412	70	233,460		
1970	3	8,014	22.0	7.3	119,687	3	17,399	47.7	16.5	139,803	26,030	71	259,490		
1971	3	8,223	22.5	7.5	127,910	2	17,399	47.7	23.8	157,202	25,622	70	285,112		
1972	3	6,632	18.2	6.1	134,542	2	17,662	48.4	24.2	174,864	24,294	67	309,406		
1973	2	3,998	11.0	5.5	138,540	2	16,862	45.8	23.1	191,726	20,860	57	330,266		
1974	2	4,123	11.3	5.6	142,663	2	16,702	46.2	22.9	208,428	20,825	57	351,091		
1975	3	3,605	9.9	3.3	146,268	3	4,472	12.3	4.1	212,900	8,077	22	359,168		
1976	3	3,432	9.4	3.1	149,700	3	12,856	35.2	11.7	225,756	16,288	45	375,456		
1977	3	2,189	6.0	2.0	151,889	3	10,912	29.9	10.0	236,668	13,101	36	388,557		
1978	3	2,638	7.2	2.4	154,527	4	12,828	35.1	8.8	249,496	15,466	42	404,023		
1979	3	2,022	5.5	1.8	156,549	4	10,485	28.7	7.2	259,981	12,507	34	416,530		
1980	3	1,424	3.9	1.3	157,973	4	8,657	23.7	5.9	268,638	10,081	28	426,611		
1981	3	1,550	4.2	1.4	159,523	3	7,105	19.5	6.5	275,743	8,655	24	435,266		
1982	4	11,237	30.8	7.7	170,760	10	15,166	41.6	4.2	290,909	26,403	72	461,669		
1983	5	20,112	55.1	11.0	190,872	13	74,867	205.1	15.8	365,776	94,979	260	556,648		
1984	5	29,536	80.9	16.2	220,408	17	84,757	232.2	13.7	450,533	114,293	313	670,941		
1985	5	11,992	32.9	6.6	232,400	17	61,310	168.0	9.9	511,843	73,302	201	744,243		
1986	5	17,553	48.1	9.6	249,953	16	51,449	141.0	8.8	563,292	69,002	189	813,245		
1987	6	20,758	56.9	9.5	270,711	16	26,213	71.8	4.5	589,505	46,971	129	860,216		
1988	6	14,651	40.1	6.7	285,362	16	17,435	47.8	3.0	606,940	32,086	88	892,302		
1989	5	12,543	34.4	6.9	297,905	14	12,460	34.1	2.4	619,400	25,003	69	917,305		
1990	5	10,089	27.6	5.5	307,994	15	10,363	28.4	1.9	629,763	20,452	56	937,757		
1991	5	9,540	26.1	5.2	317,534	15	8,058	22.1	1.5	637,821	17,598	48	955,355		
1992	5	8,243	22.6	4.5	325,777	14	7,963	21.8	1.6	645,784	16,206	44	971,561		
1993	5	4,679	12.8	2.6	330,456	13	5,260	14.4	1.1	651,044	9,939	27	981,500		
1994	5	2,554	7.0	1.4	333,010								984,054		
						Secondary oil recovery		Cumulative incremental							
1994							4,971	14		4,971			989,025		
1995							193,472	530		198,443			1,182,497		
1996							318,043	871		516,486			1,500,540		
1997							168,340	461		684,826			1,668,880		
1998							162,261	445		847,087			1,831,141		
1999							138,225	379		985,312			1,969,366		
2000							91,467	251		1,076,779			2,060,833		
2001							48,305	132		1,125,084			2,109,138		
2002							30,630	84		1,155,714			2,139,768		
2003							20,804	57		1,176,518			2,160,572		
2004							6,771	19		1,183,289			2,167,343		

All production unitized in 1994 and reported from the Chaparral Energy well in C SE¼ sec. 15, T. 3 N., R. 10 ECM

Sources: Harpham (1996) and IHS Energy (2005).

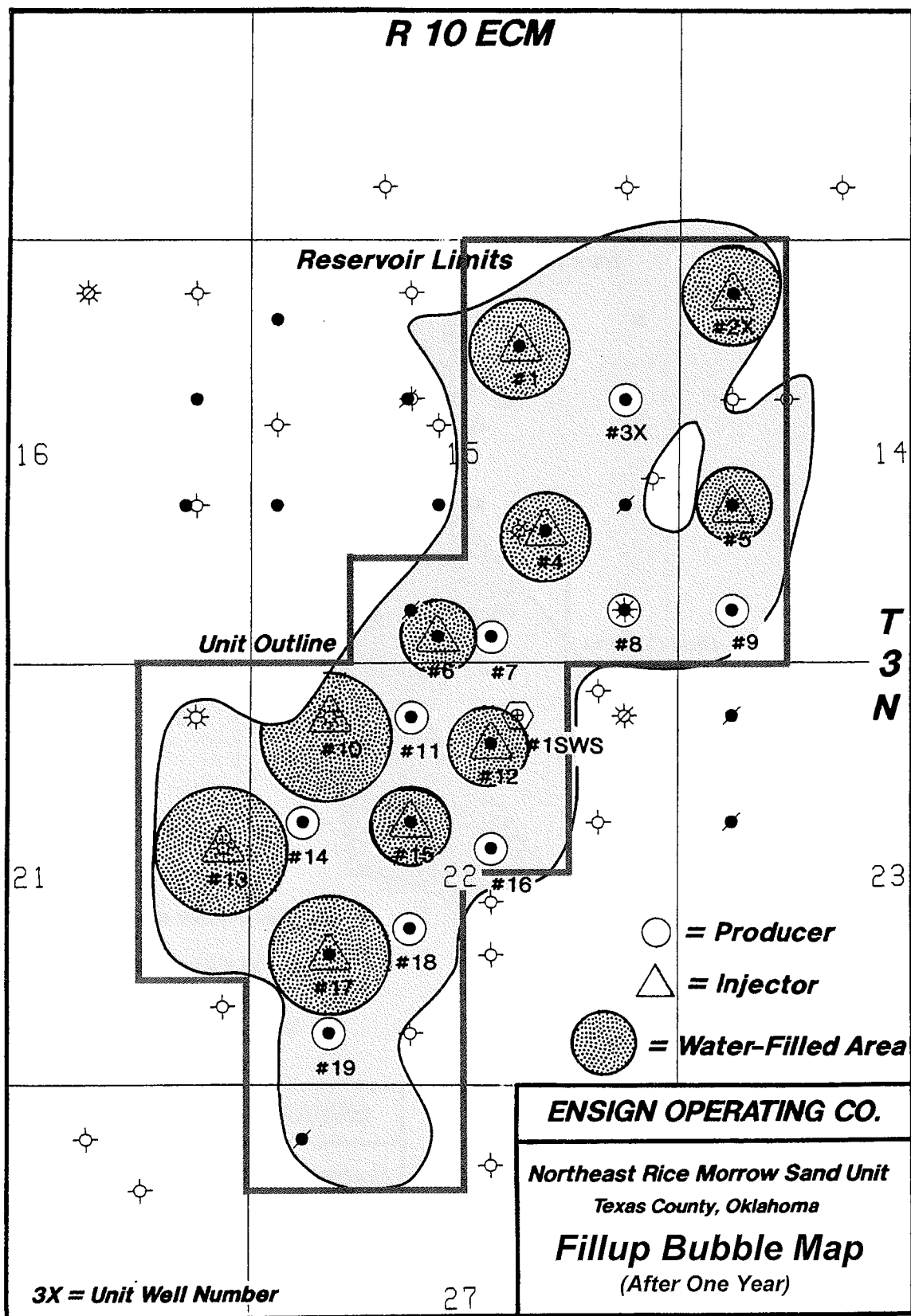


Figure 11. Water fill-up bubble map of Northeast Rice Morrow Sand Unit (NERMSU) a year after initial water injection. From Harpham (1996).

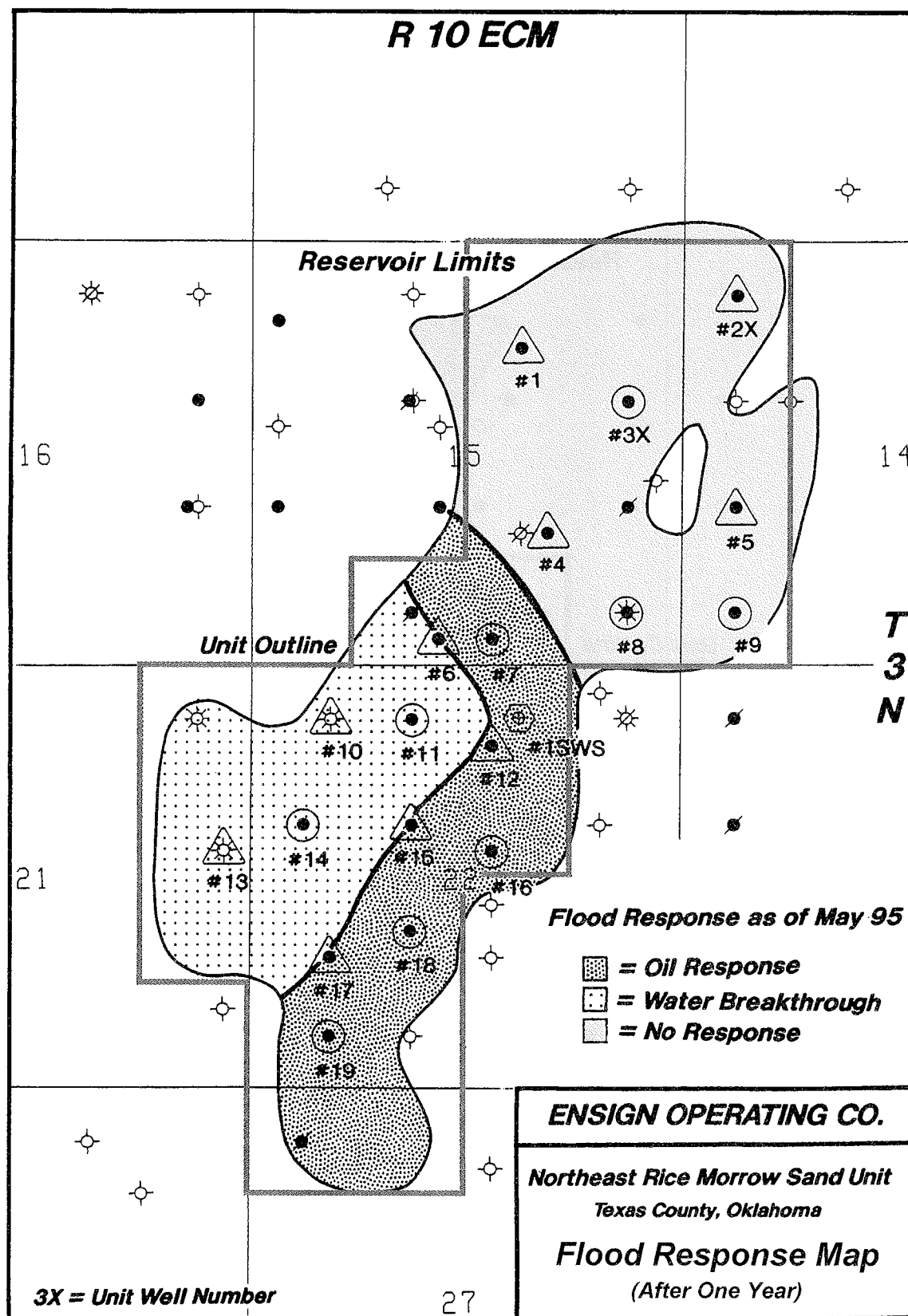


Figure 12. Waterflood-response map of NERMSU a year after water injection. From Harpham (1996).

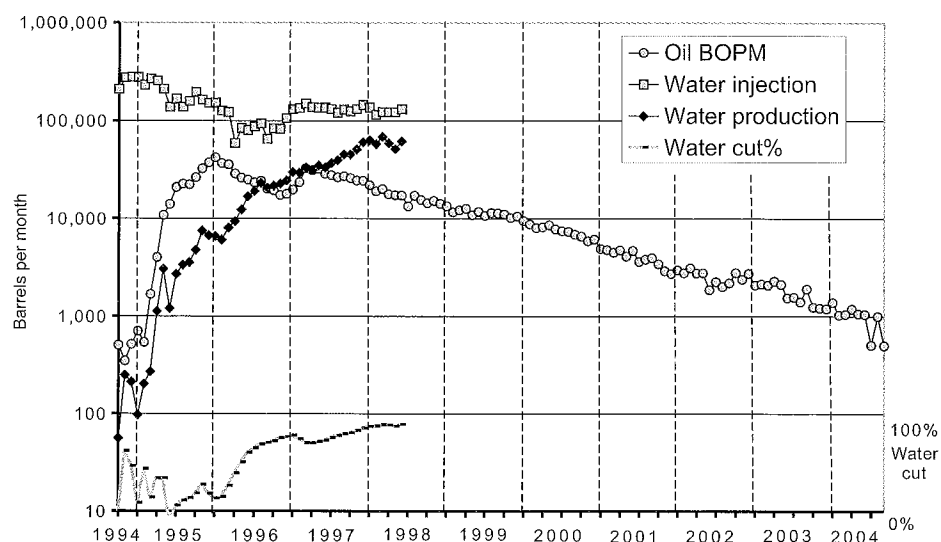


Figure 13. Plot showing annual oil production, water production, water injection, and water cut for NERMSU. Data from Harpham (1996) and IHS Energy (2005).

TABLE 3.—Geological/Engineering Data for the Upper Morrow Sandstone in Rice NE Field, Texas County, Oklahoma

	Morrow sandstone	
	Upper Purdy "B"	Lower Purdy "C"
Reservoir size	450 acres	940 acres
Oil–water contact	about –1,650 ft	about –1,720 ft
Gas–oil contact	about –1,587 ft	about –1,540 ft
Reservoir thickness (net sandstone $\geq 10\% \phi$)	5–20 ft (avg. 9 ft)	5–38 ft (avg. 14 ft)
Porosity	5–24% (avg. ~14%)	5–24% (avg. ~17%)
Permeability	1–184+ md average ~12 md	average ~20 md
Water saturation	25–50% (avg. 35%)	22–50% (avg. 35%)
Reservoir temperature	130°F	130°F
Oil gravity	30–39° API	34–42° API (avg. 37°)
Initial formation-volume factor	1.156 reservoir bbl/stock-tank bbl	
OOIP ^a (volumetric)	2,473 MSTBO ^b	9,759 MSTBO
Cumulative primary oil	333 MSTBO (82 BO/ac-ft)	651 MSTBO (50 BO/ac-ft)
Primary oil-recovery efficiency	13.5%	6.7%
Secondary oil recovery		1,186 MBO
Primary- + secondary-recovery efficiency		18.8%
Cumulative gas	117 MMCF(?)	3,260 MMCF

^aOriginal oil in place.

^bThousand stock-tank barrels of oil.

Fighting the Tide: Morrow–Springer Gas in Oklahoma

Dan T. Boyd

Oklahoma Geological Survey
Norman, Oklahoma

ABSTRACT.—In spite of our image as an oil producer, natural gas has been Oklahoma's most important energy resource for decades and today represents 80% of our total hydrocarbon production. Morrow–Springer and equivalent reservoirs are the State's most important gas producers, accounting for 28% of daily production. Development drilling in older fields, combined with production from Potato Hills Field, has maintained a Morrow–Springer contribution that equals 1994 production. This helped reduce the latest annual (2003) Oklahoma gas-production decline to ~1%, which, since 1990, has averaged nearly 3% annually. Maintaining State production requires an approach that includes the addition of new (usually deeper) reservoirs and infill drilling in existing fields. Prolific Morrow and Springer reservoirs remain prime exploration and development objectives that complement ongoing activity in other producing intervals, including nonconventional sources of natural gas, especially coalbed methane.

INTRODUCTION

To most, the image of Oklahoma is that of an oil pumpjack, but based on a barrel of oil equivalence (BOE), natural gas is by far our most important energy resource. Equating 6,000 cubic ft (6 MCF) of gas to a barrel of oil, the State progressed from being primarily an oil producer to being primarily a gas producer in 1963. On the same basis, in 2000, cumulative State gas production exceeded that of oil, in spite of oil having more than a 50-year head start (Fig. 1).

Natural gas today constitutes roughly 80% of both Oklahoma's drilling activity and hydrocarbon production on a BOE basis. If oil and natural gas are combined, the 1927 peak in

Oklahoma's hydrocarbon production of 333 million (MM) BOE can be seen only as an intermediate high in overall hydrocarbon production. The State reached its all-time annual production high of 527 MMBOE in 1970 and nearly the same level in 1984, when 518 MMBOE was produced.

Although most of Oklahoma's major gas fields were discovered well before 1950, the lack of an early market delayed their development. As a result, the earliest years of the Oklahoma gas industry were generally sustained by gas produced in association with shallow oil from fields on the shelf in the northeastern part of the State (Fig. 2). Most early natural gas was found in conjunction with oil exploration, but it was not marketable. At this time, gas was regarded as a drilling hazard

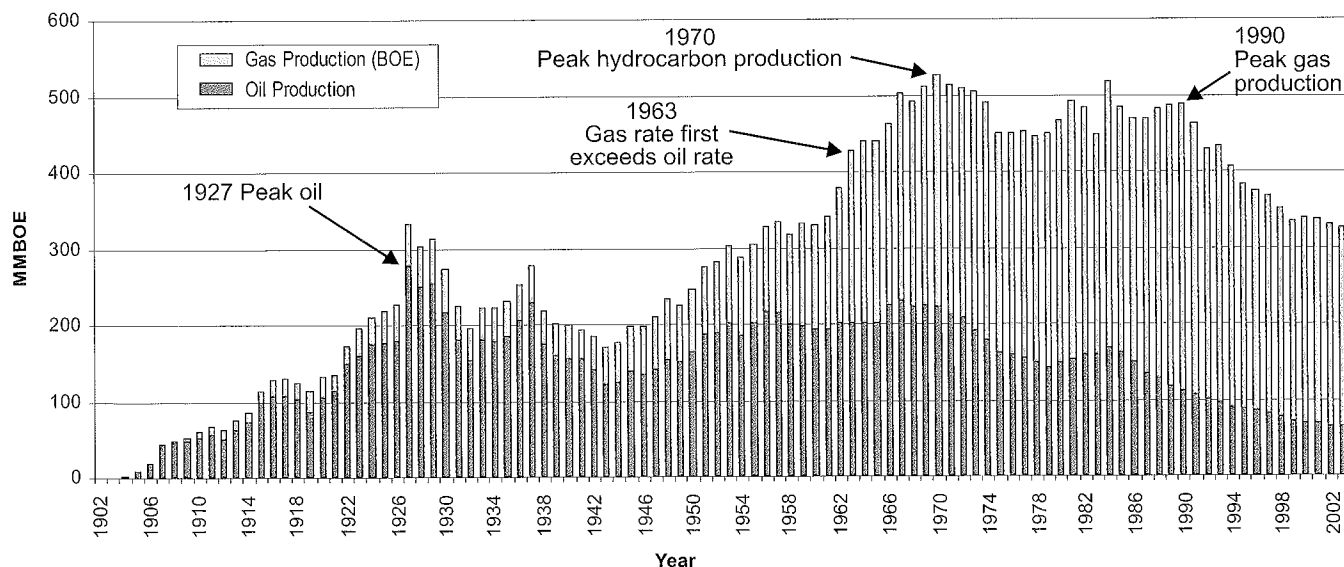


Figure 1. Graph showing Oklahoma annual hydrocarbon production (6 MCF/bbl). BOE = barrel of oil equivalence; MMBOE = millions of barrels of oil equivalence. Data from Claxton (2004).

and was usually vented or flared. Delays in developing a gas market are why Oklahoma did not reach peak gas production of 6.2 billion cubic ft per day (BCFPD) until 1990 (Fig. 3), 63 years after peak oil production (Claxton, 2004).

Oklahoma now produces about 4.3 BCFPD day, which is 1.6 trillion cubic ft (TCF) per year or roughly two-thirds its peak rate. This gas is produced from >3,000 fields and a wide range of reservoirs scattered across the State. The largest of these are the Morrow-Springer and their stratigraphic equivalents. These reservoirs represent 1,191 MMCFPD, or 28% of Oklahoma's 2003 production, and roughly the same

proportion of the State's 94 TCF of cumulative gas production (IHS Energy, 2004).

GEOLOGIC BACKGROUND

The Anadarko, Arkoma, and Ardmore Basins (and associated province shelves) are responsible for the bulk of Oklahoma's oil and gas production (Fig. 4). These basins were present as broad depressions throughout the lower Paleozoic, but did not exist as currently defined until major orogenic events that began in the Late Mississippian–Early Pennsylvanian

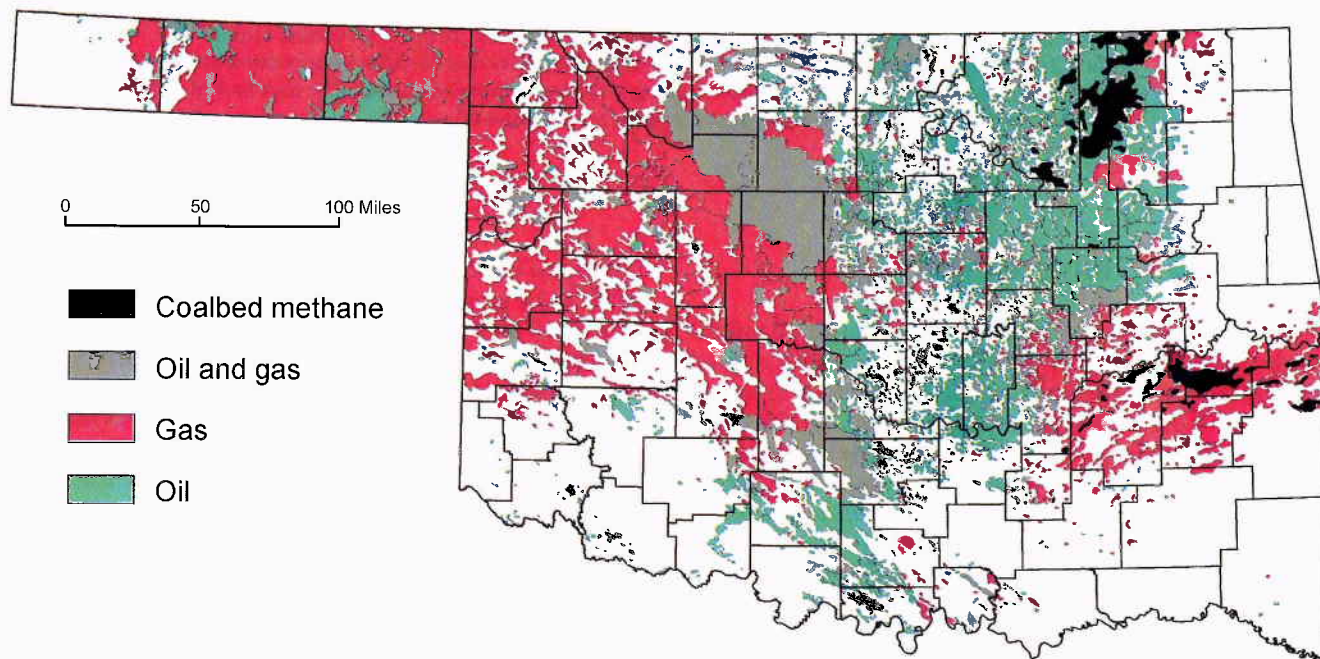


Figure 2. Map of Oklahoma oil and gas fields distinguished by gas to oil ratio (GOR), and coalbed-methane production. Modified from Boyd (2002). GOR cutoffs (in cubic feet per barrel): oil, <5,000; oil and gas, 5,000–20,000; gas, >20,000.

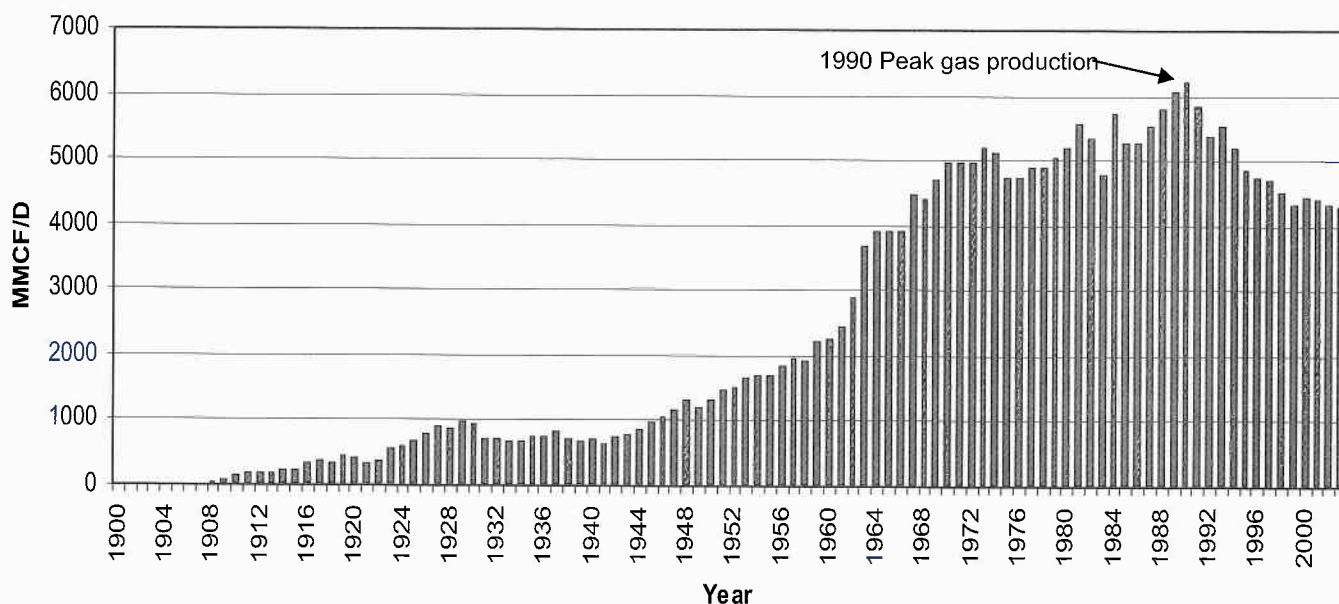


Figure 3. Graph showing Oklahoma annual natural gas production. Data from Claxton (2004).

(Johnson and others, 2001). Major subsidence that began during this period persisted throughout the Pennsylvanian and provided the accommodation space for deposition of most of Oklahoma's productive oil and gas reservoirs.

Springer sedimentary rocks, which record the first pulse of these orogenic events, straddle the boundary between the Mississippian and Pennsylvanian Systems. They mark a change from the dominantly carbonate and shale deposition of the Mississippian to the clastic deposition characteristic of the succeeding Pennsylvanian. In most areas, the overlying Morrowan rocks consist of shallow-marine and fluvial-deltaic clastics deposited on a surface of eroded Mississippian rocks (Johnson, 1989). In the deep Anadarko Basin this sequence of clastic rocks can be very thick, with a Morrow section of >1,000 ft overlying as much as 5,000–7,000 ft of Springer sedimentary rocks (Andrews and others, 2001).

The bulk of the Morrow–Springer stratigraphic section is composed of shale that acts as both source and seal for the productive interbedded sandstones. This shale contains mostly Type III (gas-prone) kerogen and has total-organic-carbon values ranging from 0.5% to 3.4% (Johnson and Cardott, 1992). Hydrocarbon traps in this interval are dominantly stratigraphic in nature. While multiple producing reservoirs can be found on structural closures, a large stratigraphic component to hydrocarbon trapping is usually present. Hydrocarbon accumulation in the Morrow–Springer commonly occurs with little or no structural assistance to trapping.

Stratigraphic nomenclature in the Morrow–Springer interval, especially as it applies to productive oil and gas reservoirs, is complex. As is true throughout the State, reservoirs were generally named after a landmark or the lease on which they first produced. Those listed here are from the 2004 IHS Energy listing of productive zones with cumulative gas production of at least 30 BCF. This production hurdle excludes the Kelly and Puryear sandstones in the Morrow interval, and the Flat Top, Velma, and Woods in the Springer. The major reservoirs are placed in their relative stratigraphic positions; however, no direct correlation is implied for those that are shown at the same level in different geologic provinces (Fig. 5).

Reservoir names are taken from the operators, with most completions designated simply as either Morrow or Springer,

even when the productive reservoir correlates with a named sandstone within either of the two sandstone groups. This reduces the apparent impact of some of the component reservoirs contained within the Morrow–Springer. Excepting the Cromwell, Jackfork, and Wapanucka reservoirs in the Arkoma Basin and Ouachita Mountain Uplift, major reservoirs tend to be concentrated in the western half of the State (Fig. 6).

PRODUCTION

Production data in this discussion come from the IHS Energy Group and are current through October 2004. This excellent database, like all others, is hampered by poor State records, especially from early years. The total production volume allocated to a reservoir in this database, including that listed as “Unknown,” is 77 TCF. This is 16 TCF less than State tax records indicate to be the cumulative production (Claxton, 2004). All reported volumes combine associated and non-associated gas.

Cumulative gas production for all Morrow–Springer-equivalent reservoirs is 21.4 TCF, or 28% of the total reported for the State. The Morrow alone, in addition to a cumulative recovery of 13.6 TCF in Oklahoma, making it by far the largest gas-producing reservoir name in the State, has also produced >8 TCF in the Texas Panhandle. Morrow-equivalent reservoirs in Oklahoma, including the Cromwell, Keyes, and Primrose, add 2.7 TCF to this total. Cumulative Springer production is 3.0 TCF, with an additional 2.1 TCF from its major component reservoirs—the Britt, Cunningham, and Boatwright sandstones being the most prominent (Fig. 7).

Reservoirs identified as Morrow and Springer, excluding their stratigraphic equivalents, rank first and eighth in terms of cumulative production. However, this measure of their past productive performance is eclipsed by their current production rate, in which the Morrow and Springer are ranked the top two gas producers in the State (Fig. 8). Its later development and high reservoir quality are responsible for today's high Springer production relative to other reservoirs. The Morrow, including its equivalent reservoirs, accounts for 710 MMCFPD, with major contributions coming from the Cromwell and Jackfork Sandstones. Springer-equivalent reservoirs produce 481 MMCFPD, with the largest contributions coming from the Cunningham, Britt, and Boatwright sandstones.

Major gas fields are defined as having produced at least 1 TCF. These fields, with their large number of high-rate wells and long production lives, represent every area's core production. Here, Morrow–Springer reservoirs figure prominently. There are 16 major gas fields in Oklahoma, mostly in and around the Anadarko Basin (Fig. 9). In many of these fields Morrow–Springer reservoirs account for a large proportion of the production. Those with the largest contribution from the Morrow–Springer include Watonga–Chickasha (4 TCF), Mocane–Laverne (2 TCF), Camrick (1 TCF), and Guymon–Hugoton, Putnam, Elk City, Cement,

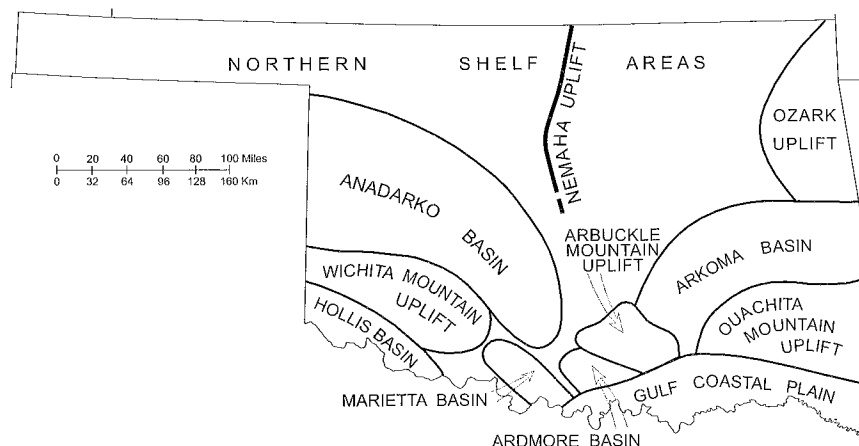


Figure 4. Map of major geologic provinces of Oklahoma.

System	Series										
Pennsylvanian	Atokan	Anadarko Basin				Ardmore Basin			Arkoma Basin		Ouachita Mountains
		Morrow Group		Morrow Formation		Dornick Hills Group		Wapanucka (Ls.)			
		Upper		Purdy				Union Valley (Ls.)			
		Lower		Keyes Primrose				Cromwell Jefferson		Jackfork	
Mississippian	Chesterian	Springer Group		Springer Fm		Springer Group		Springer Fm			
				Cunningham				Markham			
				Britt				Aldridge			
				Boatwright				Humphreys			
						Goddard Fm		Goodwin Goddard			

Figure 5. Stratigraphic chart showing positions of major (>30BCF cumulative production) producing Morrow–Springer reservoirs in Oklahoma. Modified from Andrews and others (2001) and Andrews (2003).

and Eakley-Weatherford (~0.5 TCF each) (Fig. 10). Hundreds of other fields produce from Morrow–Springer-equivalent reservoirs. These are scattered over a wide area and account for >11,000 active wells. Morrow–Springer producing wells represent nearly one-third of all producing gas wells in the State, with >3,000 within the confines of the Watonga-Chickasha and Mocane-Laverne Fields.

A great deal of Morrow–Springer drilling and gas production took place early, in a low-price environment. This was economically feasible only because of the high per-well production rates and recoveries that were attainable from these reservoirs, many of which were first identified during early oil exploration. There are 924 gas wells in Oklahoma that have produced >10 BCF, and, despite their age, >80% are still producing. These “all-stars” represent 1.5% of the State’s gas wells, but they account for 20% (15.7 TCF) of Oklahoma’s cumulative gas production. A total of 380 all-star wells produce from Morrow–Springer reservoirs, a number that is greater than the next seven reservoirs combined: Spiro, Chase, Hunton, Red Oak, Red Fork, Hoover, and Atoka, in order of importance. The fields that encompass the highest volume Morrow–Springer wells are Watonga-Chickasha (68), Camrick (31), Reydon (30), Cheyenne West (22), and Eakley-Weatherford (21).

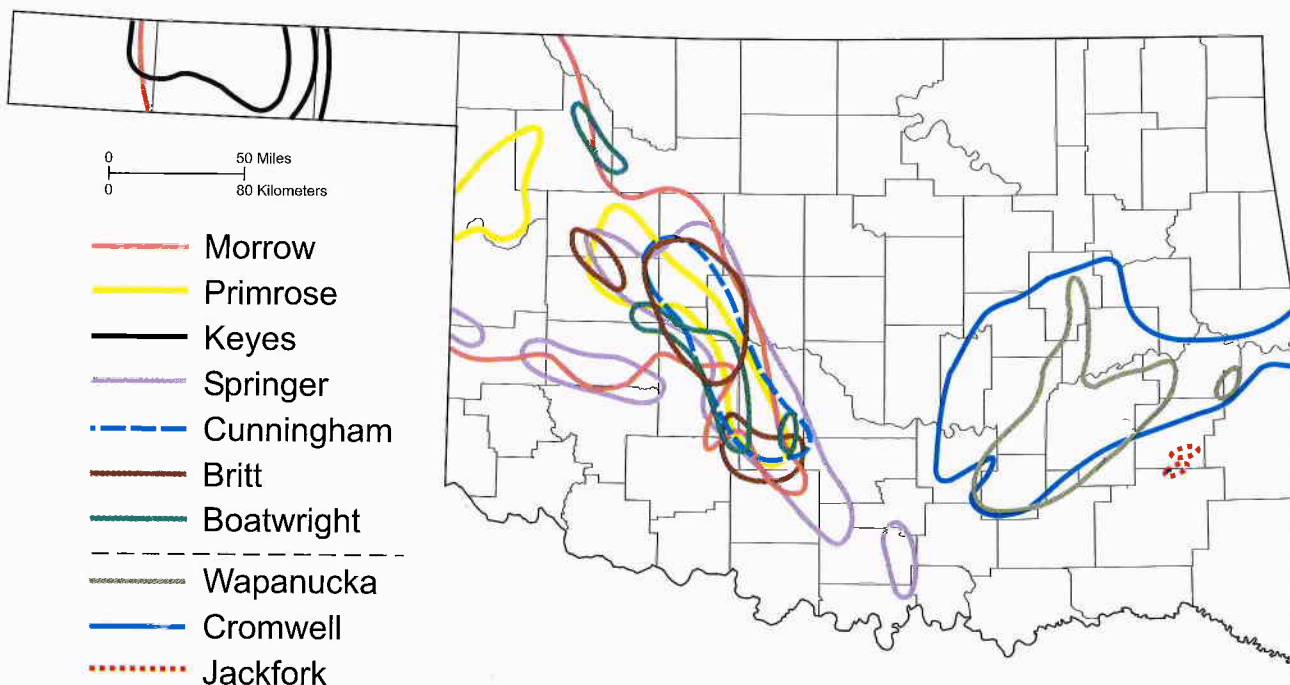


Figure 6. Map showing outlines of major Morrow and Springer gas-producing areas in Oklahoma.

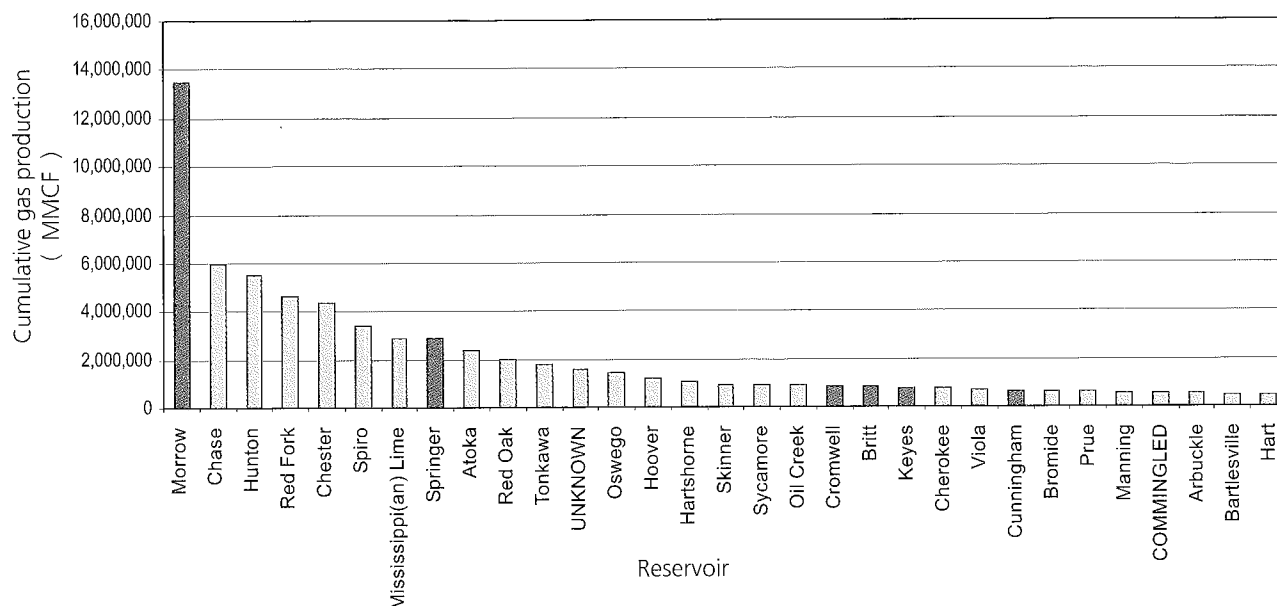


Figure 7. Graph showing Oklahoma cumulative gas production by reservoir. Data from IHS Energy (2004).

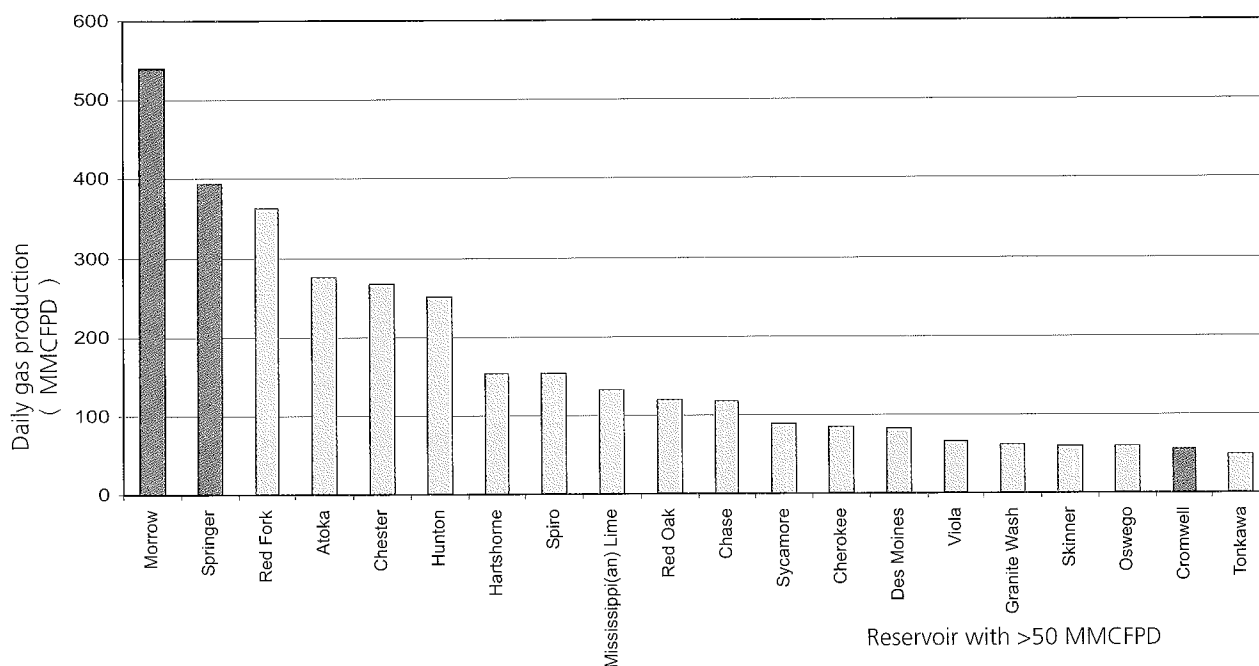


Figure 8. Graph showing Oklahoma daily gas production by reservoir (>50 MMCFPD). Data from IHS Energy (2004).

Reydon and Cheyenne West Fields are in the Anadarko Basin just west of Strong City Field. Six of the most recent 10+ BCF producers are in Potato Hills Field, 12 mi southeast of Wilburton Field (IHS Energy, 2004).

GAS PRICE AND DRILLING ACTIVITY

Natural gas was commercially produced in Oklahoma for 73 years before its value rose significantly. This price increase was the result of an unlikely chain of events when a Middle East war precipitated an oil embargo in 1973. The resulting dramatic domestic price increase of crude oil led to the dereg-

ulation of natural-gas prices and their ensuing rise. Increasing demand for natural gas brought the isolated North American market to the point at which supply (productive capacity) and demand are now roughly equal. The nation's inability to import significant quantities of liquefied natural gas (LNG) from overseas means that, in the short term, domestic U.S. production (~85%), combined with imports from Canada (~15%), must keep pace with demand. A lack of excess productive capacity is the underlying reason for the record natural-gas prices that the industry now enjoys (Boyd, 2004) (Fig. 11).

The history of gas drilling in Oklahoma, as in the rest of the country, closely matches the major ups and downs in the

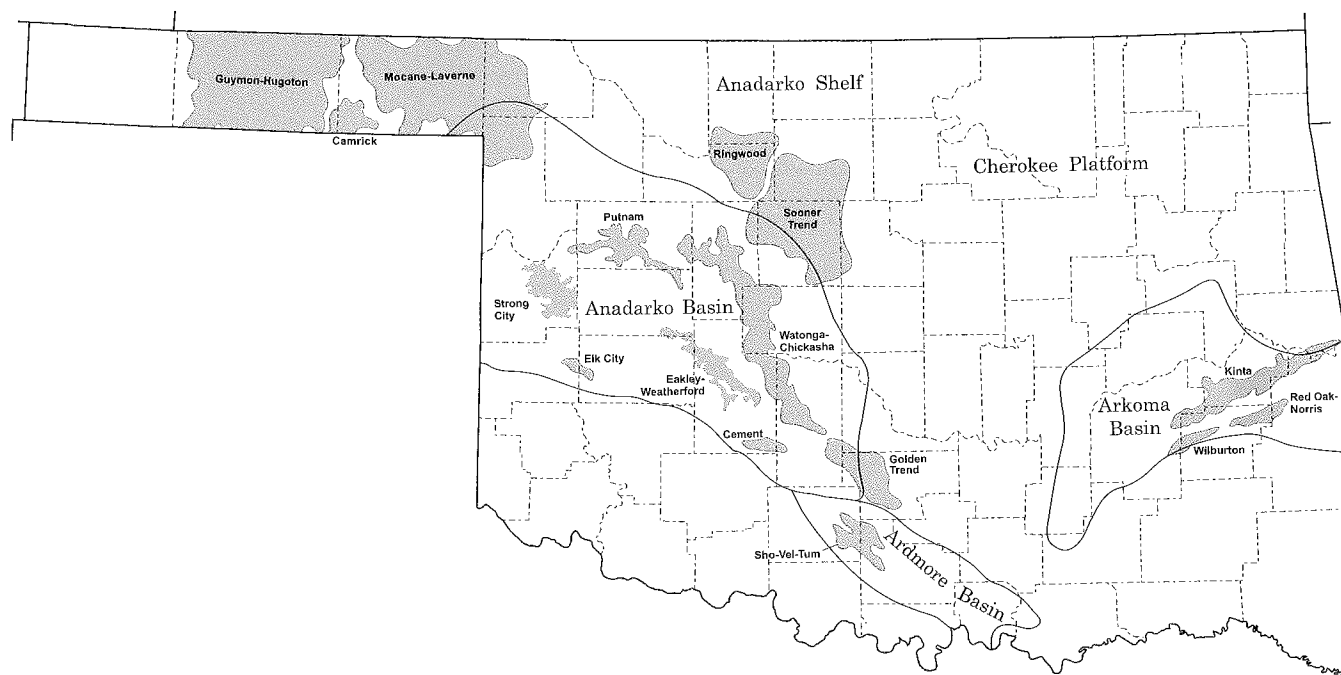


Figure 9. Map showing major Oklahoma gas fields having >1 TCF (trillion cubic feet) cumulative recovery.

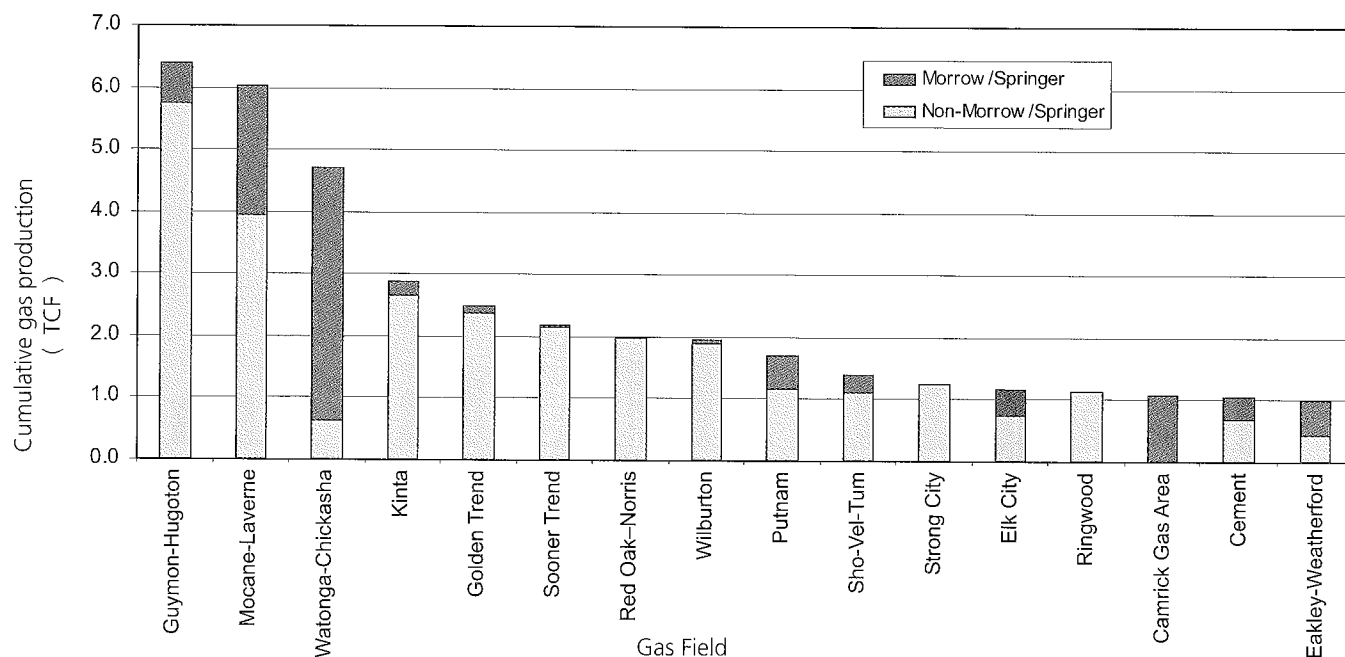


Figure 10. Graph showing cumulative gas production of major Oklahoma gas fields having >1 TCF (trillion cubic feet) cumulative recovery. Data from IHS Energy (2004).

price of natural gas. The first major increase in the price of gas began in the late 1970s and lasted through 1985. This was followed by a 10-year period of relatively low prices that ended gradually with modest improvements that began in the late 1990s. The year 2000 saw a dramatic price increase that, with the exception of 2002, has continued to rise to record levels in each succeeding year. In Oklahoma these prices have averaged almost \$4 per MCF for the last 4 years; during 2004 this average moved above \$5 per MCF (Fig. 11).

Following rising prices, gas drilling was also highlighted by a flurry of activity in the late 1970s and early 1980s. This period, better known as the "drilling boom," started when natural-gas prices began their sharp rise. The drilling boom was followed by a relative lull in activity that ended gradually through the late 1990s. Activity has accelerated since 2000, when prices began their rapid rise to the record levels of today.

The increased value of natural gas, combined with a decline in the size and number of oil discoveries, has brought the share of gas-targeted wells to about 80% of those drilled

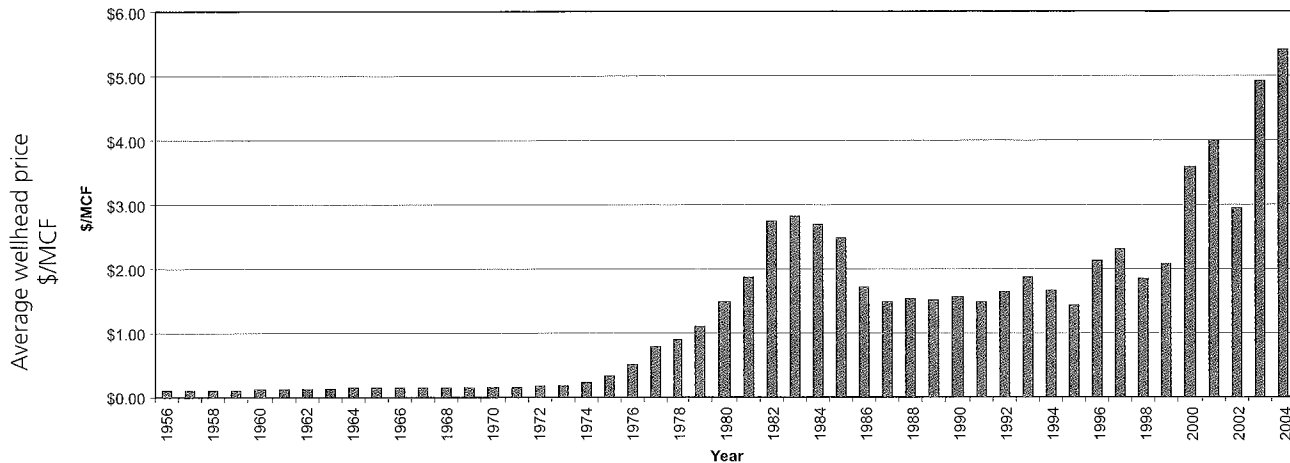


Figure 11. Graph showing average wellhead price of natural gas in Oklahoma by year (not inflation adjusted). Data from Claxton (2004).

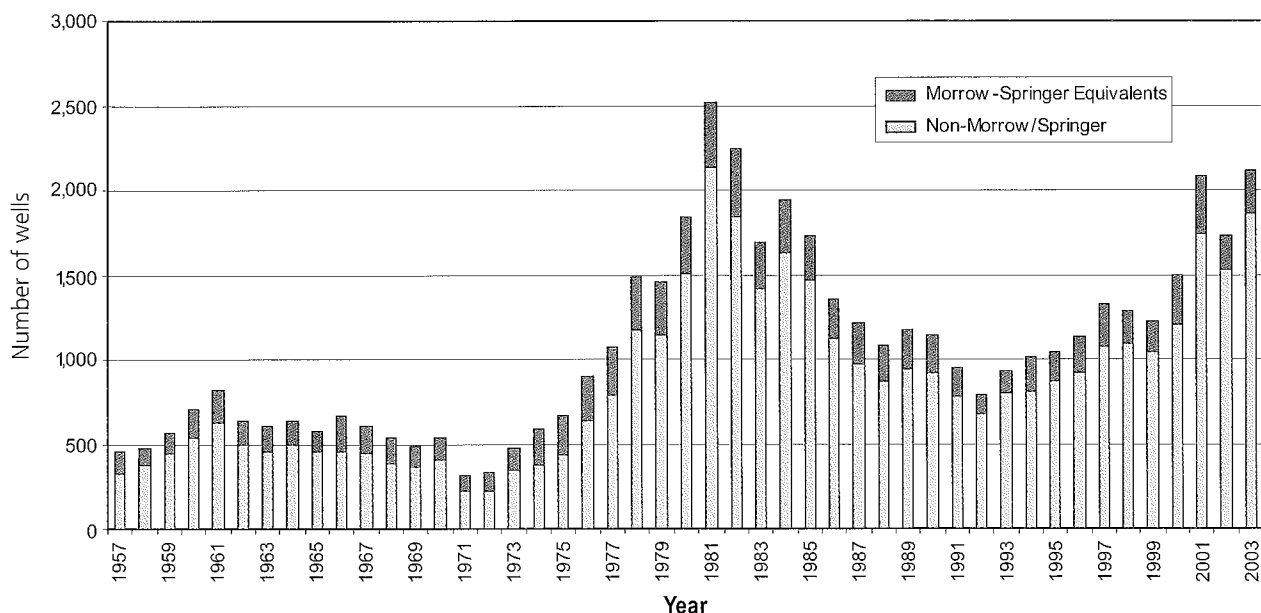


Figure 12. Graph showing annual gas-well completion history in Oklahoma (based on first production date). Data from IHS Energy (2004).

in the State. With 2004 projected to add >2,000 gas completions to the production mix, Oklahoma's gas activity is now at its highest level since 1982 (Fig. 12). The relative quality of Morrow-Springer reservoirs and their importance in the State's core production is revealed by the fact that although in any given year they represent one-eighth to one-tenth of gas completions, one-third of active wells produce from Morrow-Springer completions. The most active gas play in the State, coalbed methane, is shallow and prospective across vast areas of the eastern part of Oklahoma (Fig. 2). In spite of generally low production rates, its shallow depth, low geologic risk, and modest declines have combined to make it the State's most active gas play (IHS Energy, 2004).

Morrow-Springer gas drilling has generally followed the overall State trend, although its share in any given year varies with development activity. Years in which the Mor-

row-Springer's share of gas drilling and production surged generally mark periods when major fields, such as Watonga-Chickasha, Mocane-Laverne, Camrick, or Guymon-Hugoton, were being developed. The increase in Springer drilling that occurred immediately after 1973 is largely due to development of the Springer in Watonga-Chickasha Field. This field, which helped spur development of the Springer elsewhere, accounted for the bulk of Springer drilling through the 1970s (IHS Energy, 2004) (Fig. 13).

PRODUCTION TRENDS

Despite a continued high level of drilling activity, Oklahoma's natural-gas production continues to decline, albeit at a reduced rate. Since the peak production year of 1990, the State has lost 1,907 MMCFPD of capacity, which equates to a 2.8% average annual decline since that time (Claxton, 2004). Drill-

ing activity, much of it targeting Morrow-Springer objectives, has slowed this decline to 0.9% from 2002 to 2003, but this still represents a loss of 41 MMCFPD for the year (Fig. 14).

Like the State as a whole, Morrow-Springer gas production is much below peak levels. However, resurgent development drilling combined with contributions from new reservoirs has generated 2 years of rising production (1999-2000) and has kept Morrow-Springer production at a level comparable to 10 years ago. Some incremental production is the result of infill drilling during 1999-2001 in Mocane-Laverne, Watonga-Chickasha, and Guymon-Hugoton Fields, in which production was flat to slightly inclined. However, the largest single factor in the resurgence of the Morrow-Springer during this time was Jackfork development of Potato Hills Field. Here, production rose from nothing in 1998 to >100 MMCFPD in 2000 (Fig. 15).

Year-to-year gas production in Oklahoma has risen only twice since its peak in 1990. The last time this occurred was in 2000 and was almost entirely due to Morrow-Springer drilling, especially in Potato Hills Field. This field is the single most significant source of Oklahoma gas in many years. It has already produced >140 BCF, but it is now in steep decline, with daily production in 2004 down to its 1999 level of ~40 MMCFPD (IHS Energy, 2004). The rapid depletion of Potato Hills Field contributed to the relatively steep decline seen in overall State production in 2001 and 2002.

The only other year since 1990 in which State production has risen was 1993, which was a result of more broad-based development in several major fields. This activity included 115 additional wells in Strong City Field (mostly Red Fork), 113

wells in Mocane-Laverne Field (mostly Springer-Chester), 93 wells in Watonga-Chickasha Field (mostly Morrow), 90 wells in Kinta Field (mostly Atoka and Hartshorne), and 88 wells in Red Oak-Norris (mostly Red Oak) (IHS Energy, 2004).

Morrow-Springer drilling and production have remained strong in recent years, maintaining their central position in Oklahoma gas production. However, the decline in Potato Hills, combined with that in the major fields elsewhere, has re-established the ongoing decline in State gas production. Morrow-Springer reservoirs have certainly been stemming this tide of declining production, but thus far they have only been able to reduce the rate of long-term decline. Although recent activity has reduced Oklahoma's annual decline to one-third the long-term average, even modest percentage declines equate to large losses in a State that produces 1.6 TCF per year. This limits the impact of fields even the size of Potato Hills Field.

THE BIGGER PICTURE

Morrow-Springer gas in Oklahoma cannot be fully appreciated without an understanding of the larger State, national, and international energy issues that ultimately control it. The world's energy economy has become progressively more integrated, making it impossible to look at any area in isolation. Thus, to fully understand Morrow-Springer activity and production trends, or pricing and resultant economic projections, one must first be familiar with the larger setting in which they occur.

In Oklahoma, as in the rest of the country, the industry's capacity to increase production has been diminished by its inability to make major discoveries. The last major gas discovery in Oklahoma, the mostly Morrow-Springer Eakley-Weatherford

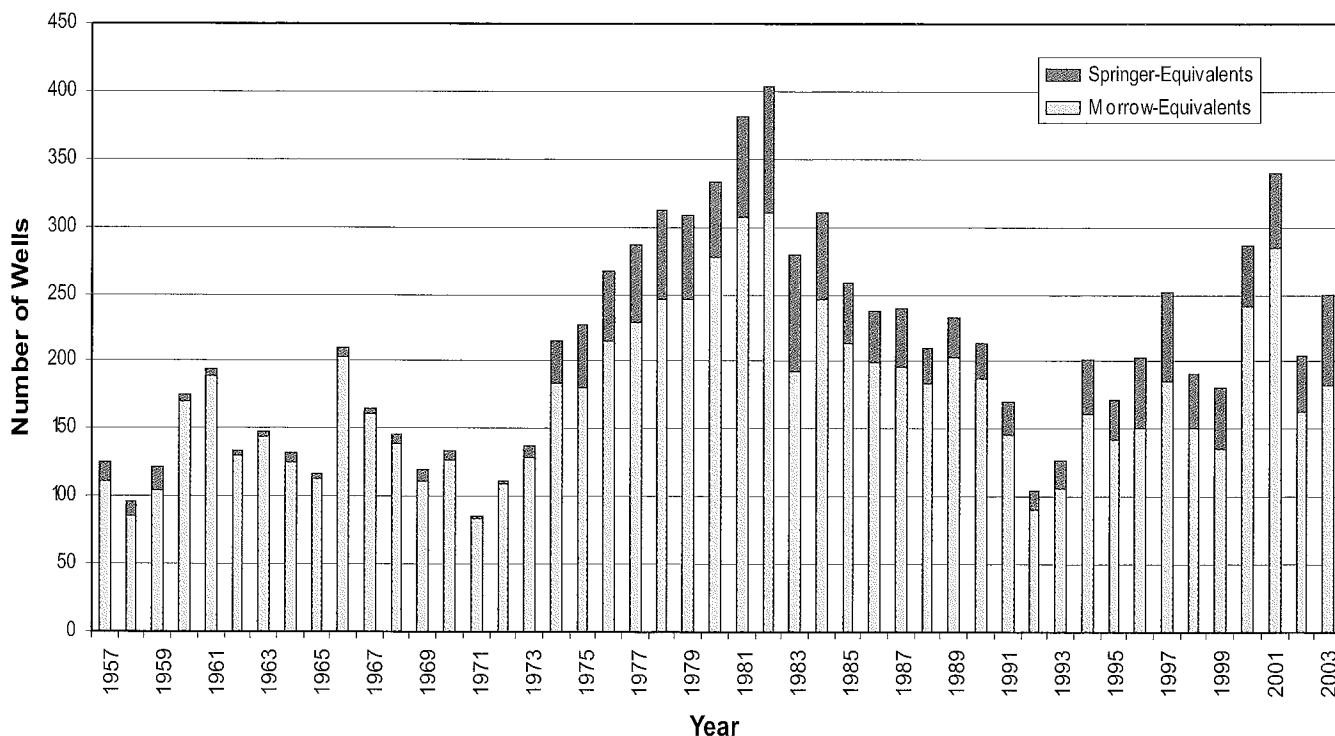


Figure 13. Graph showing annual gas-well completions for the Morrow and Springer in Oklahoma (based on first production date). Data from IHS Energy (2004).

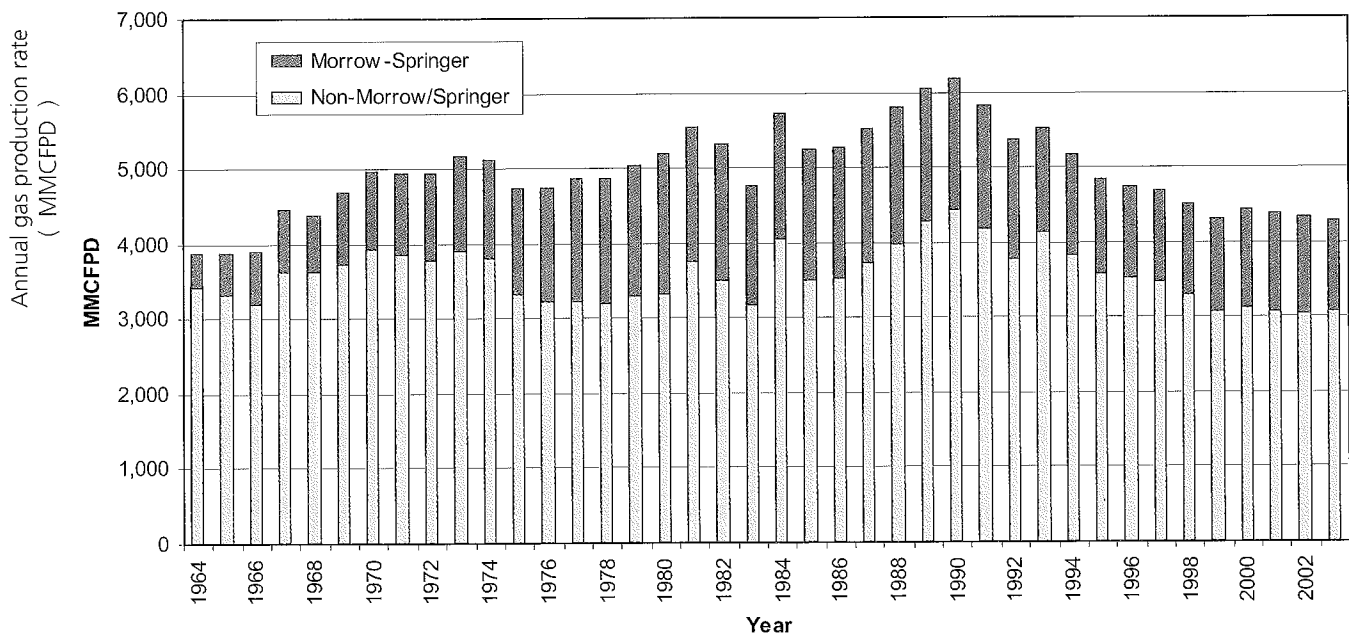


Figure 14. Graph showing annual gas production (MMCFPD = million cubic feet per day) for the Morrow and Springer in Oklahoma (includes associated gas). Data from Claxton (2004) and IHS Energy (2004).

Field, occurred in 1980 (Boyd, 2002). The scarcity of new, large discoveries is not surprising, given the fact that exploration has been active in the State for more than a century, and during that time nearly half a million wells have been drilled. However, the net effect has been to place natural gas on the same path as oil, with an ever-increasing share of its production load sustained by numerous low-rate wells. The average gas well in Oklahoma now produces ~150 MCF per day (Fig. 16).

Stemming gas-production declines today is now largely dependent on the drilling of many wells that decline rapidly.

According to the Energy Information Administration of the U.S. Department of Energy, 22% of Oklahoma's wellhead gas capacity is now being produced from wells that are <1 year old. Should drilling cease for 1 year, this would equate to the loss of 1 BCF per day of productive capacity. In the same vein, roughly 50% of the State's gas capacity is coming from wells that are <3 years old (Energy Information Administration, 2004). Oklahoma is not unique in this regard, as a similar situation exists for much of the rest of the country. However, this situation does highlight the critical importance of sustaining high levels of drilling activity to maintain oil, and especially gas, production (Fig. 17).

Given the age of the gas industry and the generally steep decline in new wells, production trends tend to match pricing trends. When prices fall, activity and production decline, and when prices rise, drilling activity follows and production declines slow or even reverse. Thus, the key to maintaining Oklahoma's natural-gas production is continuous drilling activity, and the key to maintaining drilling activity is price.

The long-term outlook for gas prices has never been better, and this can be demonstrated by a closer look at the production data presented for the Morrow-Springer (Fig. 15). The wide seasonal differences seen in Morrow-Springer gas production in the early years mirror those seen in both State and national production. Such variations are caused by the contrast between periods of maximum production

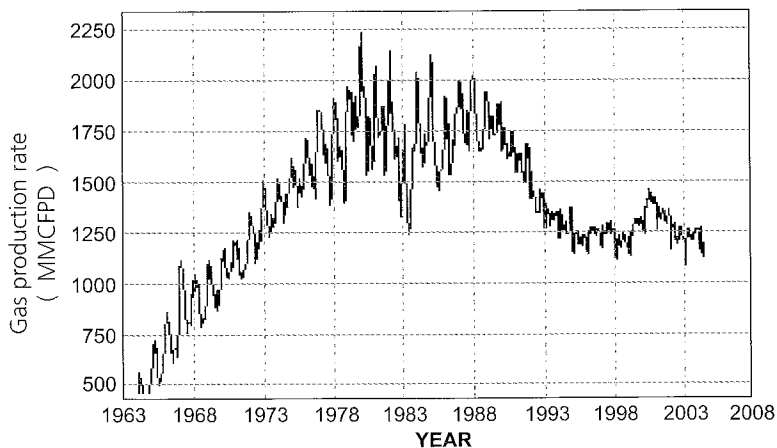


Figure 15. Graph showing average annual gas production rate in Oklahoma for Morrow-Springer (and equivalent) reservoirs. Data from IHS Energy (2004).

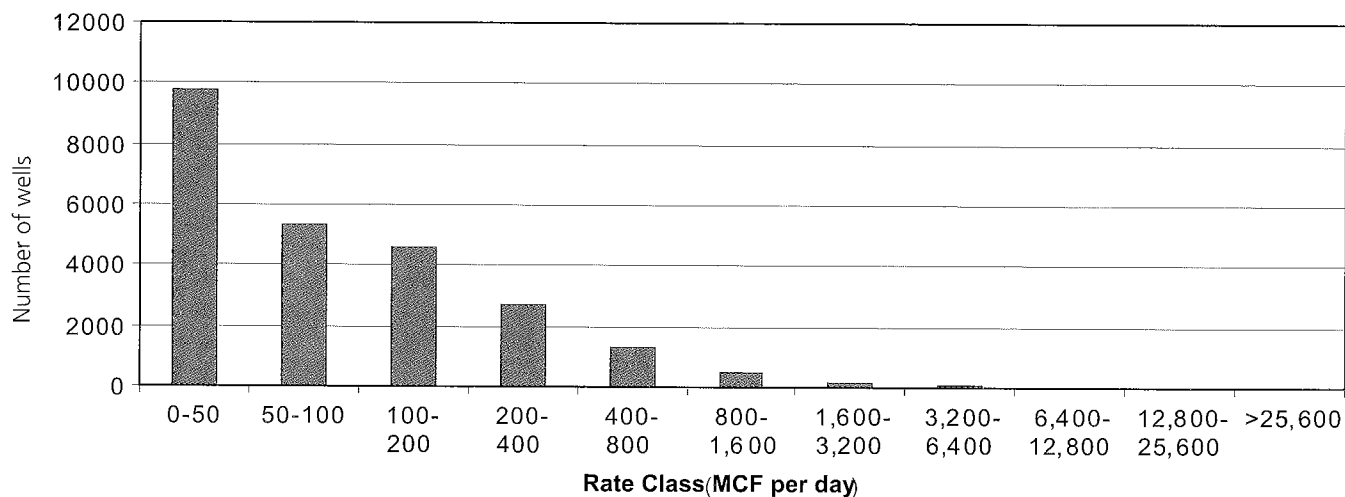


Figure 16. Graph showing Oklahoma gas-well production rates (1999). Data from Energy Information Administration (2004).

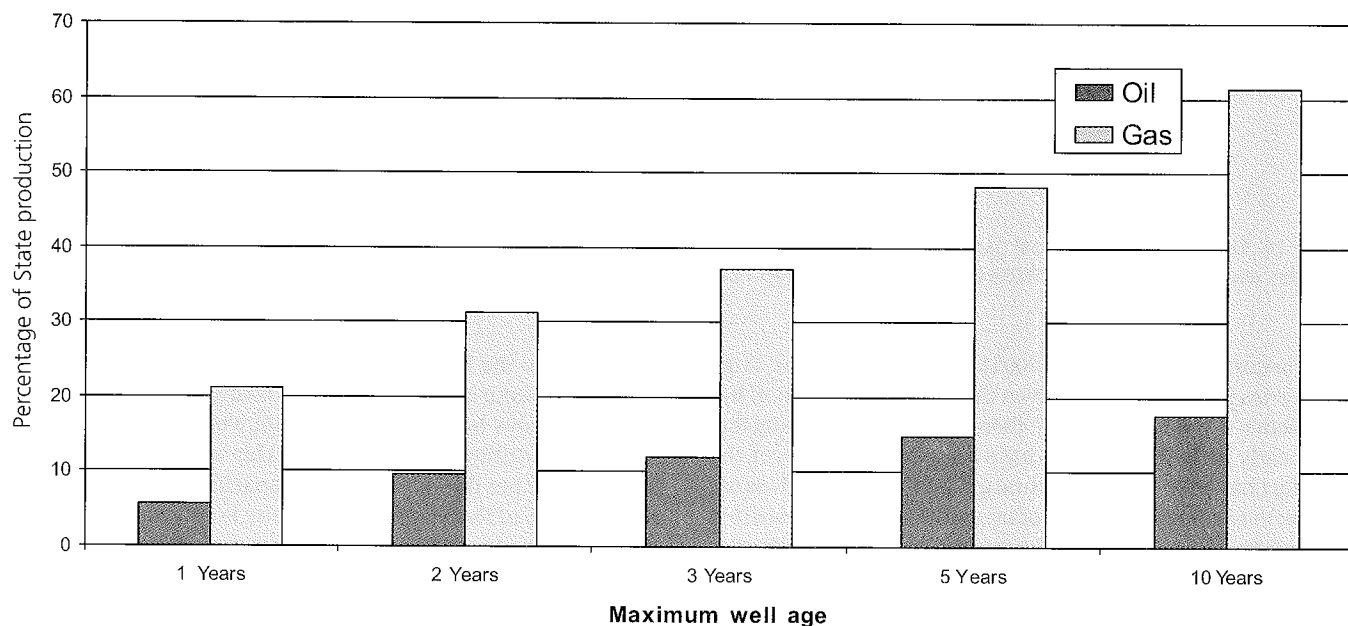


Figure 17. Graph showing proportion of oil versus gas production in Oklahoma during 2003 on the basis of well age. Data from IHS Energy (2004).

during high-demand winter months, and summers, when demand abates and production can be curtailed. (Minor monthly variations, which are apparent only in recent years, are caused by the differing numbers of days in each month. This is highlighted by the pronounced drop seen each February.)

The difference between winter- and summer-month gas production is indicative of the magnitude of excess productive capacity. Through the late 1980s, seasonal variations were gradually reduced as winter demand exceeded production. This made it necessary to store larger volumes of gas (>3 TCF nationally) to continuously meet demand. The lack of major seasonal swings since the late 1990s shows that production has been near capacity year-round for some time. This has created a widening gap between U.S. consumption and production, which in turn has forced an increasing reliance on

imports. At present, these imports come via pipeline from Canada; however, Canadian gas production is also at near capacity (Boyd, 2005) (Fig. 18).

LNG (liquified natural gas) imports from overseas will be necessary to meet long-term U.S. natural-gas demand. However, the lack of facilities to import significant quantities of LNG means that, for at least the next few years, gas supplies should stay tight and prices should remain relatively high (Boyd, 2005). It will take years to build the infrastructure necessary to open the U.S. market to the abundant gas reserves that exist overseas. However, once this is done, the price for natural gas in Oklahoma, like oil, will be tied to the international market. This is encouraging, because an outgrowth of a tightening gas market has been that, on a barrel of oil equivalency, the price of gas is now roughly equal to oil. High oil demand and an abundance of natural gas for decades have led

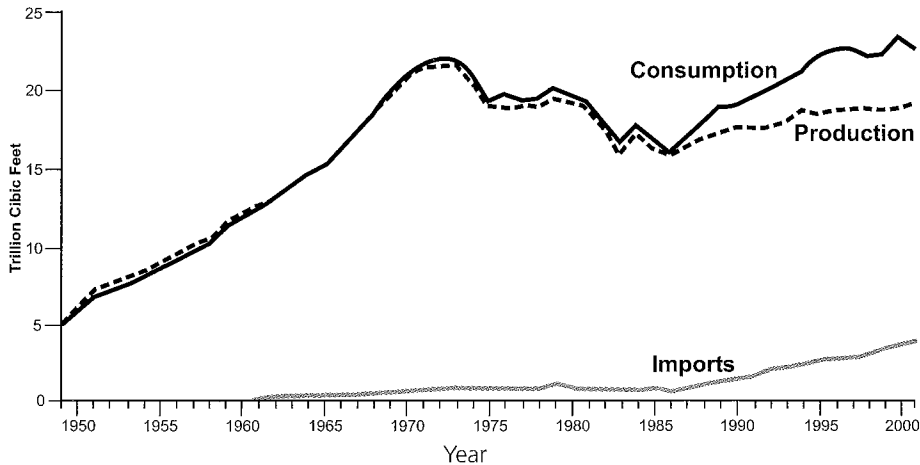


Figure 18. Graph showing annual natural-gas consumption, production, and imports in the United States during 1949–2001. Data from Energy Information Administration (2004).

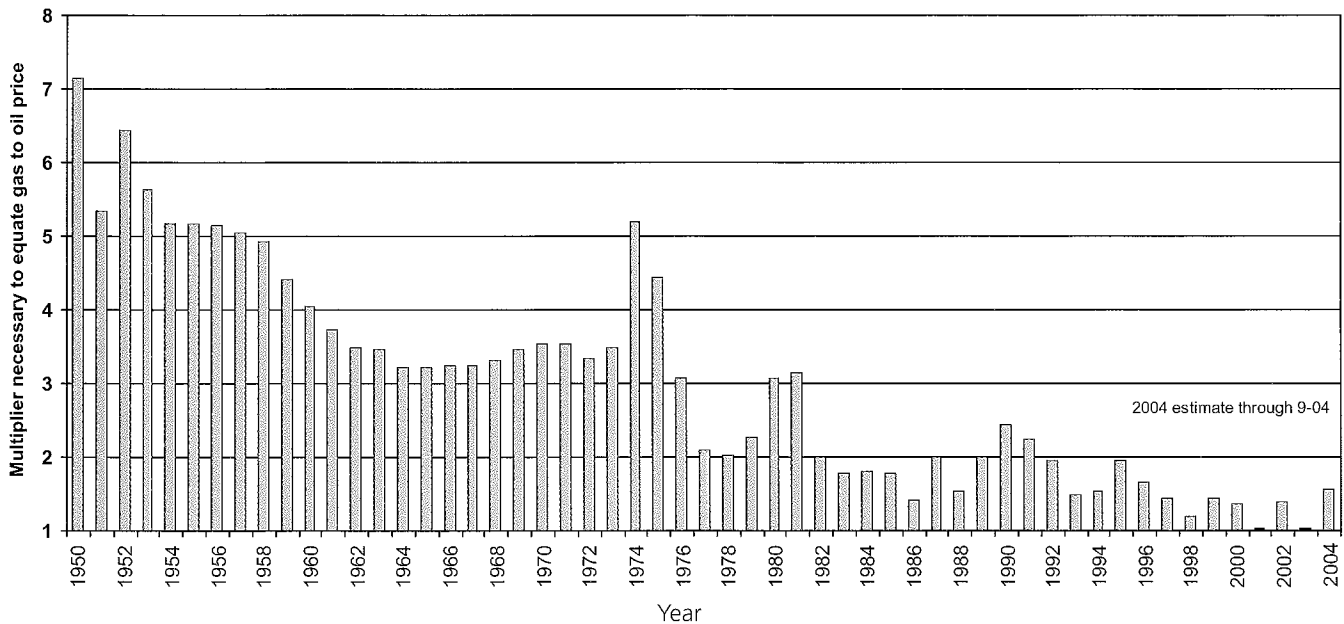


Figure 19. Graph showing average annual gas-price undervaluation relative to oil in Oklahoma. Data from Claxton, (2004).

to gas being sold for a fraction of its heating value relative to oil. Through the 1950s this oil-price premium was 5 to 7 times more, and in the late 1970s and early 1980s 2 to 3 times more, than natural gas. The rough parity of oil and gas, combined with the fact that LNG prices are designed to follow oil prices, should ensure that average gas prices in the long term should also remain strong (Fig. 19).

SUMMARY AND CONCLUSIONS

Natural gas is Oklahoma's primary energy resource, and Morrow–Springer-equivalent reservoirs will continue to be key components. These reservoirs represent 28% of the State's cumulative production and today are the most prolific producers in the State. Morrow–Springer reservoirs account for >40% of high-volume (long-lived) wells, making them the

most important component of the State's core gas production. In addition to exploratory potential, many untapped reservoirs in existing fields, as well as those that require infill drilling, are in this stratigraphic interval. Morrow–Springer development drilling in several major fields, combined with the addition of the high-rate Jackfork Sandstone reservoir in Potato Hills Field, were responsible for the last year-to-year increase in Statewide gas production.

Maintaining the State's gas production requires continued exploration, as the addition of small (<10 BCF) and occasional medium-sized (100+ BCF) discoveries is still possible. In the vast areas that are already producing, a continued effort to add new reservoirs to existing fields, especially deeper reservoirs, is needed. The Morrow–Springer is bound to account for a large proportion of both exploratory and development future successes. Continued active development of noncon-

ventional reservoirs, especially coalbed methane, will remain critical to the continued health of Oklahoma's gas industry.

High prices have vastly improved the economics of gas production. However, although the resultant rebound in drilling has reduced the rate of decline, and may even modestly increase production in the short term, the long-term production profile for Oklahoma will at best be flat. This flat production profile in the face of increasing demand is responsible for today's high prices and has made the short- to medium-term price outlook very favorable. The long-term outlook for prices, as always, is more difficult to predict. However, because LNG imports follow crude oil prices, the price for natural gas should also remain strong.

REFERENCES CITED

- Andrews, R. D., 2003, Cromwell play in southeastern Oklahoma: Oklahoma Geological Survey Special Publication 2003-2, 87 p.
- Andrews, R. D.; and others, 2001, Springer gas play in western Oklahoma: Oklahoma Geological Survey Special Publication 2001-1, 123 p.
- Boyd, D. T., 2002, Oklahoma oil and gas fields (distinguished by GOR and conventional gas vs. coalbed methane: Oklahoma Geological Survey Map GM-36, scale 1:500,000.
- 2004, Oklahoma oil, natural gas, and our place in the big picture: Oklahoma Geological Survey Information Series Publication 10, 50 p.
- 2005, Oklahoma oil and gas production: its components and long-term outlook: Oklahoma Geology Notes, v. 65, no. 1, p. 4-23.
- Claxton, Larry (ed.), 2004, Oil and gas information: Oklahoma Corporation Commission: 2003 report on crude oil and natural gas activity within the State of Oklahoma; retrieved October 2004 at: [http://www.occ.state.ok.us/Divisions/OG/Annual Reports/2004%20OIL%20AND%20GAS%20REPORT.pdf](http://www.occ.state.ok.us/Divisions/OG/Annual%20Reports/2004%20OIL%20AND%20GAS%20REPORT.pdf).
- Energy Information Administration, 2004, Natural gas productive capacity for the lower-48 states 1985-2003: Retrieved October 2004 at: http://www.eia.doe.gov/pub/oil_gas/natural_gas/analysis_publications/ngcap2003/ngcap2003.html.
- IHS Energy Group, 2006, PI/Dwights Plus southern Mid-Continent production data, Version 1.7, July 25, 2006, v. 16, no. 7, electronic edition, CD-ROM
- Johnson, K. S., 1989, Geologic evolution of the Anadarko basin, in Johnson, K. S. (ed.), Anadarko basin symposium, 1988: Oklahoma Geological Survey Circular 90, p. 3-12.
- Johnson, K. S.; and Cardott, B. J., 1992, Geologic framework and hydrocarbon source rocks of Oklahoma, in Johnson, K. S.; and Cardott, B. J. (eds.), Source rocks in the southern Midcontinent, 1990 symposium: Oklahoma Geological Survey Circular 93, p. 21-37.
- Johnson, K. S.; Northcutt, R. A.; Hinshaw, G. C.; and Hines, K. E., 2001, Geology and petroleum reservoirs in Pennsylvanian and Permian rocks of Oklahoma, in Johnson, K. S. (ed.), Pennsylvanian and Permian geology and petroleum in the southern Midcontinent, 1998 symposium: Oklahoma Geological Survey Circular 104, p. 1-19.

Iodine Production from Morrowan Sandstones, Anadarko Basin, Northwestern Oklahoma

Stanley T. Krukowski

Oklahoma Geological Survey
Norman, Oklahoma

ABSTRACT.—Iodine production in the United States comes from iodine-rich natural brines in the Anadarko Basin of northwestern Oklahoma. A 12-year program conducted by Amoco Production Company analyzed brine samples collected from subsurface units near Woodward, Oklahoma. Amoco observed high concentrations of iodine in these brines as high as 1,560 parts per million (ppm) in Chesterian (Mississippian) limestones and 700 ppm in Morrowan (basal Pennsylvanian) sandstones. Morrowan sandstones, up to 100 m thick, are preserved as channel sands in a south-trending paleovalley (the Woodward Trench) in the Chesterian surface. The Chesterian limestones do not yield large volumes of water; however, the Morrowan sandstones yield a large volume of brine whose average iodine content is ~300 ppm.

The Woodward Trench averages 1.6 km wide and ~115 km long. Brine-production and -injection wells are >2,000 m deep at the northern end of the Woodward Trench; wells in the southern end of the Woodward Trench near Vici, Oklahoma, are at least 3,000 m deep. Near Dover, Oklahoma, an oil-field-brine-injection/disposal site collects waste oil-field brines from oil and gas wells in northwestern Oklahoma. These brines are processed for iodine extraction prior to injection into wells for disposal.

INTRODUCTION

Iodine is a heavy, grayish-black crystalline solid with a metallic luster. It has a density of 4.9 g/cm³ and is a solid at ordinary temperatures. It is a member of the halogen family, along with fluorine, chlorine, bromine, and astatine. Iodine melts at 114°C, and at 184°C it will volatilize to a blue-violet gas that has an irritating odor. It is only slightly soluble in water. Its solubility increases with temperature. At low temperatures, iodine is made up of diatomic molecules and readily dissociates, or sublimates, at moderately elevated temperatures.

Iodine does not occur as an element in nature but as iodates, iodides, or other combined forms. It is the 47th most abundant element in the earth's crust. Iodine was discovered by Bernard Courtois in 1811. He observed an unknown substance in the crude soda ash that resulted from the burning of seaweed. Samples of this unknown substance were identified to be a new element, and in 1813 Gay-Lussac named the substance *iode* in French, from the Greek word *ioeides*, meaning violet-colored.

Most people know iodine is a dietary supplement in iodized table salt used to prevent goiter. It also is remembered for its use as an antiseptic and disinfectant (tincture of iodine) found in first-aid kits and most medicine cabinets. The uses of iodine are much more diverse: it is used in animal feed, photography, catalysts, and other applications.

GEOLOGY

Compounds of iodine are minor constituents in seawater and brines, in certain marine organisms, and in minerals of

the Chilean nitrate deposits. Seawater contains ~0.05 ppm iodine, and certain marine organisms, such as seaweed, sponges, fish, and some brown algae, are able to further concentrate iodine (Lyday, 1999). Some seaweed can extract and accumulate iodine up to 0.45% of its dry weight. The northern Chilean nitrate deposits in the Atacama Desert, contain iodine minerals: lautarite, Ca(IO₃)₂ (calcium iodate); dietzeite, Ca₂(IO₃)₂·(CrO₄) (calcium iodate-chromate); and bruggenite, Ca(IO₃)₂·H₂O (Erickson, 1981).

Various subsurface brines also contain iodine compounds. Some gas-field brines in the United States and Japan may contain 30 to 1,300 ppm iodine. Several coals in Germany also contain iodine compounds. Iodine has been recovered from brines mainly in Japan and the United States but also in Java, Indonesia, Italy, England, and the former USSR.

Subsurface Brines

About 45% of the iodine currently consumed in the world comes from brines processed in Japan, the United States, the Commonwealth of Independent States (CIS; the former Soviet Union), and Indonesia (Lauterbach and others, 2001). The remainder (55%) is produced from desert evaporite deposits in Chile. In Japan, iodine is produced from brines associated with natural-gas wells. The iodine content of Japanese subterranean brines ranges up to 150–160 ppm. In Oklahoma, iodine content in older iodine-producing rock formations (Mississippian–Pennsylvanian) may range up to 1,500 ppm, but typically the iodine content of produced brines is ~300 ppm. Iodine production in the CIS is associated with oil recovery, principally in Turkmenistan, Azerbaijan, and Russia,

which account for 97% of CIS production (Lauterbach and others, 2001; Lyday, 2004a). Uzbekistan also produces minor amounts of iodine. Table 1 shows iodine production by country and the corresponding known reserves.

In Indonesia, iodine is present with trace amounts of bromine in oil-field brines in Pliocene sandstones and diatomaceous marls in the Gujangan Anticline (Lyday, 1985); however, Indonesian iodine typically comes from brines not associated with oil and gas deposits (Lauterbach and others, 2001).

All iodine production in the United States now comes from iodine-rich (300 ppm iodine) natural brines in the deep subsurface of the Anadarko Basin of northwestern Oklahoma (Fig. 1). Oklahoma's first iodine operation, the Woodward Iodine Corporation, opened early in 1977. The discovery of iodine-rich brines at Woodward resulted from a 12-year program of analyzing brine samples collected by Amoco Production Company (Cotten, 1978). Amoco noted unusually high concentrations of iodine in the Woodward area as high as 1,560 ppm in Chesterian (Mississippian) limestones and 700 ppm in Morrowan (basal Pennsylvanian) sandstones. Morrowan sandstones in the area are as thick as 100 m and are preserved as channel sands in a south-trending paleovalley (the Woodward Trench) cut into the Chesterian surface (Fig. 2). Although iodine concentrations are higher in the Chesterian strata, the Chesterian limestones have low permeability and do not yield large volumes of water. On the other hand,

TABLE 1.—Crude Iodine: World Production and Reserves (thousand kilograms)

Country	Mine Production		Reserves
	2003	2004 ^a	
Azerbaijan	300	300	170,000
Chile	11,650	16,200	9,000,000
China	500	500	4,000
Indonesia	75	75	100,000
Japan	6,500	6,500	4,900,000
Russia	300	300	120,000
Turkmenistan	300	300	170,000
United States	1,750	1,340	250,000
Uzbekistan	2	2	NA
World Total ^b (rounded)	21,400	25,500	15,000,000

^aEstimated.

^bExcludes other countries.

Source: Lyday (2005).

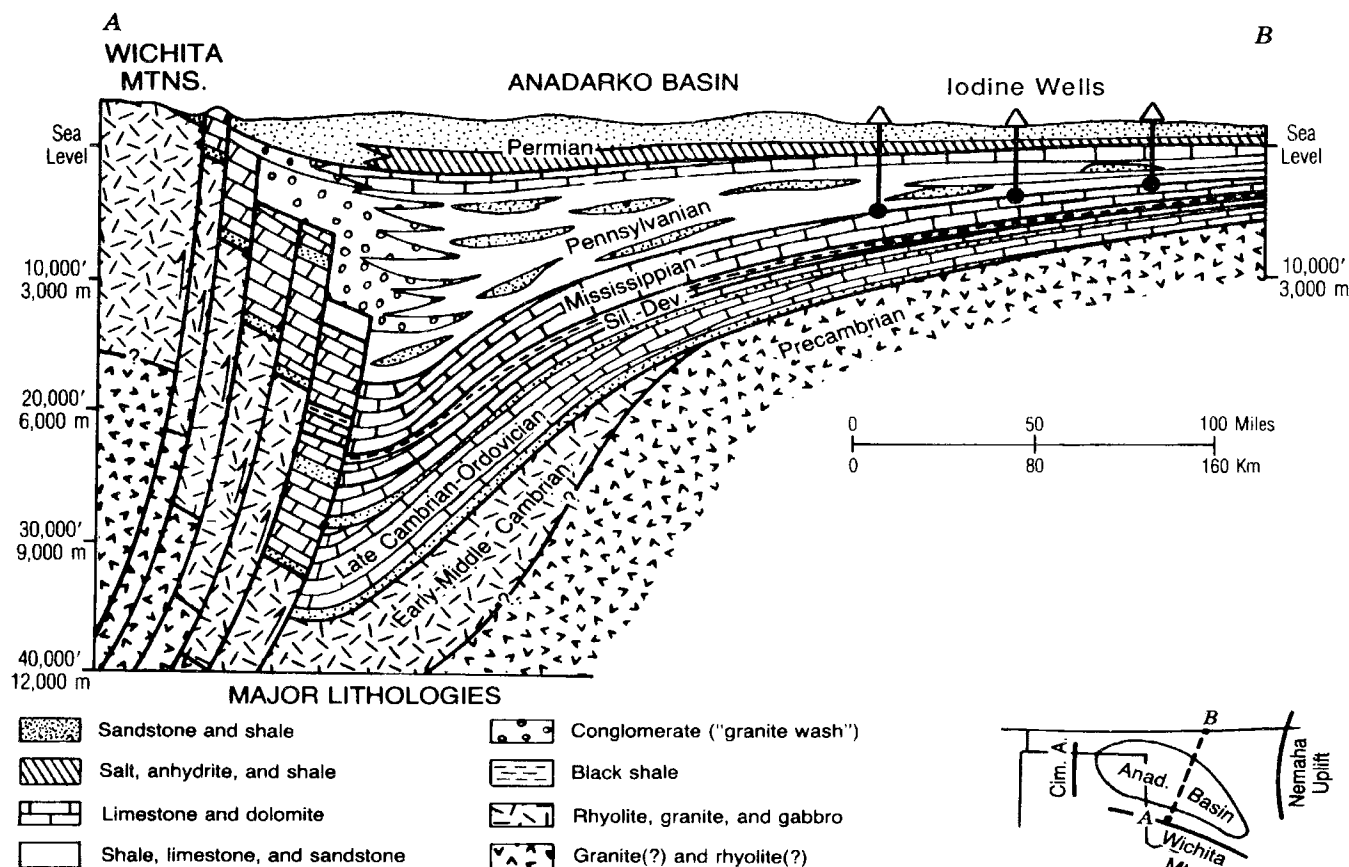


Figure 1. Generalized south-north structural cross section through the Anadarko Basin of western Oklahoma (modified from Johnson, 1989). Iodine-rich brines are produced from basal Pennsylvanian sandstones on the north flank of the basin.

Morrowan sandstones here have higher porosity (~14%) and higher permeability of ~20–40 millidarcies (md), and yield large volumes of brine averaging ~300 ppm iodine. Production wells yield 5,000–10,000 barrels (200,000–400,000 gal) of brine per day (Johnson and Gerber, 1999).

The Woodward Trench has an average width of 1.6 km and a known length of ~115 km (Cotten, 1978). Brine-production wells and injection wells are 2,130 to 2,290 m deep toward the northern end of the Woodward Trench. Extraction of iodine-rich brines from Morrowan sandstones in a southern extension of the Woodward Trench near Vici, Oklahoma, occurs at depths of 3,000 to 3,183 m. A miniplant near Dover, Oklahoma, serves as an oil-field-brine-injection/disposal site, collecting waste oil-field brines from a number of producing oil and gas wells in nearby parts of northwestern Oklahoma. Johnson and Gerber (1999) reported that these oil-field brines contain concentrations of iodine in the range 100–1,000 ppm. The oil-field brines are processed in the miniplant, where iodine is extracted before the brines are injected into wells at the site for disposal.

For many years the origin of iodine-rich brines associated with sedimentary rocks of the northern flank of the Anadarko Basin has provided a challenge for oil-field scientists. The high concentration of iodine in the Chester limestone (Mississippian) led to speculation that its source was the limestone. Moran's (1996) work with iodine isotope ratios indicated that the organic-rich Woodford Shale (Upper Devonian–Lower Mississippian) was the probable source rock for the high concentrations of iodine. The iodine-rich brines probably migrated from the Woodford Shale into several brine reservoirs in northwestern Oklahoma (Johnson and Gerber, 1999).

PRODUCTION AND TRADE

The major iodine-producing nations, in descending order, are Chile, Japan, and the United States, with lesser amounts being produced in China, Azerbaijan, Russia, Turkmenistan, Indonesia, and Uzbekistan (Fig. 3; Table 1). Annual world production in 2002, 2003, and 2004 was, respectively, 20.7 million kg, 21.4 million kg, and an estimated 25.5 million kg, of which about 32% is consumed in the United States (Lyday, 2003, 2004a, 2005).

Iodine was first produced in the United States between 1917 and 1921, from seaweed harvested in California; after distillation to produce acetic acid, the residue was processed for potash fertilizers and iodine (Lyday, 1986). The first U.S. commercial production of iodine from brines was in Louisiana between 1928 and 1932; some of the Louisiana oil-field brines contained ~35 ppm iodine (Lyday, 1986). Oil-field brines in parts of California contain 30–70 ppm iodine (Fig. 4) in the Monterey Formation (Miocene) and Repetto Formation (Pliocene); production from these units occurred at various times between 1928 and 1966. In Michigan, natural brines containing 15–30 ppm iodine are present in the Sylvania Formation (Devonian) at a depth of ~1,300 m. The Michigan brines were processed mainly for bromine, and byproduct iodine, by Dow Chemical Company until the wells were plugged and abandoned in 1987.

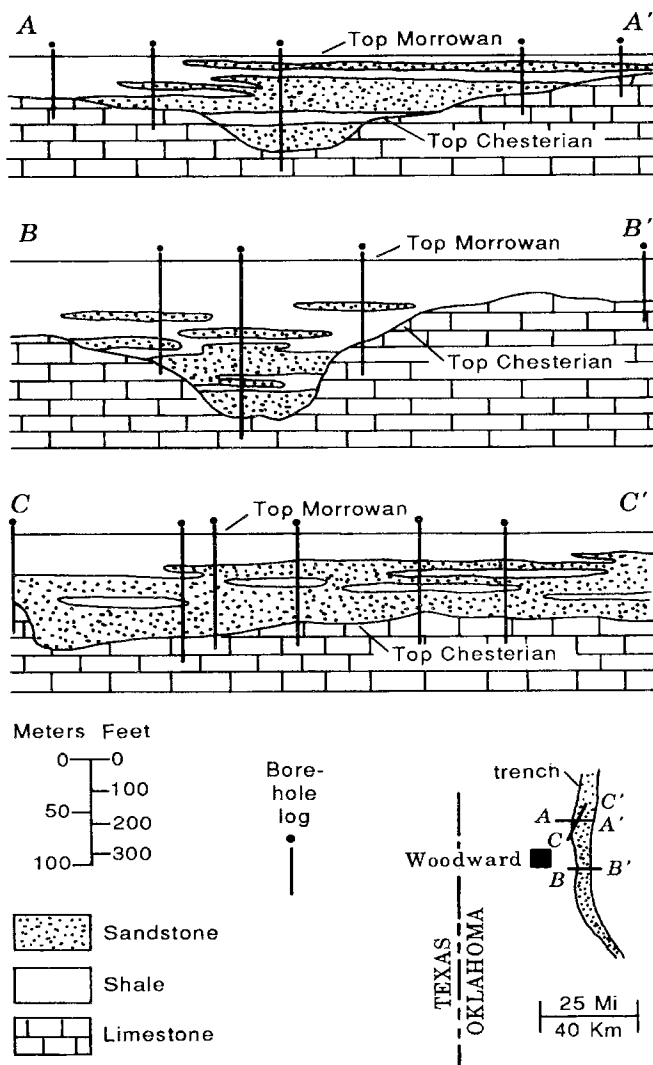


Figure 2. Cross sections showing iodine-bearing Morrowan channel sandstones preserved in the Woodward Trench that has been cut into Chesterian limestones (modified from Cotten, 1978; Johnson, 1989). Datum is top of Morrowan strata. Length of A–A' and B–B' is ~10 km; length of C–C' is ~15 km.

Today U.S. production comes from iodine-rich (300 ppm iodine) natural brines on the north flank of the Anadarko Basin in northwestern Oklahoma (Fig. 1). In Oklahoma, three companies operate two major plants and one miniplant for the recovery of iodine. The total production from the three companies in 2002 was 1.42 million kg; and production in 2003 was estimated to be 1.75 million kg, with an estimated value of \$19.7 million (Table 1). Woodward Iodine Corporation began operating early in 1977 as a joint venture between Amoco Production Company and Houston Chemicals, a subsidiary of Pittsburgh Plate Glass Industries (Cotten, 1978); in 1984 the company was purchased by Asahi Glass Company of Japan (Lyday, 1986), and then sold in 1994 to Ise Chemical Industries Company, Ltd., of Japan (U.S. Geological Survey, 1998; Johnson and Gerber, 1999). Woodward Iodine Corporation operates 12 production wells in the Woodward Trench,



Figure 3. Map showing countries that produce iodine, with estimated production given in kilograms (kg) during 2004.

just north of Woodward, and injects the waste brine back into the trench through four injection wells; three additional wells are operated as disposal wells. Brine-production and -injection wells are 2,130 to 2,290 m deep.

A second iodine plant near Vici in Oklahoma was started in late 1987 by Iochem Corporation of Japan. It also extracts iodine-rich brines in a southern extension of the Woodward Trench, operating nine production wells and four injection wells at depths of 3,000 to 3,183 m.

North American Brine Resources (NABR) operates the remaining iodine installation in Oklahoma at a miniplant near Dover, where oil-field brines, collected from many producing oil and gas wells of northwestern Oklahoma, are processed. The company also had a major operation in the Woodward Trench ~35 km north of Woodward, which included two production wells and three injection wells at a depth of ~1,800 m; this facility began operations in 1989 and recently was dismantled (Krukowski, 2005). NABR began in 1989 as a joint venture of Beard Oil Company (40% share) and two Japanese firms (Godoe USA, Inc., 50% share, and Inorgchem Development, Inc., 10% share) (Ohl and Arndt, 1988). In 2003, NABR, as a joint venture between Mitsui & Company of Japan and Beard Oil Company, was sold to a group of U.S. private investors and is now operated as a limited liability company (Krukowski, 2004).

TECHNOLOGY

Exploration Techniques

Iodine production has historically been a consequence of either oil and natural-gas production or nitrate-fertilizer processing. The commercial extraction of iodine from seaweed was practiced from 1811 to 1959; however, seaweed is no longer an economical option. Cotten (1978) and Johnson and Gerber (1999) describe how Amoco Production Compa-

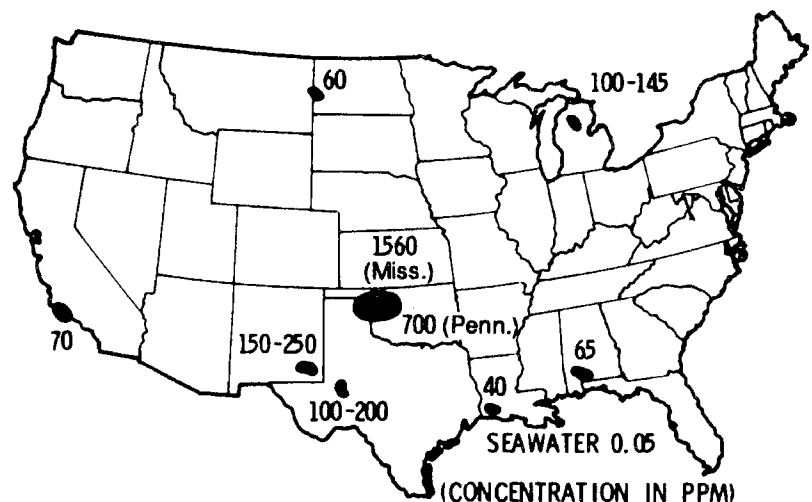


Figure 4. Map showing areas of known iodine concentrations in the United States (from Cotten, 1978). Exceptionally high iodine concentrations in northwestern Oklahoma are in Mississippian (Miss.) and Pennsylvanian (Penn.) strata.

ny approached the prospect of producing iodine from brines associated with oil and natural-gas exploration drill holes in the Woodward Trench of northwestern Oklahoma. Reports on the chemistry of subsurface water samples from these exploratory wells showed that a variety of potentially economic minerals was present. Feasibility studies indicated that iodine was the most favorable mineral for development, based on the fact that its concentrations were relatively high and that the United States was almost entirely dependent on foreign imports for its supplies.

Scientists at the Amoco Research Center determined that 60,000 barrels per day of 300 ppm iodine-rich brine had to be produced over a 10-year period to be an economically viable project. Additional holes on 640-acre centers were drilled into the Morrow Formation (Pennsylvanian) in the trench, and their electric logs examined to determine the thickness of water-bearing sands with porosities >10%. These criteria helped determine the concentration (grade) of iodine and the amount (reserves) of resources present. A joint venture by Pittsburgh Plate Glass Industries and Amoco Production Company brought the necessary expertise together to form the Woodward Iodine Corporation in 1977.

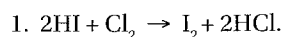
Iodine geochemical data obtained from surface soil samples are used as an exploration tool in the petroleum industry (Tedesco, 1994; Tedesco and Goudge, 1994; Tedesco and Andrew, 1995; Leaver and Thomasson, 2002). Positive anomalies of trace iodine geochemistry have been used as an indirect indicator of hydrocarbon accumulation in the subsurface. Perhaps future study of this phenomenon will lead to new exploration techniques in the search for subterranean iodine-rich brines.

Mining

Iodine is produced from underground brines pumped to the surface, using electric submersible pumps. Through a system of pipelines the brine is transported to the processing facility. Natural gas is either flared off or extracted from the brines in a gas separator in which the natural gas is physically separated from the brine. The brine is collected in storage tanks before entering the processing plant for iodine extraction. Corrosion-resistant pipe and storage tanks are necessary to contain fluids and vapors during transport and storage; in addition, calcium-scale inhibitors are introduced to prevent calcium carbonate-scale buildup on exposed metallic surfaces (W. W. Hamon, Jr., Vice President, Iochem Corporation, written communication, 2002).

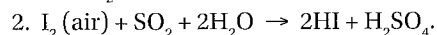
Production Process

The blow-out process (also known as the air-stripping process) is the principal method for extracting iodine from brines. Initially the brine undergoes skimming and settling which removes impurities such as oil, clay, and other undesirable materials. Chlorine is then injected into the brine, which causes oxidation:

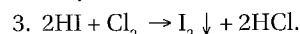


The I_2 remains in solution and is extracted from the brine with a counter-current air blow-out process where free iodine is stripped from solution as it is exposed to large volumes of air (Johnson and Gerber, 1999; Lauterbach and others, 2001).

The iodine-depleted brine is discarded (or injected) into wells, returning the brine to the original underground formation. This also serves to maintain fluid pressures in the reservoir and helps to prevent subsidence. The iodine-rich air leaves the stripping column and enters an absorption column where the vapor is submitted to a co-current desorption process. A reducing environment is maintained by adding sulfur dioxide (SO_2) and water. The iodine is reduced to iodide:



This hydriodic- and sulfuric-acid solution is maintained in an interim-storage vessel. When chlorine gas is injected into this hydriodic-acid solution, it undergoes oxidation and iodine crystallization:



The oxidized crystallizer liquor is a mixture of water, sulfuric acid, hydrochloric acid, and iodine crystals (Johnson and Gerber, 1999).

The next step separates the iodine crystals from this liquor. This is accomplished through batch filtration, followed by vacuum drying of the filter cake. Wet iodine filter cake is transferred to a fusion kettle. Sulfuric acid, coming into contact with the melted product, helps in controlling humidity (drying) and removes impurities. The final step converts the fused iodine into a flaked or prilled product; and then it is packed for shipping (Johnson and Gerber, 1999; Lauterbach and others, 2001).

MARKETING

Uses

Iodine products were first used commercially in the early 20th century as a remedy for goiter, as a disinfectant for cuts and abrasions, and for sanitation (Lyday, 1999). Since then, iodine has been used in a variety of specialty chemicals for many commercial applications. Major uses include X-ray contrast media, iodophors and biocides, catalysts, stabilizers, animal feeds, disinfectants, pharmaceuticals, photography, and colorants. It is difficult to report the end use of iodine accurately, because iodine-containing intermediates are marketed before being used in their ultimate form. Table 2 shows the U.S. consumption (by principal end use during 2002). The following description of uses is from Lyday (1999, 2002), Lauterbach and others (2001), and Harben (2002).

X-Ray Contrast Media

Iodine absorbs X-rays, so it is included in a class of drugs called radiopaques—that is, drugs used in the diagnoses of medical problems by media contrast. Radiopaques containing iodine are introduced into the body in anatomical areas that have insufficient natural contrast. The iodine absorbs the X-rays to a greater extent than do natural soft tissues or blood, thereby casting a light shadow on X-ray film and thus

TABLE 2.—U.S. Consumption (apparent^a) of Iodine in 2002

Use	Thousand kg	% of total
Sanitation	2,934	45
Animal Feeds	1,760	27
Pharmaceuticals	652	10
Catalysts	522	8
Stabilizers	326	5
Other ^b	326	5
Total	6,520	100

^a Domestic production plus imports minus exports plus adjustments for government and domestic industry stock changes.

^b Includes inks and colorants, photographic chemicals, laboratory reagents, production of batteries, high-purity metals, motor fuels, and lubricants.

Source: Lyday (2002).

enhancing the contrast. The main X-ray procedures using iodine-contrast media diagnostically are angiography, CT scans, gastrointestinal series, and colicography.

As populations of industrialized nations age, the need grows for diagnostic testing to keep patients healthier longer and to reduce hospitalization costs (Lyday, 2002). Increasing medical testing of older populations with X-ray contrast media will result in additional iodine consumption in radiopaque drugs.

Iodophors and Biocides

An iodophor is an iodine complex weakly bound to a carrier molecule, or surfactant that increases iodine solubility in water, permitting its gradual release and giving a residual effect to the compound (Lauterbach and others, 2001). The germicidal action of iodine is a result of its ability to quickly penetrate the cell walls of microorganisms, rupturing their proteins and nucleic acid. For that reason, iodophors and iodine-based biocides are used for their disinfectant and antiseptic properties in sanitation and cleansing applications in hospitals, dairies, laboratories, food-processing plants, dish-washing detergents, food processing, restaurants, herbicides, swimming pools, and water supplies. In some instances, toxic biocides (for example, pentachlorophenol, PCP; and tributyltin oxide, TBTO) have been replaced with iodine-based alternatives in certain preservative applications, including cosmetics, paints, wood preservation, metalworking fluids, leather processing, inks, and starches (Lauterbach and others, 2001).

Catalysts

Monsanto developed the process for producing acetic acid (using an iodide-promoted rhodium complex as catalyst) in the 1960s and ~90% of new acetic-acid production capacity uses this process. Acetic acid is used as a solvent in the

production of terephthalic acid, a major component of polyethylene terephthalate, a plastic used for soft-drink containers. Iodide catalysts also are used in the dehydrogenation of butane and butene to butadiene, and in the preparation of stereoregular polymers.

Stabilizers

Iodine is used as a stabilizer in the manufacture of nylon for tire cord and carpets, and for converting rosins, tall oil, and other wood products to more stable forms.

Animal Feeds

About 27% of U.S. domestic consumption of iodine is used as additives for animal feed (Lyday, 2002). Cattle and sheep are fed iodized salt and other iodine compounds to regulate metabolism and to reduce certain livestock ailments such as soft-tissue lumpy jaw and goiter. Iodine supplements are especially important for breeding cows and calves, because an iodine deficiency during pregnancy and lactation increases risk of weakness or stillbirths in cattle, pigs, and horses.

Photography

Almost all photography is based on the light-sensitive character of silver halides, particularly silver iodide and silver bromide. Up to 7% of the silver salt in emulsions for negatives is iodide and ammonium iodide is used as a photographic developer. See Harben (2002) for more details on photographic emulsions.

Pharmaceuticals and Human Health

Potassium iodide (KI) is widely used as an expectorant in cough medicine and iodine compounds are used in the synthesis of amphetamine, methamphetamine, ethyl amphetamine, antibiotics, corticosteroids, and other drugs. KI also is used to prevent thyroid cancer. It is recommended by the U.S. Food and Drug Administration as a safe and effective means of blocking radioiodines by the thyroid in a radiation emergency such as a nuclear accident. During nuclear accidents a portion of the radioactivity is released as ¹³¹I, a major radioisotope of nuclear power plants.

Iodine is necessary for healthy human life. The thyroid gland requires iodine to produce the hormone thyroxine. Iodine Deficiency Disorder, or IDD, occurs when people lack iodine in their diets. It is especially serious for pregnant women and young children. Deficiencies may result in retarded fetal development, and physical and mental retardation (cretinism being an extreme condition). IDD also may lead to goiter (enlargement of the thyroid gland, manifested in a swelling of the neck), abnormal physical development, and reproductive loss (Lauterbach and others, 2001). IDD has been eliminated effectively in the industrialized nations by adding potassium iodide or potassium iodate to table salt and vitamin supplements.

Colorants

Iodine is a coloring agent in some dyes used in foods and on materials. Red food coloring has been used in cherries,

candies, carbonated soft drinks, powdered drinks, gelatin desserts, icings, and pet foods, as well as in dyeing and/or printing cotton, half-silk, jute, and straw products. It is also used as a coloring agent in drugs, cosmetics, printer inks, and photographic sensitizers.

Other Uses

Iodine is used as an intermediate in the synthesis of fluorochemicals used in water- and oil-repellent emulsions in textiles and leather, and in fire-extinguishing foams. Iodine also is used in the modification of selenium to make semiconductors; the manufacture of high-purity metals, such as titanium, zirconium, boron, and hafnium; the production of motor fuels; additives in rechargeable dry cells; smog inhibitors; and cloud seeders to induce rainfall.

Product Grades and Specifications

Iodine and its compounds are generally marketed in the form of crude iodine, resublimed iodine, calcium iodates, calcium iodide, potassium iodide, sodium iodide, and numerous organic compounds.

Commercial-grade crude iodine normally has a minimum purity of 99.5% to 99.8% I_2 . The main impurities in order of quantity are iron, sulfuric acid, and water. Specifications of U.S. Pharmacopoeia call for crude iodine to be not less than 99.8% I_2 . The Committee on Analytical Reagents of the American Chemical Society allows a maximum of 0.005% total bromine and chlorine and 0.010% nonvolatile matter (Lyday, 2003).

Prices

Actual prices for iodine are negotiated on long- and short-term contracts between buyers and sellers (Lyday, 2004b). U.S. prices for iodine (including cost, insurance, and freight charge-

es for imported iodine) have fluctuated, peaking at \$17.46 per kilogram in 1988 (Johnson, 1994). Prices decreased because of economic recession (1989–1992; 2002–2004) and oversupply (for example, when Chile began increasing production in the early 1990s and at the turn of the new century). Trends that caused prices to increase included additional demand for X-ray contrast media, potassium iodide production for U.S. Government contracts, and efforts to eliminate the effects of IDD. U.S. producers believed that large inventories of iodine sold by the National Defense Stockpile since 1989 depressed the price of iodine produced domestically; domestic production is competing with about 1 million pounds of excess stockpile (Lyday, 2002). Figure 5 shows the price trends for the years 1977–2003 (Lyday, 2004b).

Substitutes

Chlorine and bromine may be substituted for iodine in some chemical applications, but they are less desirable. Antibiotics, boron, chlorine, bromine, and Mercurochrome™ may be used instead of iodine in sanitation and biocide uses. Salt crystals and finely divided carbon may be used for cloud seeding (Harben, 2002; Lyday, 2004a, 2005). There are no substitutes, however, for iodine in some cattle feed and in catalytic, nutritional, pharmaceutical, and photographic uses (Lyday, 2004a, 2005).

Recycling

Lauterbach and others (2001) report that several iodine-consuming companies recover iodine from side streams generated in their production processes. Iodine is recovered as a derivative from the incineration of process impurities that have been captured before being discharged into the environment.

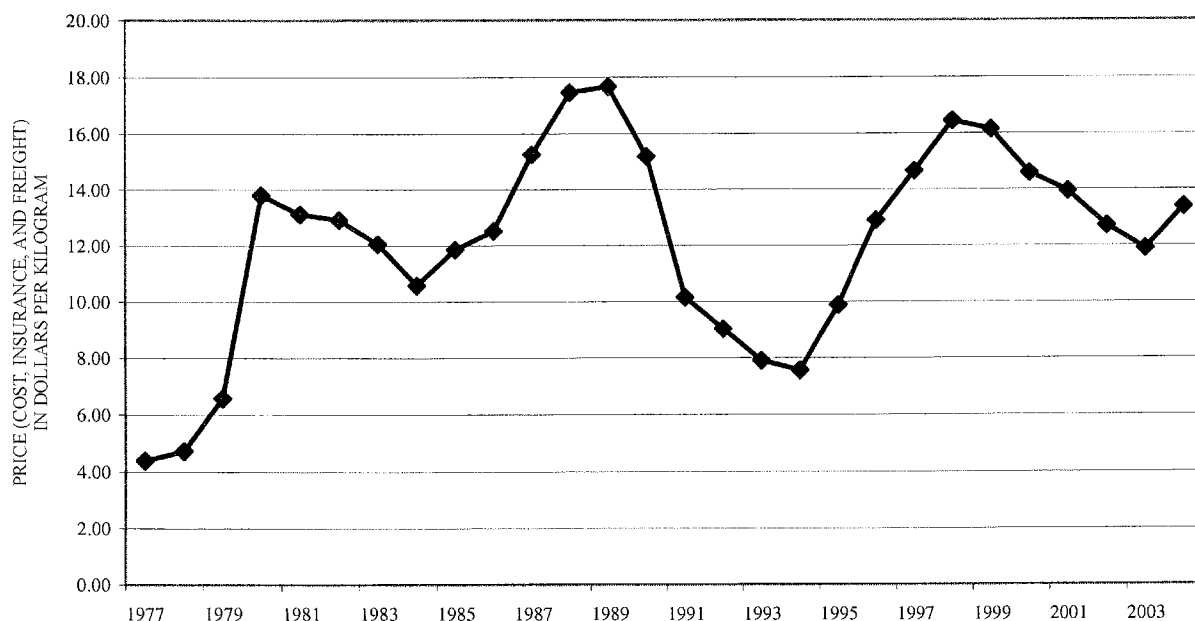


Figure 5. Graph showing trend of iodine prices in 1977–2003 (Lyday, 2004b).

U.S. Consumption, Imports, and Exports

Reported U.S. apparent consumption of iodine decreased from 5,420,000 kg in 2000 to 4,730,000 kg in 2001. In 2002, U.S. apparent consumption was 6,520,000 kg; however, apparent consumption continued to decrease to an estimated 5,210,000 kg in 2004 (Lyday, 2005). A breakdown of consumption and uses during 2003 is presented in Table 2. In 2004, about 5,200,000 kg (estimated) was imported to the United States, and about 1,330,000 kg (estimated) was exported (Lyday, 2005). U.S. imports during the years 2000–2003 were from Chile (67%), Japan (22%), Russia (10%), and other countries (1%).

Packaging and Transportation

Crude iodine is shipped in double polyethylene plastic-lined fiber drums holding 45–90 kg each. Resublimed iodine is shipped in the same type of container, and also in 11.3-kg glass jars and smaller bottles. Iodine also is shipped in 350-kg bulk bags and 1,800-kg tote bags, depending on the mode of transportation.

The mode of transportation depends on plant location, infrastructure in the region, and destination of the product. In Oklahoma, iodine is shipped by rail and truck, which can also accommodate bulk shipments in fiber drums, bulk bags, and tote bags. For destinations along major waterways and overseas, barges and cargo ships, respectively, are the norms. Freight classification is “chemicals, not otherwise indexed by name” (NOIBN) and requires no special label.

ECONOMIC FACTORS

Depletion Allowances, Tariffs, and Stockpiles

Depletion allowances for iodine from both domestic and foreign production is 14%. Tariffs on iodine are reported in Table 3. Since 1989, the U.S. Government Defense National Stockpile Center has sold surplus iodine stocks at a rate of about 454 metric tons (1 million pounds) per year. These are released on a quarterly basis and are sold at the prevailing market price at the time.

REGULATORY AND ENVIRONMENTAL CONSIDERATIONS

Health and Safety

Iodine is relatively safe to handle because it is a crystalline solid at normal room temperature and pressure; it has a relatively low vapor pressure of 1 kilopascal (kPa) @ 25°C in comparison to other halogens (for example, 700 kPa for chlorine). Personal protective equipment (PPE) is not necessary when handling properly packaged containers; however, chemically approved gloves, clothing, eyewear, and masks or respirators should be worn when solid iodine is not packaged properly (Lauterbach and others, 2001).

An upper limit of 0.1 ppm iodine in air was set by the U.S. Occupational Safety and Health Administration, because unprotected short-term exposure (up to 1 hour) can be hazardous to lungs and eyes. Severe irritation to the eyes and the respiratory tract, which may lead to pulmonary edema, can

TABLE 3.—Tariffs on Iodine, 2004

Item	Number	Normal Trade Relations 12/31/03
Iodine, crude	2801.20.0000	Free
Iodide, calcium and cuprous	2827.60.1000	Free
Iodide, potassium	2827.60.2000	2.8% ad valorem
Iodides and iodide oxides, others	2827.60.5000	4.2% ad valorem

Source: Lyday (2005).

occur from exposure to concentrations >0.1 ppm over extended periods. Burns also may result if contact with the skin is prolonged. Chronic absorption of iodine results in iodism, a condition whose symptoms include insomnia, inflammation of eyes and nasal passages, bronchitis, tremors, diarrhea, and weight loss (Lauterbach and others, 2001).

Land Use and Zoning

Permits for brine wells are similar to those for oil and natural-gas wells, particularly if there is coproduction of these resources or if injection wells are part of the iodine-extraction operation. The Oklahoma Corporation Commission regulates and permits borehole drilling, maintenance, abandonment, and reclamation. Most iodine operations are in remote areas, so industrial zoning is not a major concern. When it is necessary to abandon iodine-producing brine wells, the boreholes are plugged with concrete so that producing formations are sealed to prevent contamination of aquifers, other rock units, and the soils where the drill pad was located.

Pollution Control and Other Environmental Considerations

In the production of iodine, special considerations for chemical reagents, such as chlorine, sulfur dioxide, ammonia, and sulfuric acid, must be taken into account and documented in risk-management plans. These considerations include emissions from nonpoint sources (fugitive emissions), and single-point sources. Fugitive emissions are those from leaking valves, corroded pipe, and other equipment. Point-source emissions such as natural-gas compressors, boilers, and scrubbers discharge noxious substances (usually as gases) into the environment.

The U.S. Environmental Protection Agency requires that risk communication be filed with appropriate governmental entities. The Superfund Amendments and Reauthorization Act of 1986 (SARA Title 3; also known as the Right-to-Know Act of 1986) sets forth guidelines for essential emergency planning for local communities. Potential chemical hazards are identified by the producer, who files various risk communications annually with the local emergency committee, fire departments, the Oklahoma Department of Environmental

Quality, and others. This notifies respective agencies of potential problems associated with hazardous materials used at the site.

In the United States, iodine is a federally regulated List II chemical under the Comprehensive Methamphetamine Act of 1996; so iodine producers are required to report all iodine buyers and customers to the U.S. Drug Enforcement Agency and other enforcement authorities. Iodine is an essential ingredient in the manufacture of methamphetamines, which are commonly produced illegally (sold as "meth" or "speed"). These customs requirements call for iodine sellers to record all sales and to report detailed information about their customers. Producers maintain close control over inventories and have tight security at warehouses and other storage facilities.

REFERENCES CITED

- Cotten, H. M., 1978, Iodine in northwestern Oklahoma, in Johnson, K. S.; and Russell, J. A. (eds.), *Proceedings of Thirteenth Annual Forum on the Geology of Industrial Minerals: Oklahoma Geological Survey Circular 79*, p. 89-94.
- Erickson, G. E., 1981, *Geology and origin of the Chilean nitrate deposits*: U.S. Geological Survey Professional Paper 1188, 37 p.
- Harben, P. W., 2002, Iodine and iodine compounds, in *The industrial minerals handybook* (4th edition): Industrial Minerals Information, Ltd., London, p. 160-164.
- Johnson, K. S., 1989, *Geologic evolution of the Anadarko Basin*, in Johnson, K. S. (ed.), *Anadarko Basin symposium, 1988*: Oklahoma Geological Survey Circular 90, p. 3-12.
- 1994, Iodine, in Carr, D. D. (ed.), *Industrial minerals and rocks* (6th edition): Society of Mining, Metallurgy, and Exploration, Inc., Littleton, Colorado, p. 583-588.
- Johnson, K. S.; and Gerber, W. R., 1999, Iodine geology and extraction in northwestern Oklahoma, in Johnson, K. S. (ed.), *Proceedings of the 34th Forum on the Geology of Industrial Minerals, 1998*: Oklahoma Geological Survey Circular 102, p. 73-79.
- Krukowski, S. T., 2004, Iodine: *Mining Engineering*, v. 56, no. 6, p. 27-28.
- 2005, Iodine: *Mining Engineering*, v. 57, no. 6, p. 39-41.
- Lauterbach, A.; Ober, G.; Rios, S.; Basinger, W.; and Shipp, A., 2001, Iodine, high performance chemistry: *Sociedad Quimica y Minera de Chile S.A.*, Santiago, Chile, 85 p.
- Leaver, J. S.; and Thomasson, M. R., 2002, Case studies relating soil iodine geochemistry to subsequent drilling results, in Schumacher, D.; and LeSchack, L. A. (eds.), *Surface exploration case histories: applications of geochemistry, magnetics, and remote sensing*: American Association of Petroleum Geologists Studies in Geology 48, and Society of Exploration Geophysicists Geophysical References Series 11, Tulsa, p. 41-57.
- Lyday, P. A., 1985, Iodine, in *Mineral facts and problems, 1985 edition*: U.S. Bureau of Mines Bulletin 675, p. 377-384.
- 1986, Crude iodine production: *Industrial Minerals*, no. 222 (March), p. 65-76.
- 1999, Iodine and iodine compounds, in Elvers, Barbara; and Hawkins, Stephen (eds.), *Ullman's encyclopedia of industrial chemistry* (6th edition, electronic release): Wiley-VCH Publishers, New York.
- 2002, Iodine, in *USGS minerals yearbook 2002*, v. 1, metals and minerals: U.S. Geological Survey, Washington, D.C., p. 38.1-38.10.
- 2003, Iodine, in *Mineral commodity summaries 2003*: U.S. Geological Survey, Washington, D.C., p. 85-86.
- 2004a, Iodine, in *Mineral commodity summaries 2004*: U.S. Geological Survey, Washington, D.C., p. 82-83.
- 2004b, Iodine, in *USGS minerals yearbook 2004*, v. 1, metals and minerals: U.S. Geological Survey, Washington, D.C., p. 37.1-38.4.
- 2005, Iodine, in *Mineral commodity summaries 2005*: U.S. Geological Survey, Washington, D.C., p. 83-84.
- Moran, J. E., 1996, Origin of iodine in the Anadarko Basin, Oklahoma: *American Association of Petroleum Geologists Bulletin*, v. 80, p. 381-391.
- Ohl, J. P.; and Arndt, R. H., 1988, The mineral industry of Oklahoma, in *Minerals yearbook*, v. 2, area reports: domestic: U.S. Bureau of Mines, Washington, D.C., p. 395-404.
- Tedesco, S. A., 1994, *Surface geochemistry in petroleum exploration*: Chapman & Hill, New York, 206 p.
- Tedesco, S. A.; and Andrew, J. A., 1995, Integration of seismic data, iodine geochemistry yields Lodgepole exploration model: *Oil and Gas Journal*, v. 93, no. 38, p. 56-60.
- Tedesco, S. A.; and Goudge, C. K., 1994, How iodine surveys help locate southeast Colorado Morrow reservoirs: *Oil and Gas Journal*, v. 92, no. 41, p. 86-89.
- U.S. Geological Survey, 1998, Iodine, in *Mineral industry surveys, 1997 annual review*: Washington, D.C., 11 p.

Trends in Composition of Morrowan Gases in Southwestern Kansas

K. David Newell

Kansas Geological Survey, University of Kansas
Lawrence, Kansas

ABSTRACT.—Compositions and heating values of 240 gases from 115 oil and gas fields producing from Morrowan rocks (Lower Pennsylvanian) in southwestern Kansas were analyzed for stratigraphic and spatial variability. Morrowan rocks in southwestern Kansas lie at depths >5,500 ft. Gas produced in these fields is generally of acceptable quality, with 95% of the analyses having heating values >950 BTU per standard cubic foot (scf). Gas production is from both oil-associated and gas-only pay zones, usually from the Keyes sandstone of the Kearny Formation. Overall, the heating value of Morrowan gases in southwestern Kansas increases slightly with increasing depth. Lesser amounts of noncombustible-component gases (mainly nitrogen) with increasing depth may account for this. The Morrowan gases also tend to be slightly drier with depth in that they are composed of lesser amounts of higher molecular weight hydrocarbons. These compositional changes probably are the result of greater thermal maturation that comes with increasing depth.

Nitrogen and helium percentages in Kansas Morrowan gases as a group are less than those in Morrowan gases to the northwest in eastern Colorado. Morrowan fields in Kansas near the Colorado state line (e.g., Arroyo Field, Taloga Field) can have >1% helium with relatively low nitrogen-to-helium ratios (i.e., <10:1), thereby suggesting that gas produced from this area perhaps could be processed for helium extraction. Nitrogen-to-helium ratios are higher in Morrowan fields to the east in southwestern Kansas.

The Sparks Field, which straddles the Morton–Stanton county line, has CO₂ locally >3%. Fields in Morton County also have relatively elevated CO₂ contents, but, in general, most Morrowan fields in southwestern Kansas register <0.2% CO₂.

INTRODUCTION

This paper attempts to characterize and outline general trends for the chemical compositions of gases in the Lower Pennsylvanian (Morrowan) Kearny Formation in Kansas. As such, it is not an attempt to discover the origin(s) of these gases, for the ultimate answers to these questions are likely best addressed with sophisticated isotopic analyses of both the main component gases and trace gases. Nevertheless, the general compositional data gathered in the routine analysis and development of oil and gas fields can have utility in understanding or at least establishing some constraints and consequent insight that may prove valuable in answering such questions about gas origins and any post-accumulation alteration of these gas products. Exploration decisions also can be aided by knowing the quality of natural gases found in a given trend of oil and gas fields.

Data generally recorded in a routine gas analysis include percentages of hydrocarbon chemical species—methane, ethane, propane, *n*-butane, isobutane, *n*-pentane, cyclopentane, and isopentane. Heavier hydrocarbon percentages are usually included as a “C6+” component. Nonhydrocarbon gases reported include nitrogen, oxygen, carbon dioxide, argon, helium, hydrogen, and hydrogen sulfide. Other physical data reported are gas gravity and heat content (reported as BTU/scf).

Data for gas compositional analyses are available from several published and unpublished sources. Published sources include technical articles on oil and gas fields, and also a series of gas-quality publications put out by the U.S. Bureau of Mines. Unpublished sources include scout cards and miscellaneous data archived at the Kansas Geological Survey. For purposes of this study, analytical data were compiled for ~240 gases from 115 Morrowan oil and gas fields in southwestern Kansas (Table 1).

Additional information added to this database by the author includes production depth and surface datums. Some updates and corrections were necessary for well locations (section, township, and range), production depths, and field names. It also was assumed that any oxygen in the sample was likely due to contamination by the atmosphere. If oxygen was present, it and other atmospheric gases were subtracted according to their atmospheric ratio to oxygen (see Weaver, 1966). The percentage of nitrogen in a natural gas is most affected by this correction, because nitrogen has a ratio of 3.72 to oxygen in the atmosphere (Weaver, 1966). After correction for any atmospheric component in the sample, the sums of all gas percentages in a sample were recalculated to 100%, and the heating value also was adjusted.

TABLE 1.—Compositions of Natural Gases Produced from Morrowan Strata in Kansas^a

COUNTY	FIELD	OPERATOR	WELL NAME	LOCATION			DEPTH SURFACE (ft)	DEPTH (ft)	HYDROCARBONS										NONHYDROCARBONS				SPEC. GRAV.	REFERENCE		
				Sec.	Tp.	R.			Gasoline (%)	Methane (%)	Ethane (%)	n-Butane (%)	Isobutane (%)	Gasoline (%)	Cyclopentane (%)	Hexanes+ (%)	Nitrogen (%)	Helium (%)	Argon (%)	Hydrogen (%)	CO ₂ (%)	Oxygen (%)			BTU	
Wallace	Saxon	Stakely Oil	Saxon #1	19	13 S	42 W	5008	-1155	31.0	2.9	2.3	0.5	0.4	0.2	0.3	0.1	0.2	59.2	2.30	0.1	trace	0.5	trace	492	0.862	Munnely and Miller (1963)
Wallace	Stockholm	TXO Production	Himits #1	7	15 S	42 W	5102	-1186	32.5	3.3	2.3	1.1	0.2	0.4	0.0	0.2	56.8	1.91	0.2	0.1	0.4	1.3	542	0.876	Hanek and Sigler (1991)	
Wallace	Stockholm	TXO Production	Johannes #1	18	15 S	42 W	5150	-1218	32.9	3.3	2.6	0.7	0.3	0.2	0.1	0.0	0.1	57.2	1.92	trace	trace	0.6	1.1	519	0.865	Hanek and Sigler (1991)
Greeley	Stockholm SW	Marathon Oil	Bergquist #3	6	16 S	42 W	5126	-1238	39.4	14.8	15.5	6.7	4.0	2.0	0.6	0.3	0.2	12.5	0.17	0.1	0.0	3.6	0.2	1559	1.092	Hanek and Gage (1992)
Haskell	Pleasant Prairie	Helmerich & Payne	Jones "O" #17	9	27 S	34 W	4936	-1945																621	(not given)	scout cards
Haskell	Minneola	Champion Petroleum	McCune "A" #1	25	29 S	25 W	5404	-2799	71.1	6.6	4.7	1.6	0.9	0.4	0.5	0.1	0.3	13.5	0.30	trace	0.0	trace	trace	1103	0.753	Moore and Hamak (1985)
Haskell	Lemon NE	Pan American Petroleum	Rohmeyer Oper. Unit #1	30	29 S	32 W	5232	-2302	73.4	5.8	3.4	1.0	0.5	0.2	0.4	0.1	0.2	14.7	0.16	trace	0.0	0.1	0.0	1026	0.720	Moore and Shrevebury (1967)
Koenig	Eubank	Cities Service	Light #D-1	1	29 S	34 W	5351	-2369	69.2	5.7	3.4	0.8	0.5	0.1	0.2	0.2	trace	0.1	19.3	0.53	trace	0.1	0.0	953	0.723	Cardwell and Benton (1971)
		United Producing	E.M. Gregg #2	4	29 S	34 W	5125	-2110	73.4	5.3	3.3	0.8	0.5	0.1	0.2	0.2	trace	0.1	15.4	0.70	trace	0.1	0.1	trace	986	0.702
Haskell	Koenig	W.J. Copinger	W.J. Copinger	12	29 S	34 W	5280	-2310	69.5	6.0	3.2	0.8	0.6	0.2	0.2	0.1	0.2	18.4	0.50	trace	0.1	0.2	trace	973	0.727	Munnely and Miller (1963)
Stanton	Sand Arroyo	Anco Production	Goaco Kilgore #1	20	29 S	39 W	5468	-2243	79.3	4.3	2.1	0.6	0.2	0.2	0.1	0.0	0.1	11.8	0.49	0.0	trace	0.1	0.1	971	0.699	Hanek and Driskill (1996)
Stanton	Arroyo	J.M. Huber	Santa Fe #9-1	9	29 S	41 W	5420	-2016	76.4	3.6	2.4	0.9	0.3	0.3	0.4	0.0	0.1	13.4	1.77	0.1	trace	0.3	0.1	1014	0.684	Sigler (1994)
Stanton	Arroyo	J.M. Huber	Cockeheim #10-1	10	29 S	41 W	5412	-2026	75.7	3.5	2.2	0.8	0.3	0.3	0.1	0.0	0.1	14.8	1.75	0.1	trace	0.3	0.1	952	0.680	Gage and Driskill (1998)
Stanton	Arroyo	J.M. Huber	Frezz #16-2	16	29 S	41 W	5452	-2032	75.0	4.3	2.9	1.0	0.4	0.3	0.1	0.0	0.1	14.0	1.33	0.1	trace	0.4	0.2	1020	0.698	Sigler (1994)
Stanton	Arroyo	J.M. Huber	Court #21-1	21	29 S	41 W	5420	-2007	74.5	4.6	3.0	1.0	0.4	0.3	0.1	0.0	0.1	14.1	1.38	0.1	trace	0.3	0.0	993	0.699	Sigler (1994)
Stanton	Arroyo	J.M. Huber	Santa Fe #26-2	26	29 S	41 W	5397	-1997	76.1	4.4	2.7	1.1	0.3	0.5	0.1	0.1	0.3	12.7	1.36	0.1	trace	0.3	trace	1048	0.676	Sigler (1994)
Stanton	Arroyo	J.M. Huber	Pro Farms #26-2	26	29 S	41 W	5386	-2009	76.7	4.6	2.9	0.8	0.3	0.2	0.5	0.0	0.1	12.2	1.21	0.1	trace	0.4	0.0	1006	0.688	Sigler (1994)
Stanton	Arroyo	J.M. Huber	Launon #28-1	28	29 S	41 W	5444	-2063	78.2	4.1	2.5	0.8	0.3	0.1	0.4	0.0	0.0	11.9	1.31	0.1	trace	0.2	0.2	1029	0.676	Sigler (1994)
Clark	Halling	Packell Drilling	Halling "B" #1	14	30 S	22 W	5300	-2889																(not given)	0.685	scout cards
Clark	Norcan E	Murrin Drilling	Peterson #1-3	3	30 S	25 W	5318	-2739	71.2	9.9	7.2	1.4	1.1	0.3	0.2	(not given)	0.0	8.7 (B)	(not given)	(not given)	(not given)	(not given)	1211	0.7552	Doyle (1985)	
Haskell	Radio Tower	John O. Farmer	Peterson #1-28	28	30 S	31 W	5409	-2561															(not given)	0.699	scout cards	
Haskell	Victory	Pan American Petroleum	W.M. Wilson "B" #2	19	30 S	33 W	5269	-2304															(not given)	0.718	scout cards	
Haskell	Victory	Pan American Petroleum	U.V. Alton "B" #1	21	30 S	33 W	5228	-2267	78.1	5.9	3.3	0.9	0.6	0.2	0.3	0.1	0.2	9.7	0.60	trace	0.0	0.1	0.0	1068	0.694	Moore and Shrevebury (1966)
Stanton	Sand Arroyo	Anco Production	Kayla Marie #1-2	2	30 S	40 W	5100	-1832	74.7	5.6	3.6	0.3	0.4	0.0	0.0	0.0	0.0	14.9	0.42	trace	trace	0.1	0.3	1013	0.691	Gage and Driskill (1996)
Stanton	Brachamp	Graham-Michaels Drilling	Bauchamp #1-19	19	30 S	40 W	5222	-1880	70.7	4.5	3.2	1.1	0.6	0.2	0.4	0.1	0.2	17.7	0.92	trace	0.0	0.4	0.0	977	0.726	Moore and Shrevebury (1967)
		Bereco	Nellie #1	16	30 S	41 W	5093	-1685	65.5	5.4	6.4	1.4	1.0	0.0	0.0	0.1	18.6	0.25	0.0	trace	0.2	0.1	1058	0.784	Hanek and Sigler (1993)	
Stanton	Brachamp	Western Natural Gas	Armstrong #1	24	30 S	41 W	5018	-1662	69.2	5.3	4.4	0.8	0.5	0.1	0.1	trace	0.1	19.0	0.30	trace	0.1	1.6	971	0.751	Munnely and Miller (1963)	
Stanton	Sparks	J.M. Huber	Sparks #1	34	30 S	42 W	5252	-1744	83.4	3.88	2.08	0.63	0.40	0.20	0.17	0.15	6.85 (B)	(not given)	(not given)	(not given)	1.80	0.00	1025	(not given)	Rupp (1959)	
Stanton	Sparks	J.M. Huber	Sparks #1	34	30 S	42 W	5277	-1769	82.4	3.7	2.0	0.7	0.4	0.3	0.2	0.1	0.3	7.5	0.86	trace	0.1	1.4	trace	1032	0.669	Boone (1958)
Stanton	Sparks	Mesa Petroleum	Daily #1-1	1	31 S	22 W	5199	-2954	87.1	4.2	1.5	0.5	0.2	0.1	0.2	0.1	0.1	5.6	0.25	trace	0.0	0.2	0.0	1042	0.635	Moore (1977)
Stanton	Thirty-One SW	Ensign Operating Co.	Court #21-1	24	31 S	32 W	5475	-2626	81.8	5.9	2.9	1.0	0.1	0.5	0.1	0.2	7.1	0.14	0.0	0.0	0.1	2.4	1086	0.715	Hanek and Sigler (1991)	
Stanton	Cutter E	Anadarko Petroleum	Belvoir #A-1	4	31 S	34 W	5231	-2359	68.6	8.9	6.7	1.5	0.6	0.0	1.2	0.1	0.1	11.9	0.11	0.0	trace	0.2	0.1	1160	0.776	Hanek and Sigler (1993)
Stanton	Cutter	Mobil Oil	Cutter #1	1	31 S	35 W	5313	-2335	66.0	7.0	4.8	1.7	0.3	0.5	0.7	0.2	4.7	0.35	0.0	0.0	0.0	0.2	0.1	1066	0.781	Moore and Shrevebury (1966)
Stanton	Cave W	Mobil Oil	Junio F Phillips #5	17	31 S	35 W	5591	-2584	73.3	6.3	5.5	0.0	2.0	0.8	0.0	0.1	0.7	11.0	0.27	0.0	0.0	0.0	0.1	1138	0.749	Hanek and Sigler (1991)
Stanton	Perm SE	Oxy USA	M.P. Gernond "A" #1	20	31 S	37 W	5378	-2245	71.5	5.1	0.0	1.7	0.5	0.0	0.1	0.0	0.0	15.4	0.54	0.0	trace	0.0	0.1	1070	0.733	Hanek and Driskill (1996)
Stanton	Perm SW	Oxy USA	M.P. Dale "A" #1	19	31 S	38 W	5648	-2458	85.3	4.5	3.1	0.0	1.4	0.6	0.0	0.0	0.0	4.5	0.33	trace	0.0	0.1	0.0	1106	0.652	Hanek and Driskill (1996)
Stanton	Youngman NW	Anadarko Production	Cayner "A" #6	38	31 S	38 W	5792	-2632															(not given)	0.678	scout cards	
Morton	Krider	Pan American Petroleum	Alton "B" #1	15	31 S	40 W	5400	-2101	78.3	6.1	3.0	0.8	0.5	0.2	0.2	0.2	10.0	0.50	trace	0.0	0.2	trace	1050	0.687	Miller and Norrell (1964a)	
Morton	Krider	Donald C. Slavson	Breeding #1-34	34	31 S	40 W	4904	-1585															(not given)	0.60	(not given)	0.60
Morton	Krider	Pan American Petroleum	Copar "B" #1	34	31 S	40 W	5310	-2004	77.6	6.6	3.5	0.8	0.4	0.1	0.2	0.2	10.0	0.50	trace	0.0	0.5	trace	1055	0.694	Miller and Norrell (1964a)	
Morton	Krider	Pan American Petroleum	G.L. Hayward "B" #1	35	31 S	40 W	5322	-2035	76.9	8.1	4.8	1.0	0.7	0.2	0.2	0.1	6.6	13.0	0.88	trace	0.3	trace	1128	0.735	Miller and Norrell (1964a)	
Morton	Brachamp SW	Musang Drilling & Expl	Bush-Hatch #2-5	5	31 S	41 W	5384	-1941	76.6	3.8	2.3	1.1	0.6	0.3	0.2	0.1	6.6	13.0	0.88	trace	0.3	trace	1029	0.706	Moore and Sigler (1986)	
Morton	Patsy	Musang Drilling & Expl	Orrison #2-9	9	31 S	41 W	5330	-1930	81.0	3.4	2.0	0.8	0.6	0.6	0.0	0.1	6.6	13.0	0.88	trace	0.3	trace	1029	0.706	Moore and Sigler (1986)	
Morton	Patsy	Midwestern Exploration	Midwestern Exploration	16	31 S	41 W	5362	-1954	82.2	3.4	1.7	0.6	0.5	0.3	0.2	0.2	9.6	1.00	trace	0.1	0.2	0.0	1007	0.656	Munnely and Miller (1963)	
Morton	Sparks	Pan American Petroleum	Patsy Roth Murphy #1	16	31 S	41 W	5362	-1954	82.2	3.4	1.7	0.6	0.5	0.3	0.2	0.2	9.6	1.00	trace	0.1	0.2	0.0	1007	0.656	Munnely and Miller (1963)	
Morton	Sparks	J.M. Huber	Collingwood #1	11	31 S	42 W	5207	-1730	83.4	3.8	2.3	0														

Trends in Composition of Morrowan Gases, Southwestern Kansas

51

Stevens	Gentzler N	Anadarko Production	Schmidt "C" #1	30	32.5	37 W	5980	-2823	85.0	3.9	2.0	0.6	0.3	0.2	0.2	0.1	0.1	7.0	0.21	trace	0.1	0.3	0.1	1040	0.652	Miller and Hertweck (1983)
Stevens	Matts	Amoco Production	Matts #A-2	12	32.5	38 W	5932	-2788	86.5	4.5	2.6	0.7	0.4	0.3	0.1	0.2	0.2	4.1	0.33	0.0	trace	0.2	0.0	1088	0.650	Hanak and Sigler (1993)
Morton	Kinsler E	Oxy U.S.A.	Yeager "B" #3	5	32.5	39 W	5830	-2574	87.3	4.4	2.3	0.7	0.3	0.3	0.1	0.5	0.4	3.4	0.33	trace	0.0	0.2	1	1104	0.633	Hanak and Sigler (1993)
Morton	Kinsler E	Oxy U.S.A.	Kansas University "A" #5	6	32.5	39 W	5448	-2172	75.7	1.5	1.4	0.6	0.2	0.2	0.0	0.1	3.5	0.05	0.0	(trace)	0.5	0.4	1283	0.749	Sigler (1994)	
Morton	Kinsler	Oxy U.S.A.	Tillet "B" #1	19	32.5	39 W	5724	-2458	86.9	3.7	1.9	0.4	0.2	0.2	0.2	trace	trace	0.0	0.0	trace	0.0	0.0	1033	0.634	Cardwell and Benton (1972)	
Morton	Kinsler	Pan American Petroleum	Drew Gas Unit "D" #1	20	32.5	39 W	5594	-2260	70.6	6.1	3.9	0.9	0.6	0.1	0.1	trace	0.1	16.9	0.30	trace	trace	0.3	0.2	991	0.727	Miller and Norrell (1964a)
Stevens	Middream	Anadarko Petroleum	Rheeler #2-2	27	32.5	39 W	5931	-2783	86.9	4.2	1.9	0.4	0.3	0.0	0.3	0.0	0.0	4.9	0.73	trace	0.1	0.3	0.0	1040	0.620	Hanak and Sigler (1991)
Morton	Kinsler	Pan American Petroleum	Fidelity Savings "B" #1	13	32.5	40 W	5684	-2385	90.5	3.9	1.3	0.3	0.2	0.1	trace	0.1	0.2	2.8	0.30	0.0	0.0	0.3	trace	1058	0.617	Miller and Norrell (1964a)
Morton	Rupp	Hugoton Energy	Maquardt #2-2	28	32.5	40 W	5250	-1892	80.8	5.4	4.2	1.1	0.4	0.4	0.1	0.0	0.0	1.6	0.20	0.0	trace	0.4	0.0	1072	0.977	Hanak and Sigler (1991)
Morton	Richfield	Anadarko Petroleum	Blancher #A-2	34	32.5	40 W	5350	-2062	93.9	1.3	0.2	0.0	0.4	0.0	0.0	0.0	0.0	4.2	0.26	trace	trace	0.2	0.0	1072	0.639	Cardwell and Benton (1970b)
Morton	Richfield	Granite-Michals Drilling	Johns #1-3	3	32.5	41 W	5224	-1830	87.8	3.9	2.0	0.6	0.3	0.2	0.2	0.1	0.2	3.1	0.28	trace	0.1	0.2	0.0	1066	(not given)	Cardwell and Benton (1970b)
Morton	Richfield	Panhandle Eastern	Murphy Gas Unit "C" #1	14	32.5	41 W	5179	-1822	90.2	3.2	1.5	0.5	0.2	0.2	0.1	0.3	0.3	3.1	0.28	trace	0.1	0.3	0.9	1067	0.624	Cardwell and Benton (1970b)
Morton	Richfield	Anadarko Production	Murphy "A" #2	15	32.5	41 W	5156	-1772	89.2	3.2	1.7	0.5	0.2	0.2	0.2	0.3	1.0	3.6	0.29	trace	0.1	0.3	0.9	1067	0.624	Cardwell and Benton (1970b)
Morton	Richfield	Pan American Petroleum	Kansas University GU "C" #1	23	32.5	41 W	5200	-1807	84.1	4.3	2.1	0.9	0.7	0.5	0.2	0.3	1.0	5.3	0.30	0.0	0.0	0.3	trace	1132	0.988	Munneyn and Miller (1963)
Morton	Richfield	Pan American Petroleum	Daniel Gas Unit #1	23	32.5	41 W	5185	-1779	90.5	3.1	1.5	0.5	0.2	0.3	0.1	0.3	0.3	2.7	0.28	trace	0.1	0.3	0.1	1073	0.628	Cardwell and Benton (1970b)
Morton	Richfield	Pan American Petroleum	Jensen Gas Unit #1	25	32.5	41 W	5280	-1868	81.9	4.6	3.5	1.2	0.9	0.8	0.1	0.3	0.9	5.2	0.25	0.0	0.1	0.2	0.1	1172	0.712	Cardwell and Benton (1970b)
Morton	Richfield	Panhandle Eastern	Gong #1-26	26	32.5	41 W	5192	-1771	70.7	6.2	3.5	1.1	0.6	0.5	0.2	0.2	0.2	16.1	0.30	0.1	0.2	0.2	7.2	1024	(not given)	Munneyn and Miller (1963)
Morton	Richfield	Panhandle Eastern	Gong #1-26	26	32.5	41 W	5200	-1779	76.0	6.3	4.1	1.1	1.1	0.6	0.1	0.4	0.6	0.38	0.0	0.0	trace	0.2	0.0	1115	0.724	Cardwell and Benton (1970a)
Morton	Richfield	Panhandle Eastern	Lemon Gas Unit "E" #1	27	32.5	41 W	5259	-1858	80.9	5.1	3.2	1.1	0.5	0.4	0.1	0.1	0.4	7.6	0.37	trace	0.1	0.2	0.0	1089	0.686	Cardwell and Benton (1970a)
Morton	Richfield	Pan American Petroleum	Bowker Gas Unit #2	35	32.5	41 W	5200	-1769	76.5	6.6	3.3	1.1	0.7	0.4	0.1	0.1	0.4	10.2	0.40	trace	0.0	0.2	0.0	1088	0.712	Munneyn and Miller (1963)
Morton	Richfield	Panhandle Eastern	Gong #1-35	35	32.5	41 W	5191	-1768	78.4	5.9	3.8	1.1	1.0	0.5	0.1	0.1	0.4	10.0	0.35	trace	0.1	0.2	0.1	1121	0.711	Cardwell and Benton (1970a)
Morton	Richfield	NCRA	Key "A" #1	36	32.5	41 W	5187	-1779	90.9	3.1	1.3	0.5	0.2	0.1	0.2	0.1	0.1	2.7	0.45	trace	0.0	0.3	0.1	1057	0.617	Cardwell and Benton (1970b)
Morton	Richfield W	Hamilton Bros.	L.D. Russell #1-1	1	32.5	42 W	4924	-1448	91.7	3.0	1.3	0.4	0.1	0.1	0.2	0.1	0.1	2.5	0.29	trace	0.0	0.3	0.0	1049	0.609	Moore and Shrevebury (1968)
Morton	Richfield W	Hamilton Bros.	E.C. Dunn #1-2	2	32.5	42 W	4974	-1499	90.9	3.1	1.4	0.5	0.2	0.3	0.3	0.1	0.2	16.5	0.59	trace	0.8	trace	0.8	988	0.726	Moore and Shrevebury (1968)
Morton	Richfield W	Hamilton Bros.	E.C. Dunn #1-2	2	32.5	42 W	5050	-1575	71.3	4.6	2.8	1.0	0.7	0.3	0.2	0.1	0.2	7.2	0.30	trace	trace	0.3	trace	1064	0.620	Moore and Shrevebury (1968)
Morton	Richfield W	Norfolk Oil	E.C. Dunn #1-2	6	33.5	20 W	5216	-5306	90.6	3.9	1.3	0.4	0.1	0.1	0.1	0.1	0.3	16.8	0.62	0.1	0.0	1.2	0.0	976	0.730	Moore and Shrevebury (1968)
Comanche	Overcorder	Quintana Petroleum	Edmonston #4-2A	3	33.5	21 W	5264	-3245	88.4	4.9	2.5	0.6	0.5	0.1	0.1	trace	0.0	3.0	0.15	trace	0.0	0.3	0.0	1052	0.616	Moore (1978)
Clark	Caley SW	Sincan O&G	Ken Mosier #1	27	33.5	21 W	5280	-3506	88.4	4.9	2.0	0.6	0.5	0.1	0.1	trace	0.1	24	0.12	0.0	0.0	0.1	0.0	1107	0.640	Hanak and Sigler (1991)
Clark	Harper Ranch	Petroleum, Inc	Cautious Trust Unit #1	29	33.5	22 W	5435	-3471	87.4	4.7	2.3	0.8	0.4	0.2	0.2	0.1	0.4	30	0.10	trace	0.0	0.3	trace	1083	0.635	Miller and Norrell (1964a)
Clark	Slicka	Seely Oil	C.A. Isak #1	18	33.5	27 W	5752	-3263	80.7	5.6	3.7	1.1	0.8	0.1	0.2	0.1	0.2	6.8	0.10	0.0	0.0	0.2	0.0	1116	0.655	Moore and Shrevebury (1966)
Meade	McKinney	Refugion Oil	Loewen #1-A	1	33.5	28 W	5672	-3142	90.0	4.7	2.2	0.6	0.4	0.2	0.1	trace	0.2	1.4	0.09	0.0	0.1	trace	1112	0.650	Munneyn and Miller (1963)	
Meade	Borchers	MM&B	Borchers #1	20	33.5	28 W	5641	-3210	78.3	5.2	3.0	0.9	0.5	0.1	0.5	0.1	0.3	9.0	0.17	trace	0.8	1.1	0.0	1059	(not given)	Cardwell and Benton (1970a)
Meade	Borchers NW	E.G. Bradley	Beschers #1	1	33.5	29 W	5564	-3053	78.3	5.2	3.0	0.9	0.5	0.1	0.5	0.1	0.3	9.0	0.17	trace	0.8	1.1	0.0	1059	0.695	Munneyn and Miller (1963)
Meade	Borchers	Seely Oil	Carl Evans #1	1	33.5	29 W	5612	-3072	84.4	5.5	3.1	0.7	0.4	0.0	0.3	trace	0.1	5.4	0.10	0.0	0.0	trace	0.0	1088	0.659	Munneyn and Miller (1963)
Meade	Angell	Imperial Oil	Collingwood #1	6	33.5	29 W	5710	-2898	78.0	6.3	4.0	0.9	0.6	0.2	0.0	trace	0.1	9.3	0.21	trace	0.0	0.3	0.1	1071	0.696	Cardwell and Benton (1973)
Meade	Singley	Gulf Oil	H.A. Holmes #1	21	33.5	29 W	5729	-3129	78.9	7.5	4.4	1.0	0.9	0.3	0.3	0.1	0.2	6.1	0.11	0.0	trace	0.2	0.0	1151	0.709	Moore and Shrevebury (1966)
Meade	Mohr NE	Shamrock O&G	Cordele #1	24	33.5	29 W	5597	-3195	80.1	6.4	3.7	0.9	0.6	0.2	0.3	0.1	0.3	7.0	0.20	trace	0.2	0.2	0.0	1115	0.695	Munneyn and Miller (1963)
Meade	Singley	Panhandle Eastern	Bahake #1	29	33.5	29 W	5782	-3161	79.6	6.3	4.2	1.2	0.6	0.3	0.2	0.1	0.3	6.9	0.10	trace	0.0	0.2	0.0	1077	(not given)	WHCS
Meade	Singley	Shamrock O&G	Iida K. Henson #8	29	33.5	29 W	5796	-3161	79.6	6.3	4.2	1.2	0.6	0.3	0.2	0.1	0.3	6.9	0.10	trace	0.0	0.2	0.0	1129	0.704	Moore and Shrevebury (1966)
Meade	Norvige E	Shamrock & Brewer O&G	Ballard #1	31	33.5	29 W	5841	-3166	85.7	5.8	3.2	0.9	0.4	0.4	trace	0.1	3.2	0.10	0.0	0.0	0.2	trace	0.2	1121	0.670	Munneyn and Miller (1963)
Meade	Karnet	Shamrock O&G	WW Langheller #1	18	33.5	30 W	5654	-2916	83.8	6.6	3.5	0.9	0.5	0.4	trace	trace	0.1	4.0	0.11	0.0	0.0	0.1	0.0	1126	0.659	Moore and Shrevebury (1966)
Meade	Karnet	Shamrock O&G	WW Langheller #1	18	33.5	30 W	5654	-2916	83.8	6.6	3.5	0.9	0.5	0.4	trace	0.1	4.0	0.11	0.0	0.0	0.1	0.0	0.1	1126	0.659	Moore and Shrevebury (1966)
Meade	Bruno	Cotton Petroleum	Gulor #1	28	33.5	30 W	5737	-3021	86.3	5.9	2.8	0.6	0.4	0.1	0.1	trace	0.1	3.5	0.14	0.0	0.1	0.2	0.0	1234	0.740	Boone (1958)
Meade	Karnet	Cabot Carbon	Massoni #1	5	33.5	31 W	5590	-2871	88.9	5.2	2.3	0.7	0.2	0.2	0.2	0.0	1.1	0.38	trace	0.0	0.1	trace	1101	0.648	Cardwell and Benton (1973)	
Seward	Karnet	Cabot Corp.	Massoni #1	5	33.5	31 W	5595	-2877	88.9	5.2	2.3	0.7	0.2	0.2	0.2	0.0	1.1	0.38	trace	0.0	0.1	trace	1101	0.648	Boone (1958)	
Seward	Karnet	Frederick #1	Frederick #1	26	33.5	31 W	5524	-2783	86.1	5.5	2.5	0.6	0.3	0.1	0.3	0.1	0.2	3.3	0.12	0.0	trace	0.2	0.0	1127	0.654	Moore and Shrevebury (1966)
Seward	Karnet	Frederick #1	Frederick #1	26	33.5	31 W	5524	-2783	86.1	5.5	2.5	0.6	0.3	0.1	0.3	0.1	0.2	3.3	0.12	0.0	trace	0.2	0.0	1127	0.654	Moore and Shrevebury (1966)
Seward	Arkalon	Anadarko Production	Danels "C" #1	31	33.5	31 W	5686	-3078	88.9	5.1	2.2	0.9	0.1	0.2	0.3	0.1	0.2	1.7	0.10	trace	0.0	0.2	0.0	1118	0.642	Moore and others (1966)
Seward	Evelyn-Condit	Cabot Corp.	Bryant "A" #1	8	33.5	33 W	5680	-2832	82.2	5.4	3.5	1.0	0.6	0.4	0.1	0.1	0.3	6.0	0.20	trace	0.0	0.2	trace	1117	0.685	Moore and others (1966)
Seward	Evelyn-Condit	Anadarko Production	Santa Fe Land Improvement "A" #1	9	33.5	33 W	5548	-2751	85.3	5.3	3.0	0.4	0.2	0.3	0.1	0.1	5.6	0.20	trace	0.0	0.2	trace	1103	0.673	Miller and Norrell (1964b)	
Seward	Evelyn-Condit	Ferguson Oil	Freeman #1	18	33.5	33 W	5692	-2812	83.1	5.2	3.5	0.9	0.6	0.3	0.3	trace	0.1	5.6	0.19	0.0	0.1	0.1	0.0	1110	0.676	Cardwell and Benton (1971)
Seward	Shuck N	Leben Oil	Hitch #1	6	33.5	34 W	5876	-2951	84.4	4.9	2.5	0.9	0.3	0.1	0.6	trace	0.1	5.7	0.20	trace	0.0	0.2	0.4	1085	0.670	Cardwell and Benton (1972)
Seward	Shuck	Snuck #2-20	Snuck #2-20	20	33.5	34 W	5987	-3050	85.1	5.2	3.0	1.0	0.5	0.2	0.2	0.1	0.2	4.2	0.14	trace	0.0	0.2	trace	1116	0.666	Boone (1958)
Seward	Shuck	Anadarko Production	Fuller "A" #1	30	33																					

TABLE 1.—Compositions of Natural Gases Produced from Morrowan Strata in Kansas^a (continued)

COUNTY	FIELD	OPERATOR	WELL NAME	LOCATION			DEPTH (ft)	DEPTH (ft)	HYDROCARBONS										NONHYDROCARBONS					SPEC. GRAV.	REFERENCE			
				Sec.	Tp.	R.			Methane	Ethane	Propane	n-butane	isobutane	i-pentane	isopentane	Cyclopentane	Hexanes+	Nitrogen	Helium	Argon	Hydrogen	CO ₂	Oxygen					
Morton	Winter	Cities Service	Facey "A" #2A	24	33.5	43.5 W	4470	-481	70.80	6.490	5.280	1.090	0.618	0.236	0.214	(not given)	(not given)	0.025	0.424	14.700	0.006	0.142	0.055	1045	(not given)	Jenden and others (1988)		
Comanche	Tuttle NE	D.T. Swanson	Woodlark "E" #1	29	34.5	20.5 W	5420	-3670	89.7	3.9	1.5	0.5	0.2	0.1	0.1	0.1	0.1	0.1	3.2	0.15	trace	0.1	0.3	0.0	1059	0.672	Moore (1980)	
Clark	Snake Creek	Keas O&G	Harper Ranch #1	16	34.5	21.5 W	5416	-3532	91.5	3.3	1.2	0.3	0.2	0.1	0.1	0.1	0.1	0.1	3.0	0.12	trace	0.0	0.1	0.1	1042	0.604	Moore (1977)	
Clark	Snake Creek	Sunray DX	R.S. Shupe #1	12	34.5	21.5 W	5580	-3743	89.1	5.0	2.2	0.8	0.2	0.3	0.1	0.3	0.1	0.2	3.3	0.13	0.12	0.004	0.0	0.2	0.2	1131	0.648	Moore and Shrevebury (1967)
Clark	Snake Creek	Rine Drilling	Baby #5-23	23	34.5	21.5 W	5383	-3611	91.00	3.800	1.400	0.169	0.382	0.120	0.106	(not given)	(not given)	0.000	0.153	3.100	0.008	0.191	0.038	1050	0.648	Moore and others (1988)		
Clark	Snake Creek	Duck Oil	Smith #1-30-34-21	30	34.5	21.5 W	5488	-3643	87.8	5.1	2.6	0.8	0.5	0.2	0.106	(not given)	(not given)	0.000	0.153	3.100	0.008	0.191	0.038	1050	0.648	Moore and others (1988)		
Clark	Snake Creek W	Galvan-McKendrick Drilling	Randall #1-11	11	34.5	22.5 W	5378	-3529	83.6	5.1	2.5	0.8	0.5	0.2	0.1	0.1	0.1	0.1	3.9	0.12	trace	0.0	0.2	0.0	1138	0.645	Moore and Hamak (1985)	
Clark	McKinney	Calvin Exploration	Herrington #1-30	30	34.5	25.5 W	5802	-3690											0.1	6.6	0.18	trace	0.0	0.2	0.0	1069	0.663	Moore and Shrevebury (1966)
McKinney	McKinney	Dehti Oil	McKinney "C" #1	23	34.5	26.5 W	5857	-3600																	1096	(not given)	scout cards	
McKinney	McKinney	Skelly Oil	McKinney "C" #1	23	34.5	26.5 W	5815	-3705	78.4	6.6	4.9	1.7	1.2	0.3	0.1	0.1	0.1	0.1	6.3	0.20	0.0	0.0	0.2	0.0	1135	(not given)	WHCS	
McKinney	McKinney	O'Brien-Barry #2-32	Adam #1-33	32	34.5	27.5 W	5944	-3707																	1150	(not given)	Muneflyn and Miller (1963)	
McKinney	McKinney	Mesa Petroleum	Adams #1-33	33	34.5	29.5 W	5896	-1432	82.9	6.6	4.4	1.2	0.5	0.3	0.4	0.1	0.2	0.1	3.1	0.12	trace	0.0	0.1	0.0	1172	0.689	Scout cards	
McKinney	McKinney	Anadarko Production	Powell "D" #1	26	34.5	34.5 W	6098	-3182	80.3	4.6	2.6	0.8	0.4	0.3	0.4	0.1	0.3	0.9	0.17	trace	0.0	0.1	0.0	1054	0.685	Moore (1977)		
Seward	Archer	Donald C. Slavson	Liberal #1-36	36	34.5	34.5 W	6230	-3337																	1054	0.685	Moore (1981)	
Seward	Liberal W	Northrup Pump	Liberal Airport #6	36	34.5	34.5 W	6185	-3289																	(not given)	0.672	scout cards	
Seward	Liberal W	Cities Service	Clodfelder "A" #2	14	34.5	35.5 W	6144	-3150	79.9	0.3	0.1	0.0	0.0	0.0	0.0	0.0	0.0	0.0	18.7	0.65	0.1	0.2	0.0	0.0	818	0.654	scout cards	
Stevens	Stevens	Cities Service	Baughman "G" #2	19	34.5	35.5 W	6218	-3179	91.8	0.1	0.0	0.0	0.0	0.0	0.0	0.0	0.0	0.0	0.1	7.3	0.31	0.1	0.2	0.0	0.0	940	0.631	Hamak and Sgier (1991)
Stevens	Stevens	Oxy U.S.A.	Wonder "A" #2	29	34.5	35.5 W	6264	-3235	87.7	5.0	2.1	0.6	0.4	0.1	0.2	0.0	0.1	0.1	3.6	0.16	trace	0.0	0.0	0.0	1081	0.637	Hamak and Sgier (1991)	
Stevens	Stevens	Terol Energy	Kraus #2-4A	20	34.5	36.5 W	6278	-3174																	(not given)	0.65	scout cards	
Stevens	Stevens	Mobil Oil	Parker Estate #4-S	32	34.5	36.5 W	6314	-3223	85.0	4.6	2.8	0.8	0.6	0.2	0.3	0.2	0.2	0.1	5.1	0.21	trace	0.0	0.0	0.0	1097	0.663	scout cards	
Stevens	Stevens	Mobil Oil	Peachey #1 Unit Well #2	24	34.5	37.5 W	6317	-3192	72.9	7.6	4.0	1.0	0.7	0.2	0.1	0.1	0.1	0.1	12.5	0.72	0.1	0.0	0.1	0.0	1054	0.717	Moore and Shrevebury (1966)	
Stevens	Stevens	Anadarko Petroleum	Kelly #D-1	22	34.5	39.5 W	5976	-2692	78.1	7.2	4.3	1.2	0.6	0.7	0.0	0.0	0.0	0.0	6.8	0.17	trace	0.0	0.0	0.0	1143	0.717	Moore and Shrevebury (1966)	
Stevens	Stevens	Cities Service	Webb #A-2	28	34.5	41.5 W	4930	-1489	80.2	6.9	4.3	1.0	0.6	0.2	0.2	0.0	0.0	0.0	4.0	0.20	trace	0.0	0.0	0.0	1124	0.890	Muneflyn and Miller (1963)	
Morton	Taloga	Cities Service	Stewart #A-1	29	34.5	41.5 W	4822	-1363	82.8	7.0	3.9	0.9	0.6	0.1	0.2	0.0	0.0	0.0	4.0	0.20	trace	0.0	0.0	0.0	1135	0.676	Muneflyn and Miller (1963)	
Morton	Taloga	Colorado O&G	Government #1-9	9	34.5	42.5 W	4280	-838	73.7	5.8	4.0	0.9	0.4	0.2	0.2	0.0	0.0	0.0	14.0	0.40	trace	0.0	0.1	0.0	1020	0.712	Moore and Shrevebury (1968)	
Morton	Taloga	Cities Service	Hamilton "B" #2	27	34.5	42.5 W	4550	-1040																	997	(not given)	WHCS	
Morton	Taloga	Panhandle Eastern	Riley #1-27	27	34.5	42.5 W	4501	-982	72.7	4.8	4.4	2.8	1.3	1.4	1.3	0.6	0.1	0.1	6.9	0.85	trace	0.1	0.7	0.0	1321	0.829	Cardwell and Benton (1970a)	
Morton	Taloga	Colorado O&G	Central Life #1-34	34	34.5	42.5 W	4424	-882	80.9	3.9	2.5	0.8	0.4	0.3	0.4	0.3	0.1	0.1	8.8	1.10	trace	0.2	0.4	0.0	1042	(not given)	Muneflyn and Miller (1963)	
Morton	Taloga	Colorado O&G	Central Life #1-34	34	34.5	42.5 W	4424	-882	80.9	3.9	2.5	0.8	0.4	0.3	0.4	0.3	0.1	0.1	8.8	1.08	trace	0.2	0.4	0.0	1042	0.673	Boone (1958)	
Morton	Taloga	Panhandle Eastern	Hill #D-1	35	34.5	42.5 W	4644	-1133																	1142	(not given)	WHCS	
Morton	Taloga	Panhandle Eastern	Watson #2-35	35	34.5	42.5 W	4182	-661	81.9	7.0	2.5	1.2	0.5	0.4	0.4	0.1	0.2	0.1	4.5	0.20	trace	0.2	0.8	0.1	1128	0.685	Muneflyn and Miller (1963)	
Morton	Greenwood Gas Area	Cities Service	Interstate #A-1	19	34.5	43.5 W	4238	-729	73.0	5.8	4.5	1.0	0.5	0.3	0.1	0.1	0.1	0.1	13.7	0.73	trace	0.0	0.1	0.0	1038	0.717	Boone (1958)	
Morton	Greenwood Gas Area	Cities Service	Interstate #A-1	19	34.5	43.5 W	4238	-729	72.1	6.1	4.9	1.1	0.5	0.4	0.1	0.1	0.1	0.1	13.8	0.70	0.0	0.0	0.0	0.0	1063	0.732	Boone (1958)	
Comanche	Tuttle E	Sinclair O&G	Alexander #1	4	35.5	20.5 W	5461	-3715	91.4	3.5	1.3	0.8	0.3	0.2	0.2	0.2	0.6	1.4	0.10	trace	0.0	0.2	0.0	1108	0.632	Miller and Norrell (1965)		
Comanche	Tuttle SE	Roberts & Murphy	Box Ranch #1-14	16	35.5	20.5 W	5324	-3587																	(not given)	0.67	scout cards	
Comanche	Tuttle SE	Midcontinent Energy	Box Ranch #1	14	35.5	20.5 W	5650	-3805																	0.67	Moore (1980)		
Clark	Snake Creek	Snake Creek	Snake Creek	13	35.5	21.5 W	5625	-3712	89.0	4.5	2.1	0.7	0.5	0.3	0.2	0.1	0.1	0.1	3.0	0.11	trace	0.0	0.3	0.0	1077	0.612	Moore (1980)	
Clark	Snake Creek	Kennedy & Mitchell	Tuttle #1-116	13	35.5	21.5 W	5577	-3779	89.6	3.5	1.5	0.5	0.3	0.2	0.2	0.1	0.3	0.2	3.0	0.11	trace	0.0	0.2	0.0	1103	0.648	Moore and Shrevebury (1968)	
Clark	Clark Creek	Robert L. Hayne	Tuttle #2	8	35.5	22.5 W	5707	-3728	87.8	4.7	2.2	0.6	0.4	0.1	0.3	0.1	0.2	0.1	4.0	0.11	0.0	0.0	0.1	0.0	1119	0.635	Moore (1975)	
Clark	Clark Creek	Pure Oil	C.H. Tuttle "D" #1	8	35.5	22.5 W	5577	-3736	86.1	4.9	2.5	0.8	0.7	0.1	0.3	0.1	0.3	3.6	0.10	0.0	0.0	0.0	0.0	0.0	1113	0.652	Muneflyn and Miller (1963)	
Meade	McKinney	Zinke & Tumbao	Minne Wyatt "C" #1-4	4	35.5	26.5 W	6002	-3761																	(not given)	0.80	scout cards	
Meade	McKinney	Donald C. Slavson	Wyatt #1-4	4	35.5	26.5 W	6018	-3743																	(not given)	0.70	scout cards	
Meade	McKinney	Zinke & Tumbao	Edgar #1-5	5	35.5	26.5 W	5910	-3739																	(not given)	0.80	scout cards	
Meade	McKinney	Zinke & Tumbao	Edgar #1-5	5	35.5	26.5 W	5895	-3730																	(not given)	0.688	scout cards	
Meade	McKinney	Mesa Petroleum	Barragee #1-8	8	35.5	28.5 W	5955	-3521	85.8	5.5	2.8	0.8	0.3	0.2	0.3	0.1	0.2	0.1	3.7	0.16	trace	0.0	0.1	0.0	1113	0.658	Moore (1977)	
Meade	McKinney	Thomas & Brewer O&G	Adams #E-1	10	35.5	30.5 W	5754	-3311	87.5	6.0																		

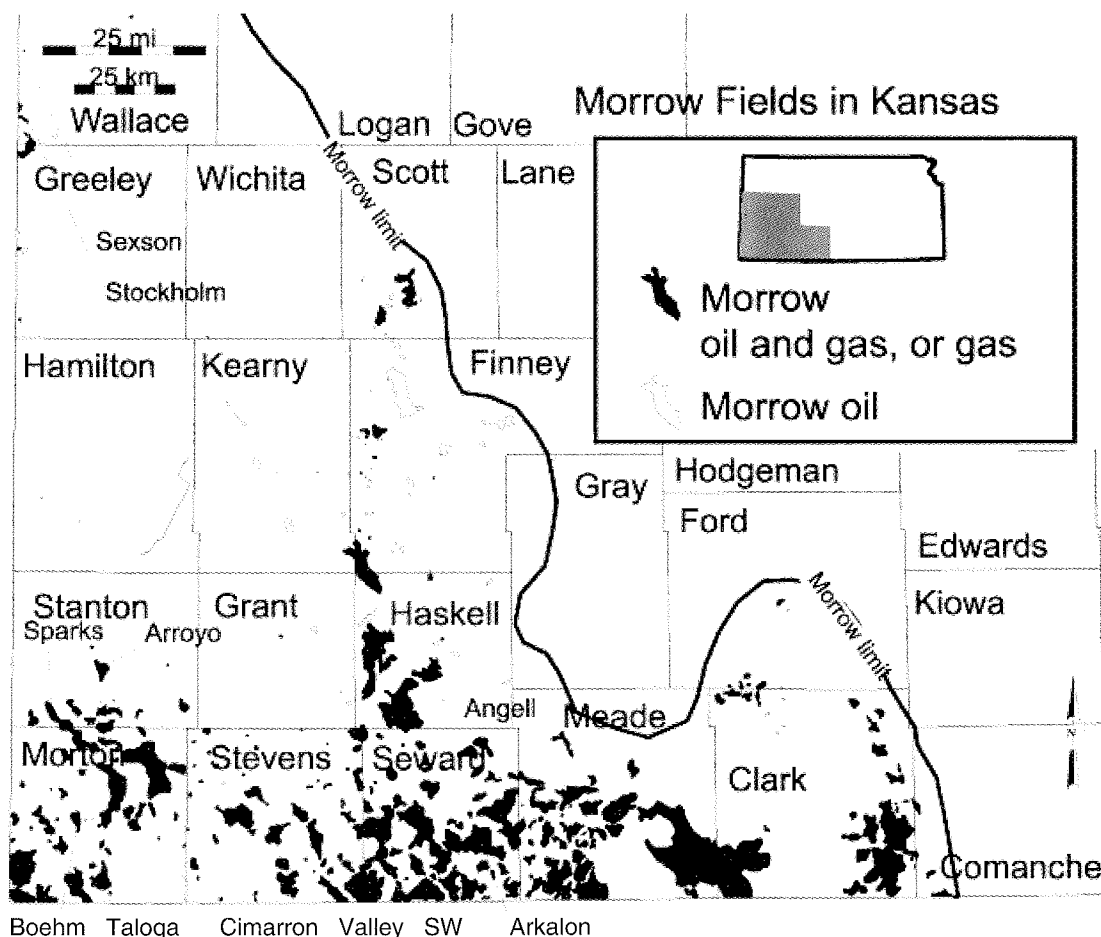


Figure 1. Map of Morrowan oil and gas fields in southwestern Kansas (from Carr and others, 1993), with limit line for Morrowan strata. Morrowan oil and gas fields specifically discussed in this article are shown on this map.

MORROW OIL AND GAS IN KANSAS

Morrowan fields are limited to the Hugoton Embayment of the Anadarko Basin in southwestern Kansas (Fig. 1). In the last decade, sandstone reservoirs in the Morrow Formation, mostly in interpreted incised valley fills, have been profitable exploration targets (Watney and others, 2008). In general, these fields produce both oil and gas, but the gas component appears to decrease northward, for along the northern limit of Morrowan fields in Kearny and Finney Counties, oil fields mostly are the norm (Fig. 1).

Morrowan rocks in southwestern Kansas lie at depths >5,500 ft (Table 1). Gas production is from both nonassociated (gas only) pay zones and pay zones associated with oil (either as a gas cap or solution gas), usually from sandstones informally identified as the Keyes sandstone of the Lower Pennsylvanian Kearny Formation.

HYDROCARBON GAS COMPOSITIONAL CHARACTERISTICS

BTU content (heating value) is a summation of all the hydrocarbon components in a natural gas—methane (CH_4 ,

1,057 BTU/scf); ethane (C_2H_6 , 1,847 BTU/scf); propane (C_3H_8 , 2,639 BTU/scf); *n*- and *i*-butane (C_4H_{10} , ~3,415 BTU/scf); *n*-, *i*-, and *c*-pentane (C_5H_{12} , ~4,215 BTU/scf); and hexane (C_6H_{14}) and heavier hydrocarbons (~4,965 BTU/scf). Any noncombustible components (e.g., nitrogen, argon, helium, carbon dioxide) will serve to decrease the heating value. A natural gas composed entirely of methane would have a heating value of 1,057 BTU/scf, so any natural gas with a heating value >1,057 BTU/scf will have higher molecular weight hydrocarbon gases present.

COMPOSITION OF GASES IN THE MORROW FORMATION

Gas produced in Morrowan fields in Kansas is generally of acceptable pipeline quality, with 95% of the analyses having heating values >950 BTU/scf (Fig. 2). The 950 BTU/scf value is a critical cutoff value, for this is usually considered the minimum quality necessary for pipeline sale without penalty.

Mapping BTU contents of Morrowan gases (Fig. 3) indicates that gases with higher BTUs are slightly more abundant along the Kansas–Oklahoma state line than they are farther

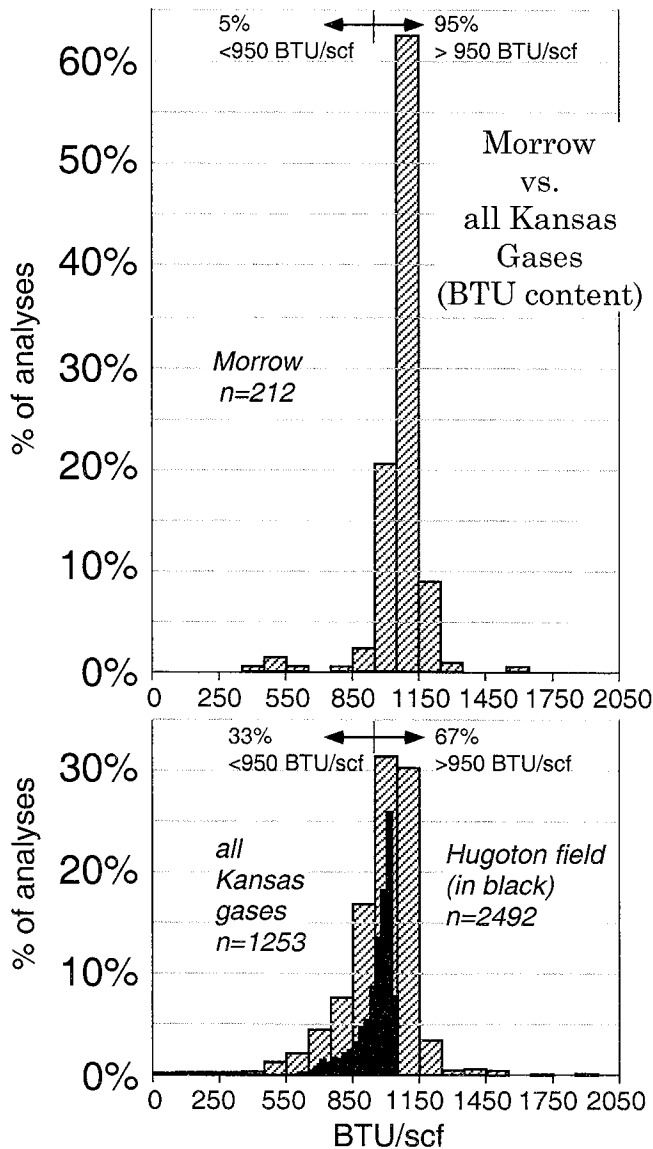


Figure 2. Histograms of the heating values recorded for Morrowan gases, as compared to Kansas gases (based on unpublished data compiled by K. D. Newell). Morrowan gases generally are of quality, with 95% of these gases having heating values >950 BTU/scf. Only 67% of Kansas gases record heating values of >950 BTU/scf. Hugoton Gas Field data are from Wilkonson (1960).

north. Lower BTU contents seem more common in natural gases produced in Stanton and Haskell Counties (cf. Figs. 1, 3). These areas may be near the distal ends of any migration paths if hydrocarbons are generally migrating northward out of more thermally mature and deeper buried Morrowan strata farther south in Oklahoma.

BTU content is a summation of all the percentages and types of component gases in a natural gas. Generally, a greater proportion of higher molecular weight hydrocarbons present in a natural gas will increase its heating value. The proportion

of higher molecular weight hydrocarbons in a natural gas is expressed by the hydrocarbon wetness of the gas, which is a ratio of methane to the total hydrocarbons in the gas, subtracted from 1, and expressed as a percentage (Schoell, 1983). Mapping hydrocarbon wetness in Morrowan gases (Fig. 4) indicates that wetter gases are more common in extreme southwestern Kansas in Morton and Stanton Counties. This trend of wetness may extend eastward into northern Stevens County, northern Seward County, and Haskell County. The increase in wetness may be an artifact of maturation and migration in that drier gases (i.e., more methane-rich gases) will dominate in gas accumulations having their source in strata with greater thermal maturation. These drier gases, generated in and migrated out of a hydrocarbon "kitchen," will displace earlier formed (and wetter components) toward the distal parts of a migration path, particularly if traps are charged by a "fill-and-spill" type of hydrocarbon movement (see Gussow, 1954). In eastern Clark County, drier gases are present close to the zero line of Morrowan strata. The reason for this pattern is unclear, but perhaps post-accumulation processes may have removed some of the ethane and heavier components of these natural gases.

NONCOMBUSTIBLE GAS CHARACTERISTICS

The major noncombustible gas that dilutes the hydrocarbon component in Morrowan gases is nitrogen (Table 1), but other gases such as argon, carbon dioxide, and helium also dilute the hydrocarbon component. Total nonhydrocarbon gases in Morrowan fields in Kansas (Fig. 5) show that these noncombustible gases compose a significant percentage (>15%) of natural gases in Stanton and Morton Counties. This region of a high percentage of noncombustible gas may extend eastward through northern Stevens County and southern Haskell County.

Nitrogen occurs in a nearly fixed ratio to helium in many gas fields in Kansas (Jenden and others, 1988). A crossplot of nitrogen percentage and helium percentage (Fig. 6) shows that Morrowan gases have highly variable nitrogen-to-helium ratios in comparison to the Permian gas produced from the overlying giant Hugoton Gas Field and other, smaller Permian gas fields east of the Hugoton Field. This likely indicates multiple sources or a more diverse or complex post-accumulation history for Morrowan gas fields, or a combination thereof.

A map of the nitrogen-to-helium ratios for Morrowan fields in Kansas (Fig. 7) shows that lower nitrogen-to-helium ratios characterize the fields along the extreme western part of the state in Stanton and Morton Counties and in western Stevens County. No obvious geological characteristic accounts for this, but the lower nitrogen-to-helium ratios and the relatively high percentages of helium in fields in this region may facilitate relatively easier extraction of helium.

Individual Morrowan fields have less variable nitrogen and helium gas contents (Fig. 8) in comparison to the entire spread of data for all the Morrowan fields. Fields in the same vicinity, such as the Boehm, Cimarron Valley SW, Sparks, and Arroyo Fields in Morton and Stanton Counties (see Fig.

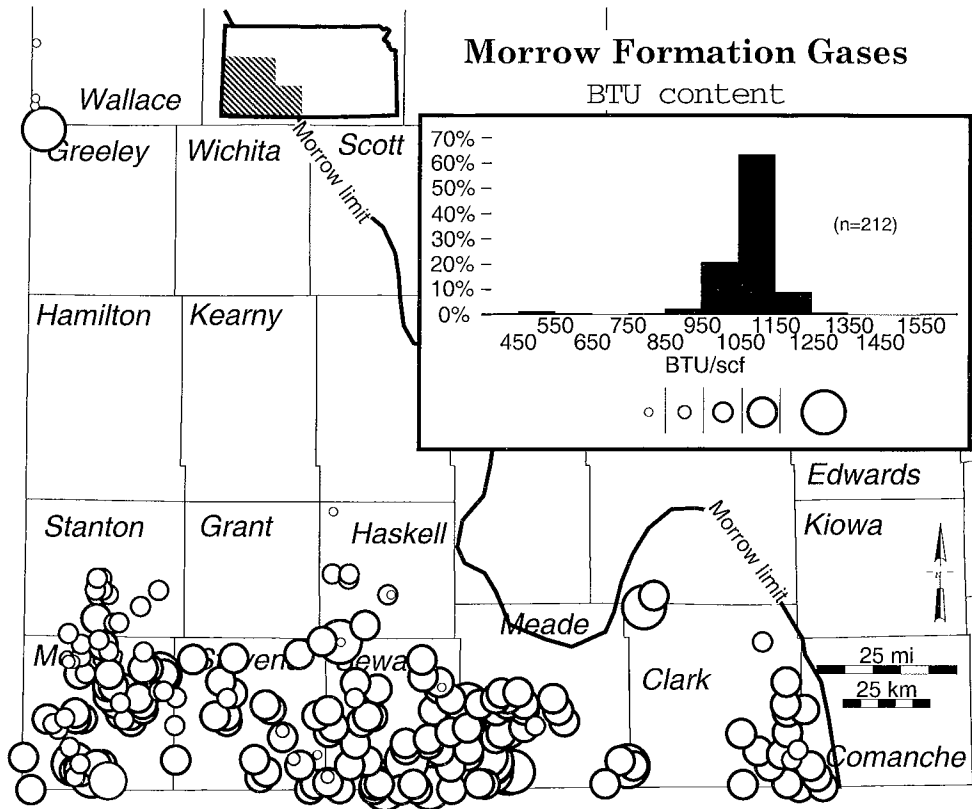


Figure 3. Map of BTU content (heating value) of Morrowan gases in southwestern Kansas. Diameter of circle corresponds to BTU content. A histogram of BTU content (superimposed on map) shows that almost all Morrow gases have >950 BTU/scf. This value is usually considered the minimum BTU content accepted by pipeline companies before any penalties are assessed.

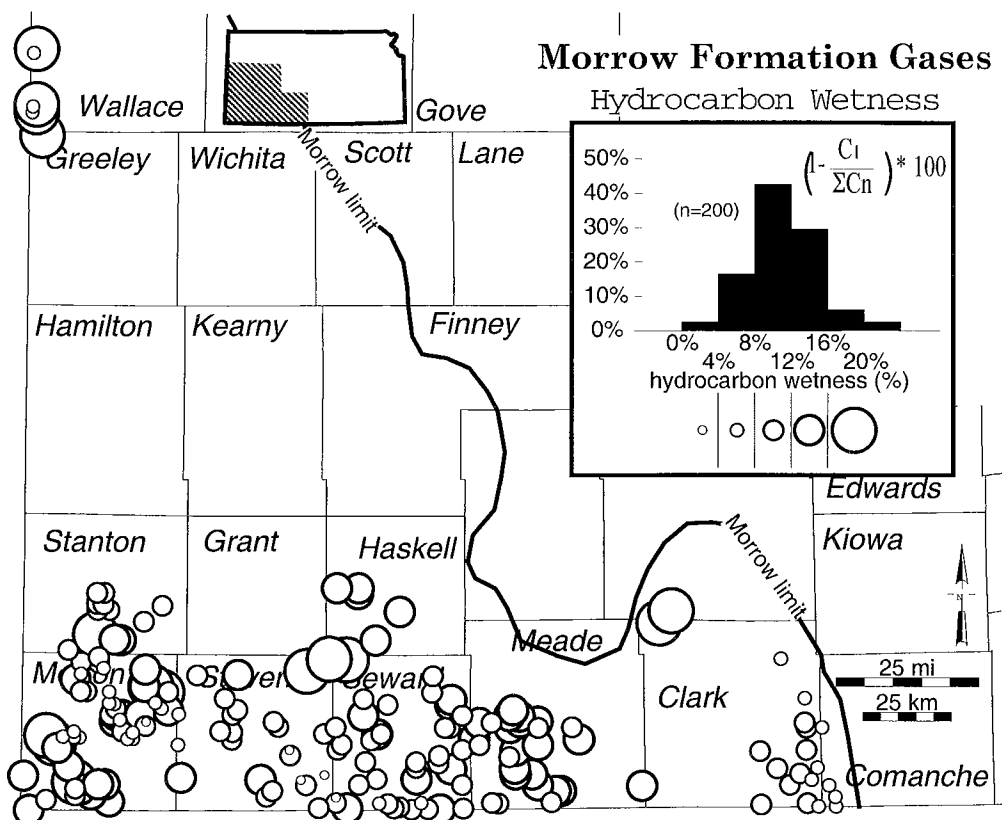


Figure 4. Map of hydrocarbon wetness of Morrowan gases in southwestern Kansas. Diameter of circle corresponds to hydrocarbon wetness. A histogram of hydrocarbon wetness (superimposed on map) shows that average wetness is between 8 and 12%.

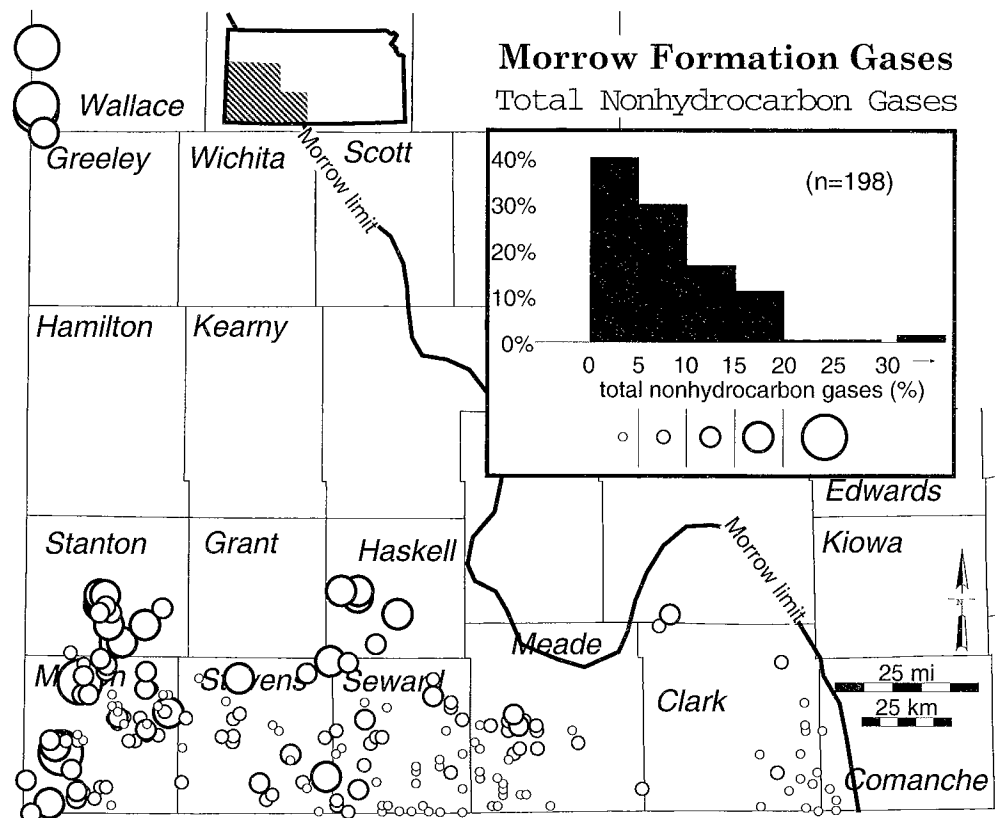


Figure 5. Map of total nonhydrocarbon gases in Morrowan natural gases in southwestern Kansas. Diameter of circle corresponds to percentage of nonhydrocarbon gas. A histogram (superimposed on map) shows that most Morrowan fields have <10% nonhydrocarbon gases.

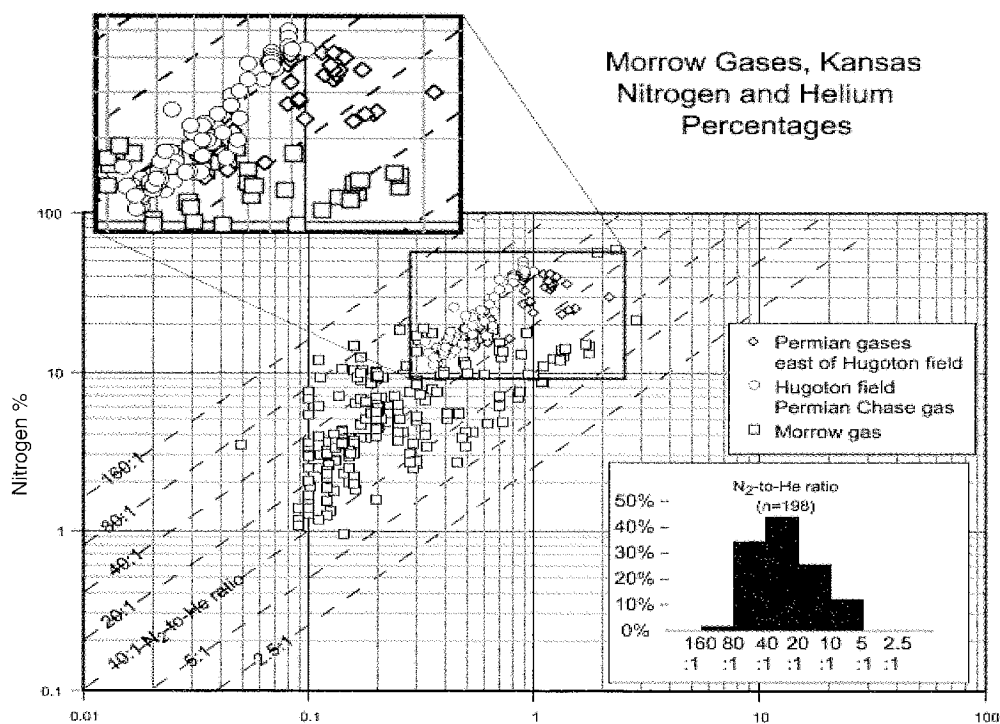


Figure 6. Crossplot of nitrogen and helium percentages of Morrowan gases in southwestern Kansas. Both axes are logarithmic. Morrowan gases have highly variable nitrogen-to-helium ratios in comparison to Permian gas produced from the overlying Hugoton Gas Field.

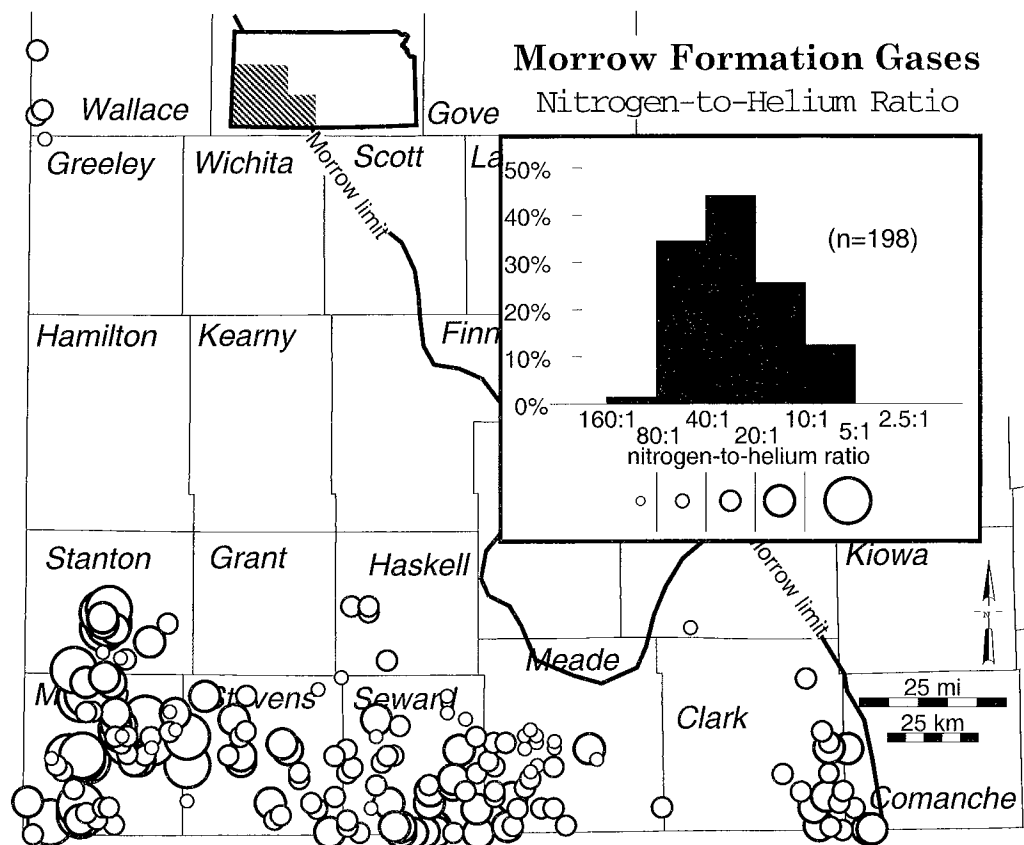


Figure 7. Map of nitrogen-to-helium ratios for Morrowan gases in southwestern Kansas. Diameter of circle corresponds to the ratio, with the larger circle corresponding to higher relative helium content (i.e., a lower nitrogen-to-helium ratio). A histogram of nitrogen-to-helium ratios (superimposed on map) shows that the average ratio is between 40:1 and 20:1.

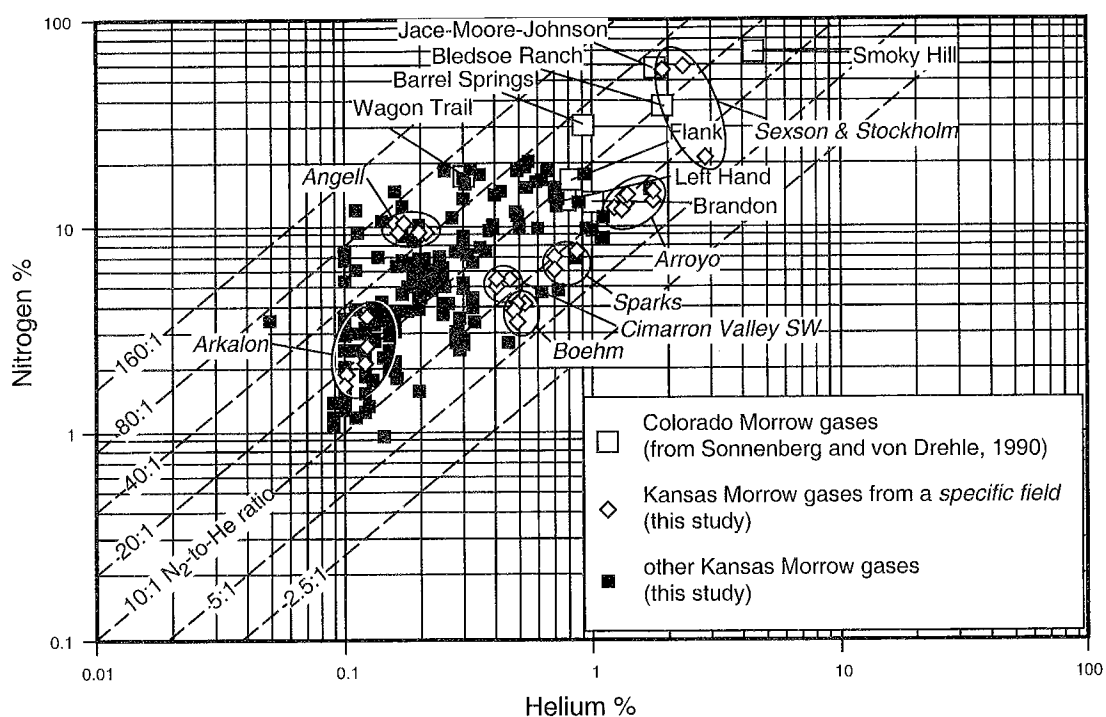


Figure 8. Crossplot of nitrogen and helium percentages from Figure 5, but with data from individual fields highlighted. Data added for Colorado Morrowan gases (from Sonnenberg and von Drehle, 1990).

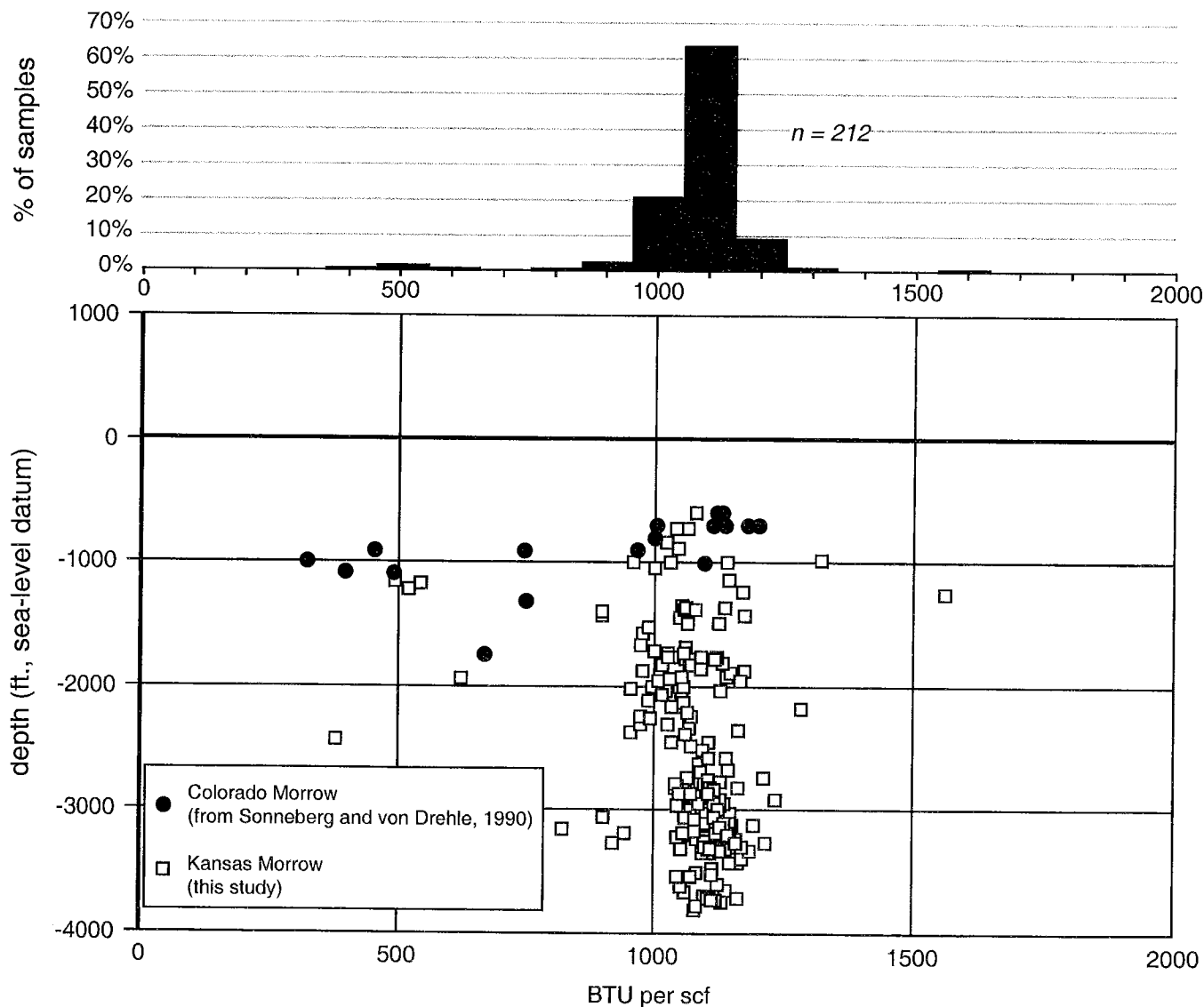


Figure 9. Crossplot of BTU content versus depth for Morrowan natural gases in southwestern Kansas. A slight increase in heating content with depth is observable in Kansas Morrowan gases. A decrease in heating content with depth observed by Sonnenberg and von Drehle (1990) in Morrowan gases in Colorado is not evident for Morrowan gases in Kansas.

1) have similar nitrogen-to-helium ratios, but with consistent northward increases in the percentages of these two gases (Fig. 9). This implies that the hydrocarbon gases in these Morrowan natural gases are essentially decreasing northward and are possibly mixing with successively higher percentages of a nitrogen-helium gas of constant composition.

Nitrogen and helium percentages reported for Morrowan fields in Colorado (from Sonnenberg and von Drehle, 1990) are generally greater than those for the Kansas Morrow fields (see Fig. 8). Sonnenberg and von Drehle (1990) also conclude that gases with relatively higher BTU content are present on the crest of the Las Animas Arch in southeastern Colorado and that lower BTU gases are on the flanks of this arch. This pattern apparently is more complicated in Kansas, for the

heating values of Morrow gases in Kansas weakly increase with depth (Fig. 9).

A nitrogen-percentage-depth crossplot (Fig. 10) shows that the nitrogen percentage in Kansas Morrowan gases decreases overall with depth and likely accounts for some of the increase in BTU content that is observable with increasing depth (see Fig. 9). A data outlier of high-nitrogen gases, corresponding to the Sexson and Stockholm Fields in Wallace County far north of most of the Morrow production in Kansas (see Fig. 1), implies that these two fields have a nitrogen origin that is different from other Kansas Morrowan fields. Hydrocarbon wetness, crossplotted with depth (Fig. 11), also shows that Morrowan natural gases have a highly variable hydrocarbon wetness with depth, but perhaps a slight decrease in hydro-

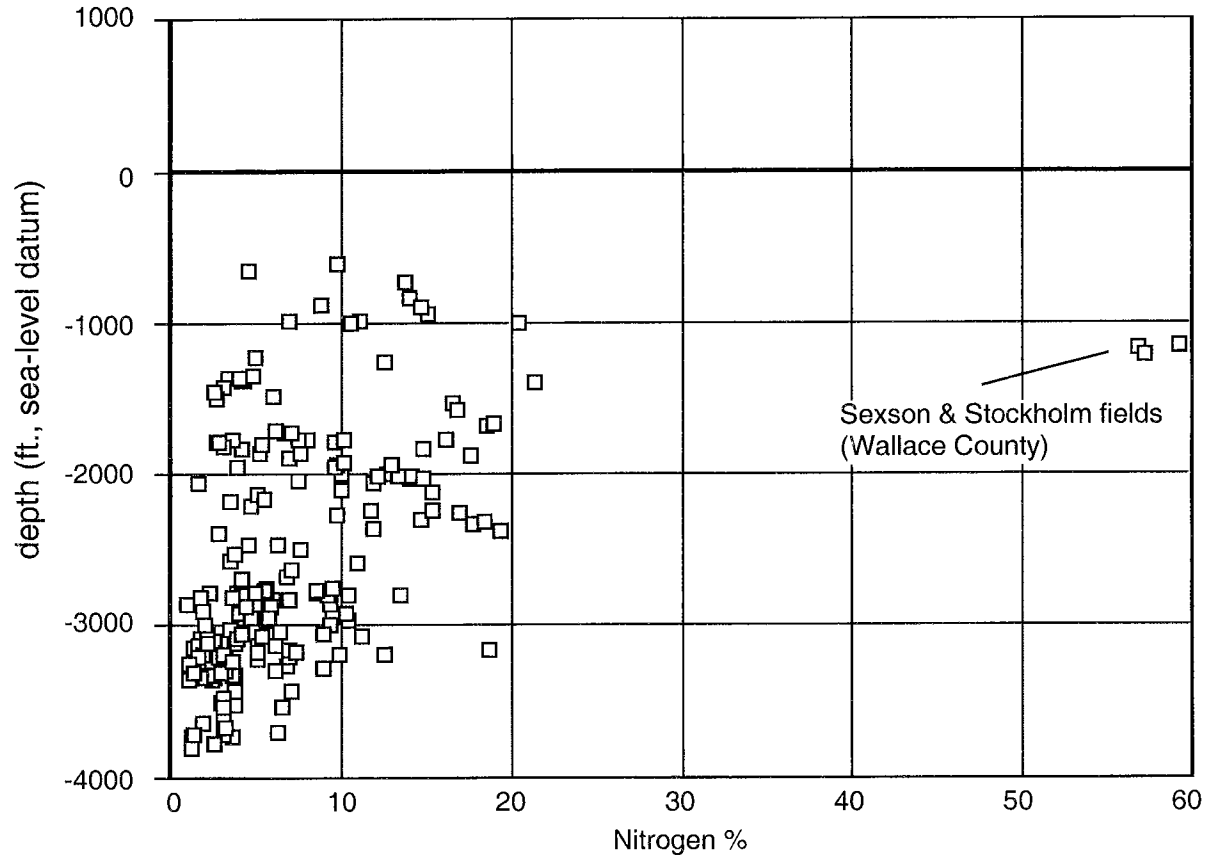


Figure 10. Crossplot of nitrogen content versus depth for Morrowan natural gases in southwestern Kansas. A general decrease in percentage of nitrogen and scatter occurs with increasing depth.

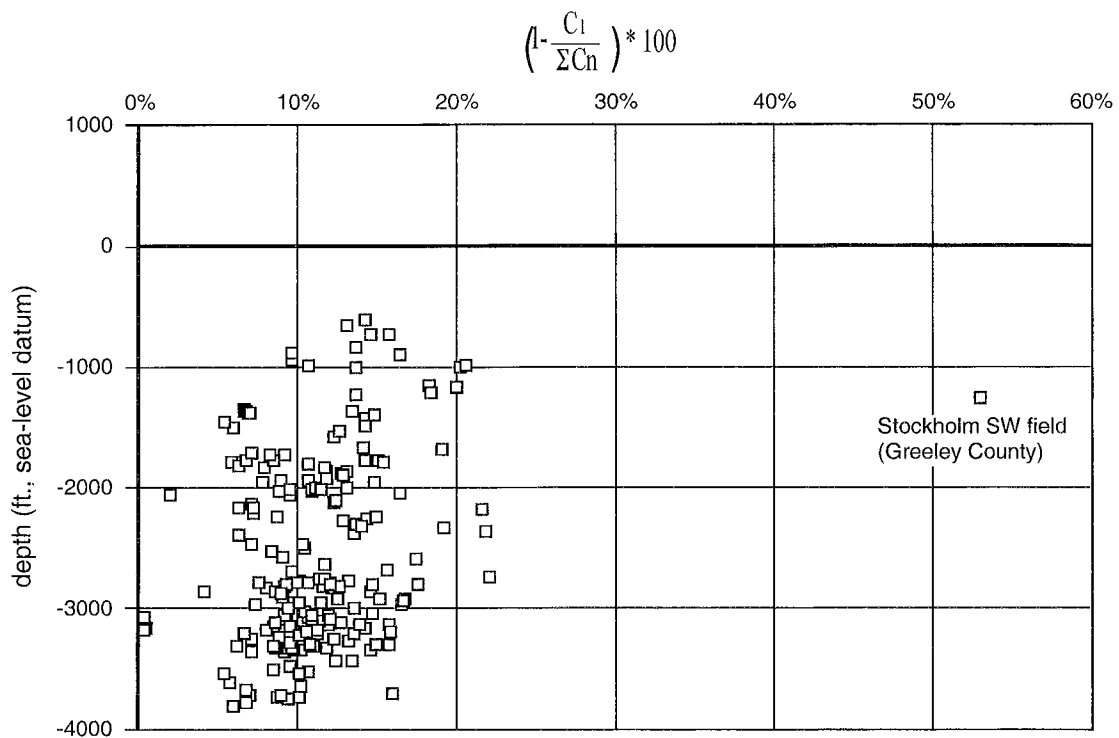


Figure 11. Crossplot of hydrocarbon wetness versus depth for Morrowan natural gases in southwestern Kansas. Less scatter and a slight decrease in hydrocarbon wetness with depth are indicated.

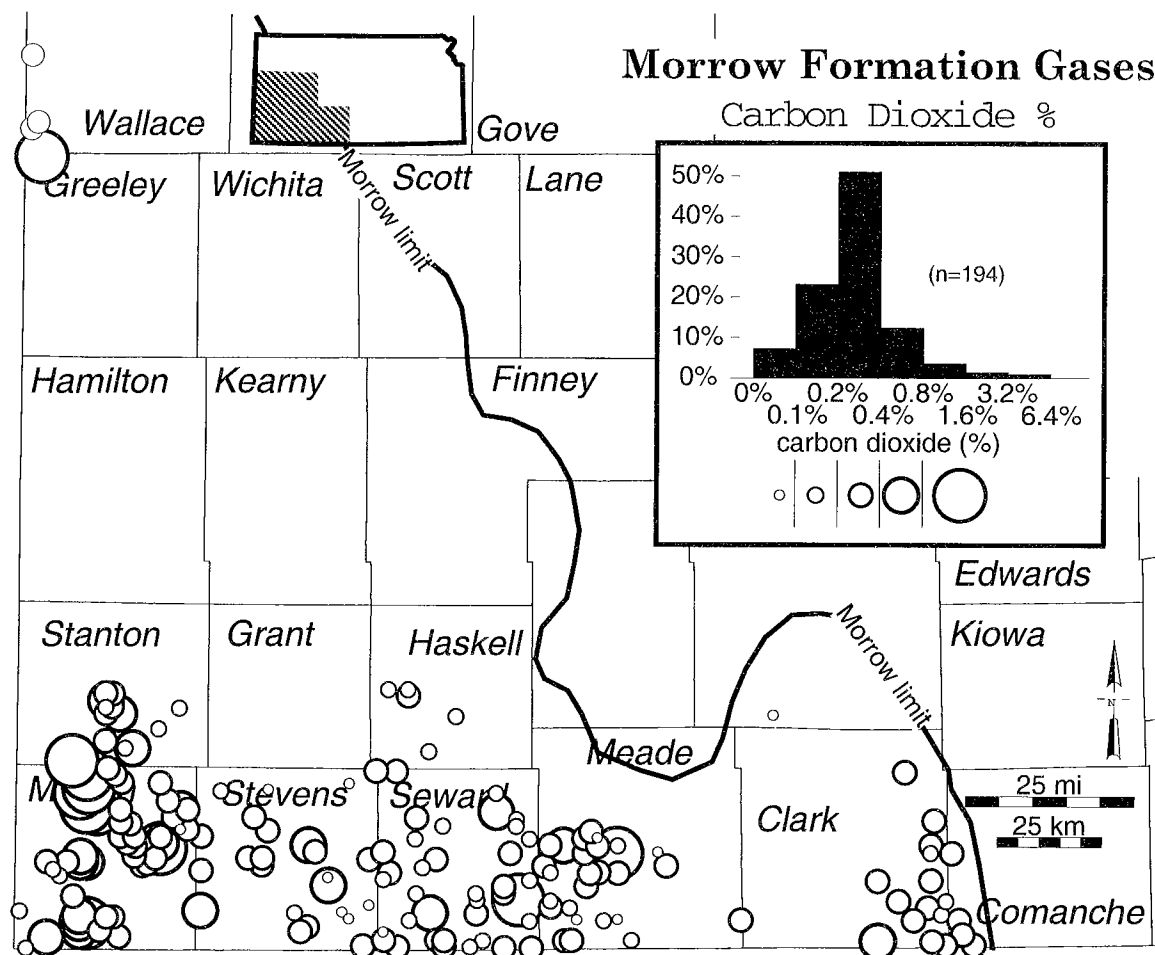


Figure 12. Map showing carbon dioxide percentages for Morrowan gases in southwestern Kansas. Diameter of circle corresponds to percentage of carbon dioxide. A histogram of CO_2 percentages (superimposed on map) shows that most fields have CO_2 contents between 0.2 and 0.4%.

carbon wetness with depth is evident. This may be a reflection of higher thermal maturation with depth.

Carbon dioxide (CO_2) is another major noncombustible gas that can decrease heating value. CO_2 , if present in sufficient quantities, can complicate acceptance of a natural gas into a pipeline system (usually by formation of dry ice, which can clog valves). A map of CO_2 percentages in Kansas (Fig. 12) shows that fields farther west in Kansas along the Morton-Stanton county line have higher CO_2 content but that most Morrowan fields in Kansas have relatively low CO_2 percentages (i.e., <0.4%). These fields in far western Kansas that have relatively high CO_2 percentages are also characterized by relatively low nitrogen-to-helium ratios (see Fig. 7), but there is no obvious geological explanation for these characteristics. The Sparks Field, which straddles the Morton-Stanton county line, contains >3% CO_2 .

SUMMARY

Several regional and local trends in gas composition can be discerned for Morrowan gases in southwestern Kansas. Morrowan oil and gas fields have gas/oil ratios that increase southward. In general, these gases are of a quality that is accept-

able to pipelines (i.e., >950 BTU/scf). The nitrogen content in these gases decreases southward and with increasing depth. Although hydrocarbon wetness also decreases with increasing depth (thus, there are fewer higher BTU components in the natural gas with increasing depth), the decrease in nitrogen with increasing depth dominates so that Morrowan natural gases generally have higher BTU contents with depth. Nitrogen-to-helium ratios and CO_2 contents are locally variable, but regionally, nitrogen-to-helium ratios decrease westward, and CO_2 contents increase westward.

ACKNOWLEDGMENTS

The author thanks Daniel F. Merriam and W. Matt Brown of the Kansas Geological Survey for critically reading the manuscript.

REFERENCES CITED

- Boone, W. J., Jr., 1958, Helium-bearing natural gases of the United States, analyses and analytical methods; supplement to Bulletin 486: U.S. Bureau of Mines Bulletin 576, 117 p.

- Cardwell, L. E.; and Benton, L. F., 1970a, Analyses of natural gases, 1968: U.S. Bureau of Mines Information Circular 8443, 169 p.
- 1970b, Analyses of natural gases, 1969: U.S. Bureau of Mines Information Circular 8475, 134 p.
- 1971, Analyses of natural gases, 1970: U.S. Bureau of Mines Information Circular 8518, 130 p.
- 1972, Analyses of natural gases, 1971: U.S. Bureau of Mines Information Circular 8554, 163 p.
- 1973, Analyses of natural gases, 1972: U.S. Bureau of Mines Information Circular 8607, 104 p.
- Carr, T. R.; Ross, J. A.; and Beene, D. L., 1993, Producing horizons of oil and gas fields in Kansas: Kansas Geological Survey Map Series M35, scale 1:250,000.
- Doyel, D., 1985, Norcan field, in Kansas oil and gas fields, v. 5: Kansas Geological Society, Wichita, p. 215–222.
- Gage, B. D.; and Driskill, D. L., 1998, Analyses of natural gases: U.S. Department of the Interior, Bureau of Land Management, Technical Note 404, 71 p.
- Gussow, W. C., 1954, Differential entrapment of oil and gas; a fundamental principle: American Association of Petroleum Geologists Bulletin, v. 38, p. 816–853.
- Hamak, J. E.; and Driskill, D. L., 1996, Analyses of natural gases, 1994–95: U.S. Department of the Interior, Bureau of Land Management, Technical Note 399, 68 p.
- Hamak, J. E.; and Gage, B. D., 1992, Analyses of natural gases, 1991: U.S. Bureau of Mines Information Circular 9318, 97 p.
- Hamak, J. E.; and Sigler, S., 1991, Analyses of natural gases, 1986–90: U.S. Bureau of Mines Information Circular 9301, 315 p.
- 1993, Analyses of natural gases, 1992: U.S. Bureau of Mines Information Circular 9356, 62 p.
- Jenden, P. D.; Newell, K. D.; Kaplan, I. R.; and Watney, W. L., 1988, Composition and stable-isotope geochemistry of natural gases from Kansas, Midcontinent, U.S.A.: Chemical Geology, v. 71, p. 117–147.
- Miller, R. D.; and Hertweck, F. R., Jr., 1982, Analyses of natural gases, 1981: U.S. Bureau of Mines Information Circular 8890, 84 p.
- 1983, Analyses of natural gases, 1982: U.S. Bureau of Mines Information Circular 8942, 100 p.
- Miller, R. D.; and Norrell, G. P., 1964a, Analyses of natural gases of the United States, 1961: U.S. Bureau of Mines Information Circular 8221, 148 p.
- 1964b, Analyses of natural gases of the United States, 1962: U.S. Bureau of Mines Information Circular 8239, 120 p.
- 1965, Analyses of natural gases of the United States, 1963: U.S. Bureau of Mines Information Circular 8241, 102 p.
- Moore, B. J., 1974, Analyses of natural gases, 1973: U.S. Bureau of Mines Information Circular 8658, 96 p.
- 1975, Analyses of natural gases, 1974: U.S. Bureau of Mines Information Circular 8684, 122 p.
- 1976, Analyses of natural gases, 1975: U.S. Bureau of Mines Information Circular 8717, 82 p.
- 1977, Analyses of natural gases, 1976: U.S. Bureau of Mines Information Circular 8749, 93 p.
- 1978, Analyses of natural gases, 1977: U.S. Bureau of Mines Information Circular 8780, 95 p.
- 1979, Analyses of natural gases, 1978: U.S. Bureau of Mines Information Circular 8810, 113 p.
- 1980, Analyses of natural gases, 1979: U.S. Bureau of Mines Information Circular 8833, 100 p.
- 1981, Analyses of natural gases, 1980: U.S. Bureau of Mines Information Circular 8856, 236 p.
- 1982, Analyses of natural gases, 1977–80: U.S. Bureau of Mines Information Circular 8870, 1055 p.
- Moore, B. J.; and Hamak, J. E., 1985, Analyses of natural gases, 1984: U.S. Bureau of Mines Information Circular 9046, 102 p.
- Moore, B. J.; Miller, R. D.; and Shrewsbury, R. D., 1966, Analyses of natural gases of the United States, 1964: U.S. Bureau of Mines Information Circular 8302, 144 p.
- Moore, B. J.; and Shrewsbury, R. D., 1966, Analyses of natural gases of the United States, 1965: U.S. Bureau of Mines Information Circular 8316, 181 p.
- 1967, Analyses of natural gases, 1966: U.S. Bureau of Mines Information Circular 8356, 130 p.
- 1968, Analyses of natural gases, 1967: U.S. Bureau of Mines Information Circular 8395, 187 p.
- Moore, B. J.; and Sigler, S., 1986, Analyses of natural gases, 1985: U.S. Bureau of Mines Information Circular 9096, 182 p.
- Munnerlyn, R. D.; and Miller, R. D., 1963, Helium-bearing natural gases of the United States, analyses; second supplement to Bulletin 486: U.S. Bureau of Mines Bulletin 617, 93 p.
- Rupp, G. E., 1959, Sparks field, in Kansas oil and gas fields, v. 2 (western Kansas): Kansas Geological Society, Wichita, p. 168–173.
- Schoell, M., 1983, Genetic characterization of natural gases: American Association of Petroleum Geologists Bulletin, v. 67, p. 2225–2238.
- Sigler, S. M., 1994, Analyses of natural gases, 1993: U.S. Bureau of Mines Information Circular 9400, 58 p.
- Sonnenberg, S. A.; and von Drehle, W. F., 1990, Morrow gas composition in southeast Colorado, in Sonnenberg, S. A.; Shannon, L. T.; Rader, K.; von Drehle, W. F.; and Martin, G. W. (eds.), Morrow sandstones of southeast Colorado and adjacent areas: Rocky Mountain Association of Petroleum Geologists, Denver, p. 233–235.
- Strohmeier, R. C., 1959, Hawks field, in Kansas oil and gas fields, v. 2 (western Kansas): Kansas Geological Society, Wichita, p. 40–42.
- Watney, W. L.; Bhattacharya, Saibal; Byrnes, Alan; Doveton, John; and Victorine, John, 2008, Geo-engineering modeling of Morrow/Atoka incised-valley-fill deposits using Web-based freeware, in Andrews, R. D. (ed.), Morrow and Springer in the southern Midcontinent, 2005 symposium: Oklahoma Geological Survey Circular 111 [this volume], p. 121–135.
- Weaver, E. C., 1966, Air, in Clark, G. L.; and Hawley, G. G. (eds.), The encyclopedia of chemistry (2nd edition): Van Nostrand Reinhold, New York, p. 31–32.
- WHCS, 2002, Data search on gas BTUs in Well History Control System data base at the Kansas Geological Survey by Melissa Moore and Kurt Look.
- Wilkinson, L., 1960, Hugoton gas field gross heating value: Kansas Corporation Commission, FPC Docket No. AR64-1 (map, scale 1:620,500).

Depositional and Diagenetic Controls of Compartmentalization in Springer Reservoirs, Southeastern Anadarko Basin, Oklahoma

James Puckette

Oklahoma State University
Stillwater, Oklahoma

Aaron Rice

Consultant
Glenpool, Oklahoma

ABSTRACT.—The Mississippian Springer sandstones are overpressured large-volume, gas-producing reservoirs in the Anadarko Basin, Oklahoma. In the Cement area of Caddo and Grady Counties, initial production rates for individual wells exceed 10 million cubic ft of gas per day. Production and pressure data confirm the highly compartmentalized nature of these sandstones. Depositional fabric and biogenic features support the interpretation that sand deposition occurred in a shallow-marine setting. Springer sandstone bodies are distributed in linear northwest to southeast trends and exhibit cleaning-upward geometries that are typical of shallow-marine shelf/bay sand ridges. Reservoirs are more prevalent in the thicker and less silty or argillaceous sections unaffected by burrowing. Primary porosity is preserved by chamosite or chlorite grain coatings that inhibited precipitation of silica and carbonate overgrowths. Secondary porosity developed as a result of dissolution of labile grains including feldspars, fossil fragments, and polycrystalline quartz. Authigenic quartz and calcite cements occluded porosity in sandstone lacking grain-coating clays. Early calcite cement was subsequently dissolved in some settings to generate secondary porosity. Zones of near-total porosity occlusion form diagenetic seals in sandstones. These seals create intraridge barriers that restrict flow and form isolated compartments in seemingly homogeneous deposits. Evidence of compartmentalization is provided by completion and production data. Within a single sandstone ridge (an apparent common reservoir), higher condensate/gas ratio fluids are produced down dip of lower ratio fluids. In one case, drilling encountered sandstone with minimal porosity separating adjacent porous and productive sandstone reservoirs.

INTRODUCTION

This study examines the impact of depositional processes and diagenesis on reservoir evolution in the Springer Britt and Cunningham sandstones in the southeastern part of the Anadarko Basin (Fig. 1). The work of Rice (1993) provides the framework for this study and further evidence that supports the sedimentological interpretations, pore-fluid pressure analysis, and the pressure architecture of the Anadarko Basin.

The highly compartmentalized nature of the Springer sandstones is well known. The discovery of nondepleted reservoirs in close proximity to depleted ones, and the rapid decline of some producing wells, attest to the existence of previously unknown boundaries to flow units. This resultant heterogeneity impacts exploration strategies and ultimate gas recoveries.

STRATIGRAPHIC FRAMEWORK

The operational term *Springer* is ambiguous in that it represents different stratigraphic intervals in its surface and subsurface applications (Fig. 2). In surface use, the name *Springer*

was applied at the formation and group rank to an interval that includes strata from the Pennsylvanian Morrow and Mississippian Chesterian Series (Westheimer, 1956; Rice, 1993). When applied to strata in the Anadarko Basin, the term *Springer* is restricted to the Chesterian Goddard Formation (Peace, 1965). For this study, the term *Springer* is used to describe the strata of the Goddard. The Springer (Goddard Formation) interval contains several parastratigraphic units that are given the operational names of Goddard, Boatwright, Spiers, Britt, and Cunningham (Peace, 1965). The Goddard Formation is part of the Noble Ranch Group, which is a clastic-dominated sequence that represents a shallow-marine, storm-dominated shelf depositional system (Rice, 1993).

The stratigraphic nomenclature employed by the oil and gas industry and adopted for this study use the operational terms *Morrow* and *Springer*, as well as the Goddard, Boatwright, Spiers, Britt, and Cunningham parastratigraphic units. As a result of the relative abundance of core and pressure data for the Britt and Cunningham sandstones, they were chosen for examination. All boundaries and unit names followed industry convention and were inferred from wireline-log sig-

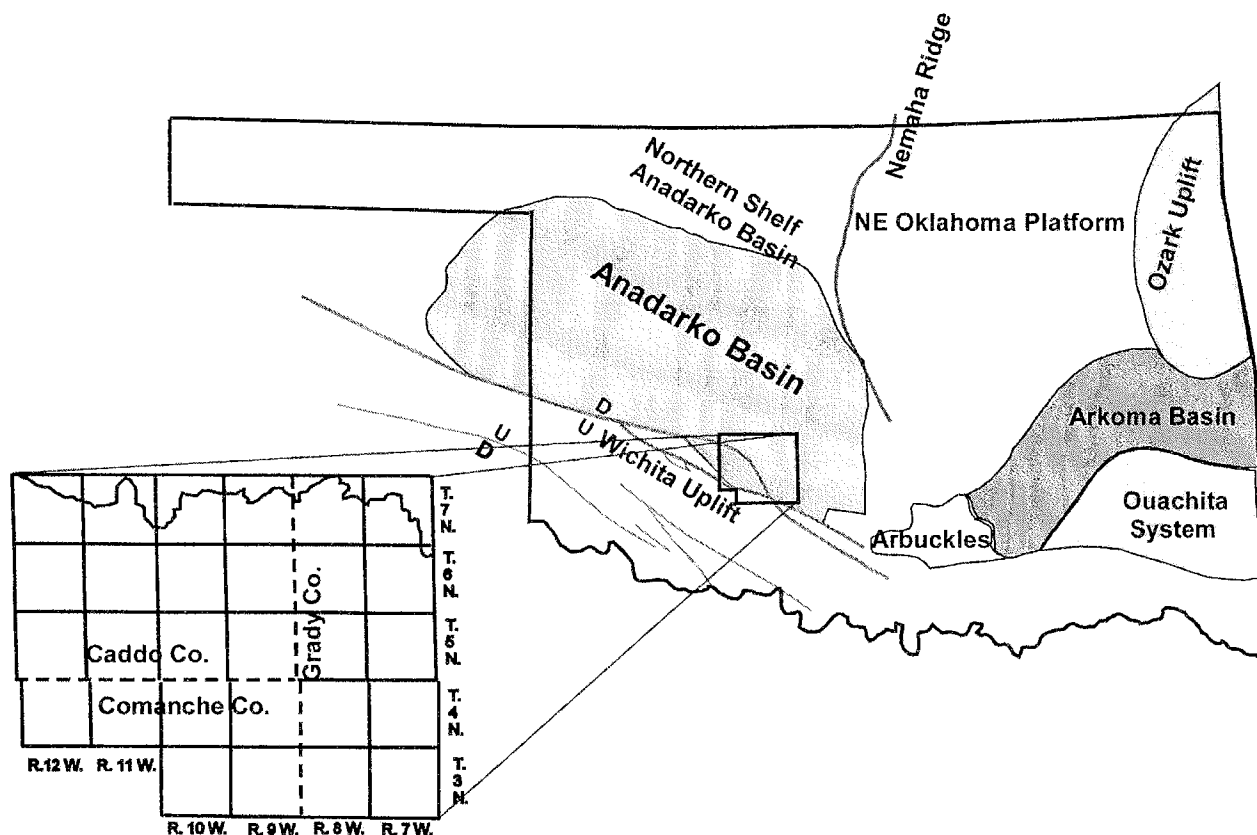


Figure 1. Map showing location of study area and major tectonic features of Oklahoma.

natures, which remained relatively similar across the study area. The top of the "Springer" interval is defined by a >650 millimhos per meter (mmho/m) deflection on the conductivity curve (Fig. 3) (Haiduck, 1987). The Cunningham and Britt intervals were further divided into upper and lower sandstone units that are separated by high-conductivity shales (Fig. 3). These shales, which appear to represent widespread flooding events in response to sea-level rises, provide a framework for correlating the intervening sandstone bodies.

The Pennsylvanian-Mississippian systemic boundary was chosen at the marked increase in conductivity that is called the "Springer conductivity marker." This change in conductivity/resistivity is attributed to the presence of intercalated sandstone laminae/beds in the Morrow interval (Haiduck, 1987).

SHELF-RIDGE SANDSTONES

In the Cement area of the Anadarko Basin, the upper part of the Springer is predominantly sandstone and shale. Based on the interpretation of gamma-ray and resistivity log signatures, sandstone bodies commonly exhibit somewhat gradational contacts with underlying shales. In contrast, the contacts between sandstones and overlying shales are sharp, giving the sandstone bodies a classic coarsening-upward geometric profile (Fig. 3).

DISTRIBUTION OF THE CUNNINGHAM AND BRITT SANDSTONES

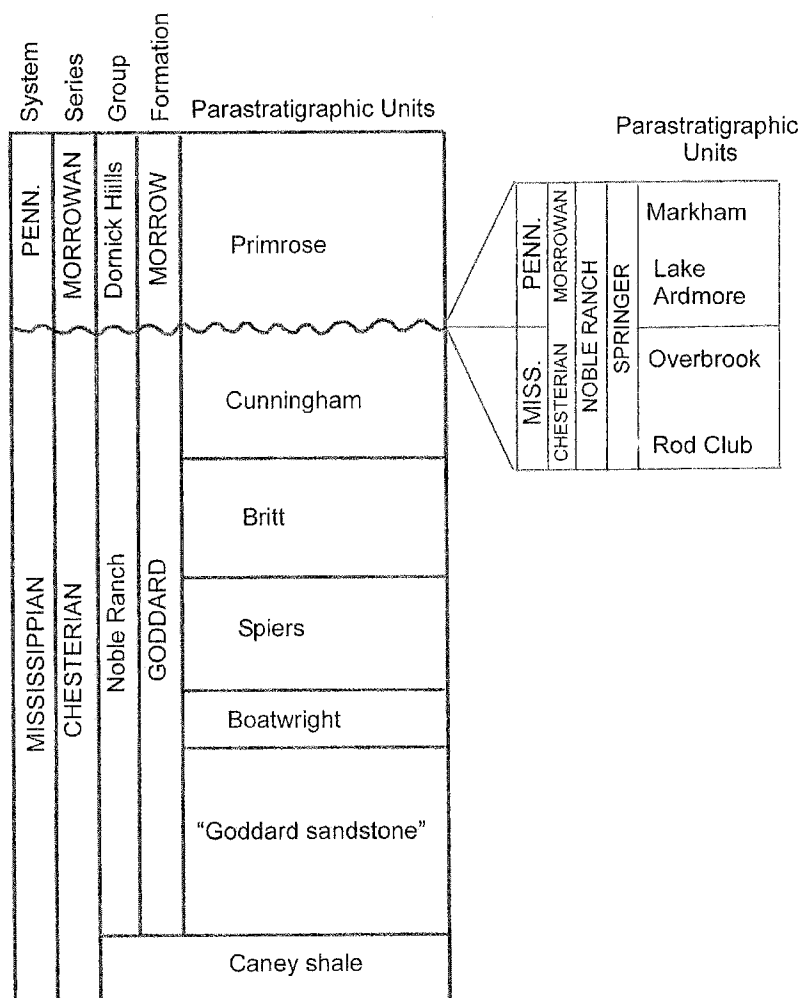
The distribution patterns of the Cunningham and Britt sandstones were mapped to determine the spatial distribution of sand bodies. Thickness maps were constructed for the upper and lower Britt and the upper and lower Cunningham sandstones. In addition, the thickness of net porous sandstone was mapped for each of the four parastratigraphic units. Sandstone was defined by a gamma-ray deflection of three chart divisions (45 API units) from the shale base line. Porous sandstone was defined by sandstone gamma-ray deflection and density porosity or equivalent sonic porosity of 8% (Fig. 3).

Lower Britt

The lower Britt sandstone (Fig. 4) forms a series of northwest to southeast-trending bodies that are concentrated in a fairway that extends from T. 7 N., R. 11 W., through T. 4 N., R. 7 W. The maximum thickness for individual sand bodies is >100 ft, whereas length to width ratios may be >15/1. One well, the Hadson No. 1-15 White, in sec. 15, T. 4 N., R. 7 W., cored the lower Britt interval.

Lower Britt Net Porosity

The distribution of net porous reservoir in the lower Britt sandstone (Fig. 5) forms a pattern that reflects the trends of



Modified from Haiduk (1987), Straka (1972), Waddell (1966), and Elias (1956)

Figure 2. Chart showing subsurface and surface stratigraphic nomenclature for the Springer. The term Springer has been applied to strata of the Mississippian and Pennsylvanian Systems. Parastratigraphic terms used in this study are shown. Modified from Haiduk (1987), Straka (1972), Waddell (1966), and Elias (1956).

total sandstone (Fig. 4). The thickest zones of porosity are concentrated in thicker sandstone bodies in T. 5 N., R. 9 W.; T. 5 N., R. 10 W.; T. 3 N., R. 7 W.; and T. 4 N., R. 8 W. The Hadson No. 1-15 White cored low-porosity sandstone.

Upper Britt

The upper Britt sandstone forms a series of ovoid to linear bodies that trend northwest to southeast (Fig. 6). Length to width ratios are generally ~3/1. Maximum thickness is >100 ft. Three cores of the upper Britt from the following wells were studied: the Kerr McGee No. 1-35 Tantequer in sec. 35, T. 5 N., R. 10 W.; the Hadson No. 1-15 White in sec. 15, T. 4 N., R. 7 W.; and the Ratliff Exploration No. 1-15 Vesper in sec. 15, T. 4 N., R. 9 W. These cored wells are identified in Figure 6.

Upper Britt Net Porosity

The distribution of porosity in the upper Britt sandstone (Fig. 7) is similar to the distribution of total sandstone. Maxi-

mum porous sandstone thickness is >40 ft. The cored wells are identified in Figure 7. Each cored well is on the margin of a porous-sandstone trend.

Lower Cunningham

The lower Cunningham sandstone is widely distributed across the study area (Fig. 8). Areas of thicker sandstone trend northwest to southeast. The maximum thickness is >125 ft. One well, the Gulf No. 1-14 Lillian Miller, in the NE NW sec. 14, T. 6 N., R. 9 W., cored the lower Cunningham sandstone.

Lower Cunningham Net Porosity

Porosity trends in the lower Cunningham sandstones are concentrated in T. 6 N., R. 8 W.; T. 6 N., R. 9 W.; T. 7 N., R. 8 W.; and T. 7 N., R. 9 W. (Fig. 9). The distribution of porosity is somewhat confined when compared to the widespread occurrence of total sandstone. The thickest porosity, which exceeds 80 ft, occurs where total sandstone thickness is >100 ft. The

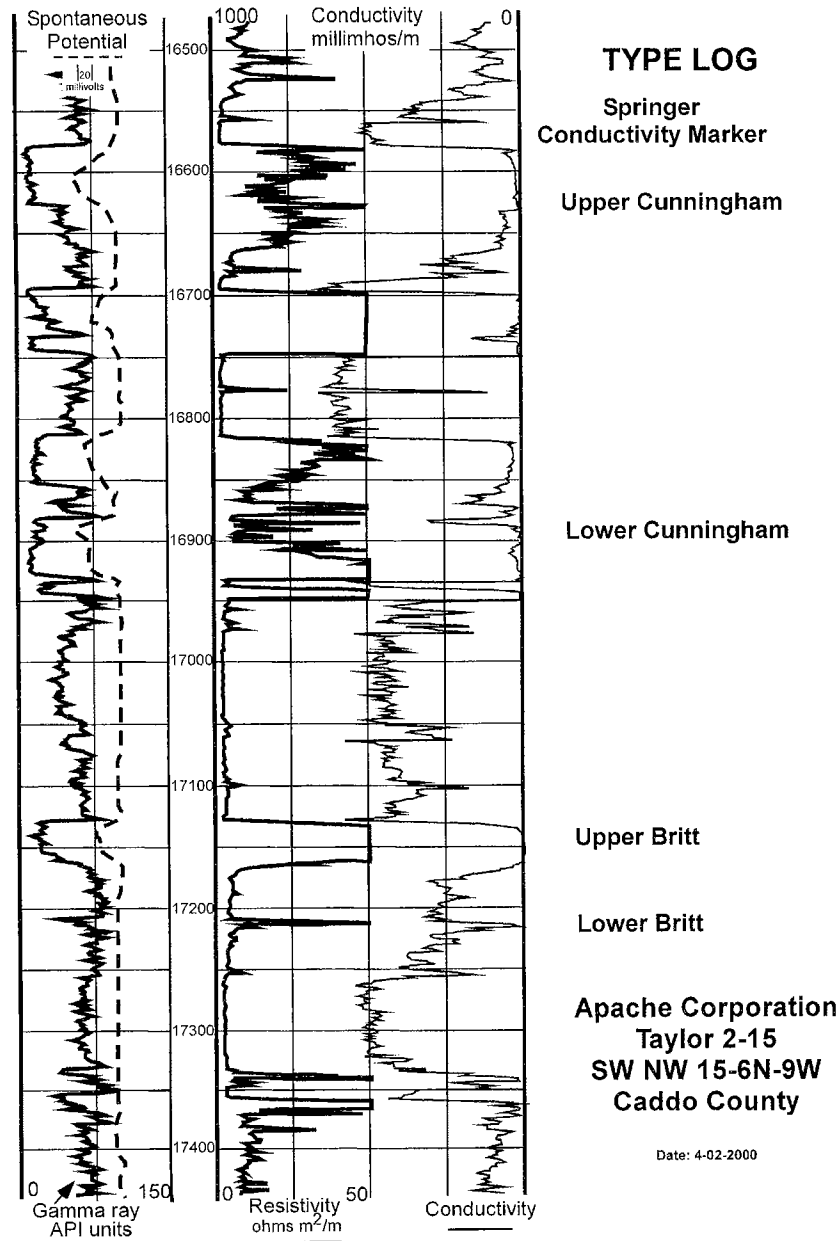


Figure 3. Type log for the Cunningham and Britt intervals of the Springer. Sandstones are characterized by clean gamma-ray signatures and a corresponding increase in shallow-resistivity measurements. Shales have characteristic low-resistivity (<10 ohm-m) and corresponding high-conductivity signatures.

core from the NE NW sec. 14, T. 6 N., R. 9 W., contains porous and tightly cemented intervals.

Upper Cunningham

The upper Cunningham is widespread, with sandstone bodies trending northwest to southeast (Fig. 10). A fairway of thicker sandstone extends from T. 7 N., R. 9 W., through T. 3 N., R. 7 W. The thickest sandstone is in T. 4 N., R. 7 W., where values reach 200 ft. Three wells cored the upper Cunningham sandstone: the Texaco No. A-1 Carr in sec. 36, T. 5 N., R. 11 W.; the Chevron No. 1-8 Berta Lay in sec. 8, T. 3 N., R. 7 W.; and the Hadson No. 1-15 White in sec. 15, T. 4 N., R. 7 W.

Upper Cunningham Net Porosity

Upper Cunningham porosity (Fig. 11) has a distribution similar to total sandstone distribution. The maximum thickness is >40 ft. The three cored wells are shown in Figure 11.

DEPOSITIONAL SETTING AND ENVIRONMENTS

During the Mississippian, the proto-Anadarko (Oklahoma) Basin trended west-northwest to east-southeast (Rascoe and Adler, 1983). The distribution of the linear Springer sandstone bodies subparallel to the paleobathymetric trend indicates an origin related to marine or paralic processes. Integrated

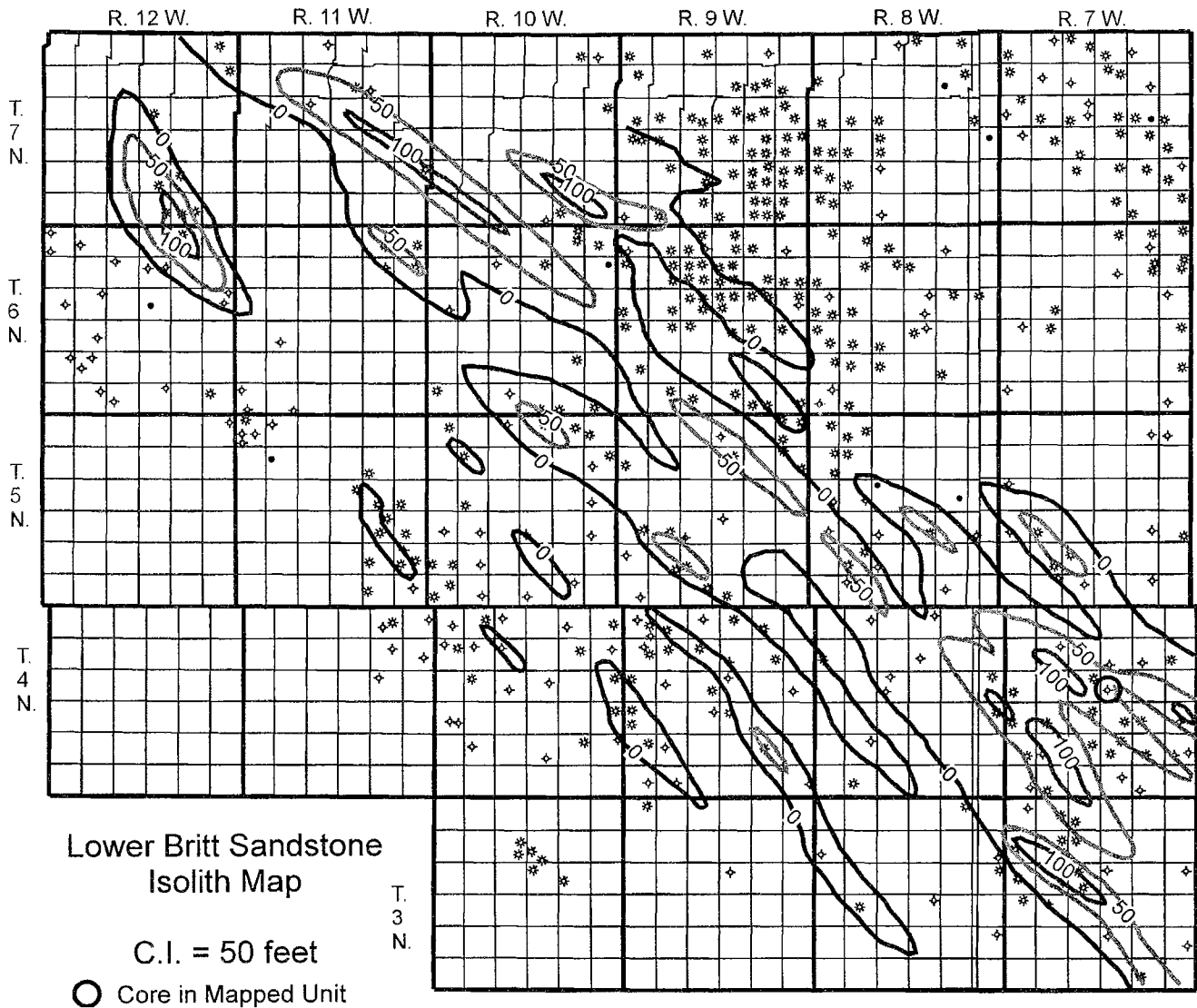


Figure 4. Lower Britt sandstone isolith map. Criterion for identifying sandstone is a gamma-ray signature of <30 API units. Sandstone bodies trend northwest to southeast and display elongate, ridgelike morphology.

subsurface and core data were interpreted to establish depositional systems and facies. Rice (1993) examined a total of six cores and identified depositional facies similar to those associated with shelf-sand ridges described by Tillman and Martinsen (1984) and Brenner and Davies (1973). The depositional facies include (1) central marine bar (Fig. 12A), (2) shelf sandstone (Fig. 12B), (3) bar margin, (4) bioturbated shelf sandstone (Fig. 13A), (5) interbar (Fig. 13B), (6) shelf storm deposits (Fig. 13C), (7) central bar (Fig. 13D), and (8) estuarine dark shale. Characteristics of these lithofacies and their cored intervals are shown in Figure 14. A generalized schematic diagram of shelf-sand ridges is shown in Figure 15.

PETROLOGY AND DIAGENESIS

Detrital and Diagenetic Constituents

The Cunningham and Britt sandstones are classified as quartz arenites. Monocrystalline quartz of plutonic origin is

the major detrital constituent and accounts for >99% of framework grains. Other detrital constituents include polycrystalline (metamorphic) quartz, feldspars, bioclasts, glauconite, colophane, tourmaline, and zircon (Rice, 1993).

Detrital clay matrix is a minor constituent in most cored intervals. In the Cunningham and Britt sandstones, detrital clay matrix appears to be recrystallized to chlorite, which is ductily deformed and forms pseudomatrix between detrital grains (Rice, 1993).

Authigenic constituents include silica, calcite, siderite, dolomite, Fe-rich chlorite/chamosite, and kaolinite. Syntaxial quartz overgrowths are common and play an important role in reservoir evolution. Calcite cement is common and appears to be an early product in the diagenetic history. Calcite fills pores between detrital quartz grains and forms syntaxial overgrowths on pelmatozoan bioclasts. Siderite may be another relatively early product in the diagenetic history, whereas

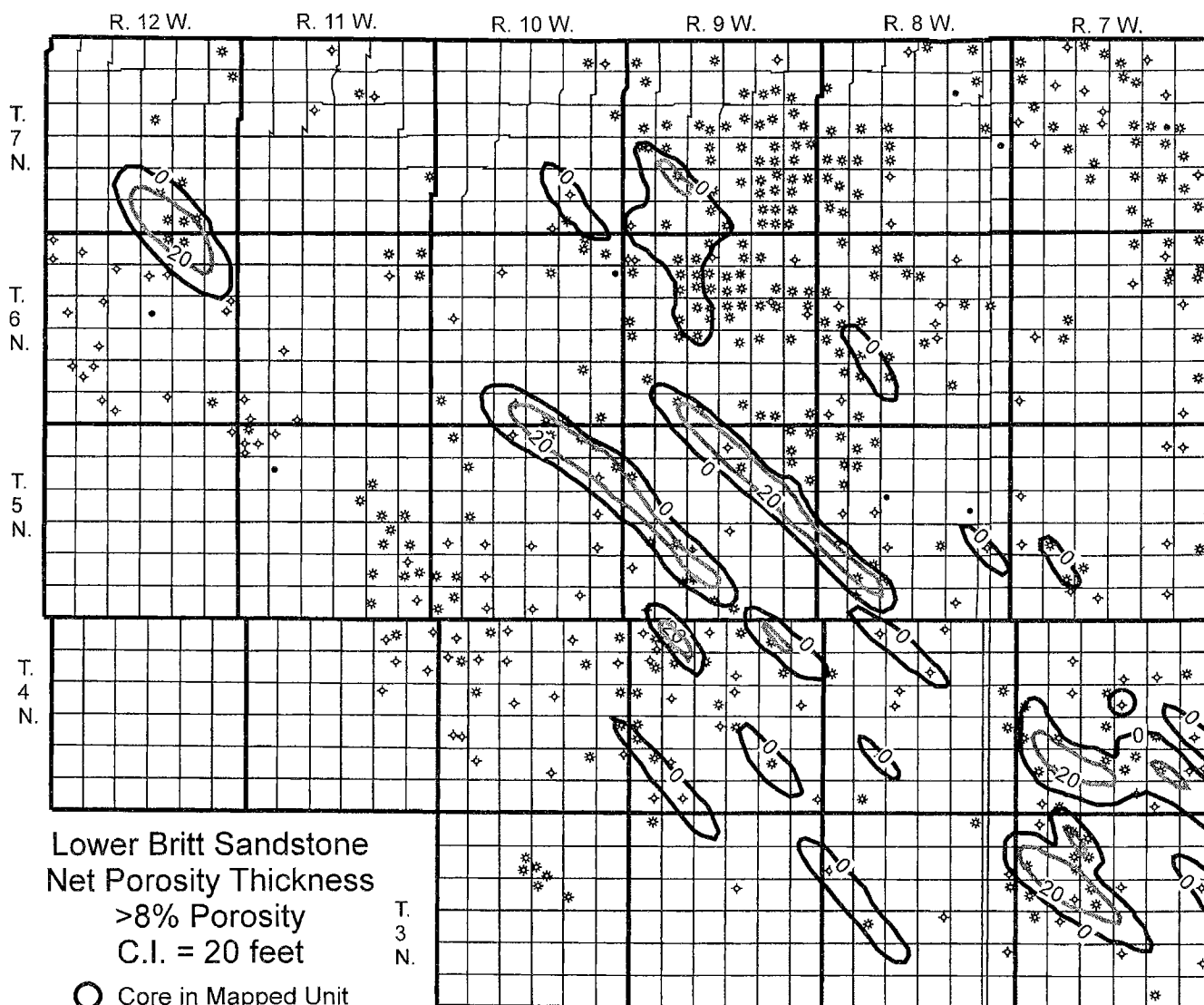


Figure 5. Map showing lower Britt sandstone net-porosity thickness. Criteria for determining net sandstone are gamma-ray measurement of <30 API units and corresponding density or sonic porosity measurement of $\geq 8\%$ (2.68 g/cm^3 density). Porosity-thickness trends are similar to those of the total sandstone.

dolomite is of thermal origin and indicates deeper burial or migration of thermal fluids through the pore network (Rice, 1993).

Porosity

The preservation of primary porosity and the evolution of secondary porosity in Springer sandstones resulted from a variety of processes. Primary porosity is significant and was preserved by authigenic chamosite and chlorite clay coatings on detrital grains (Fig. 16A,B,C) that inhibited precipitation of calcite and silica cements. Secondary porosity is common and includes moldic, intragranular, and intergranular. Moldic porosity develops in marine facies by the dissolution of bioclasts. Intragranular porosity forms by the partial dissolution of feldspar, bioclasts, and polycrystalline grains (Fig. 16D).

Intergranular porosity developed as early calcite cement was dissolved (Fig. 17). Oversized pores resulted from the dissolution of calcite cement that earlier replaced quartz grains.

Early calcite cementation was important to the evolution of reservoirs in the Britt sandstone. Calcite-cemented grains were sequestered from fluids that precipitated silica cement in the form of syntaxial quartz overgrowths. As fluid chemistry changed in response to burial and the generation of organic acids from source rocks, the calcite cement was dissolved, leaving secondary pores.

Chamosite/Fe-rich chlorite grain coatings prevented the nucleation of both carbonate and silica cements and allowed primary porosity to be preserved in these deeply buried Springer sandstones (Pittman, 1979; Rice 1993). Chamosite occurs as thick rinds (0.05–0.08 mm) on detrital quartz grains and bioclasts that are chamosite ooids (Fig. 16B). Authigenic

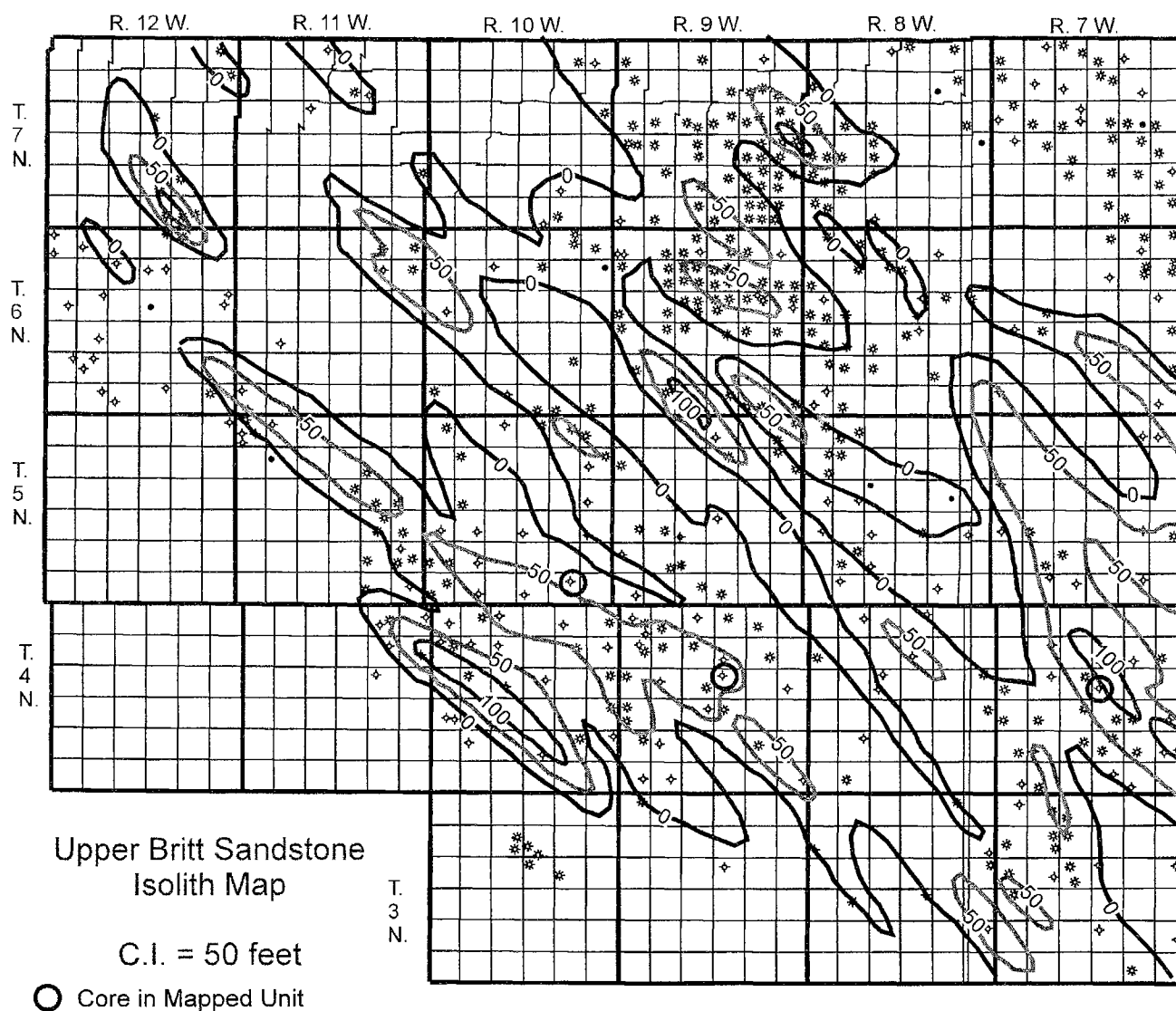


Figure 6. Upper Britt sandstone isolith map. Upper Britt sandstone-thickness trends are similar to those of the lower Britt. Sandstone was determined by using the same criterion as for Figure 4.

Fe-rich chlorite forms thin grain coatings (Fig. 16C) that effectively inhibit precipitation of intergranular silica and carbonate cements.

Microporosity can be intragranular or intercrystalline. Intercrystalline microporosity exists between the plates of authigenic chlorite crystals (Fig. 16C). Additional microporosity is intragranular and occurs within partially dissolved detrital grains and bioclasts (Fig. 16D).

RESERVOIR EVOLUTION AND COMPARTMENTALIZATION

Some reservoir facies in Springer sandstones contain mostly primary porosity that is the result of clay grain coatings. However, the preservation of primary porosity is vital to evolution of secondary porosity in the Springer sandstones. Primary porosity provided the conduits whereby pore fluids

could come in contact with detrital grains. Detrital grains not coated by clay were cemented first with early calcite, or secondly with silica that effectively occluded porosity. Early calcite cement played an important role in the evolution of secondary porosity. As pore-water chemistry changed in response to burial, acidic conditions developed that favored the dissolution of calcite and the precipitation of quartz. In some sandstones, grain-coating calcite partially dissolved, which resulted in increased porosity. More importantly, the calcite cement prevented nucleation of quartz overgrowths on detrital grains, thus limiting silica cementation, which occludes nearly all porosity in some intervals. With continued burial, thermal maturation of organic material, and generation of organic acids, Springer rocks were subjected to an additional phase of acidic dissolution. In this phase, organic acid-rich pore fluids, which migrated through the rock prior to oil and

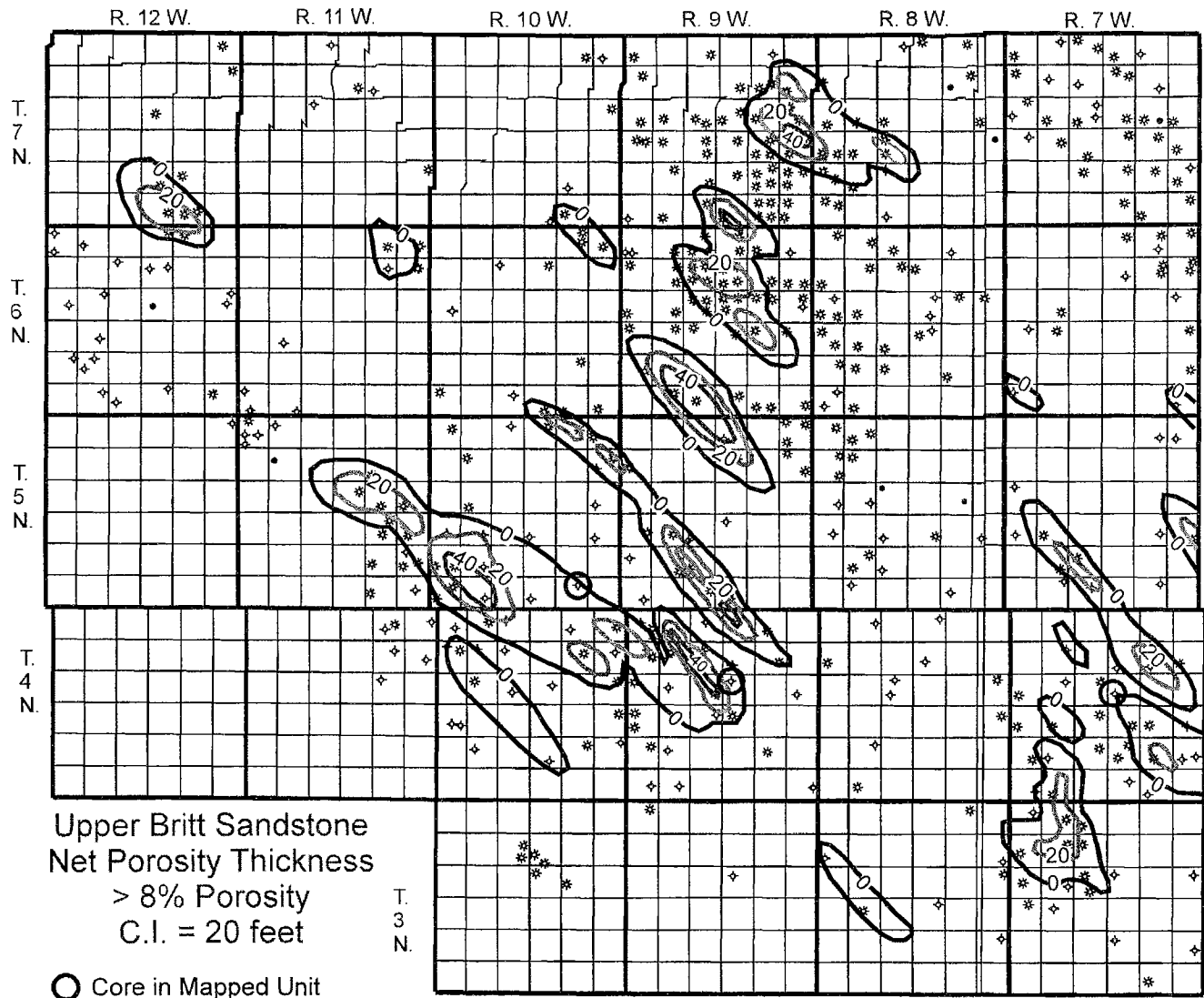


Figure 7. Map showing upper Britt sandstone net-porosity thickness. Net porous sandstone was determined by using the same criteria as for Figure 5.

gas, dissolved additional calcite and enlarged the secondary pore network.

Thin-section analysis reveals that fine-grained textures are more silica cemented than coarser textures. This phenomenon is likely the result of several processes. One is the result of mechanochemical processes (Ortoleva and others, 1995) that preferentially affect finer grained sands, which have greater surface area per given volume than coarser grained sands. A second process involves the preferential movement of fluid through coarser grained sands, which resulted in early calcite cement that was subsequently dissolved. A third factor is clay coating, which appears to preferentially affect coarser grained sands, thereby protecting them from silica cementation.

Geochemical modeling shows that in rapidly subsiding basins with considerable chemical disequilibrium, finer grained sandstones appear to undergo pressure solution and cementation at a faster rate than those that are coarser grained (Or-

toleva and others, 1995). This process leads to the preferential cementation of finer grained textures and the formation of silica-cemented zones between porous areas. The isolation of porous areas by cemented sandstone is called auto-isolation and contributes to compartmentalization of seemingly continuous sandstone bodies (Ortoleva and others, 1995).

AUTO-ISOLATION OF THE LOWER CUNNINGHAM SANDSTONE

Auto-isolation in the lower Cunningham interval is responsible for compartmentalization of a seemingly laterally continuous sand ridge. Evidence from pressure data, fluid content, structural position, production data, and core data was integrated with wireline-log and completion data to delineate compartments.

In the northern part of the study area (T. 6 N., R. 8-9 W.) the lower Cunningham sandstone interval consists of three

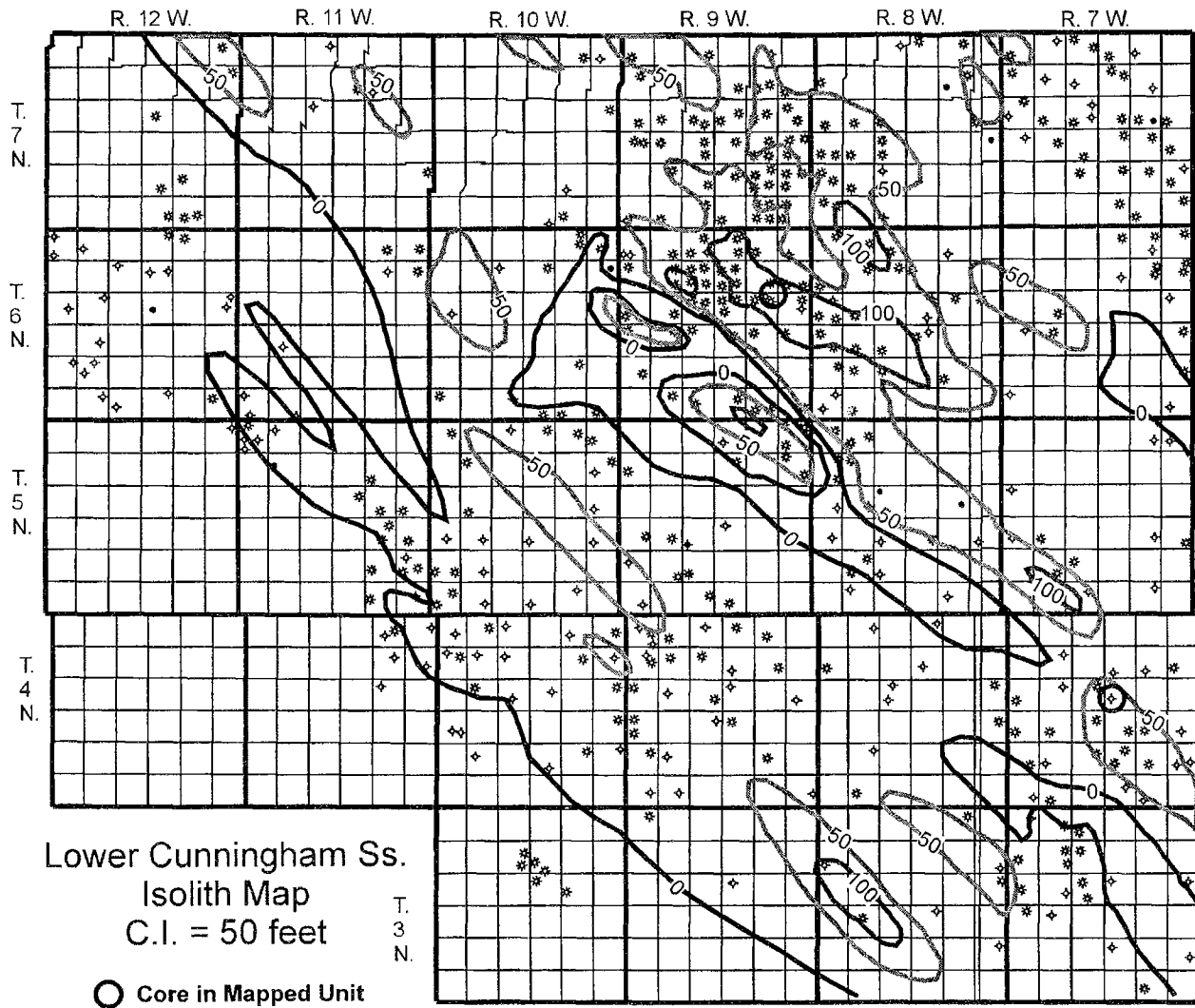


Figure 8. Lower Cunningham sandstone isolith map. The lower Cunningham is widespread across the study area and contains thicker linear sandstone bodies that trend northwest to southeast. Sandstone was determined by using the same criterion as for Figures 4 and 6.

vertically stacked sand ridges (Fig. 18). These ridges are distinguished by clean gamma-ray signatures (<30 API units) that show a ≥ 45 unit deflection from the shale baseline (Figs. 3, 18). The units were assigned identifying letters, A, B, and C, in descending order. Each unit was mapped for thickness to determine its spatial distribution. The lowermost sandstone, unit C, was examined petrologically from the three wells shown in Figure 18. Core from the C unit was examined in the Gulf No. 1 Lillian Miller well in the NW NE sec. 14, T. 6 N., R. 9 W. Bit cuttings were examined from the Gulf No. 1 Moody in the C NE sec. 10, T. 6 N., R. 9 W., and the IFE Energy Exploration No. 1 Van Zandt in the C NE sec. 14, T. 6 N., R. 9 W. Cuttings and core were correlated and compared with various petrophysical (wireline) logs to help assess reservoir properties.

Two distinct compartments were identified in unit C on the basis of evidence from pressure measurements, petrologic

analysis, and fluid data (Fig. 19). Compartment 1 was encountered by the Gulf No. 1-10 Moody well in sec. 10, T. 6 N., R. 9 W. The No. 1-10 Moody tested an original pressure/depth gradient of 0.60 psi/ft. We believe that liquids and gas production from the unit C reservoir is a high ratio at only 1-2 barrels of condensate per million cubic feet of gas (MMCFG). The date of first production was October 1981. Petrophysical-log measurements indicate a porosity of $\sim 10\%$ across the perforated interval in unit C (Fig. 18).

Compartment 2 was encountered by the IFE Energy No. 1-14 Van Zandt well in the C NE sec. 14, T. 6 N., R. 9 W. (Fig. 19). The No. 1-14 Van Zandt tested an original pressure/depth gradient of 0.62 psi/ft. The liquids to gas ratio is 7-9 barrels of condensate per MMCFG. The date of first production was October 1982. Petrophysical-log measurements indicate a porosity of $\sim 11-12\%$.

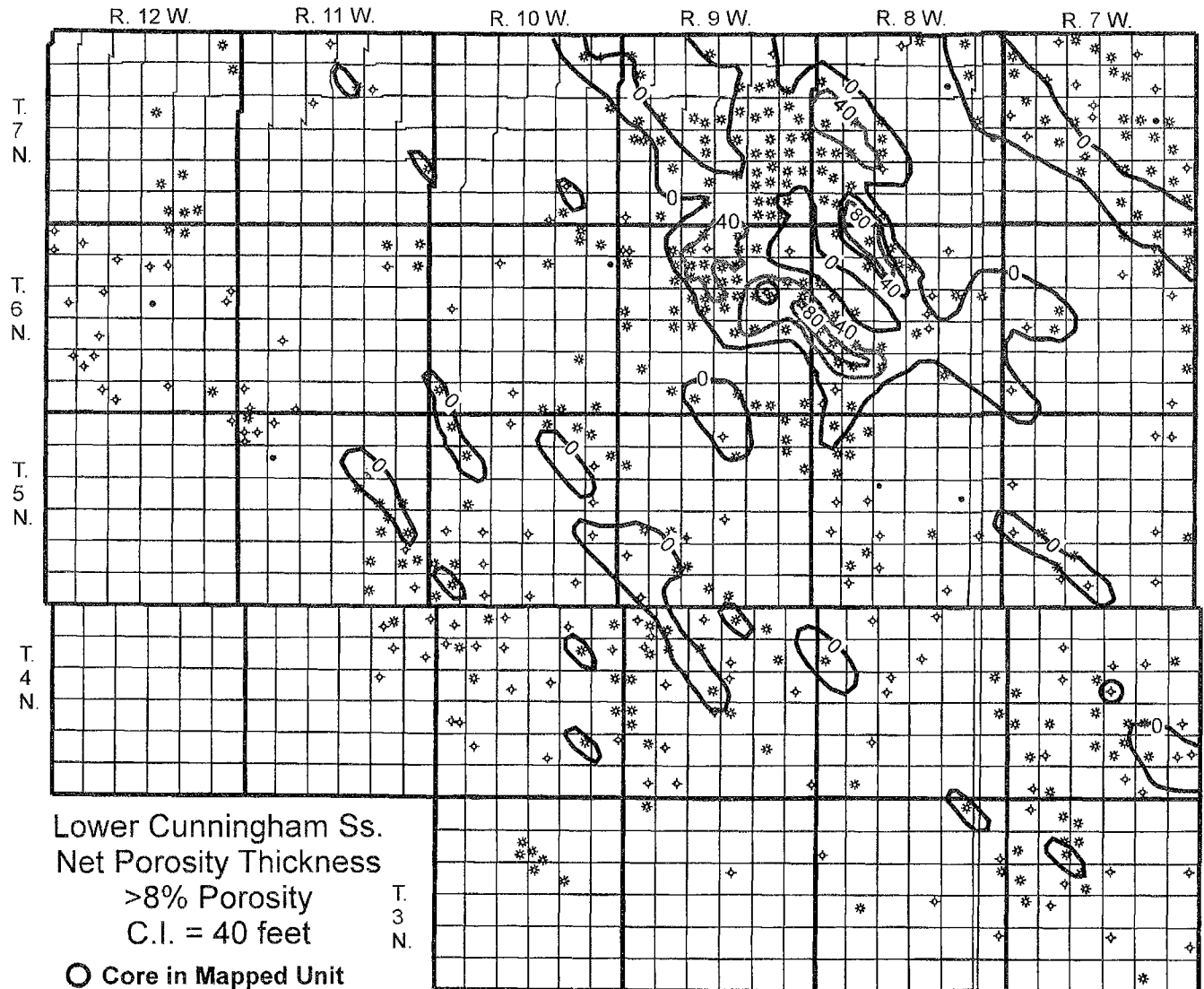


Figure 9. Map showing lower Cunningham net-porosity thickness. Lower Cunningham porosity is mostly limited to the four square township areas. However, total thickness of porous sandstone can exceed 80 ft in this area. Criteria for determining net porosity are the same as for Figures 5 and 7.

The Gulf No. 1-14 Lillian Miller encountered the unit C sand ridge at a position between the No. 1-14 Van Zandt and the No. 1-10 Moody wells (Fig. 19). The unit C sandstone cored by the No. 1-14 Miller well is stylolitized and extensively cemented with silica. Thin-section petrography revealed that porosity is rare in unit C and consists of secondary moldic porosity following dissolution of sparsely distributed fossil fragments. Porosity from thin-section analysis was estimated at 2%, whereas maximum porosity measurements obtained from sonic petrophysical logs were near 3%.

Grain mounts of bit cuttings from the No. 1-10 Moody and No. 1-14 Van Zandt wells were examined, as no cores were available. Petrographic analysis of these cuttings revealed that grain-coating chlorite was present at both locations. Therefore, it is hypothesized that grain-coating chlorite preserved primary porosity in the unit C sandstone from the No. 1-10 Moody and No. 1-14 Van Zandt wells. In contrast, the lack

of grain-coating clay in the sandstone cored in the No. 1-14 Miller well allowed quartz to nucleate, resulting in the near total occlusion of porosity by syntaxial quartz overgrowths. The limited porosity that developed in the sandstone from the Miller well is the result of dissolution of labile bioclast grains.

Mapping unit C thickness revealed no evidence to suggest that the No. 1-10 Moody, the No. 1-14 Van Zandt, and the No. 1-14 Miller wells did not encounter the same sand ridge (Fig. 19). Gamma-ray-log signatures indicate that each well contains "clean" sandstone. The thickness of sandstone is similar in each and is >30 ft. The thickness map shows a laterally continuous sandstone ridge that trends northwest to southeast across the northern part of T. 6 N., R. 9 W. All three wells were drilled near the crest of the Laverty Anticline, so structural position is not believed to influence productivity (Rice, 1993).

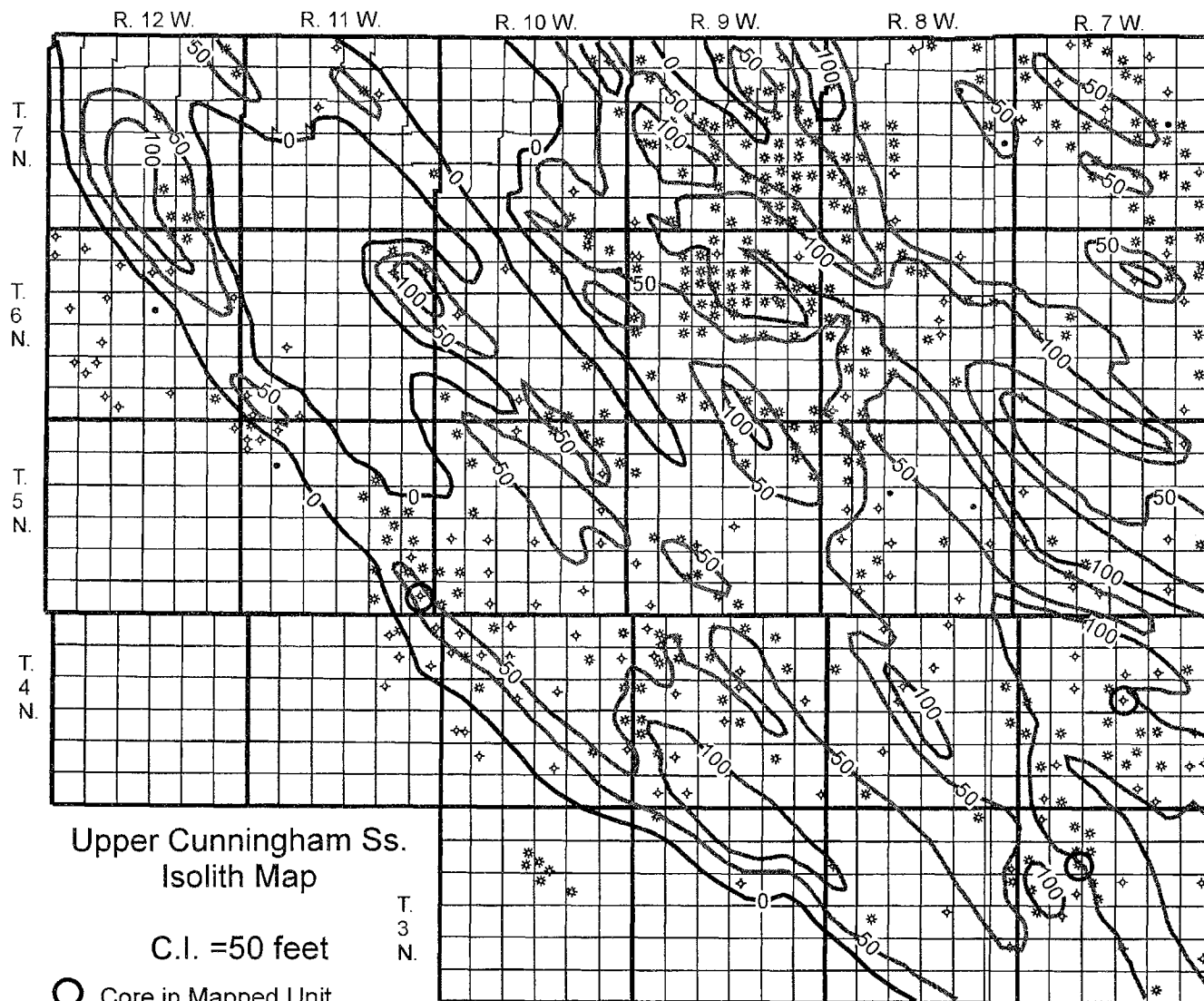


Figure 10. Upper Cunningham sandstone isolith map. The upper Cunningham is another widespread sandstone unit that displays thicker bodies with northwest to southeast trends. The criterion for determining sandstone is the same as for Figures 4, 6, and 8.

The evidence just presented supports the presence of two compartments in unit C of the lower Cunningham sandstone. If the No. 1-10 Moody, the No. 1-14 Miller, and the No. 1-14 Van Zandt wells were completed in a common reservoir, the Van Zandt well should have the higher liquids/gas ratio. However, the production data indicate that the reverse is true and that the No. 1-10 Moody has a higher liquids/gas ratio. In addition, the reported reservoir pressure and resultant pressure/depth gradient were higher for compartment 2 than for compartment 1, which was completed 1 year earlier. The petrologic and petrophysical data support the hypothesis of two compartments. The unit C sandstone encountered by the No. 1-10 Moody and No. 1-14 Van Zandt wells is porous ($\geq 10\%$), as indicated by wireline logs, whereas the sandstone encountered by the No. 1-14 Miller well has a very low porosity ($< 3\%$).

IMPLICATIONS

Compartmentalized sandstones offer exploration opportunities. As shown in the previous example, porous compartments exist in close proximity to seal zones. In the case of the unit C sandstone ridge, the lithofacies remains constant, and sealing appears to be the result of diagenetic processes. Mapping individual sandstone ridges is a tool for delineating trends of thicker sandstone and thicker porosity. Petrographic analysis may provide textural data that could be useful in predicting where coarser grained sandstones and/or sandstones with clay-coated grains, which are the better reservoir facies, are present.

SUMMARY AND CONCLUSIONS

Integrated core, petrophysical, and subsurface-mapping data support the interpretation that the Springer Cunning-

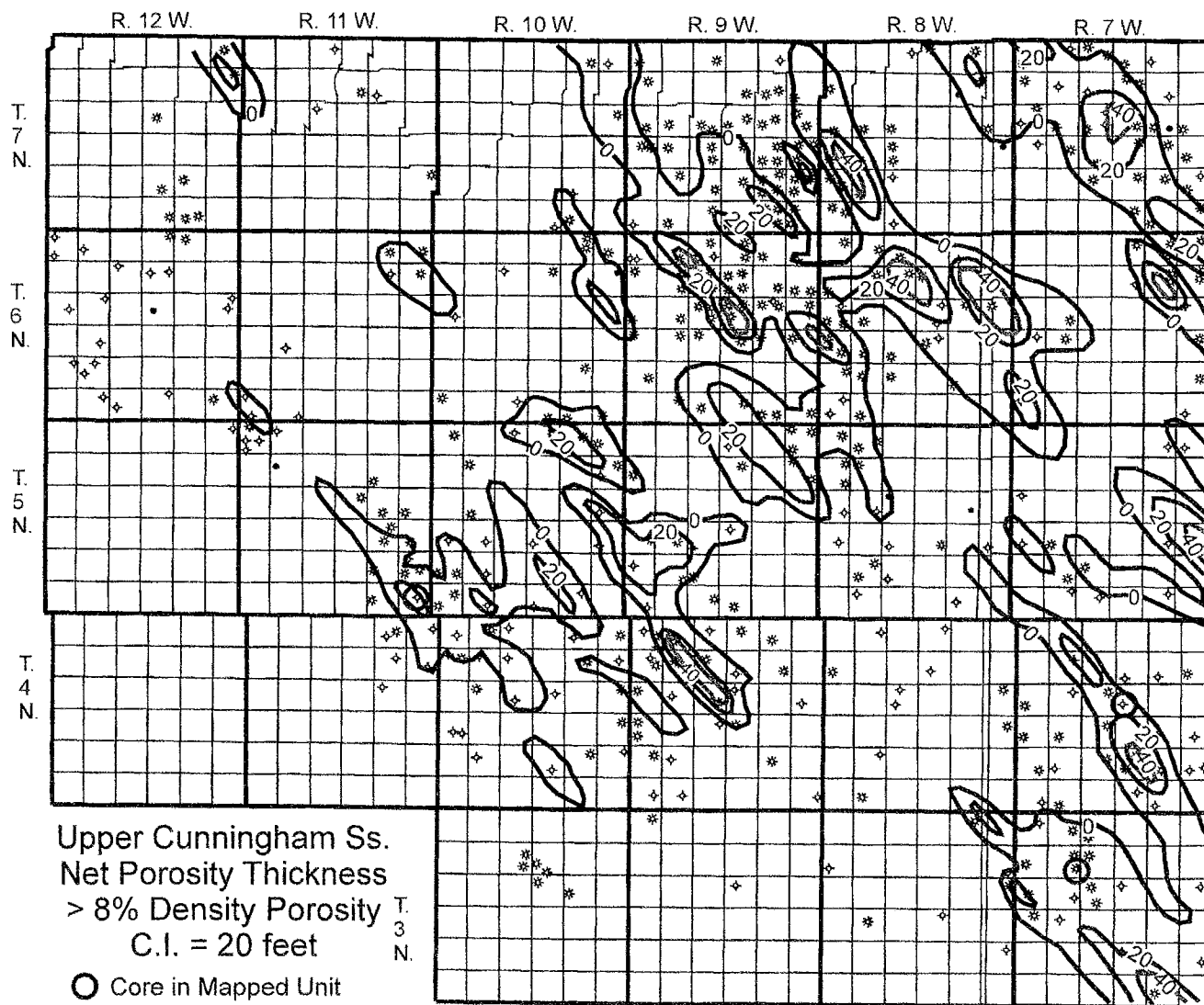


Figure 11. Upper Cunningham net-porosity thickness. Upper Cunningham porosity is more widespread than porosity in the lower Cunningham. However, the total thickness of net porosity in a given sandstone body is somewhat less and does not exceed 60 ft. Criteria for determining net porosity are the same as for Figures 5, 7, and 9.

ham and Britt are shelf/bay sand ridges. Invertebrate-fossil bioclasts and glauconite are evidence that some sandstones are marine. The absence of normal invertebrate fossils in shale intervals suggests a restricted bay setting with disaerobic conditions. The operational units in the Cunningham and Britt intervals map as linear sand ridges. Sandstones display cleaning-upward log signatures typical of shallow-marine settings. The trend of sand ridges subparallel to the depositional shoreline is indicative of a shallow-marine setting.

Compartmentalization of the Cunningham and Britt sandstones is related to original depositional texture and composition. Mapping indicates that porosity trends follow thickness trends. Vertical isolation of operational units is achieved by the separation of sandstone bodies by intervening shale strata. Intra-sandstone-ridge compartmentalization can be

related to diagenetic processes. The clean quartz arenites of the Springer interval were highly susceptible to silica cementation and underwent near-total porosity occlusion with deep burial. Porosity in porous compartments is both primary and secondary. Primary porosity is preserved to depths >15,000 ft by chamosite or chlorite grain-coating clays. Secondary porosity is important in sandstone cemented early by calcite cement, which was subsequently dissolved by acidic fluids that were generated during burial.

ACKNOWLEDGMENTS

The authors wish to express their appreciation to Walter Esry and the staff of the Oklahoma Geological Survey Core and Sample Library for providing cores examined in this study. We are also grateful to Zuhair Al-Shaieb and Azhari

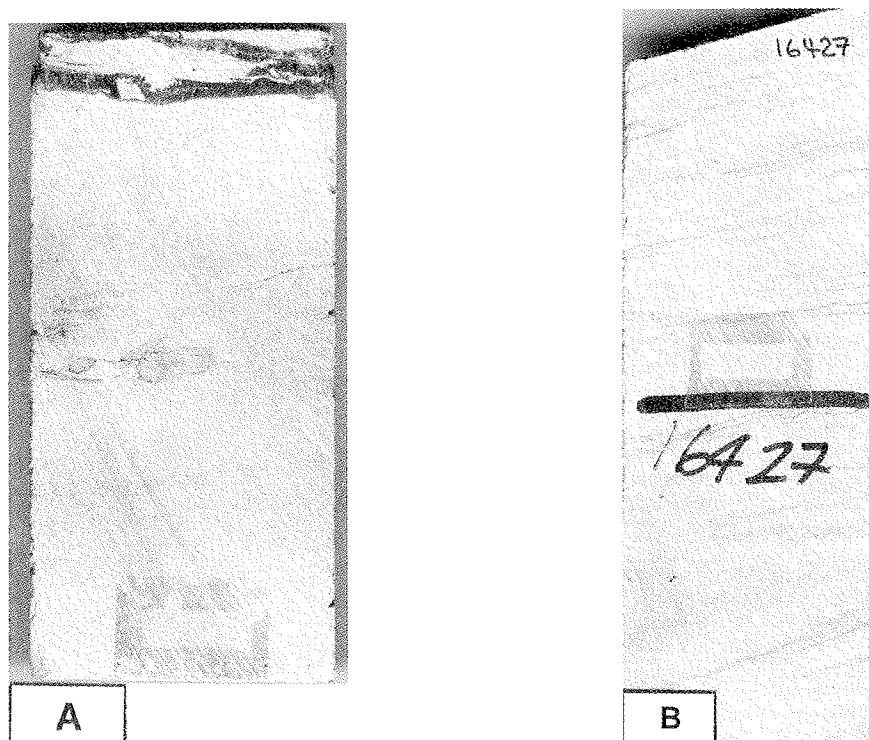


Figure 12. Core slabs representing examples of shelf sandstone and central bar lithofacies described by Rice (1993). (A) Central marine-bar lithofacies, upper Britt sandstone, Hadson No. 1-15 White. Depth, 16,429 ft. (B) Shelf-sandstone lithofacies with planar cross-bedding and microstylolitization. Upper Britt sandstone, Hadson No. 1-15 White. Depth, 16,427 ft.

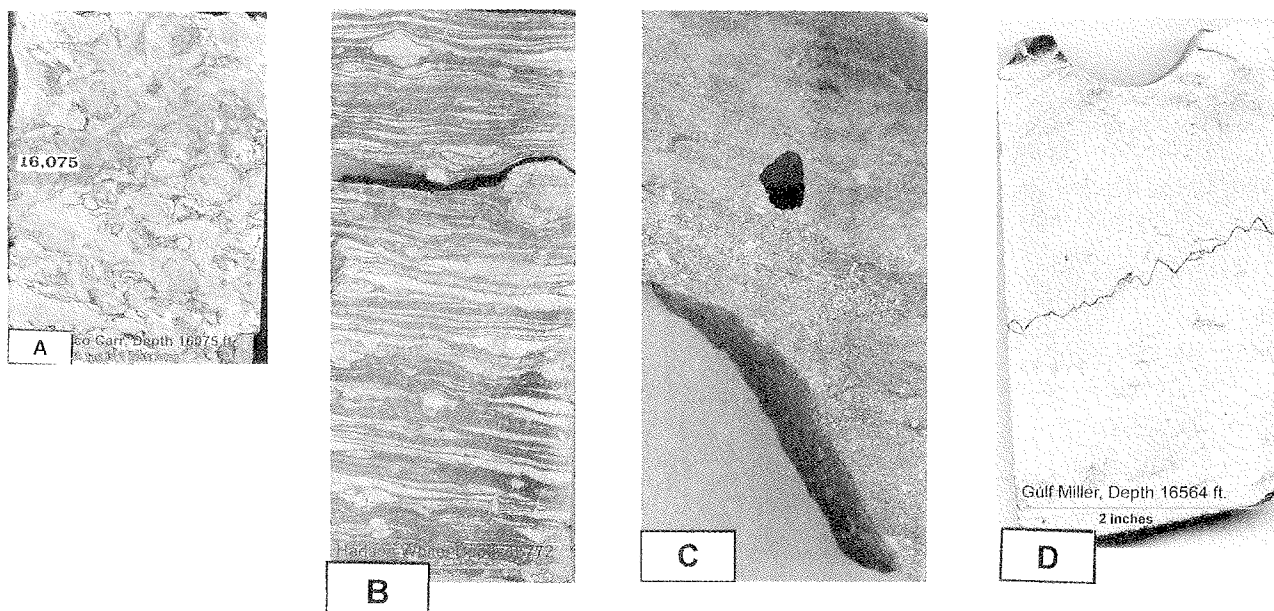


Figure 13. Core slabs representing interbar and bar lithofacies. (A) Bioturbated clayey sandstone of the bioturbated shelf-sandstone lithofacies. Biotic activity was intense and destroyed all bedding features. Upper Cunningham sandstone, Texaco No. A-1 Carr. Depth, 16,075 ft. (B) Interlaminated sandstone and shale of the interbar lithofacies. Horizontal burrowing is common, but no shelly marine invertebrate fauna is evident. Lower Britt sandstone, Hadson No. 1-15 White. Depth, 16,772 ft. (C) Bioclastic sandstone of the shelf storm lithofacies. Lower Cunningham sandstone, Gulf No. 1-14 Lillian Miller. Depth, 16,516 ft. This unit is composed primarily of pelmatozoan bioclasts. (D) Stylolitized sandstone of the central bar lithofacies, lower Cunningham sandstone, Gulf No. 1-14 Lillian Miller. Depth, 16,564 ft. Dissolution sand grains along stylolite are a source of silica that may occlude porosity in the host sandstone.

Facies	Characteristics	Core and Interval
Central bar	Fine- to medium-grained quartzose sandstone with subhorizontal, tabular planar cross-bedding, sandstone ripples and minor shale	Gulf, Lillian Miller: 16,451-16,479; 16,547.5-16,578
Central marine bar	Glauconitic quartz sandstone that locally contains siderite clasts. Structures include trough cross beds and planar tangential cross-bedding with trough sets that are commonly truncated	Ratliff Expl., Vesper: 18,805-18,826
Bar margin	Glauconitic fine- to medium-grained sandstone and shale with rip-up clasts. Sedimentary structures include low angle trough cross beds and current ripples with shale clasts that occasionally show preferred orientations.	Ratliff Expl., Vesper: 18,826-18,839
Interbar	Glauconitic and interbedded fine- to very fine-grained silty sandstone and silty shale. Horizontal ripple-form bedding surface marked by interbedded shale and sandstone are common. Current ripples are more common than symmetrical wave forms	Gulf, Lillian Miller: 16,479-16,510 Chevron, Berta Lay: 16,628-16,663 Hudson, White: 16,010-16,030 Hudson, White: 16,751-16,800
Bioturbated shelf sandstone	Shaly sandstone to slightly sandy dark gray siltstone with traces of glauconitic. Sedimentary structures include scattered thin rippled sandstone with horizontal and vertical burrowing	Texaco, Carr: 16,067-16,110 Kerr McGee, Tantequer: 18,075-18,081
Shelf sandstone	Very fine grained sandstone with traces of interlaminated shale. Sedimentary structures are subhorizontally inclined to low angle laminations with rare trough cross bedding	Gulf, Lillian Miller: 16,519-16,545 Kerr McGee, Tantequer: 18,083-18,112 Chevron, Berta Lay: 16,625-16,628 Hudson, White: 16,054-16,070 Hudson, White: 16,416-16,435 Hudson, White: 16,800-16,810
Shelf storm	Graded coquina sandstones of pelmatozoan bioclasts	Gulf, Lillian Miller: 16,510-16,519 Gulf, Lillian Miller: 16,578-16,580 Kerr McGee, Tantequer: 18,081-18,082
Estuarine dark shale	Dark gray to black, fissile mudrocks that lack marine invertebrate fossil content, but contain coal fragments	Kerr McGee, Tantequer: 18,112-18,117 Texaco, Carr: 16,110-16,111

Figure 14. Tabular listing of depositional facies types, their characteristics, and the core and depth encountered.

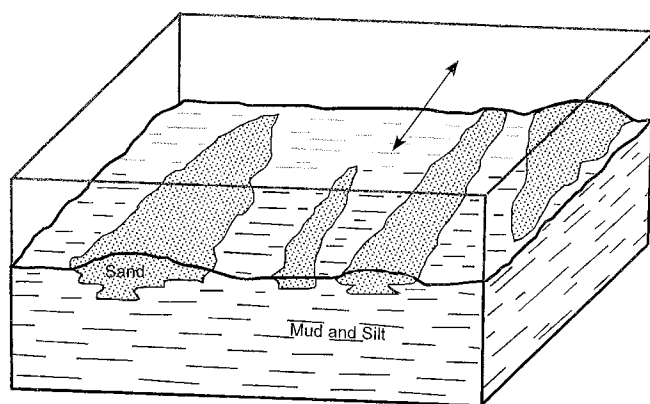


Figure 15. Depositional model for shelf-sand ridges. Sand is indicated by stippled pattern, and mud and silt by lined pattern. Arrow indicates primary current direction. (Modified from Brenner, 1980.)

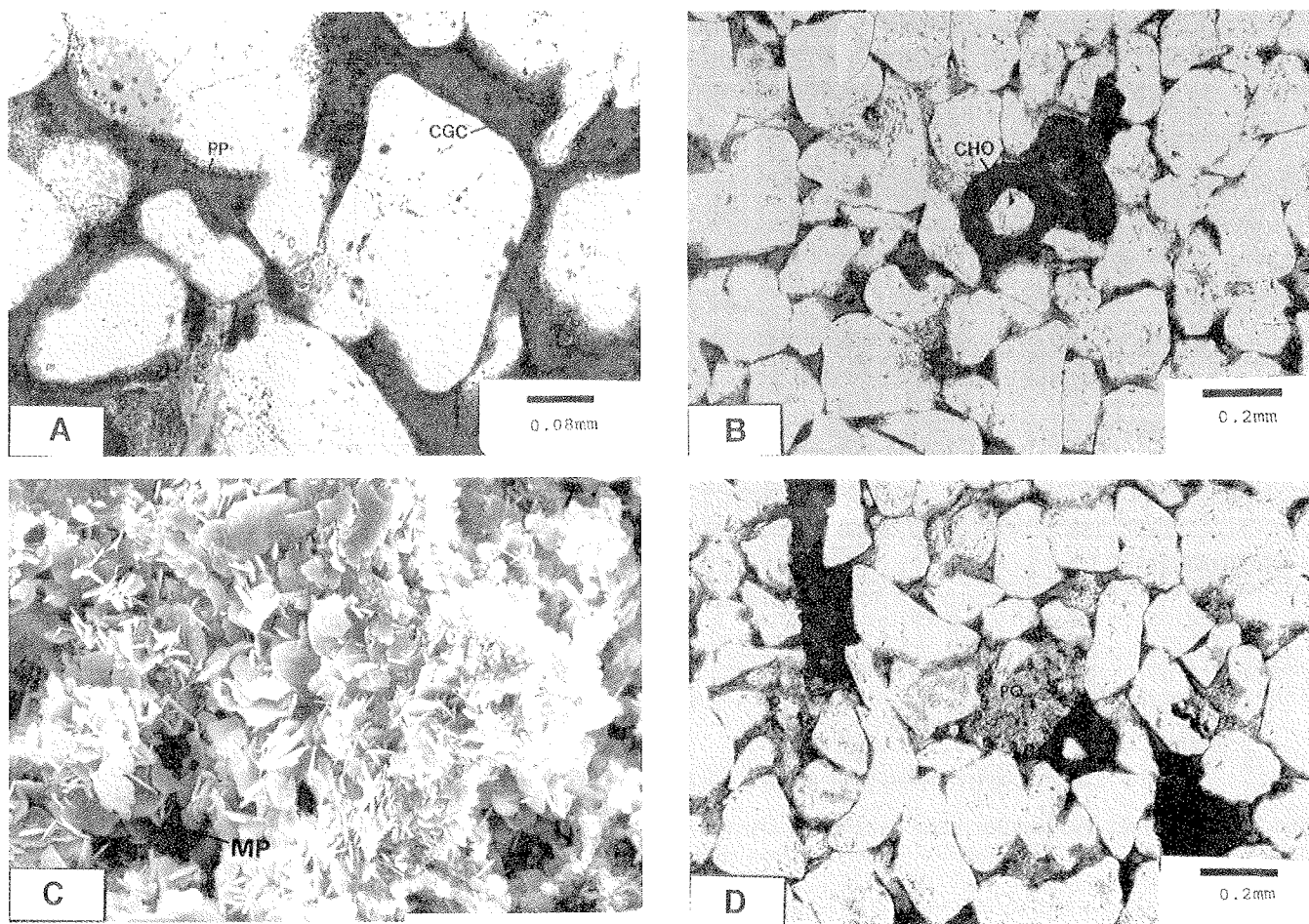


Figure 16. Examples of porosity types in the Cunningham and Britt sandstones. (A) Photomicrograph of primary porosity (PP) in the lower Cunningham sandstone at a depth of 16,474 ft. Clay grain coating (CGC) prevented nucleation of quartz overgrowths, preserving the smooth, noncorroded grain boundary. (B) Photomicrograph of primary porosity preserved by chamosite clay grain coatings. Chamosite ooids are evident in center of photomicrograph. Left ooid (CHO) nucleated on a quartz grain, whereas the right ooid formed on bioclast. Gulf No. 1-14 Lillian Miller. Depth, 16,474.6 ft. Plane-polarized light. (C) Scanning electron microscope photograph, showing microporosity (MP) that developed between chlorite crystals that coat quartz grains. (D) Photomicrograph of intragranular porosity that developed by the partial dissolution of polycrystalline quartz grains. Gulf No. 1-14 Lillian Miller. Depth, 16,474.5 ft. Plane-polarized light.

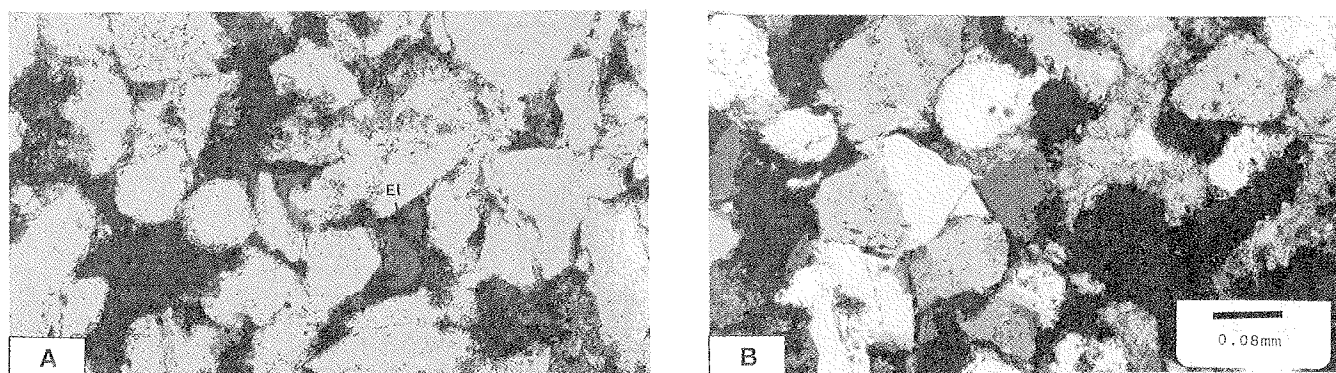
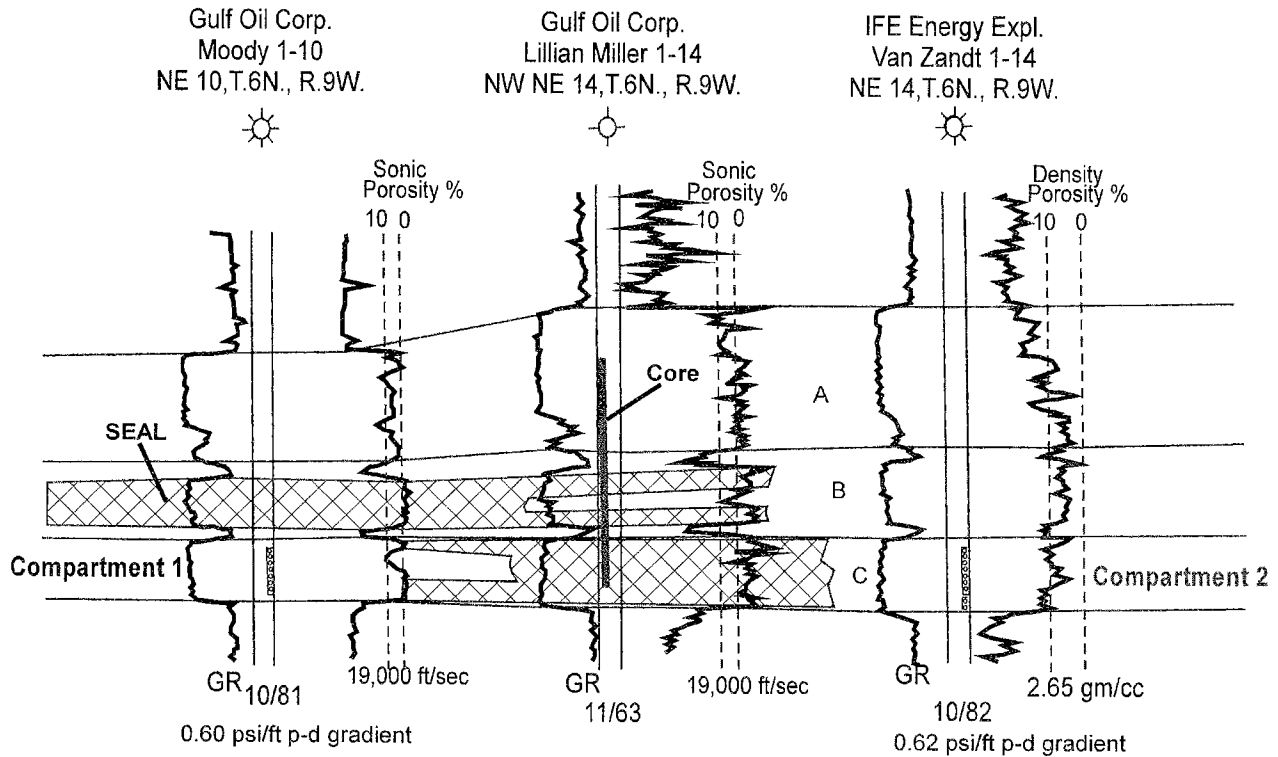


Figure 17. Photomicrograph of enlarged intergranular porosity (EI) formed by dissolution of early calcite cement. Chevron No. 1 Berta Lay. Depth, 16,630.5 ft. (A) Plane-polarized light. (B) Cross-polarized light.



Compartments in Lower Cunningham Sandstone "Unit C"

Figure 18. Schematic cross section with wireline-log signatures, showing cemented (cross-hatching) and porous zones in lower Cunningham unit C. Unit C is cemented, as encountered in the Gulf No. 1-14 Lillian Miller in the NW NE sec. 14, T. 6 N., R. 9 W., but is porous, as encountered in the IFE No. 1-14 Van Zandt in the C NE sec. 14, T. 6 N., R. 9 W. Unit C is also porous in the Gulf No. 1-10 Moody in the C NE sec. 10, T. 6 N., R. 9 W. In addition, the No. 1-14 Van Zandt has a higher pressure/depth gradient than the No. 1-10 Moody, which was completed 1 year earlier.

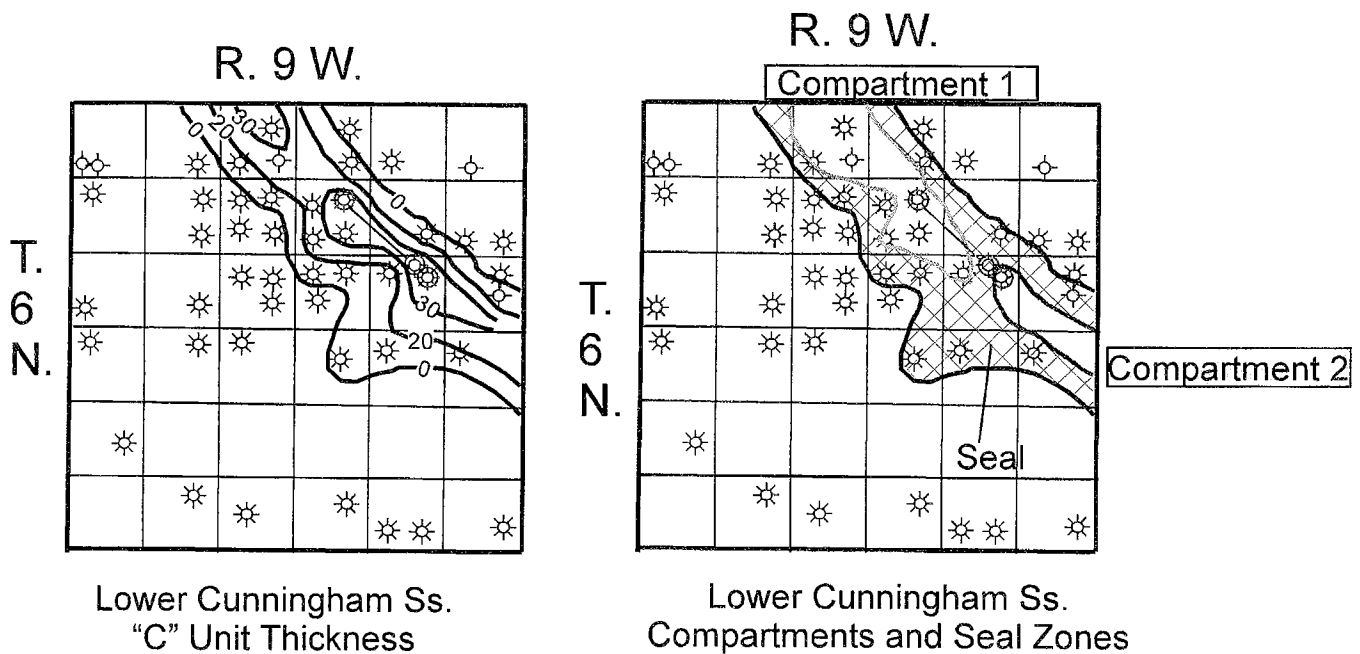


Figure 19. Map representation of the proposed compartments and seals shown in Figure 18. The Gulf No. 1-14 Lillian Miller drilled the cemented barrier between compartments 1 and 2, which were encountered by the No. 1-10 Moody and No. 1-14 Van Zandt wells, respectively.

Abdalla, who asked thought-provoking questions and made suggestions that stimulated the research.

REFERENCES CITED

- Brenner, R. L., 1980, Construction of process-response models for ancient epicontinental sea deposition using partial analogs: *American Association of Petroleum Geologists Bulletin*, v. 64, p. 1223–1244.
- Brenner, R. L.; and Davies, D. K., 1973, Storm-generated coquinoid sandstone: genesis of high-energy marine sediments from the Upper Jurassic of Wyoming and Montana: *Geological Society of America Bulletin*, v. 84, p. 1685–1698.
- Elias, M. K., 1956, Upper Mississippian and Lower Pennsylvanian formations of south-central Oklahoma, in *Petroleum geology of southern Oklahoma—a symposium sponsored by the Ardmore Geological Society*: American Association of Petroleum Geologists, Tulsa, p. 56–134.
- Haiduk, J. P., 1987, Facies analysis, paleoenvironmental interpretation, and diagenetic history of Britt sandstone (Upper Mississippian) in portions of Caddo and Canadian Counties, Oklahoma: Oklahoma State University unpublished M.S. thesis, 188 p.
- Ortoleva, P.; Al-Shaieb, Z.; and Puckette, J., 1995, Genesis and dynamics of basin compartments and seals: *American Journal of Science*, v. 295, p. 345–427.
- Peace, H. W., II, 1965, The Springer Group of the southeastern Anadarko Basin in Oklahoma: *Shale Shaker*, v. 15, no. 5, p. 81–99.
- Pittman, E. D., 1979, Porosity, diagenesis, and productive capability of sandstone reservoirs: *Society of Economic Paleontologists and Mineralogists Special Publication* 26, p. 159–173.
- Rascoe, Bailey, Jr.; and Adler, F. J., 1983, Permo-Carboniferous hydrocarbon accumulations, mid-continent, U.S.A.: *American Association of Petroleum Geologists Bulletin*, v. 67, p. 979–1001.
- Rice, A. R., 1993, Depositional environment, petrology, and compartmentalization of Cunningham and Britt sandstones in parts of Caddo, Grady, and Comanche Counties, Anadarko Basin, Oklahoma: Oklahoma State University unpublished M.S. thesis, 192 p.
- Straka, J. J., II, 1972, Conodont evidence of age of Goddard and Springer Formations, Ardmore Basin, Oklahoma: *American Association of Petroleum Geologists Bulletin*, v. 56, p. 1087–1099.
- Tillman, R. W.; and Martinsen, R. S., 1984, The Shannon shelf-ridge sandstone complex, Salt Creek anticline area, Powder River Basin, Wyoming, in Tillman, R. W.; and Siemers, C. T. (eds.), *Siliciclastic shelf sediments*: Society of Economic Paleontologists and Mineralogists Special Publication 34, p. 84–142.
- Waddell, D.E., 1966, Pennsylvanian fusulinids in the Ardmore basin, Love and Carter Counties, Oklahoma: *Oklahoma Geological Survey Bulletin* 113, 128 p.
- Westheimer, J. M., 1956, The Goddard Formation, in *Petroleum geology of southern Oklahoma—a symposium sponsored by the Ardmore Geological Society*: American Association of Petroleum Geologists, Tulsa, v. 1, p. 292–396.

Sequence Stratigraphy, Lithofacies, and Reservoir Quality, Upper Morrow Sandstones, Northwestern Shelf, Anadarko Basin

James Puckette and Zuhair Al-Shaieb (deceased)

Oklahoma State University
Stillwater, Oklahoma

Erin Van Evera

UNOCAL 76
Sugar Land, Texas

ABSTRACT.—Upper Morrow valley-fill sandstones are a major oil and gas exploration target on the northwestern shelf of the Anadarko Basin. Integrated core, production, and wireline-log data from wells in Kansas and Oklahoma were used to interpret lithofacies and depositional history of the late Morrowan interval. Three major assemblages were recognized: marine, fluvial, and estuarine. The primary marine lithofacies are dark fossiliferous (shelly) shale and bioclastic sandstone. Fluvial facies are dominantly medium- to coarse-grained sandstones and granule conglomerates characteristic of braided- to meandering-stream to point-bar channel sequences. Sedimentary features include trough cross-bedding containing stacked fining-upward sequences, low-angle cross-beds, and fine- to coarse-grained sandstones with interbedded or laminated silty, shaly, and coaly intervals. Estuarine facies consist of interbedded fine- to medium-grained sandstones and mudrocks with abundant trace fossils such as burrows or feeding traces.

Core and wireline-log evidence indicates that the upper Morrow contains several depositional sequences whose boundaries are defined by valley incision. Valleys developed in response to major drops in relative sea level and regression. Lowstand systems tract (LST) deposits are limited to a few thin, clay-clast conglomerates within the valleys. Subsequent sea-level rise during the transgressive systems tract (TST) resulted in valley filling by fluvial and estuarine facies. With continued rise and transgression, sediment deposition shifted landward. Marine silt and mud were deposited within the valley and in the interfluvial areas. These marine facies contain the maximum flooding surface (MFS). Subsequent sea-level stabilization resulted in deposition of the overlying highstand systems tract (HST) sediment assemblage.

Reservoir quality is controlled by the sequence-stratigraphic framework coupled with compositional and textural parameters. Braided-stream/point-bar sequences deposited during the TST contain better reservoir lithology. Average porosity and permeability are 13.4% and 50.6 millidarcies, respectively. Marine sandstones contain abundant skeletal grains and carbonate cement that occluded porosity. Fine-grained estuarine sandstones are typically poor-quality reservoirs as the result of high detrital-clay content and biogenic modification that destroyed primary porosity.

INTRODUCTION

Late Morrowan (Pennsylvanian) sea-level fluctuation influenced depositional style and lithofacies on the northwestern shelf of the Anadarko Basin. Deposition on the shelf was dominated by fluvial and marine processes that are represented by channel-fill sands encased in marine mud (Puckette and others, 1996). Over the past decade, a number of studies concluded that cyclic sea-level fluctuation was responsible for the formation of these transgressive/regressive depositional sequences, which consist of lowstand valleys, heterogeneous valley fills of predominantly transgressive origin, and highstand muds. Sequence boundaries were defined at the ero-

sional base of valleys, whereas maximum flooding occurred in the mudrock sections above valley fills.

Integrated core, geophysical-logging, and production data indicate that valley fills are complex heterogeneous mixtures of fluvial and estuarine rocks. Marine influence within valley fills is suggested by the presence of fossiliferous sandstones. Fluvial lithofacies, especially coarse-grained sandstones and granule conglomerates, are highly porous and permeable. In contrast, mud-rich estuarine rocks and calcite-cemented, marine-influenced rocks have very low values of porosity and permeability. In this study, we examine the lithofacies assemblages within late Morrowan valleys and provide quantitative assessment of porosity and permeability. Furthermore, we present conceptual models that may explain discontinuities

Puckette, Jim; Al-Shaieb, Zuhair; and Van Evera, Erin, 2008, Sequence stratigraphy, lithofacies, and reservoir quality, upper Morrow sandstones, northwestern shelf, Anadarko Basin, in Andrews, R. D. (ed.), Morrow and Springer in the southern Midcontinent, 2005 symposium: Oklahoma Geological Survey Circular 111, p. 81–97.

in sandstone bodies that could enhance exploration and development success.

STRATIGRAPHY AND GEOLOGIC SETTING

The term *Morrow Formation* is an informal operational term used to describe the stratigraphic unit that represents

the Pennsylvanian Morrowan Series (Fig. 1). Another informal term, the "Squaw Belly limestone," is used to separate upper and lower Morrow intervals (Puckette and others, 1996). The use of the terms *late Morrowan*, *upper Morrow*, *early Morrowan*, and *lower Morrow* follows convention established by the oil and gas industry. Sandstone bodies within the Morrow

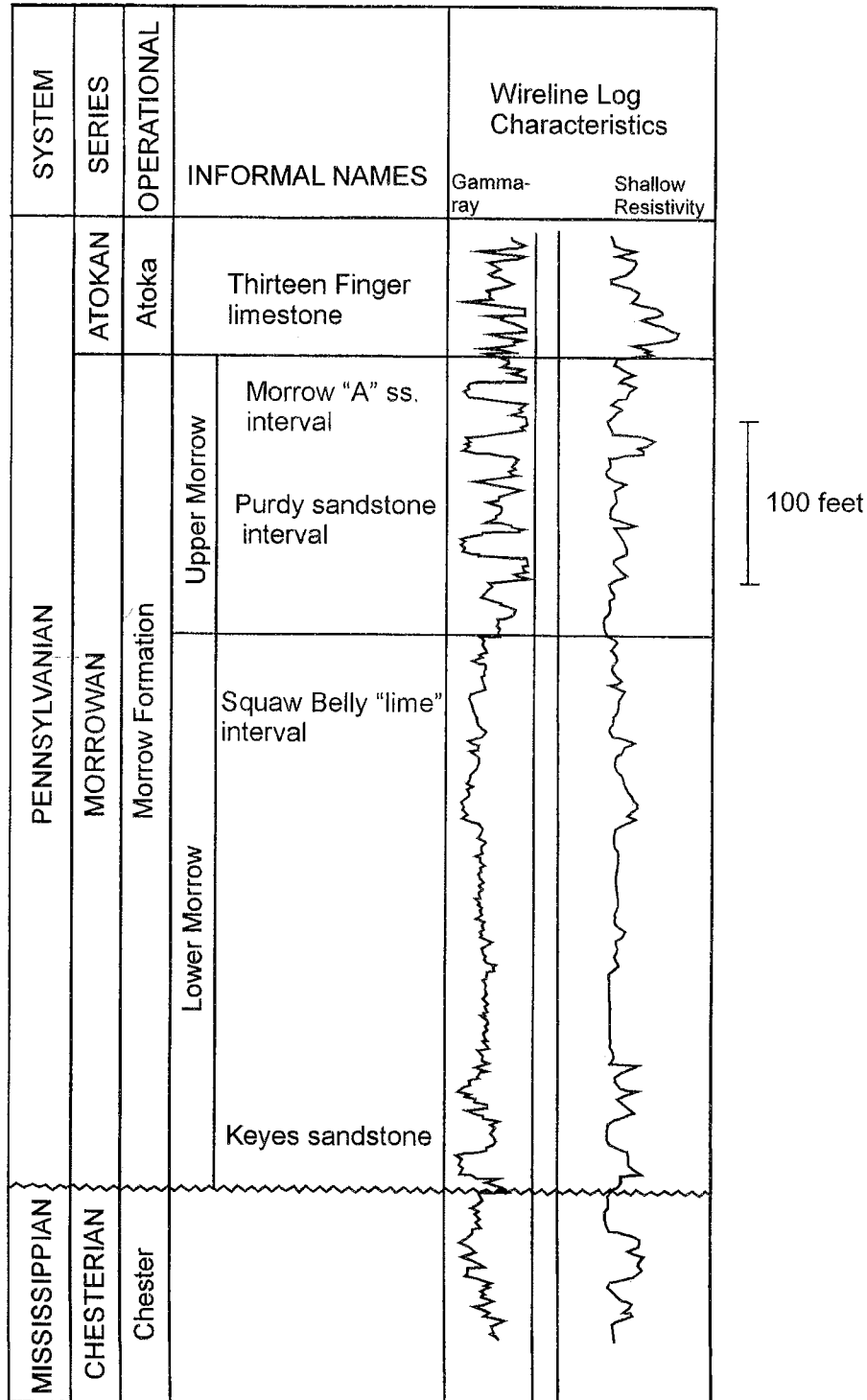


Figure 1. Stratigraphic-nomenclature chart, showing informal divisions and operational terminology for the Morrowan Series in the study area.

are commonly given locally derived names that command widespread use.

The upper Morrow examples in this study are all from oil- and gas-producing fields on the northwestern shelf of the Anadarko Basin/Hugoton Embayment region of the Oklahoma and Texas Panhandles, southeastern Colorado, and western Kansas (Fig. 2). In later Morrowan time, this area was transected by south-

ward-flowing, fluvial-dominated sediment-dispersal systems. The positions of these systems were influenced by positive elements, including the Apishapa-Sierra Grande Uplift to the west, the Ancestral Front Range and Transcontinental Arch to the north, the Central Kansas Uplift to the northeast, and the Wichita-Amarillo Uplift to the south (Sonnenberg and others, 1990). Stream gradients in the region are reported to be 0.4 to 0.9

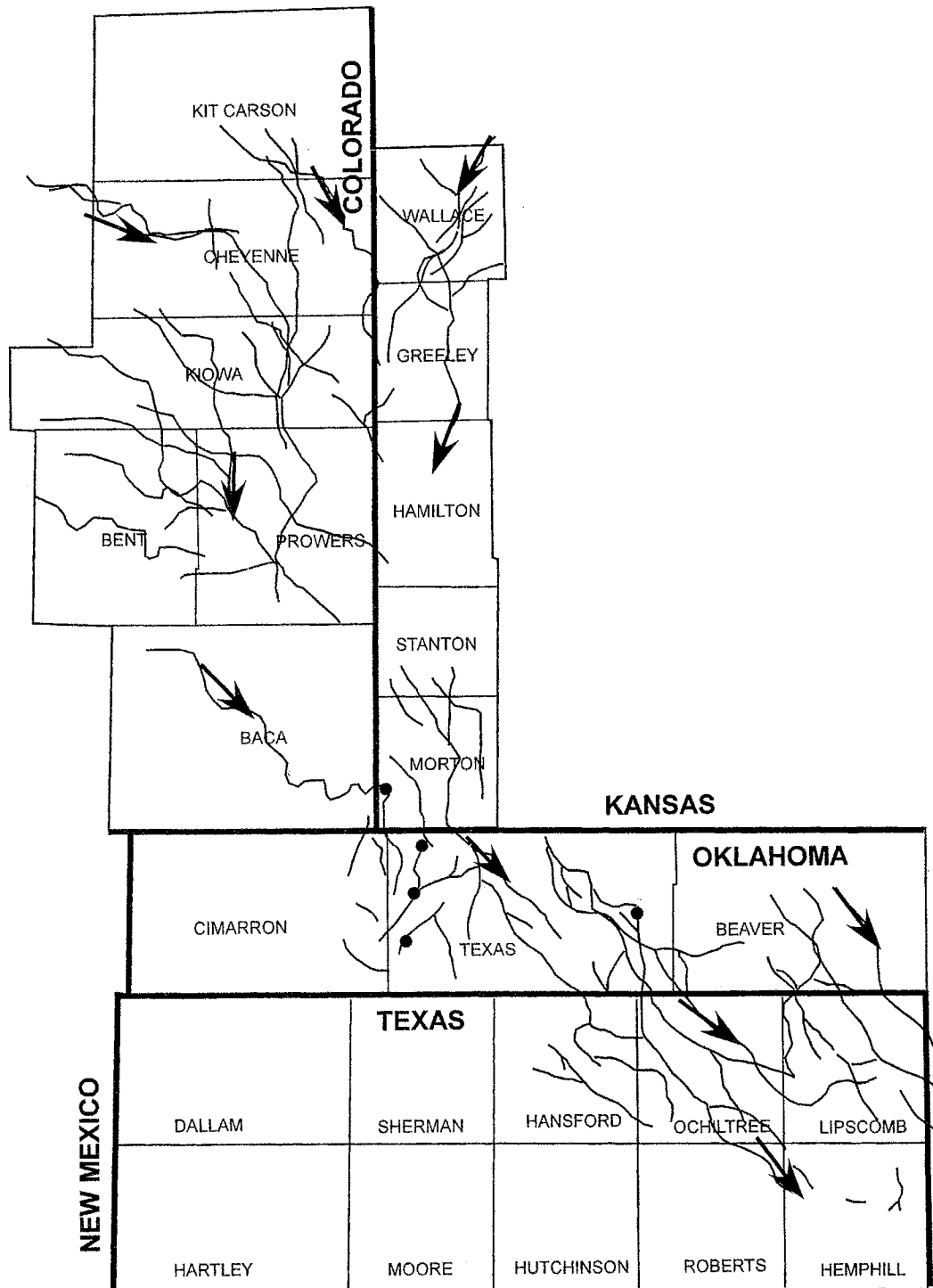


Figure 2. Map showing sediment-dispersal systems for the late Morrowan. Trends indicate the general southerly flow of streams toward the Anadarko Basin (after Puckette and others, 1996; Blakeney and others, 1990; Bowen and others, 1990; and Sonnenberg and others, 1990). Wells from which cores were examined are shown as black circles.

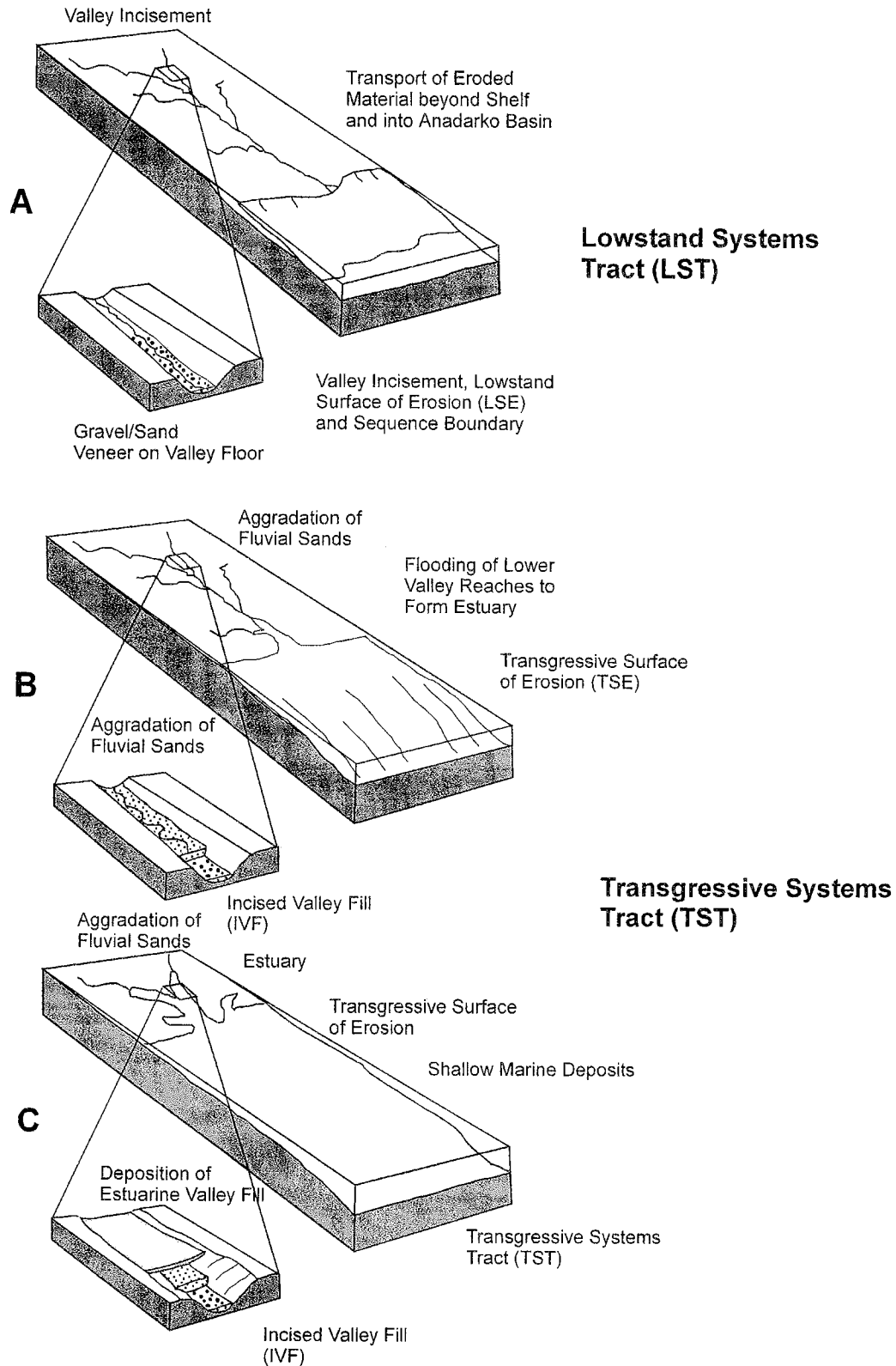


Figure 3. Diagram illustrating the systems tracts that controlled upper Morrowan deposition. (A) Lowstand systems tract (LST), showing position of valley incisement and area of deposition, and valley containing thin veneer of fluvial sediments. (B) Transgressive systems tract (TST), showing aggradation of fluvial sands and incipient flooding of valley to form an estuary. (C) TST continued, showing deposition of estuarine sediments in flooded valley and deposition of marine sediments over former lower reaches of the stream (diagram from Wheeler and others, 1990).

ft/mi (Cornish, 1982) and <2.5 ft/mi (Swanson, 1979), indicating flat topography. This low-relief shelf was vulnerable to flooding and subaerial exposure as the Morrowan sea level fluctuated in response to glacio-eustatic or tectonic processes.

PREVIOUS STUDIES

The economics of drilling upper Morrow reservoirs make them a primary drilling target in the Oklahoma and Texas Panhandles, southeastern Colorado, and western Kansas. Upper Morrow reservoirs in these four states have produced >320 million barrels of oil and 3.5 trillion cubic ft of gas from reservoirs at drilling depths of <6,000 ft. These reservoirs are the focus of numerous studies. More recent ones that examine specific fields include DeVries (2005), Al-Shaieb and Puckette (2002), Shepherd (2000), and Luchtel (1999). The sequence-stratigraphic framework for the Morrowan Series was established by Al-Shaieb and others (1995), Puckette (1993), Gerken (1992), Wheeler and others (1990), Sonnenberg and others (1990), Kristinik and Blakeney (1990), Harrison (1990), and Bowen and others (1990). Rascoe and Adler (1983), Cornish (1982), Swanson (1979), Benton (1971), and Forgotson and others (1966) published papers that provided the foundation for the later studies.

SEQUENCE STRATIGRAPHY

The strata that constitute the Morrow interval on the northern shelf of the Anadarko Basin are interpreted to have formed as the result of cyclic sea-level fluctuation induced by tectonic or glacio-eustatic processes (Sonnenberg and others, 1990; Kristinik and Blakeney, 1990; Wheeler and others, 1990;

Al-Shaieb and others, 1995). During sea-level lowstands, late Morrowan streams eroded the underlying rocks or sediments to form valleys (Fig. 3). During subsequent transgressions, the valleys filled with sediments that were trapped within their walls (Fig. 3). As transgression continued, the valleys and the surrounding interfluvial areas were flooded and covered by shallow-marine muds (Fig. 4). Maximum flooding occurred in this transgressive phase. Marine-mud deposition dominated highstand conditions, which continued until the regression associated with the next lowstand. Lowstand erosional surfaces form the sequence boundaries that define each cycle.

SEDIMENT SUPPLY AND DEPOSITIONAL PROCESSES

Core and wireline-log evidence indicates that sand-sized and coarser clastic material is confined to the stream valleys and that overbank or flood deposits are rare in the upper Morrow. In addition, there is no evidence on the northern shelf to support the formation of extensive deltaic complexes during the Morrowan. In this respect, the Morrowan is much different than the younger Desmoinesian Red Fork and Skinner systems, which built large deltaic complexes in the Anadarko Basin (Puckette, 1990; Puckette and Al-Shaieb, 2003; Al-Shaieb and others, 1995). Skinner and Red Fork dispersal systems drained large areas of the continent, including large exposures of Precambrian igneous and metamorphic basement rocks on the Transcontinental Arch and the Canadian Shield (Rascoe and Adler, 1983). In contrast, the late Morrowan drainage basin was located primarily on relatively mud- and carbonate-rich sedimentary-rock outcrops (Rascoe and Adler, 1983; Rader, 1990). As a result, the supply of coarser grained

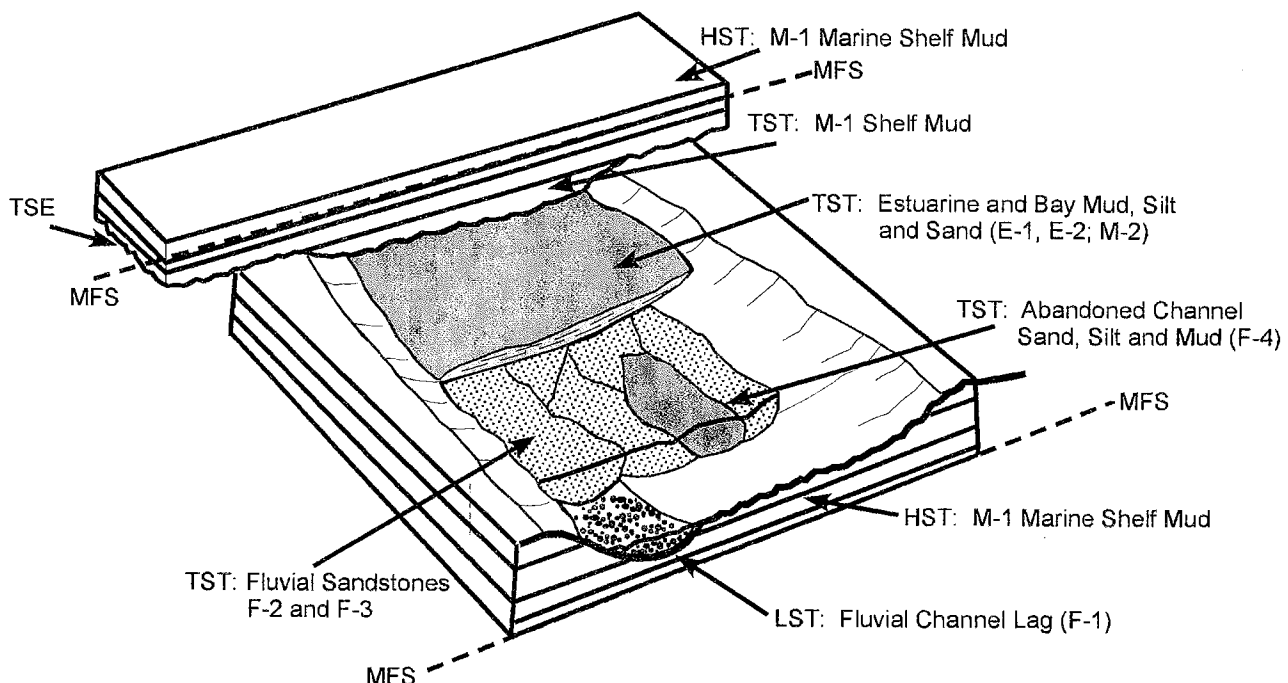


Figure 4. Diagram of setting for depositional sequence of Morrowan strata in the study area (diagram modified from Wheeler and others, 1990). See text and Figure 7 for explanation of abbreviations and lithofacies designations.

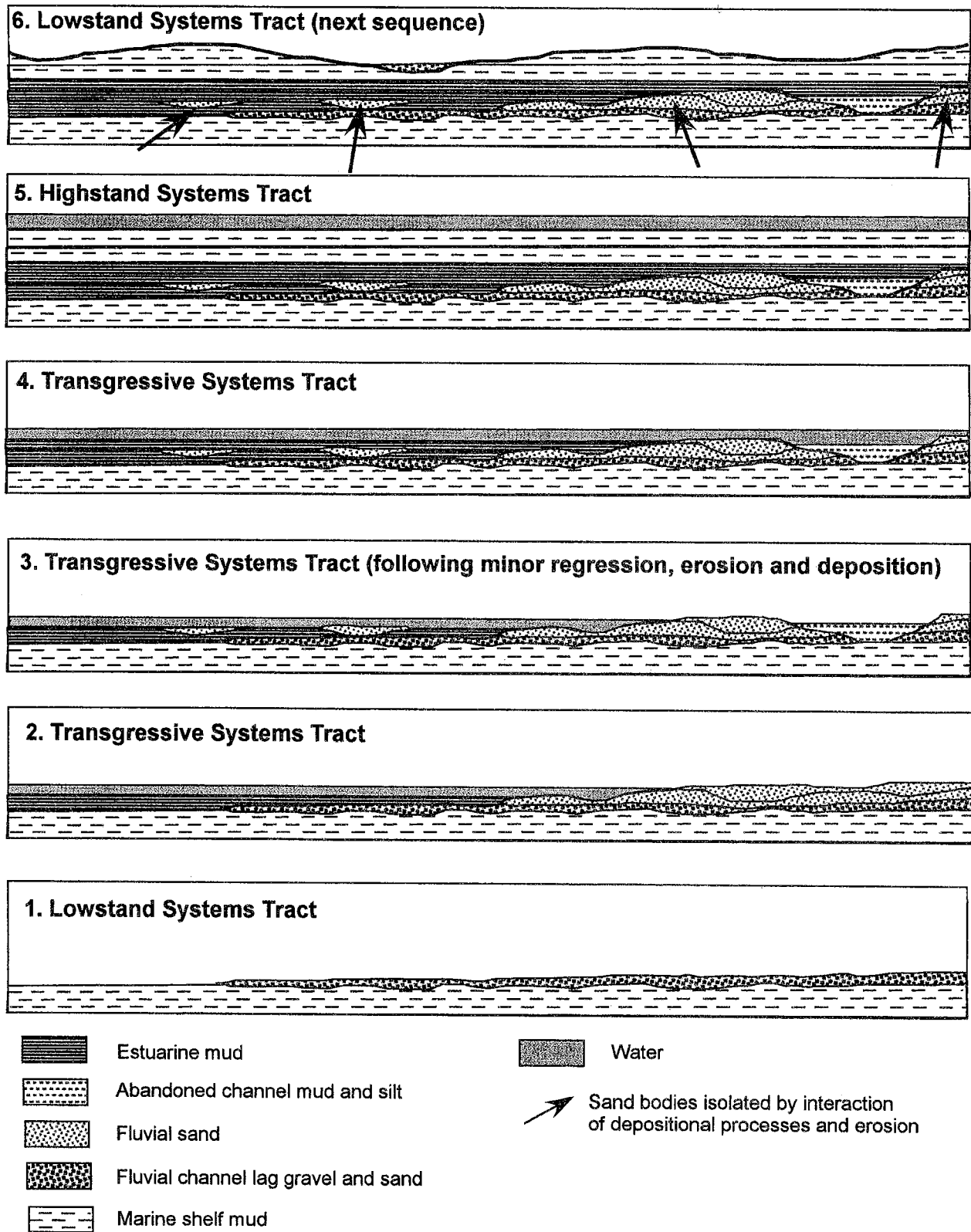


Figure 5. Diagrammatic depositional dip-oriented cross section, illustrating the spatial relationships between sand bodies and intervening mud fill. (1) LST fluvial-channel lag gravel and sand are deposited on unconformity surface, which is a sequence boundary. (2) TST estuarine mud deposited on lowstand gravel as sand accumulated upstream. (3) TST continues after minor regression, erosion, and deposition. Channelization, abandonment, and deposition of mud and silt form low-permeability barrier in previously continuous deposit. (4) TST continues with flooding of previous deposits. (5) HST marine-mud deposition, following maximum flooding. (6) LST, following drop in sea level. Eroded surface is sequence boundary.

(sand-sized and larger) siliciclastic material was limited. Low sediment supply combined with the relatively dry climatic conditions to generate sediment-starved streams that apparently remained confined to their channels during base flow and flooding. As a result, during sea-level lowstands, most sediment was transported beyond the shelf and deposited in the rapidly subsiding Anadarko Basin.

During subsequent sea-level rises, flooding of the valleys trapped sediment within the channels. As stream energy decreased with rising base level, proximity to the shoreline influenced depositional processes. Coarser grained material was deposited in braided streams that were relatively unaffected by the advancing shoreline. Lower gradient sections developed meanders that resulted in the deposition of finer grained sands. Within the developing estuary, mud and silt were the dominant sediments. The backstepping channel fill allowed the simultaneous deposition of sand in updip stretches of the stream while mud-rich sediments were deposited close to the estuarine-fluvial interface. As a result, a valley could contain a number of fluvial sand bodies of slightly different ages separated by younger mud-rich fill (Fig. 5).

Where transgression proceeded uninterrupted, older braided fluvial deposits were succeeded by sediments of meandering-stream or estuarine origin. In some areas a drop in sea level forced regression, and existing sediments were eroded and/or succeeded by more proximal ones (Puckette, 1993). These processes contributed to the heterogeneity of fill in late Morrowan valleys (Fig. 3). Consequently, accumulations of coarse sand were frequently isolated or partitioned by later processes, causing the heterogeneity evident in some upper Morrow fields.

UPPER MORROW LITHOFACIES

Cores of upper Morrow sandstones were examined from five fields in Oklahoma and Kansas. Eight distinct lithofacies were recognized: (1) matrix-rich paraconglomerate, F-1; (2) coarse-grained sandstone to granule conglomerate that exhibits stacked fining-upward intervals and planar and trough cross-bedding, F-2; (3) ripple to low-angle cross-bedded, coarse- to fine-grained sandstone containing clay clasts and carbonaceous material, F-3; (4) fine-grained sandstone interbedded with silt, shale, and coaly material, F-4; (5) interbedded fine- to medium-grained sandstone and shale containing abundant trace fossils, E-1; (6) fine- to medium-grained burrowed sandstone and dark shale interbedded with thin coarse-grained sandstone, E-2; (7) thinly laminated dark mudrocks that contain abundant marine invertebrate fos-

sils, M-1; and (8) fine- to coarse-grained, calcite-cemented, fossiliferous sandstone, M-2. The descriptions, reservoir properties, and origins of these facies are explained as follows and are shown in Figure 6. Reservoir properties were determined from thin-section analysis, measurements of core porosity and permeability, and fluid-production data.

Fluvial Lithofacies

Matrix-Rich Paraconglomerate (F-1)

The F-1 lithofacies is composed of thin (<1- to 2-ft-thick) pebble conglomerates consisting of claystone clasts in a clay-rich matrix. These have generally low porosity and permeability as the result of abundant pseudomatrix and cement. F-1 conglomerates are poor-quality reservoirs.

F-1 lithofacies is interpreted as a high-energy deposit that formed during sea-level lowstand. F-1 represents the LST and contains clasts eroded from the channel floor and banks.

Lithofacies	Sedimentary Structures and Depositional Facies	Reservoir Characteristics
Fluvial (F)		
F-1	Matrix-supported paraconglomerate. <i>High current-energy stream</i>	Generally poor quality. Low porosity and permeability are result of cement and pseudomatrix.
F-2	Coarse-grained sandstone to conglomerate. This package is characterized by trough and planar cross-bedding and contains stacked fining-upward sets. <i>High-energy braided stream of middle to lower channel sequence</i>	Generally fair to good quality. Primary and enlarged intergranular porosity types are common.
F-3	Ripple to low-angle planar cross-bedded, fine- to coarse-grained sandstone with scattered clay clasts and carbonaceous material. <i>Meandering stream of upper channel sequence</i>	Generally fair to good quality. Porosity reduction a result of clay matrix, carbonate cement and/or pore-filling, authigenic kaolinite.
F-4	Fine-grained sandstone sporadically interbedded/interlaminated with silty, shaly and coaly interval. Plant fossils scarce to common. <i>Channel abandonment</i>	Generally poor to fair quality. Significant amount of pore space is filled with clay matrix.
Estuarine (E)		
E-1	Interbedded fine- to medium-grained sandstone and shale containing abundant trace fossils. <i>Mid-estuary with minimal fluvial and marine influence. Low energy.</i>	Generally poor quality. Low porosity and permeability are result of carbonate cement and pseudomatrix.
E-2	Fine- to medium-grained, burrowed sandstone and dark shale that is interbedded with thin, coarse-grained sandstone. <i>Upper estuary: tidally influenced with variable energy and possible fluvial input</i>	Generally fair quality. Primary and enlarged intergranular porosity types are common.
Marine (M)		
M-1	Dark shale and/or claystone. Calcareous intervals contain abundant marine invertebrate fossils. <i>Marine low-energy environment. Disaerobic offshore shelf setting</i>	Seal-forming lithofacies
M-2	Fine- to coarse-grained, calcite-cemented and fossiliferous sandstone. <i>Shallow-marine high-energy environment</i>	Poor-quality reservoir as a result of extensive calcite cement.

Figure 6. Chart of sedimentary structures, along with depositional facies and reservoir characteristics, in upper Morrow strata in the study area (modified from Luchtel, 1999; Al-Shaieb and Puckette, 2002).

Coarse-Grained Sandstone to Granule Conglomerate (F-2)

The F-2 lithofacies consists of graded intervals of granule conglomerate to coarse-grained sandstone that contains planar and trough cross-bedding. These poorly sorted sandstones are composed of multiple-stacked, fining-upward sets that are typically <2 ft thick. F-2 sandstones are fair- to good-quality reservoirs with primary and secondary porosity.

The coarse grain size, graded fining-upward character, and lack of burrowing or marine indicators support the interpretation that the F-2 lithofacies is of high-energy fluvial origin and resembles deposition documented in a braided-stream environment.

Coarse- to Fine-Grained Sandstone with Ripple- and Low-Angle Cross-Bedding (F-3)

The F-3 lithofacies is coarse- to fine-grained sandstone that is ripple- to low-angle cross-bedded and contains scattered clay clasts and carbonaceous material. F-3 is of generally fair to good reservoir quality but contains less porosity and permeability than F-2. Porosity and permeability are commonly reduced in F-3 sandstones by authigenic, pore-filling kaolinite and carbonate cement.

The finer grain size, sedimentary structures, and lack of marine indicators support the contention that F-3 represents deposition in the decreased energy of a meandering-stream deposit. This interpretation is corroborated by the spatial distribution pattern of sand bodies and paleocurrent directions determined by dipmeter data (DeVries, 2005).

Fine-Grained Sandstone, Siltstone, Shale, and Coaly Material (F-4)

The F-4 lithofacies includes planar-laminated, very fine to fine grained sandstone, shale, and siltstone. Carbonaceous material is common, including leaf and stick impressions, root traces, and coaly material, is common. F-4 lithologies are poor to fair for reservoir quality, as pore space is commonly filled with clayey matrix.

The abundant plant material and lack of marine indicators suggest that F-4 represents abandoned channel fill or swamp deposits within the fluvial valley.

Estuarine Lithofacies

Burrowed Fine- to Medium-Grained Sandstone (E-1)

The E-1 lithofacies is burrowed, fine- to medium-grained sandstone interbedded with dark shale. E-1 sandstones are generally poor-quality reservoirs as a result of burrowing that homogenized sediment and introduced clayey matrix into sandy intervals.

The burrowing, the interbedded sandstone and shale, and the lack of a normal-marine invertebrate fauna, are evidence that E-1 was deposited in a mid-estuarine, low-energy environment that was not influenced greatly by fluvial or marine processes.

Thinly Bedded, Fine- to Medium-Grained Burrowed Sandstone, Shale, and Coarse-Grained Sandstone (E-2)

The E-2 lithofacies contains silt- and clay-rich burrowed fine- to medium-grained sandstones, thin shales, and thin

nonburrowed coarse-grained sandstones. The coarse-grained sandstones are generally <1.5 ft thick. The fine-grained sandstones are ripple laminated and form wavy to planar beds within the interbedded shales. The fine- to medium-grained sandstone is poor-quality reservoir rock as a result of biotic homogenization. The coarse-grained sandstones have fair to good reservoir properties.

The discrepant grain sizes and the relative amount of biotic indicators suggest that E-2 facies was influenced by fluvial and estuarine processes. Horizontally laminated, burrowed sandstone and shale suggest an estuarine environment, whereas the coarse-grained sandstone without burrowing indicates higher energy fluvial or tidal processes. This facies may represent deposition in the upper estuary, where tidal or fluvial processes influenced energy input.

Marine Lithofacies

Fossiliferous Dark Shale or Claystone (M-1)

The M-1 facies consists of thinly laminated dark shale and claystone, so M-1 is not a reservoir facies. Normal-marine invertebrate fossils, including brachiopods and echinoderms, are common.

The invertebrate fossils and dark color indicate that M-1 was deposited as marine-shelf mud. The bioclast-rich, conglomeratic zone near the base of the M-1 facies is interpreted as a transgressive lag deposit.

Fossiliferous Sandstone (M-2)

The M-2 lithofacies is coarse- to fine-grained, planar-cross-bedded sandstone that contains marine invertebrate bioclasts, including brachiopod, echinoderm, and bryozoan fragments. M-2 sandstones become finer grained upward and increasingly rich in clay and silt matrix. Burrowing is common in the clay- and silt-rich intervals. M-2 is a poor-quality reservoir facies as a result of abundant carbonate cement in clay-poor sandstones and abundant clayey matrix in the mud-rich intervals.

Abundant bioclastic debris and cross-bedding suggest that the mud-poor M-2 facies was deposited within a high-energy, marine-influenced environment. As the distribution of lithofacies M-2 appears to be limited to the valley trends, it is believed to represent a marine incursion into the estuary. Increasing matrix toward the top indicates lower energy, deeper water, and a possible transition to widespread flooding that inundated the interfluvial areas.

SEQUENCE STRATIGRAPHY AND LITHOFACIES SUCCESSION

Lithofacies successions reflect the response of depositional processes to changing sea level. Luchtel (1999) developed a depositional dip-oriented schematic cross section that shows the generalized succession (Fig. 7). This schematic diagram illustrates the following stages:

A. HST.—Sea level is near maximum, and mud dominates deposition across the flooded shelf.

B. LST.—Sea level is near lowest level; forced regression exposes the shelf to erosion, and valleys form. Deposition is

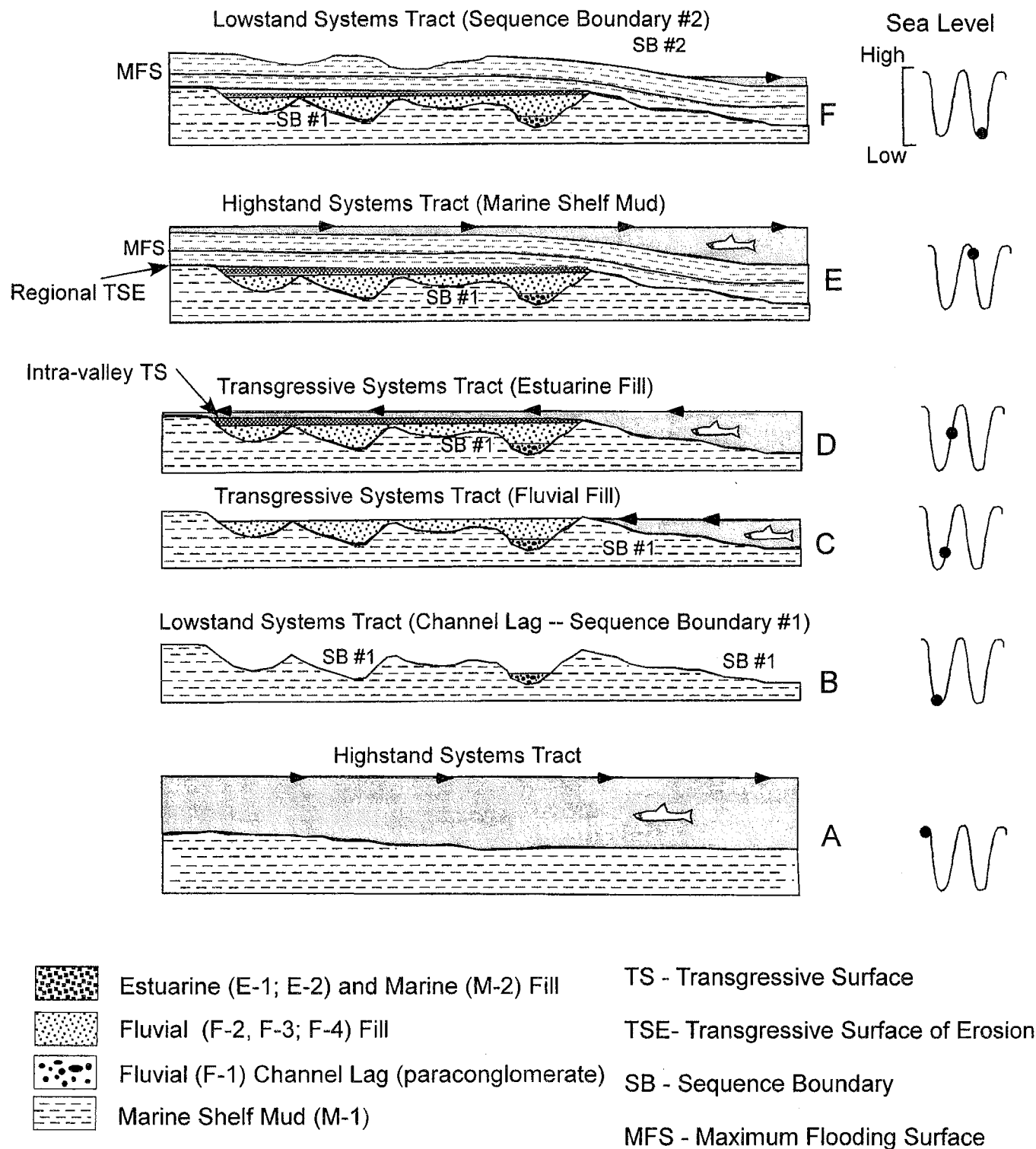


Figure 7. Schematic diagram showing evolution of upper Morrowan successions (from bottom to top) in the study area. Depositional settings in response to sea-level change are shown in cross sections oriented along depositional dip (modified from Luchtel, 1999). See text for details.

restricted to channel lag deposits. The erosional surface in this stage is a sequence boundary.

C. TST.—Sea level begins to rise, and the valley floods, causing deposition of fluvial sands in the valley.

D. TST.—Transgression continues with rising base level. Valleys fill with fluvial, estuarine, and marine sediment. Flooding of the interfluvium occurs. At maximum water depth (not shown), the maximum flooding surface (MFS) formed.

E. HST.—Maximum flooding occurred, and sea level begins to decline. Deposition across the flooded shelf is dominated by mud and silt.

F. LST.—Sea level has dropped to its lowest level. Forced regression occurs, causing retreat of the shoreline toward the basin axis. Erosion of the valley complex occurs, and a sequence boundary is formed.

The lithofacies successions recorded in cored intervals examined in this study are similar to those illustrated by Luchtel (1999) and Wheeler and others (1990). Similar facies successions are described in a number of other studies, including those of DeVries (2005), Krystinik and Blakeney (1990), and Sonnenberg and others (1990).

Cores from the Carthage, Eva NW, and Hardesty NE Fields are used to illustrate examples of upper Morrow lithofacies successions.

The core from the No. 3 Hendrix well in the Carthage Field is composed of sandstone and shale. The core contains six lithofacies: E-1, E-2, F-1, F-2, M-1, and M-2 (Fig. 8). Wireline logs suggest that the basal sandstone is in sharp contact with the underlying (marine) shale, which was not cored. The lowest cored interval (4,566–4,567 ft) contains burrowed, inter-

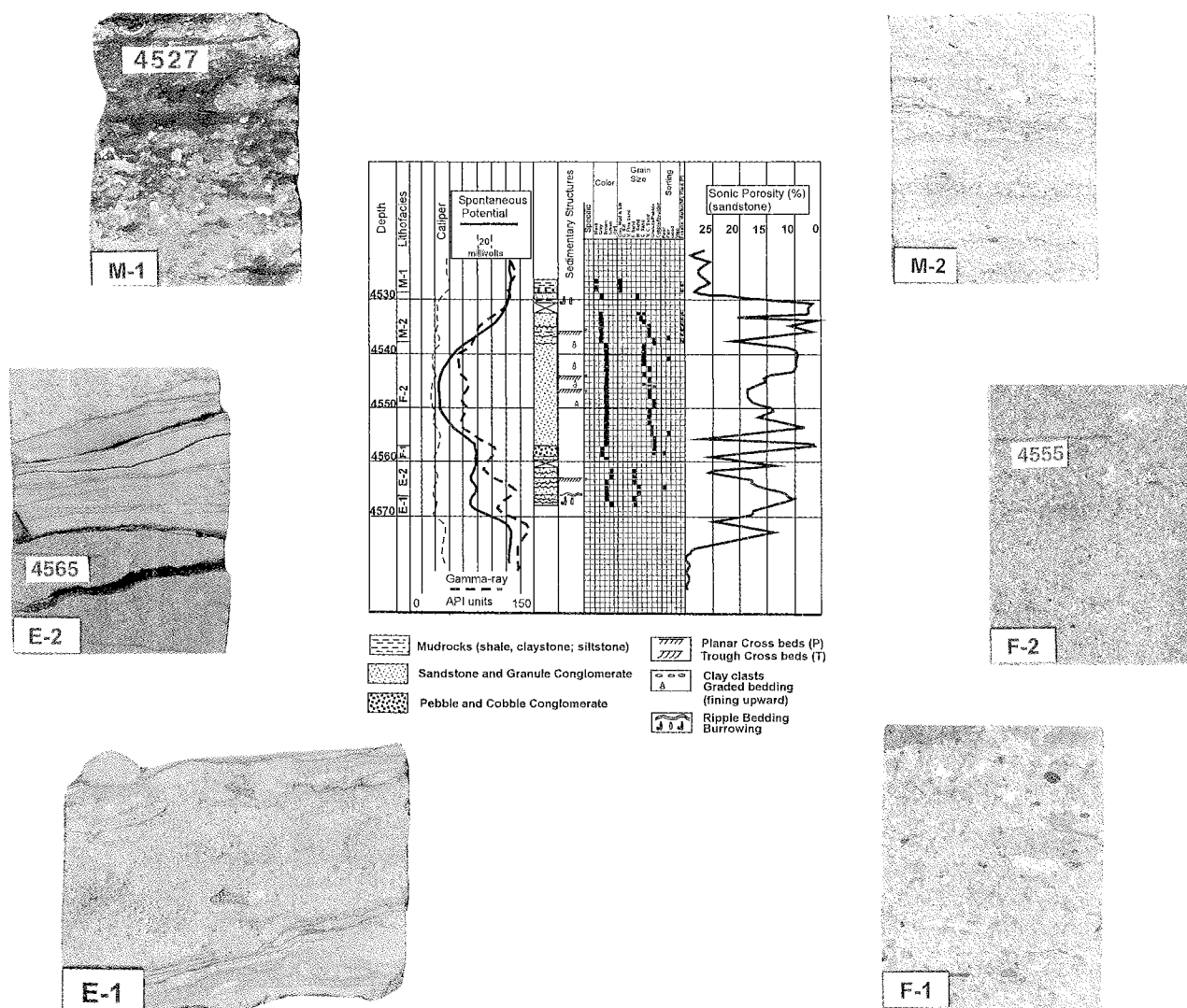


Figure 8. Photographs of lithofacies in core, and relative positions and responses of wireline-log curves. Lower Purdy sandstone, Petroleum Inc. No. 3 Hendrix, Carthage Field, Texas County, Oklahoma. F-1, fluvial paraconglomerate; F-2, braided-stream sandstone; E-2, estuarine sandstone with ripple-like bedding; E-1, burrowed estuarine sandstone with flowage features; M-2, fossiliferous sandstone; M-1, fossiliferous dark shale.

bedded very fine to fine grained sandstone and dark shale of lithofacies E-1. The next interval, E-2 lithofacies (4,559.5–4,566 ft), is burrowed fine- to medium-grained sandstone and shale interbedded with thin coarse-grained sandstone. F-1 lithofacies overlies E-2 and is separated by a sharp contact. F-1 (4,557–4,559.5 ft) is sandy pebble conglomerate with abundant clay clasts. F-2 overlies F-1 and is separated by a sharp contact. F-2 is planar- to trough-cross-bedded coarse-grained sandstone to granule conglomerate (4,538–4,557 ft) that forms four stacked, fining-upward sets. M-2 lithofacies is superjacent to F-2 (4,527.5–4,538 ft) and consists of fossiliferous, coarse- to fine-grained sandstone. The uppermost interval in the Hendrix core (4,526–4,527.5 ft) is dark-gray fossiliferous shale of M-1 lithofacies. M-1 contains a zone

of fossil debris at the base that marks the boundary with the underlying M-2. This fossil-hash zone is typical of the transgressive surface of erosion developed by a regional marine transgression (Weimer, 1984, 1988).

The core from the No. 11-2 Hardesty well in the Hardesty NE Field contains five lithofacies that represent a succession from marine-shelf mud to fluvial-channel to abandoned-channel depositional environments (Fig. 9). The lowermost cored interval (6,266.5–6,268 ft) is dark fossiliferous M-1 lithofacies. Its upper contact is sharp with the overlying F-1 conglomerate (6,261–6,266.5 ft). The superjacent F-2 interval (6,232–6,261 ft) contains four granule-conglomerate to coarse-grained sandstone graded sets. The overlying F-3 lithofacies (6,228–6,232 ft) is coarse- to fine-grained sandstone (fining-

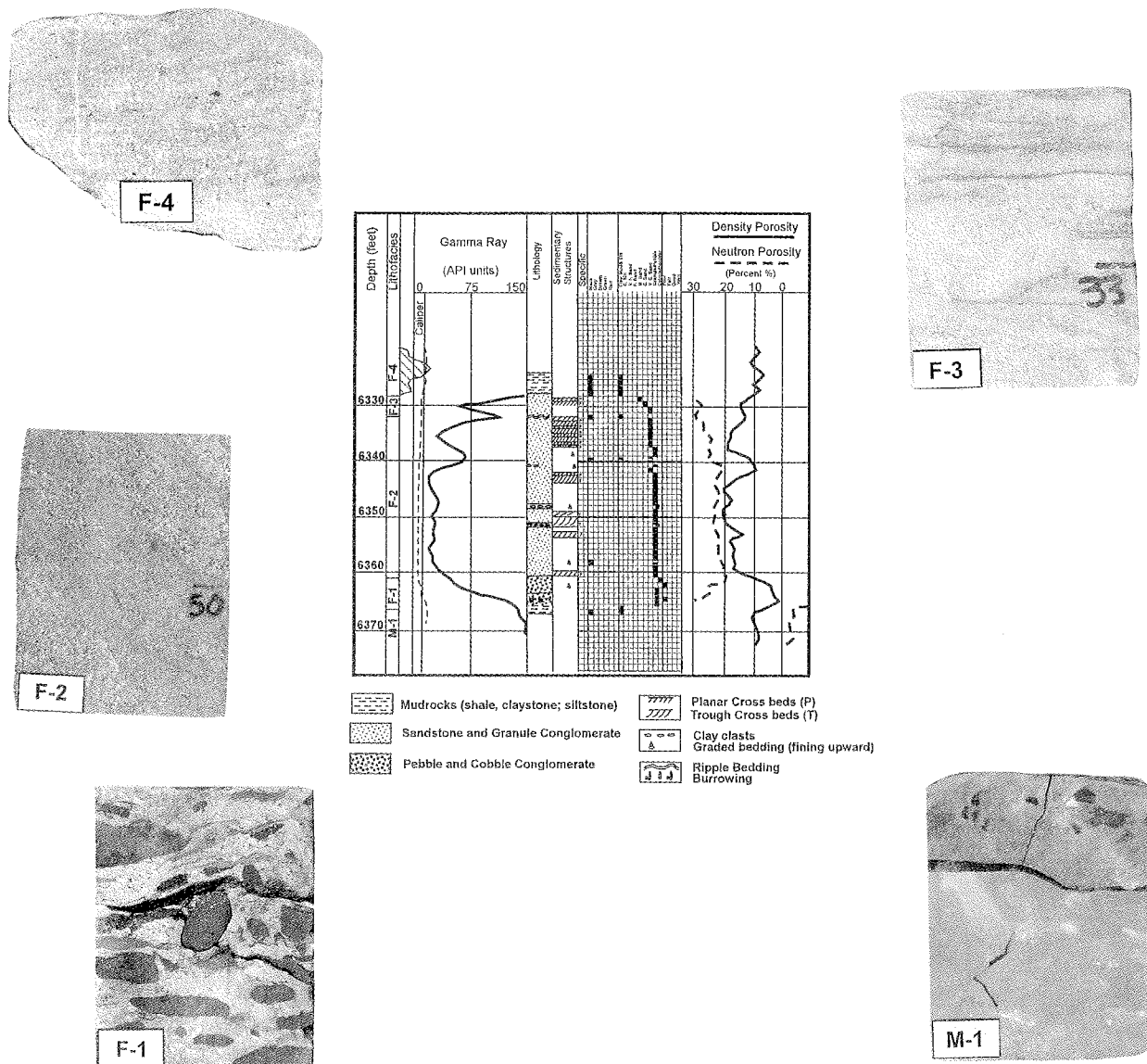


Figure 9. Photographs of lithofacies in core, and relative positions and responses of wireline-log curves. Purdy sandstone, No. 11-2 Anadarko Hardesty NE Unit, Hardesty NE Field, Texas County, Oklahoma. F-1, fluvial paraconglomerate; F-2, braided-stream sandstone with trough cross-bedding; F-3, meandering-stream sandstone with low-angle cross-stratification; F-4, abandoned-channel sandy claystone; M-1, fossiliferous dark claystone.

upward interval) that contains ripple to low-angle planar cross-beds and carbonaceous material. The uppermost lithofacies in this core is dark shale that contains carbonaceous material but no marine fossils. This interval is interpreted as F-4 abandoned-channel fill.

RESERVOIR CHARACTERIZATION

Petrology and Diagenesis

Thin-section petrography reveals that, on the basis of the relative abundance of detrital framework grains, the upper Morrow sandstones are classified primarily as subarkoses,

sublitharenites, and quartz arenites (Puckette, 1993). The most abundant detrital grains are of monocrystalline (plutonic) quartz. Other common framework grains are plagioclase, orthoclase, microcline, granitic-rock fragments, and sedimentary-rock fragments (Fig. 10).

Important diagenetic constituents include kaolinite, chlorite, calcite, and thermal dolomite (Fig. 11). Authigenic chlorite is grain coating, whereas kaolinite is pore filling. Thermal dolomite is an important pore-occluding cement that appeared relatively late in the paragenetic sequence of diagenetic events (Puckette and others, 1996). Calcite is early



Figure 10. Detrital constituents in upper Morrow sandstones. (A) Quartz (Q) sand grains (plane-polarized light [ppl]). (B) Sedimentary-rock fragment (SRF) (cross-polarized light [cpl]). (C) Plagioclase (Pl) in fine- to medium-grained sandstone (cpl). (D) Granitic-rock fragment (GRF) (cpl).

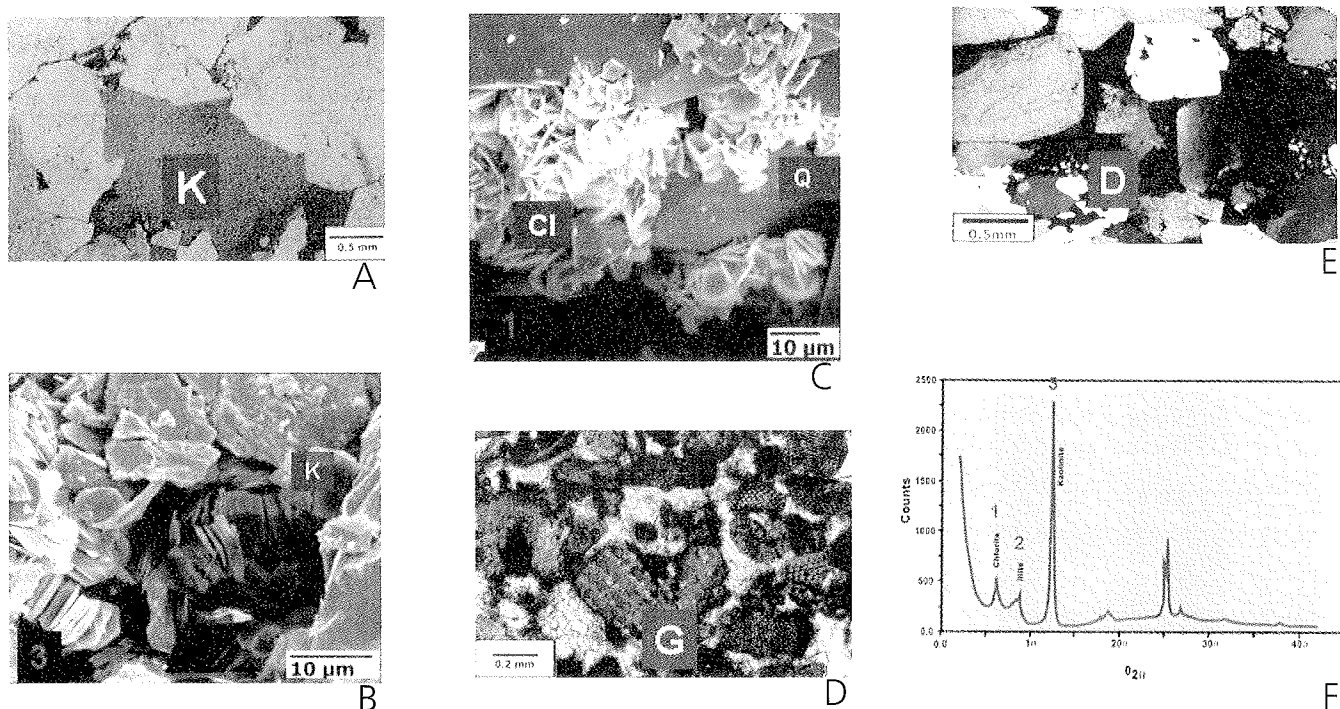


Figure 11. Diagenetic constituents in upper Morrow sandstones. (A) Authigenic kaolinite (K) derived from dissolution of feldspar (ppl). (B) Scanning electron microscopy (SEM) photograph of kaolinite (K), showing "booklet" morphology. (C) SEM photograph of pore-lining chlorite (Cl) on quartz overgrowths (Q). (D) Bioclast filled with intraparticle glauconite (G) (ppl). (E) Thermal dolomite (D) with sparry calcite (cpl). (F) Powder X-ray diffractogram, showing characteristic peaks for chlorite, illite, and kaolinite.

pore-occluding cement in marine facies. Glauconite cements the intraparticle porosity in bioclasts.

Kaolinite, a dissolution product of feldspars, is especially abundant in upper Morrow sandstones. It forms masses of stacked “booklets” that partially or totally fill pore spaces (Fig. 11B). Kaolinite partitions pores, reducing permeability and creating barriers to fluid flow if booklets break free and accumulate in pore throats.

Porosity, Permeability, and Reservoir Quality

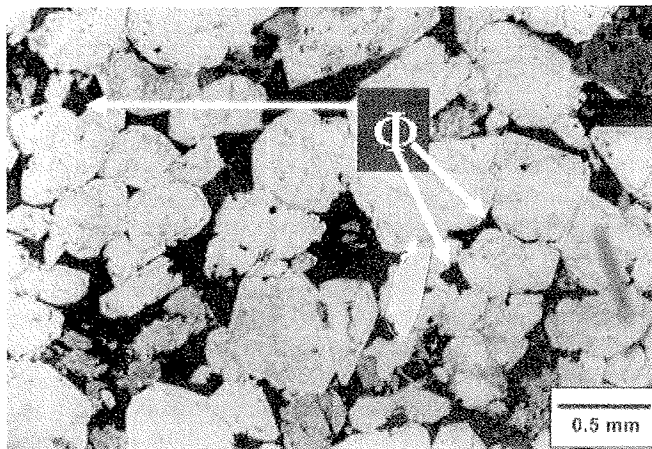
Porosity is highly variable in upper Morrow sandstones and includes several types (Fig. 12). Primary porosity is abundant, especially in the F-2 lithofacies. Secondary porosity, created by the dissolution of detrital grains, contributes to the higher permeability values measured in F-2 and F-3 lithofacies. Secondary intragranular porosity developed within partially dissolved detrital feldspars and rock fragments. Interparticle

microporosity in pore-filling kaolinite masses is abundant in F-2 and F-3 sandstones.

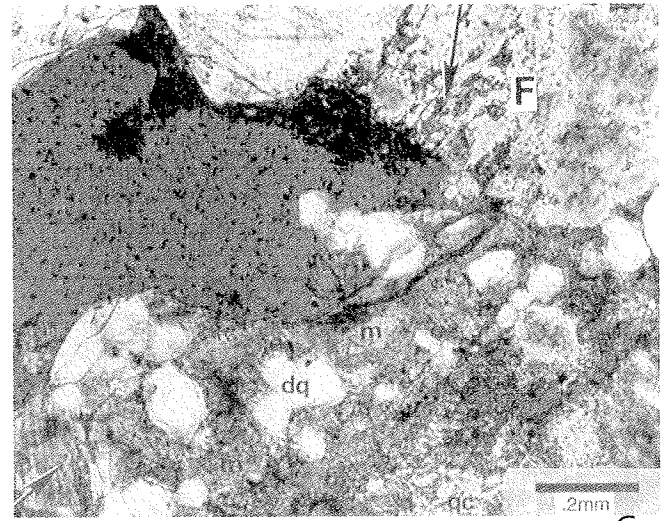
Porosity and permeability values for upper Morrow lithofacies from the Hardesty NE Field were plotted to analyze the relationship between these two parameters in the various lithofacies. The crossplot (Fig. 13) indicates five distinct porosity-permeability groupings: (1) *zone A*: high porosity (16–24%) and high permeability (>122 md); (2) *zone B*: medium to high porosity (13–18%) and lower permeability (22–122 md); (3) *zone C1*: medium to high porosity (13–17%) and low permeability (10–22 md); (4) *zone C2*: low porosity (3–13%) and low permeability (<1–22 md); and (5) *zone D*: very low porosity (<3%) and low permeability (1–22 md).

Zone A includes mostly samples from F-2 lithofacies. Porosity is primary and secondary enlarged pores. Clay matrix and cementation are minimal.

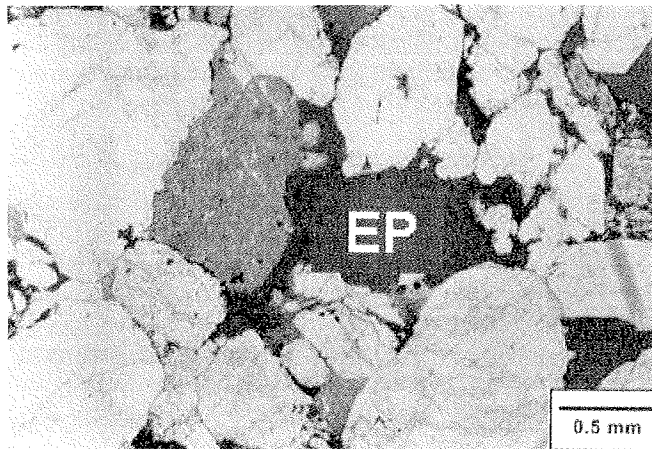
Zone B includes samples from F-2 and F-3 lithofacies. Porosity remains high, but permeability values are reduced by



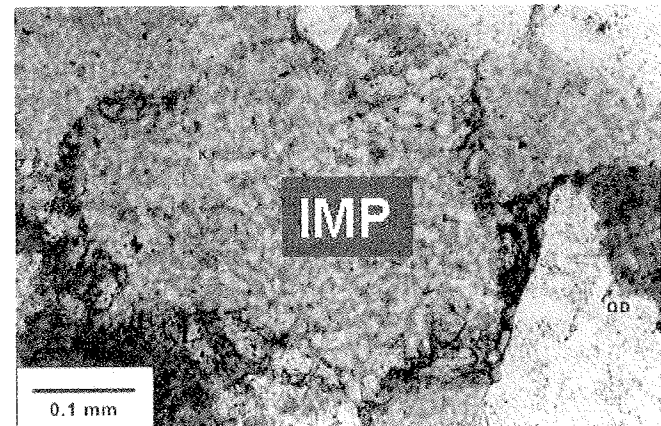
A



C



B



D

Figure 12. Photomicrographs of upper Morrow sandstones, showing porosity types. (A) Primary porosity (arrows), with planar euhedral quartz overgrowths bounding pores. (B) Enlarged intergranular porosity (EP). (C) Intragranular porosity resulting from partial dissolution of feldspar grain (F). (D) Intercrystalline microporosity (IMP) within patch of pore-filling kaolinite. All photomicrographs are plane-polarized light.

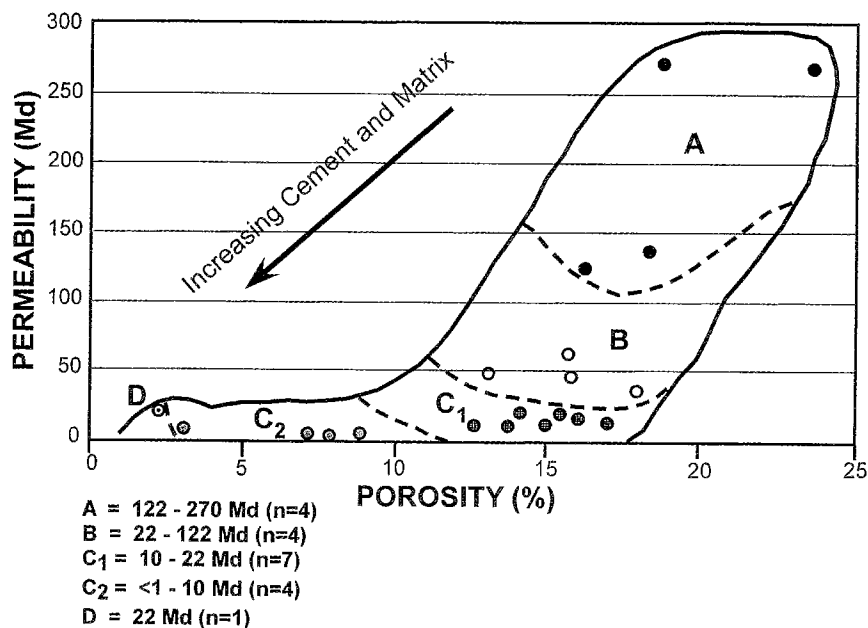


Figure 13. Crossplot of porosity and permeability measurements, upper Morrow sandstones, Hardesty NE Field, showing the five fields or zones of similar porosity and permeability.

authigenic kaolinite and clay matrix (Fig. 14). Zone B samples are typically finer grained than zone A samples and are more susceptible to permeability reduction by cementation.

Zone C₁ includes samples of F-1, F-4, and E-1 lithofacies. Porosity remains relatively high (12.5–17%), but permeability is reduced (10–22 md) by carbonate cement and pseudomatrix in facies F-1, and by clay and silt matrix in the F-4 and E-1 lithofacies (Fig. 14).

Zone C₂ contains samples of F-1 and E-1 sandstones that are of lower porosity (3–12.5%) and low permeability (<1–10 md). Porosity and permeability are reduced by matrix, pseudomatrix, and carbonate cement.

Zone D is composed of tightly cemented M-2 sandstone (Fig. 14) and M-1 marine mudrocks with low porosity (<3%) and permeability (<1–22 md; the lowest permeability includes a measurement from Carthage Field).

These results indicate that F-2 and F-3 sandstones are of better reservoir quality. M-1 mudrocks and M-2 sandstone facies have low permeabilities and could serve as seals that isolate porous sandstone bodies. Facies F-1, F-4, E-1, and E-2 are typically thin (<3 ft thick), but they may contain adequate permeability-reducing cement or matrix to contribute to heterogeneity within the valley fills.

SEQUENCE STRATIGRAPHY AND RESERVOIR EVOLUTION

Reservoir-quality lithologies in the upper Morrow sandstones are closely linked to sequence-stratigraphic history. Valleys eroded during lowstands contain F-1 clay-clast conglomerates that are not of reservoir quality. Infilling of the channels occurred during the TST produced by rising sea level. Flooding of the stream channels produced mud-rich estuarine (E-1 and E-2) deposits along the lower reaches,

while coarser sediments (sand and gravel) aggraded along the upper reaches. Sand aggradation produced F-2 and F-3 facies that became reservoir-quality sandstones. As sea level continued to rise, nonreservoir-producing estuarine facies backstepped older fluvial ones. Concurrently, rising base level forced a reduction in stream gradients upstream and the formation of meander belts along more distal reaches. Simultaneously, braided processes operated along more proximal stretches. Meandering streams produced point-bar sands (F-3), abandoned-channel sands and muds (F-4), and marshes where plant material was preserved (F-4). Some F-3 sands became reservoirs, whereas mud-rich facies did not. F-4 facies are typically clay-rich and do not become reservoirs. Eventually, marine facies (M-2 and M-1) backstepped fluvial and estuarine ones, filling the channel with mud and silt that evolved into sealing lithofacies, contributing to isolation of sandstone reservoirs within the channel fill.

SUMMARY AND CONCLUSIONS

The upper Morrow on the northwestern shelf of the Anadarko Basin is represented by three major lithofacies: fluvial, estuarine, and marine. Each lithofacies was subdivided using textural, sedimentological, depositional, and paleontological parameters. Fluvial facies consist of F-1 (channel lag), F-2 (braided stream), F-3 (meandering stream), and F-4 (abandoned channel). Estuarine facies are E-1 (lower estuary) and E-2 (upper estuary). Marine facies are E-1 (shelf) and E-2 (valley fill).

Lithofacies are controlled by sequence stratigraphy. LST deposits are limited to F-1 clay-clast conglomerate. TST deposits are fluvial F-2 sandstone, F-3 sandstone, and F-4 sandstone and shale; estuarine E-1 and E-2 sandstone and shale;

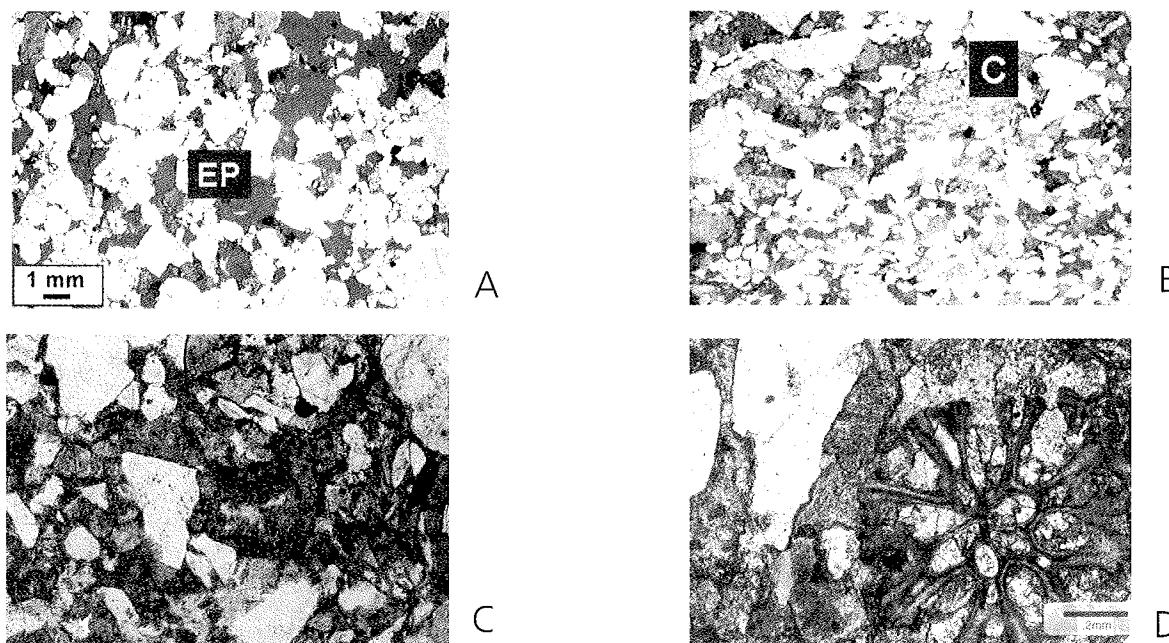


Figure 14. Photomicrographs of selected examples that represent the porosity-permeability zones identified in Figure 13. (A) Zone A sandstone (facies F-2) with enlarged pores (EP). Porosity is 17%, and permeability is 127.1 md. (B) Zone B sandstone (facies F-2) with abundant authigenic clay (C) that partitions pore space. Porosity is 18%, and permeability is 34 md. (C) Zone C sandstone (facies E-1) with clay matrix. Porosity is reduced to 13%, and permeability to 0.02 md. (D) Zone D sandstone (facies M-2) with abundant bioclastic material and carbonate cement. Porosity is <3%, and permeability is <0.01 md. All photomicrographs are plane-polarized light.

and marine M-2 sandstone. HST deposits are represented by M-1 shale.

Measured porosity and permeability from petrographic, petrophysical, and core analysis support the conclusion that F-2 and F-3 lithofacies are the better quality reservoirs and have the highest potential for producing large volumes of oil and gas. Authigenic kaolinite is abundant and poses a risk for blocking pore throats and restricting flow. Carbonate cement and, to a lesser extent, dolomite reduce porosity and permeability in most lithofacies.

Depositional models indicate that sediments that form marine, estuarine, and fluvial facies were deposited simultaneously along the various stretches of a stream valley. Furthermore, minor, higher frequency sea-level changes introduced heterogeneity to valley fills. As a result, (1) reservoir-quality lithofacies are widely distributed along valley trends, and (2) these reservoir-quality lithofacies are separated by intervening low-porosity, low-permeability lithofacies that act as seals.

ACKNOWLEDGMENTS

The authors wish to acknowledge Amy Close, Melanie McPhail, Ken Rechlin, Julie Turrentine, and Chris Wiggers for their contributions to data collection and compilation of material used in this study. We also express our appreciation to Walter Esry and the staff of the Oklahoma Geological Survey Core and Sample Library, who made available the cores that were essential to the completion of this work.

REFERENCES CITED

- Al-Shaieb, Z.; and Puckette, J., 2002, Sequence stratigraphic control on reservoir quality in Morrow sandstone reservoirs, northwestern shelf, Anadarko Basin: American Association of Petroleum Geologists Search and Discovery Article no. 10023 (2002), www.searchanddiscovery.net/.
- Al-Shaieb, Z.; Puckette, J.; and Abdalla, A., 1995, Influence of sea-level fluctuation on reservoir quality of the upper Morrowan sandstones, northwestern shelf of the Anadarko Basin, in Hyne, N. J. (ed.), Sequence stratigraphy of the Mid-continent: Tulsa Geological Society Special Publication 4, p. 249-268.
- Benton, J. W., 1971, Subsurface stratigraphic analysis, Morrow (Pennsylvanian), north central Texas County, Oklahoma: University of Oklahoma unpublished M.S. thesis, 60 p.
- Blakeney, B. A.; Krystinik, L. F.; and Downey, A. A., 1990, Reservoir heterogeneity in Morrow valley fills, Stateline trend: implications for reservoir management and field expansion, in Sonnenberg, S. A.; and others (eds.), Morrow sandstones of southeast Colorado and adjacent areas: Rocky Mountain Association of Geologists, Denver, p. 131-142.
- Bowen, D. W.; Krystinik, L. F.; and Grantz, R. E., 1990, Geology and reservoir characteristics of the Sorrento-Mt. Pearl field complex, Cheyenne County, Colorado, in Sonnenberg, S. A.; and others (eds.), Morrow sandstones of southeast Colorado and adjacent areas: Rocky Mountain Association of Geologists, Denver, p. 67-77.
- Cornish, F. G., 1982, Fluvial environments and paleohydrology of the upper Morrow 'A' (Pennsylvanian) meander belt sandstone, Beaver County, Oklahoma: Shale Shaker Digest, v. 11, p. 73-83.
- DeVries, A., 2005, Sequence stratigraphy and micro-image analysis of the upper Morrow sandstone, Mustang East field, Morton County, Kansas: Oklahoma State University unpublished M.S. thesis, 79 p.

- Forgotson, J. M.; Statler, A. T.; and David, M., 1966, Influence of regional tectonics and local structure on deposition of Morrow Formation in western Anadarko Basin: American Association of Petroleum Geologists Bulletin, v. 50, p. 518–532.
- Gerken, L. D., 1992, Morrowan sandstones in south-central Texas County, Oklahoma: Oklahoma State University unpublished M.S. thesis, 140 p.
- Harrison, J. C., 1990, "Upper" Morrow Purdy sandstones in parts of Texas and Cimarron Counties, Oklahoma: Oklahoma State University unpublished M.S. thesis, 95 p.
- Krystinik, L. F.; and Blakeney, B. A., 1990, Sedimentology of the upper Morrow Formation in eastern Colorado and western Kansas, *in* Sonnenberg, S. A.; and others (eds.), Morrow sandstones of southeast Colorado and adjacent areas: Rocky Mountain Association of Geologists, Denver, p. 37–50.
- Luchtel, K. L., 1999, Sequence stratigraphy and reservoir analysis of the Upper Kearney Formation (Morrowan Series) (Lower Pennsylvanian System) within three Kansas fields: University of Kansas unpublished M.S. thesis, 149 p.
- Puckette, J., 1990, Depositional setting, facies, and petrology of Cabaniss (Upper Cherokee) Group in Beckham, Dewey, Custer, Ellis, Roger Mills and Washita Counties, Oklahoma: Oklahoma State University unpublished M.S. thesis, 144 p.
- 1993, The petrography and diagenetic history of an upper Morrow valley fill sandstone: Oklahoma State University unpublished report, 31 p.
- Puckette, Jim; and Al-Shaieb, Zuhair, 2003, The Red Fork Sandstone: overview of marine and deep-marine reservoirs, *in* Boyd, D. T. (ed.), Finding and producing Cherokee reservoirs in the southern Midcontinent, 2002 symposium: Oklahoma Geological Survey Circular 108, p. 119–133.
- Puckette, Jim; Abdalla, Azhari; Rice, Aaron; and Al-Shaieb, Zuhair, 1996, The upper Morrow reservoirs: complex fluvio-deltaic depositional systems, *in* Johnson, K. S. (ed.), Deltaic reservoirs in the southern Midcontinent, 1993 symposium: Oklahoma Geological Survey Circular 98, p. 47–84.
- Rader, K., 1990, Petrography of Morrow sandstones in southeast Colorado, southwest Kansas and northwest Oklahoma, *in* Sonnenberg, S. A.; and others (eds.), Morrow sandstones of southeast Colorado and adjacent areas: Rocky Mountain Association of Geologists, Denver, p. 51–58.
- Rascoe, Bailey, Jr.; and Adler, F. J., 1983, Permo-Carboniferous hydrocarbon accumulations, mid-continent, U.S.A.: American Association of Petroleum Geologists Bulletin, v. 67, p. 979–1001.
- Shepherd, S. K., 2000, Depositional history and reservoir characterization of the Northeast Hardesty field, Texas County, Oklahoma: University of Texas, Austin, unpublished M.S. thesis, 105 p.
- Sonnenberg, S. A.; Shannon, L. T.; Rader, K.; and Von Drehle, W. F., 1990, Regional structure and stratigraphy of the Morrowan Series, southeast Colorado and adjacent areas, *in* Sonnenberg, S. A.; and others (eds.), Morrow sandstones of southeast Colorado and adjacent areas: Rocky Mountain Association of Geologists, Denver, p. 1–8.
- Swanson, D. C., 1979, Deltaic deposits in the Pennsylvanian upper Morrow Formation of the Anadarko Basin, *in* Hyne, N. J. (ed.), Pennsylvanian sandstones of the Mid-continent: Tulsa Geological Society Special Publication 1, p. 115–168.
- Weimer, R. J., 1984, Relation of unconformities, tectonics, and sea-level changes, Cretaceous of Western Interior, USA, *in* Schlee, J. S. (ed.), Interregional unconformities and hydrocarbon accumulation: American Association of Petroleum Geologists Memoir 36, p. 7–35.
- 1988, Record of sea level changes, Cretaceous of Western Interior, USA, *in* Wilgus, C. K.; and others (eds.), Sea level changes: an integrated approach: Society of Economic Paleontologists and Mineralogists Special Publication 42, p. 285–288.
- Wheeler, D. M.; Scott, A. J.; Coringrato, V. J.; and Devine, P. E., 1990, Stratigraphy and depositional history of the Morrow Formation, southeast Colorado and southwest Kansas, *in* Sonnenberg, S. A.; and others (eds.), Morrow sandstones of southeast Colorado and adjacent areas: Rocky Mountain Association of Geologists, Denver, p. 9–35.

Potential Stratigraphic Reservoirs in the Morrowan Jackfork Group, Southeastern Oklahoma

R. M. Slatt, B. Omatsola,¹ A. M. Garich-Faust,¹ and G. A. Romero

University of Oklahoma
Norman, Oklahoma

ABSTRACT.—Gas from the Jackfork Group (Lower Pennsylvanian, Morrowan) in southeastern Oklahoma is generally considered to be trapped in large structures and to be producing from associated fractures. Yet outcrops from various locales show the potential for other reservoir types, including stratigraphic pinch-outs and diagenetically altered sandstones associated with tight sandstones. Identifying these potential reservoir types can be challenging in structurally complex areas where there are little or no seismic profiles and only conventional well logs.

Outcrop studies in Oklahoma and Arkansas have shown that the Jackfork is composed mainly of deep-water sheet (lobe) and channel-fill sandstones. Each of these classes of sandstone has distinctive features that allow their differentiation from core (when obtained), dipmeter or borehole-imaging logs, and some conventional well logs. Sheet sandstones tend to be interbedded with shale to give a relatively low net sand; beds are laterally continuous for long distances, and stratigraphic dips are uniform and of relatively low angle. Channel-fill sandstones tend to be thick bedded with higher net sand and lenticular external geometry, and with variable quality, magnitude, and orientation of stratigraphic dips. These patterns are readily identified on borehole-image logs, and to a lesser extent on conventional and dipmeter logs.

Outcrop and subsurface studies in southeastern Oklahoma have indicated that sheet sandstones are highly cemented, brittle, and with little primary porosity; fracture porosity prevails in these sandstones. Channel-fill sandstones are more poorly sorted, contain clay, and are moderately to poorly cemented, so that matrix porosity is predominant.

Using outcrop and well-log criteria, it is possible to differentiate potential fracture- and matrix-predominant reservoir types in the subsurface on a well-to-well basis. A depositional sequence-stratigraphic framework has also been developed for the outcrops, which serves as a model for the subsurface. Identification and subregional to regional subsurface mapping of components of Jackfork depositional sequences may provide potential new stratigraphic/diagenetic plays in a large area of southeastern Oklahoma.

INTRODUCTION

The Morrowan Jackfork Group produces gas in the Potato Hills, Buffalo Mountain, and Talihiina NW fields of southeastern Oklahoma. Gas production is generally believed to be from fractured rock because the Jackfork is a notorious “hammer ringer,” and because in these areas the Jackfork is highly folded and faulted. These characteristics make drilling difficult and unpredictable, often leading to economically marginal wells (Montgomery, 1996). Although much of the Jackfork is quartz-cemented sandstone, making it brittle and subject to fracturing, some Jackfork is weakly cemented and has substantial matrix porosity and permeability (Pauli, 1994). If this more porous Jackfork lithology could be located in the subsurface and combined with favorable structures for gas accumulation, production economics might improve substantially.

Wherever outcrops of the same facies are present—preferably of the same formation or group—as subsurface res-

ervoirs, they should be studied. This is because outcrops provide a much more complete, scaled characterization of reservoir properties than can be obtained with traditional subsurface measurements such as seismic techniques, which provide good lateral information but limited vertical resolution, and conventional well logs, which provide reasonable vertical resolution but poor lateral information (Slatt, 2000). With this thought in mind, outcrops of the Jackfork Group in southeastern Oklahoma were investigated (Omatsola, 2003), and the results were applied to subsurface reservoir intervals (Garich, 2004; Romero, 2004) to evaluate the Jackfork in this area from a stratigraphic perspective.

ORIGIN AND SEDIMENTARY ARCHITECTURAL ELEMENTS OF THE JACKFORK GROUP

Turbidites of the Jackfork Group of eastern Oklahoma and south-central Arkansas were deposited in the east-west-trending Ouachita Basin during Morrowan (early Pennsylvanian) time from diverse source areas (Fig. 1). The onset of Jackfork deposition corresponds to a major global drop in sea level

¹Current address: BP, Houston, Texas.

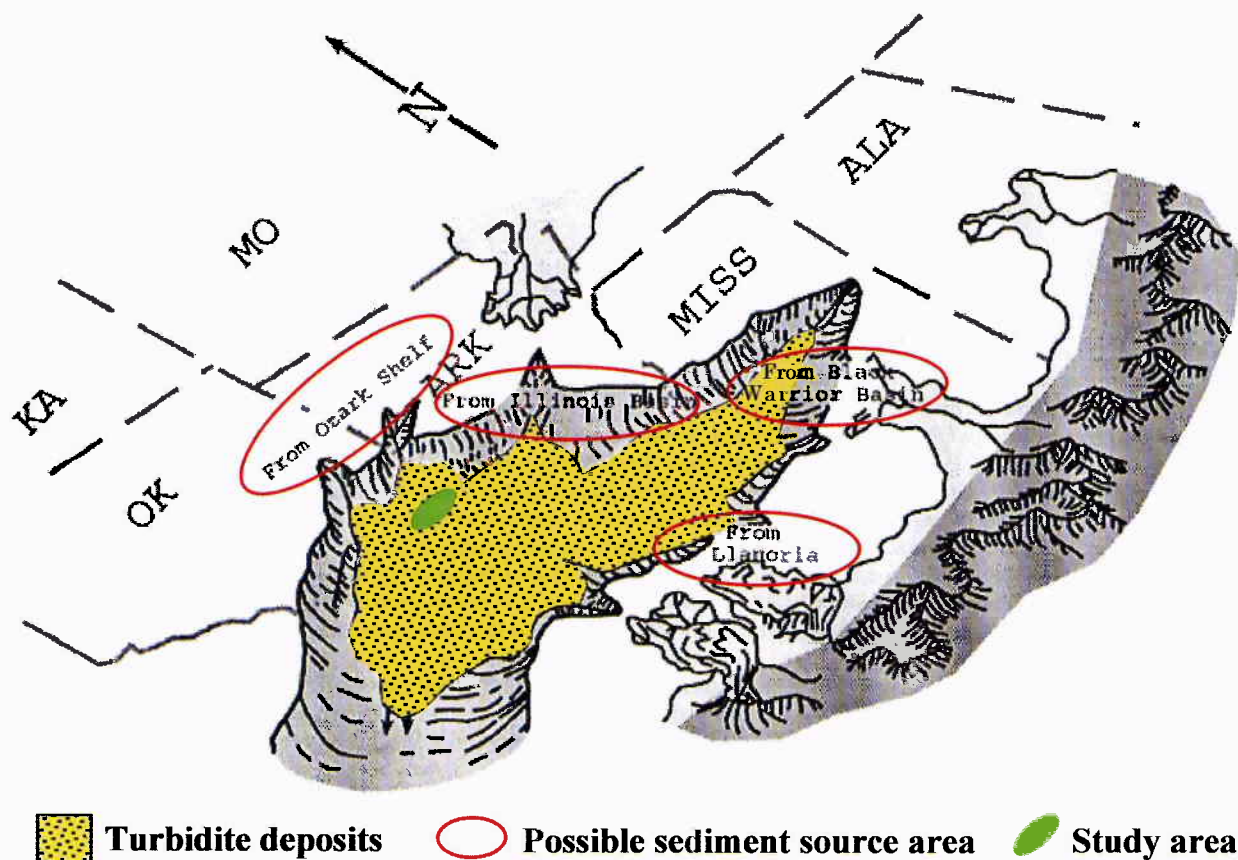


Figure 1. Map showing Ouachita Basin during deposition of the Jackfork Group rocks. Multiple sediment-source areas are shown from the northeast, north, and south. General sediment transport directions within the basin were from east to west, along the orientation of the basin axis (from Slatt and others, 2000).

at ~320 Ma (Fig. 2). Tectonically induced perturbations were superimposed on several periods of glacio-eustatic sea-level fluctuations throughout deposition of the Jackfork.

Studies presented here for southeastern Oklahoma rely heavily on several years of prior outcrop studies of the Jackfork Group in south-central Arkansas (Slatt and others, 2000). The main architectural elements of deep-water depositional and reservoir systems, including the Jackfork, are sheet sands, channel sands, and levee beds (Fig. 3) (Weimer and Slatt, 2006).

Levee beds are not thought to constitute an important reservoir rock in much of the Jackfork and so are not discussed further. Sheet sandstones were subdivided by Chapin and others (1994) into two types, layered and amalgamated sheets; both are common in Jackfork outcrops and quarries (Fig. 3). Layered sheets are a series of alternating sandstones and shales. Amalgamated sheets are a series of individual sandy gravity flows that were deposited one atop another, with little to no intervening shale beds. Both types of sheet sandstones were deposited in a basin-floor setting (Fig. 3). Amalgamated sheets tend to be deposited in the central parts of basin-floor fans, whereas layered sheets tend to occupy the peripheries of fans.

Slatt and others (2000) developed a set of criteria for differentiating sheet and channel sandstones of the Jackfork

Group. For sheet sandstones, criteria include flat tops and bases of beds, relatively uniform bed thickness, few if any scour surfaces, relatively uniform grain size throughout the thickness of a bed, and a general lack of shale rip-up clasts. For channel sandstones, criteria include lenticular geometries of beds, scour surfaces, cut-and-fill features, slump and deformation features, undulatory beds, and the presence of a significant number of shale rip-up clasts in beds. These criteria have been used in the present study to differentiate sheet from channel sandstones.

JACKFORK GROUP OUTCROPS IN SOUTHEASTERN OKLAHOMA

Outcrop Characteristics

Several hundred feet of strata in the upper part of the Wildhorse Mountain Formation (Jackfork Group) of Briggs (1973) are superbly exposed along moderately dipping bedding planes on the north flank of the Lynn Mountain Syncline on U.S. Highway 259 just west of Three Sticks Monument (Fig. 4).

Omatsola's (2003) outcrop A-2 consists of a lower section of interbedded, highly cemented Jackfork sheet sandstones and interbedded shales (Fig. 5) and an upper section of more massive (i.e., no shale interbeds), friable channel sandstones.

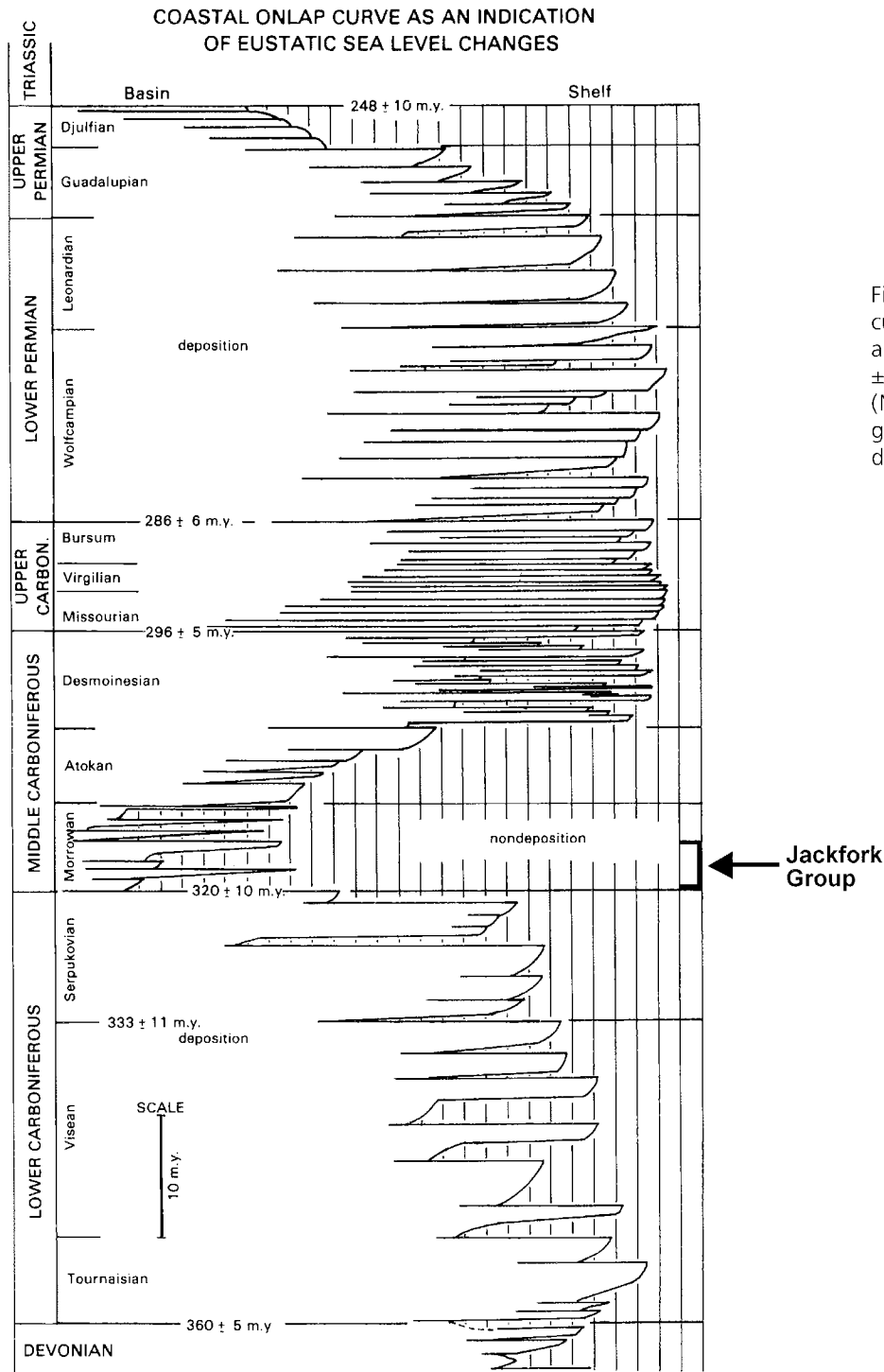


Figure 2. Diagram showing coastal onlap curve (from Ross and Ross, 1988), depicting a major third-order drop in sea level at 320 ± 10 Ma at the onset of Jackfork deposition (Morrowan time). Multiple episodes of glacio-eustatic sea-level fluctuations occurred during Jackfork deposition.

The quartz-cemented sandstones are very fine to fine grained, moderately to well sorted, and planar-tabular bedded with characteristic deep-water sedimentary structures; bases and tops of beds are sharp and generally non-erosive. By contrast, the friable sandstones are fine to medium grained, predominantly poorly to moderately sorted, massive and amalgamated, and commonly have undulatory bed boundaries.

In the same general area, Omatsola (2003) described a 165-ft-thick outcrop, A-3 (Fig. 6). This outcrop exhibits a similar

upper, channelized sequence (Fig. 6), but the lower interval is somewhat more stratigraphically complex. It consists of a lower set of layered sheet sandstones, similar to those shown in Figure 5, overlain by a thick interval of very thin bedded shales and siltstones, interpreted as either levee or basin-plain facies, and then another interval of layered sheet sandstones. The upper, thick, friable channel sandstones are in erosional contact with these sheet sandstones. Sheet sandstones in the interval 90–132 ft contain significantly more organic detritus

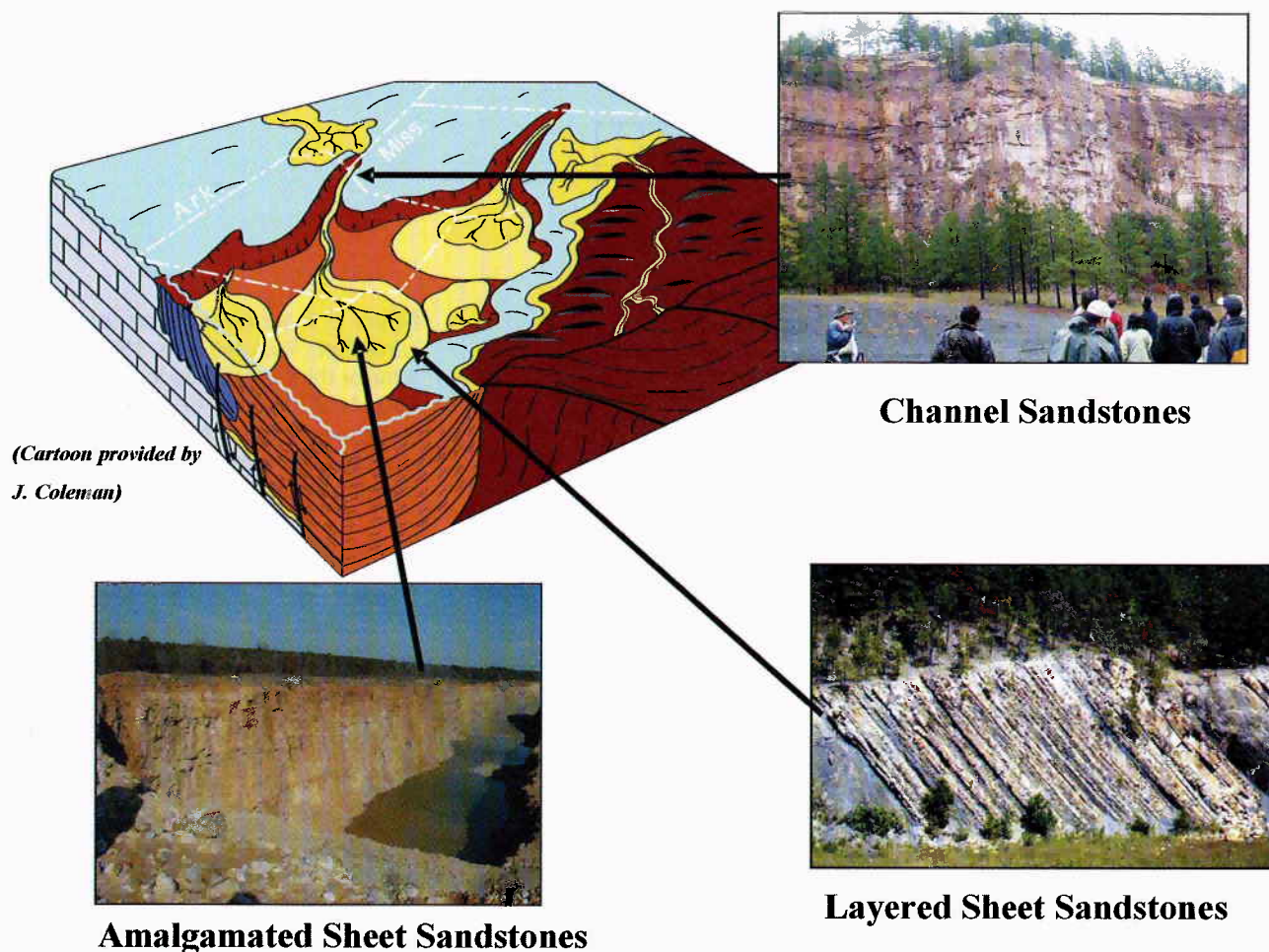


Figure 3. Generalized depositional model for the Jackfork in the Ouachita Basin (provided by J. Coleman). Photograph of the thick-bedded channel sandstone is from Big Rock Quarry, Arkansas; photograph of amalgamated sheet sandstone is from the Martin-Marietta Quarry, southern Oklahoma; photograph of the layered sheet sandstone is from DeGray Lake Spillway, Arkansas (Slatt and others, 2000).

and trace fossils than other sheet sandstones in either outcrop A-2 or A-3. Sheet sandstones at both locales are highly fractured.

SUBSURFACE JACKFORK GROUP IN SOUTHEASTERN OKLAHOMA

Description of Cuttings

Well logs, including dipmeter logs, and well cuttings from wells in Potato Hills and Talihina NW gas fields were studied by Garich (2004) and Romero (2004). Cuttings were from 10-ft Jackfork stratigraphic intervals within three of the studied wells. Cuttings were first examined to identify the different lithologies, and then representative samples were placed in ice-cube trays and epoxy-resinated. Standard thin sections were then cut from the hardened "blocks" of cuttings chips. The thin sections provided more detail on the petrographic aspects of the cuttings chips than could be determined from examining the whole chips.

Thin-section analysis showed three sandstone types: friable, highly quartz cemented, and siderite cemented (Fig. 7). Bitumen is locally present in all three sandstone types.

The stratigraphic distribution of the sandstone (and finer grained rocks) was documented by counting the proportion of each rock type within each 10-ft interval of cuttings in the same manner as one would point-count a thin section. The results for two intervals in a well are shown in Figure 8; one interval is composed mainly of friable sandstone, and the other is composed mainly of quartz-cemented sandstone cuttings chips.

Well-Log Description

Dipmeter logs can be useful in differentiating deep-water depositional facies, once the structural dip has been removed (Hansen and Fett, 2000; Witton-Barnes and others, 2000; Browne and Slatt, 2002). Dipmeter logs were available for some of the wells, and a borehole-image log was available from one well. On all of these logs, the structural dip was

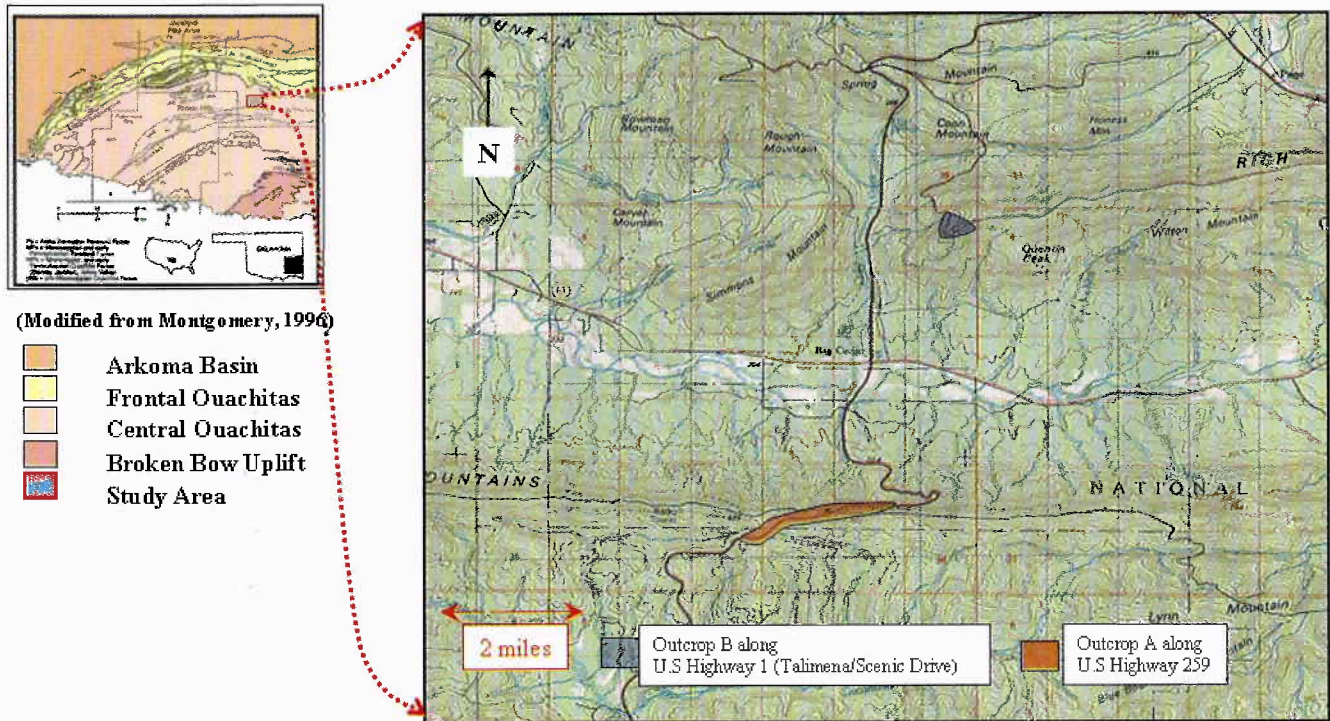


Figure 4. Topographic-map location of outcrops studied by Omatsola (2003) along U.S. Highway 259 near Three Sticks Monument (elongate highlighted area), along Talimena Drive (NE $\frac{1}{2}$ N $\frac{1}{2}$ W $\frac{1}{4}$ NW $\frac{1}{4}$ sec. 34, T. 2 N., R. 25 E., and SE $\frac{1}{4}$ SW $\frac{1}{4}$ SW $\frac{1}{4}$ sec. 27, T. 2 N., R. 25 E.) on north side of U.S. Highway 259, Le Flore County, Oklahoma.

estimated from thick shale intervals; structural dip was then removed from the dip data. Two stratigraphic dip patterns are particularly common on the logs: one pattern consists of a relatively uniform, low angle of dip (Fig. 9), and the other pattern consists of diverse, higher angles of dip and common low-quality dips (Fig. 10, open circles). These dip patterns are typical of what one would expect for channel and sheet sandstones on the basis of comparison with outcrop characteristics described previously and in Slatt and others (2000).

There is also a qualitative relation between the characteristics of the gamma-ray log and those of the dipmeter log. Intervals of relatively low-angle, uniform dip correspond to gamma-ray-log intervals, which exhibit a serrated pattern (Fig. 9). This pattern corresponds to the interlayered (sandstone-shale) nature of layered sheet sandstones seen in outcrop (Fig. 3, and Slatt and others, 2000). By contrast, intervals of relatively higher angle, variable dip correspond to the channelized, thickly bedded sandstones, with slump and scour structures seen in outcrop (Fig. 3, and Slatt and others, 2000).

On the basis of these criteria, well logs through Jackfork channel sandstones are interpreted to be characterized by relatively high-angle and variable dips and the common occurrence of low-quality dips on dipmeter logs, and by a blocky, sand-rich gamma-ray-log pattern. Jackfork sheet sandstones are interpreted to be characterized by relatively low-angle and

uniform dips on dipmeter logs, and by an interbedded sandstone-shale appearance on gamma-ray logs.

Correlation of Sandstone Types and Well-Log Characteristics

Through most of the stratigraphic intervals examined in the subsurface, quartz-cemented sandstones, as determined from cuttings analysis, are associated with the sheet-sandstone log patterns. Friable sandstones are associated with the channel sandstones. These same relationships are observed in outcrop (Figs. 5, 6). Thus, it is concluded that in the subsurface, the friable sandstones are associated with channel facies, and cemented sandstones are associated with sheet facies. This association provides a means of differentiating matrix porosity from fracture porosity, using conventional well logs (Fig. 11).

DEPOSITIONAL HISTORY AND SEQUENCE-STRATIGRAPHIC MODEL OF THE JACKFORK GROUP IN SOUTHEASTERN OKLAHOMA

The similarity between outcrop and subsurface observations is evidence that the outcrop exposures of the Jackfork Group described previously are excellent analogs to potential subsurface Jackfork gas sandstones, and that it may be pos-



Figure 5. Lower sheet sandstones in outcrop A-2 of Omatsola (2003). Note the highly fractured nature of these well-cemented sandstones. Photograph is of the lower, yellow (sheet-sandstone) interval of the measured section. Orange color denotes the upper channel-sandstone interval.

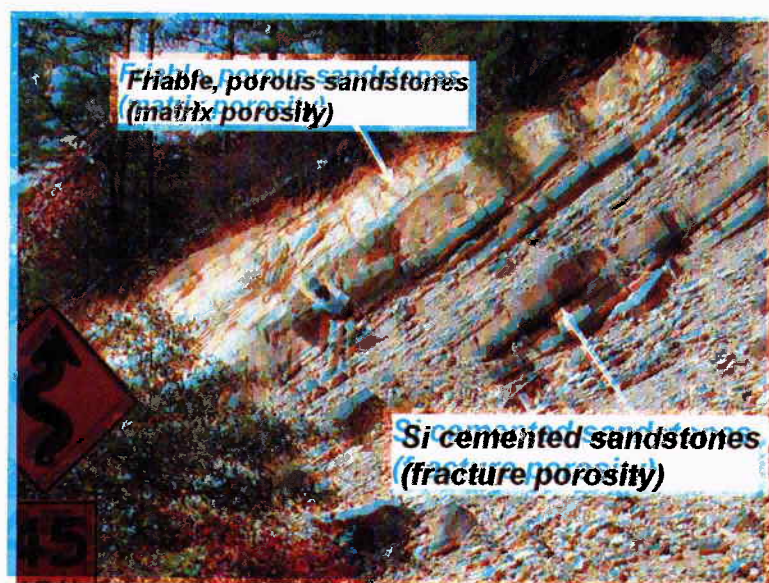
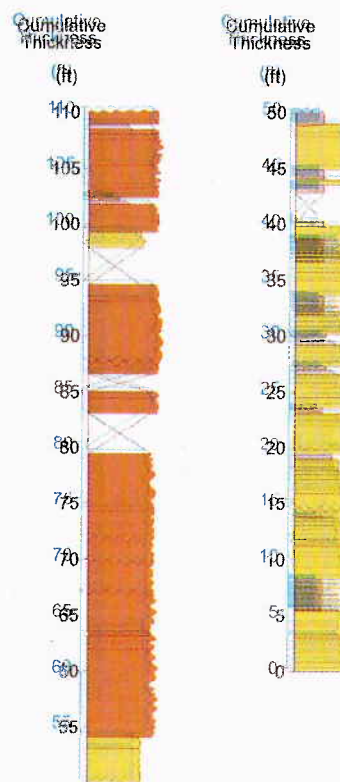
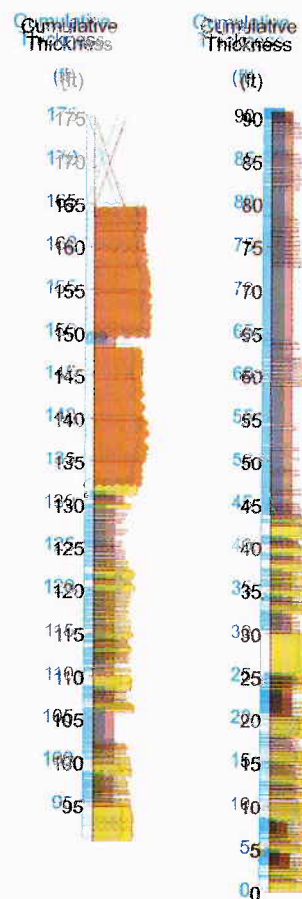


Figure 6. Upper section of Omatsola's (2003) outcrop A-3, showing upper channel sandstone, middle thick silty/shaly interval, and lower layered sheet sandstones. Channel sandstone is very friable, and the lower sheet sandstones are highly silica-cemented and fractured. Contact between the friable and cemented sandstones is at 132 ft on the measured stratigraphic section. Same colors are used for this section as the one in Figure 5.



sible to improve well-log correlations by using a sequence-stratigraphic approach.

Principles of Sequence Stratigraphy

Sea level does not remain constant over periods of geologic time but rather fluctuates on a global scale owing to global climatic and tectonic processes (eustatic sea level), and on a more local scale owing to tectonic activity (Fig. 2). Characteristic depositional sequences resulting from sea-level fluctua-

tions over geologic time provide a conceptual framework for predicting the spatial and temporal distribution of sedimentary-rock bodies deposited in deep water (Fig. 3).

A generalized, relative sea-level curve is shown in Figure 12, and a set of cartoons is provided in Figure 13 to explain the principles of sequence stratigraphy as applied to deep-water sequences such as the Jackfork Group. During a falling stage of sea level, the shelf margin becomes unstable owing to change in hydrostatic and sediment pore pressure. Such instability dislodges large slump masses, which then move

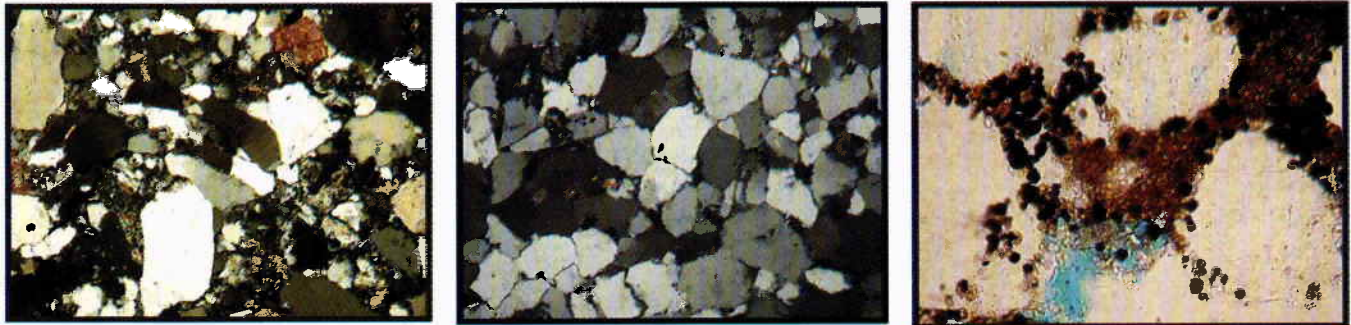


Figure 7. From left to right, thin-section photomicrographs of friable, quartz-cemented, and siderite-cemented (orange) sandstone cuttings. Note the more poorly sorted nature of the friable sandstone relative to the quartz-cemented sandstone. Modified from Romero (2004).

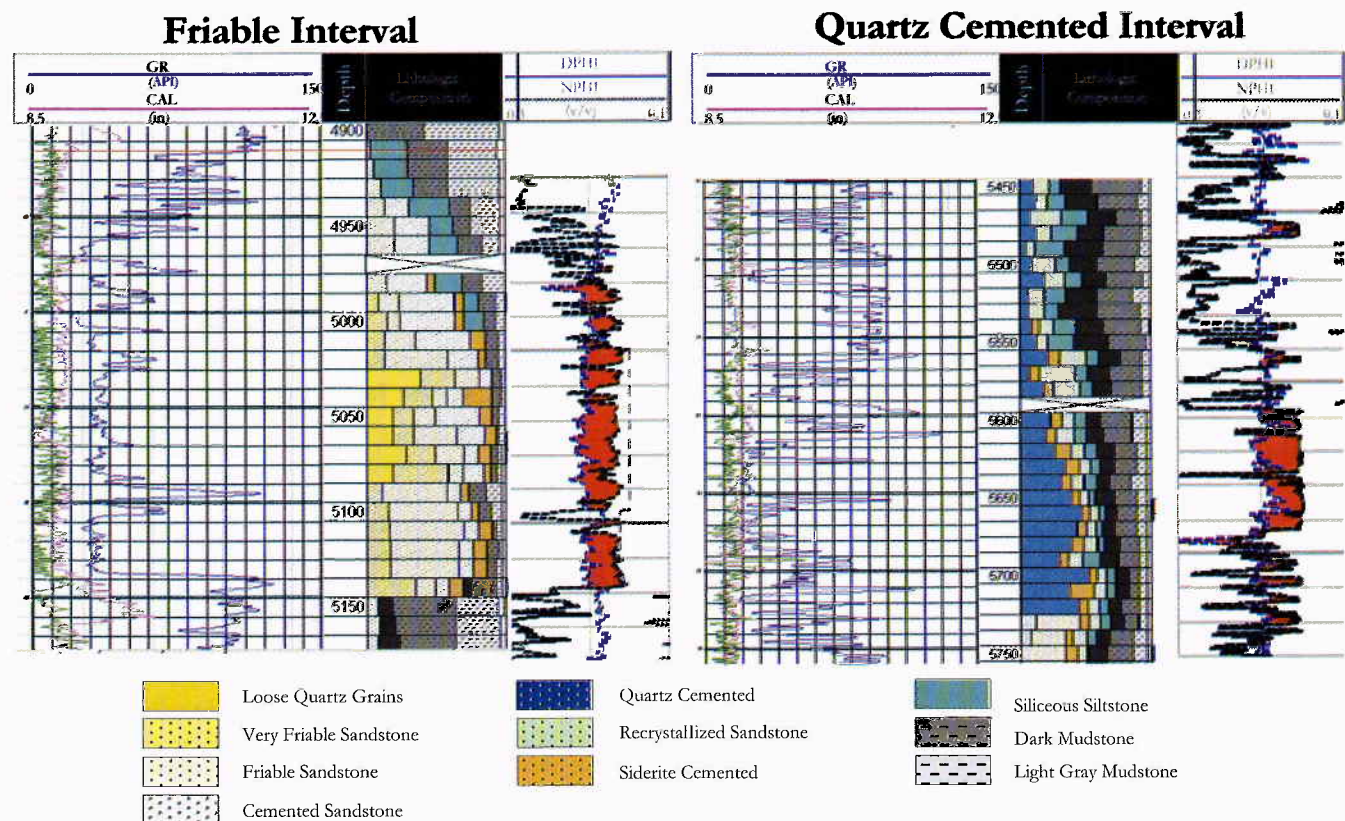


Figure 8. Parts of logs with examples of cuttings-chip descriptions from a friable interval and a quartz-cemented interval. Different lithologies identified in the cuttings are shown by the color code. Gamma-ray (GAPI), caliper (CAL), density-porosity (DPHI), and neutron-porosity (NPHI) logs are also shown for the two intervals. Symbol v/v indicates volume-for-volume decimal fraction.

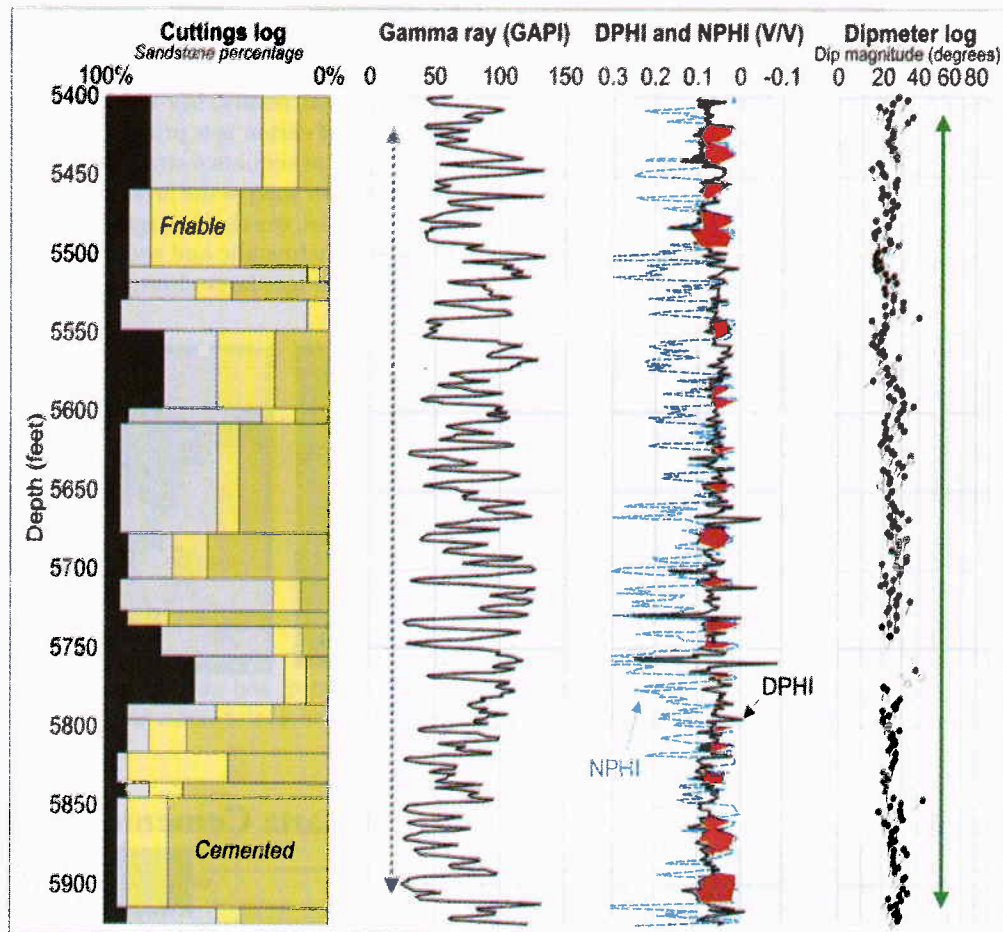


Figure 9. Cuttings log, gamma-ray log, density- and neutron-porosity logs, and dipmeter log for a 500-ft Jackfork interval in a well. Gas crossover is shown in red. Lithologies: black, shale; gray, siltstone; yellow, friable sandstone; and greenish-yellow, quartz-cemented sandstone. Except for one interval between 5,460 and 5,510 ft, quartz-cemented sandstone is the dominant sandstone in this well. Note the relative uniformity of dip patterns and the serrated nature of the gamma-ray log.

downslope under the influence of gravity. Shelf-margin and upper-slope slump scars may become the precursors to submarine canyons, which form later by a combination of incision by sediment gravity flows and by headward erosion of the submarine scars. With a continued drop in sea (base) level, rivers increase their discharge and erosive capabilities so that more and coarser grained sediments are transported through incised valleys and onto the slope and basin floor. With early turnaround in sea level, the discharge of rivers diminishes, and fewer and finer grained sediments are deposited in leveed channels. As sea level rises, the axis of deposition migrates landward with the shoreline so that submarine canyons, as well as incised valleys on the previously exposed shelf, back-fill with sediments. During this rise, and through the rest of a sea-level cycle (transgression and highstand: not shown in Fig. 13), mostly fine-grained sediments are deposited in deep water, in front of prograding deltas. The three sedimentary deposits that form during the falling stage and the early turnaround and rise of sea level are collectively termed a *lowstand systems tract* (Fig. 13).

Application of Sequence Stratigraphy to the Jackfork Group

Applying the sequence-stratigraphic concept to Jackfork outcrops, sheet sands within outcrop A-2 (Fig. 5) are interpreted to have been deposited in a basinal or base-of-slope setting, and channel sands are interpreted to have been deposited in a somewhat more proximal slope setting in the Ouachita Basin. During an early stage of lowstand of sea level, sheet sands were deposited in the basin or at the base of slope (Fig. 14). With a rise in sea level, thinner beds and more mud were deposited over the sheet sands, and the axis of deposition moved in a paleo-landward direction, but highstand deltas prograded basinward. With the next stage of falling sea level, the axis of deposition moved basinward, and channel sands were deposited over the preceding, progradational highstand deposits. The two sets of strata are now separated by a depositional sequence boundary.

Outcrop A-3 (Fig. 6) is interpreted as containing a more complete lowstand to highstand systems tract. Lower, falling-stage sheet sandstones are overlain by thin-bedded levee beds

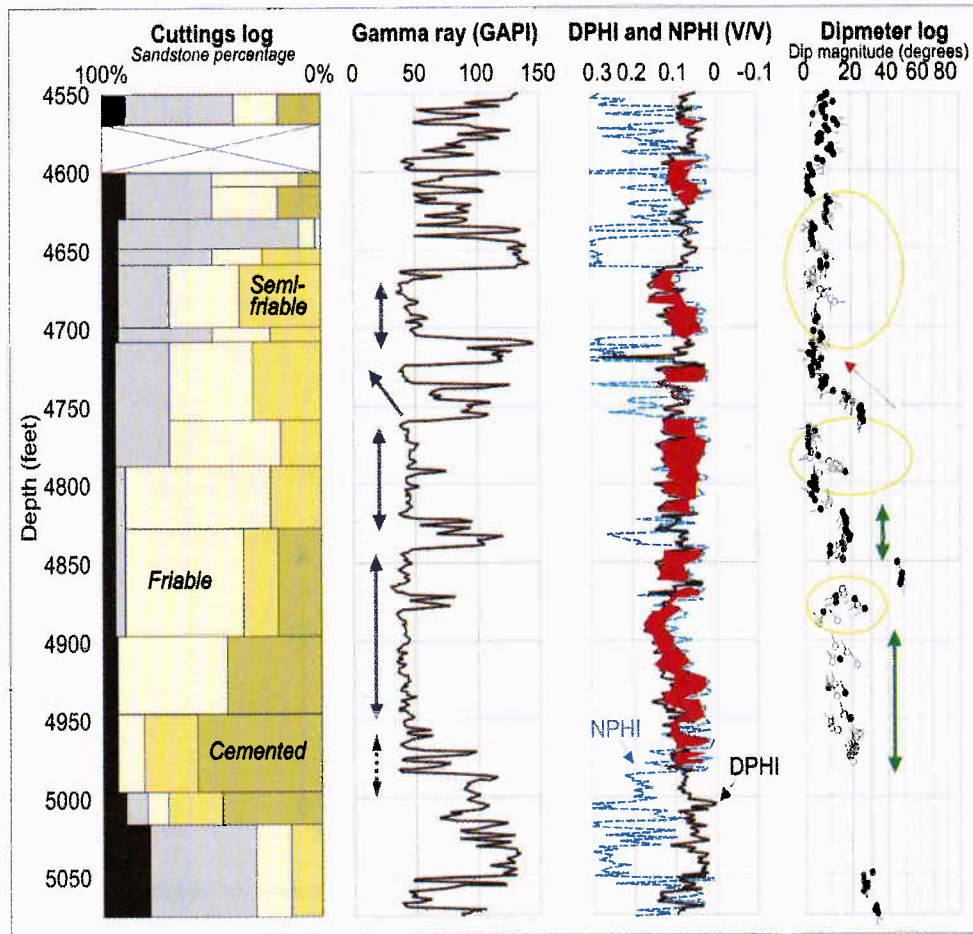


Figure 10. Same logs as in Figure 9, but within another Jackfork stratigraphic interval. With the exception of one zone of quartz-cemented sandstones at 4,950–5,000 ft, the dominant sandstone in this interval is friable to semifriable sandstone. Note the more massive-appearing sandstones on the gamma-ray log and the higher and more variable dips on the dipmeter log (with the exception of a siltstone interval from 4,550 to 4,650 ft).

deposited during early turnaround of sea level, which are in turn overlain by highstand prodelta, organic-rich sandstones and mudstones. The erosion surface upon which the friable channel sandstones sit is a sequence boundary that represents a renewed stage of falling sea level.

Because the stratigraphy and sedimentary features of the Jackfork cannot be directly observed in subsurface wells, it is somewhat more difficult to develop a subsurface sequence-stratigraphic framework. In this case, conventional well logs, dipmeter logs, and one borehole-image log were compared with the outcrop observations to interpret the sequence stratigraphy. Before a sequence-stratigraphic interpretation can be made from well logs, it is critical that faults are identified from the log intervals to ensure that only a continuous stratigraphic interval is interpreted.

An example interpretation is shown in Figure 15 for the Jackfork interval in two logs from wells ~2 mi apart. Many layered sheet sandstones are interpreted to occur at the bases of the logged intervals. These are directly overlain by a thick channel sandstone. The intervals from 7,600 to 7,900 ft in the

left well and 4,600 to 5,200 ft in the right well are considered analogous to outcrop A-2 (Fig. 5); a sequence boundary is placed between the lower sheet sandstones and the upper channel sandstones. Above the channel sandstones is a shaly interval interpreted as a condensed section and a transgressive systems tract, which is overlain in both wells by a coarsening-upward, progradational highstand deposit of probable deltaic origin.

CONCLUSIONS: SIGNIFICANCE TO GAS EXPLORATION IN THE JACKFORK GROUP OF SOUTHEASTERN OKLAHOMA

Based upon the results of our outcrop and subsurface studies, the following conclusions have been reached:

- Sheet sandstones exhibit diagnostic dipmeter, and somewhat diagnostic gamma-ray, log patterns; these sandstones are prone to be highly cemented and brittle, and to contain fracture porosity;

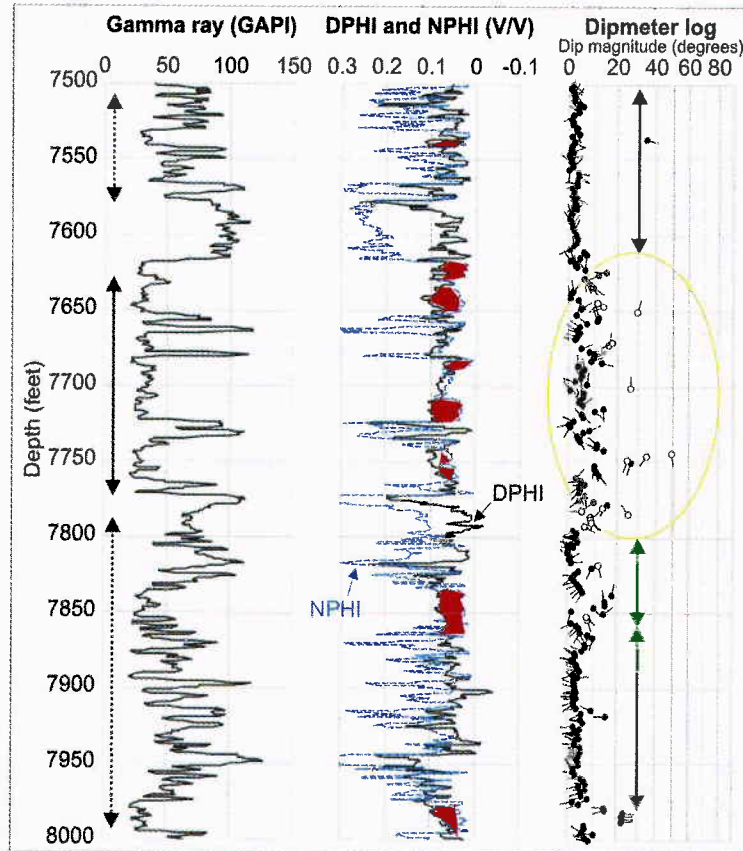


Figure 11. Part of the Jackfork interval in a well, showing two zones of cemented sheet sandstone characterized by interbedded sandstones and shales and uniformly low dips above and beneath a zone of friable channel sandstone characterized by blocky-sandstone log response and diverse dips.

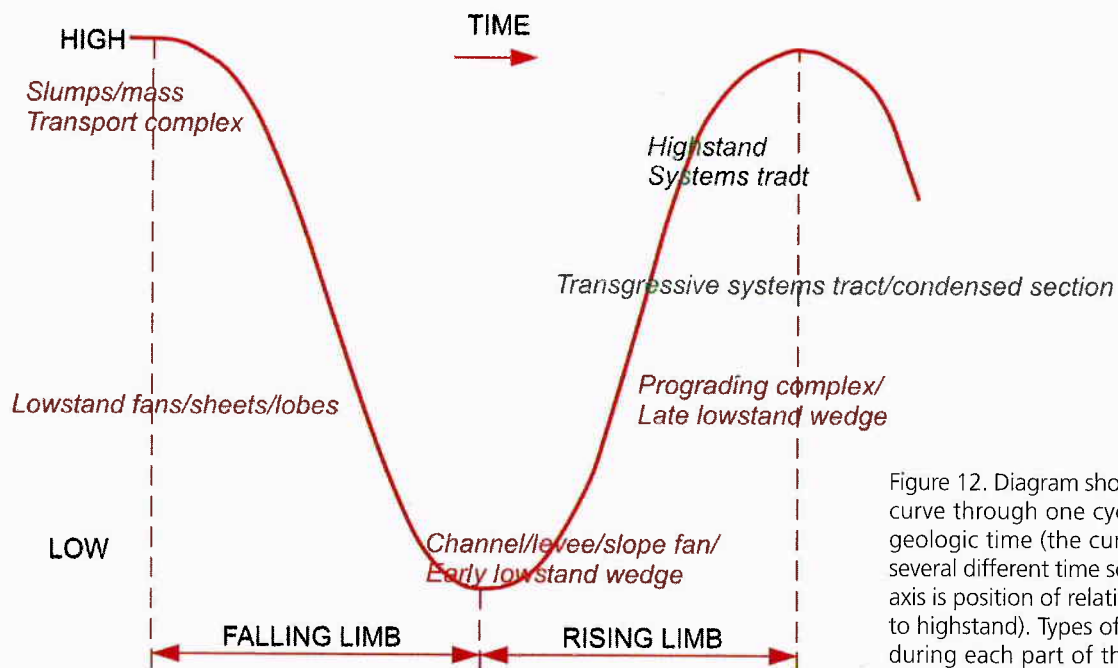


Figure 12. Diagram showing relative sea-level curve through one cycle. Horizontal axis is geologic time (the curve can be applied to several different time scales), and the vertical axis is position of relative sea level (lowstand to highstand). Types of sediments deposited during each part of the lowstand cycle are provided on the curve.

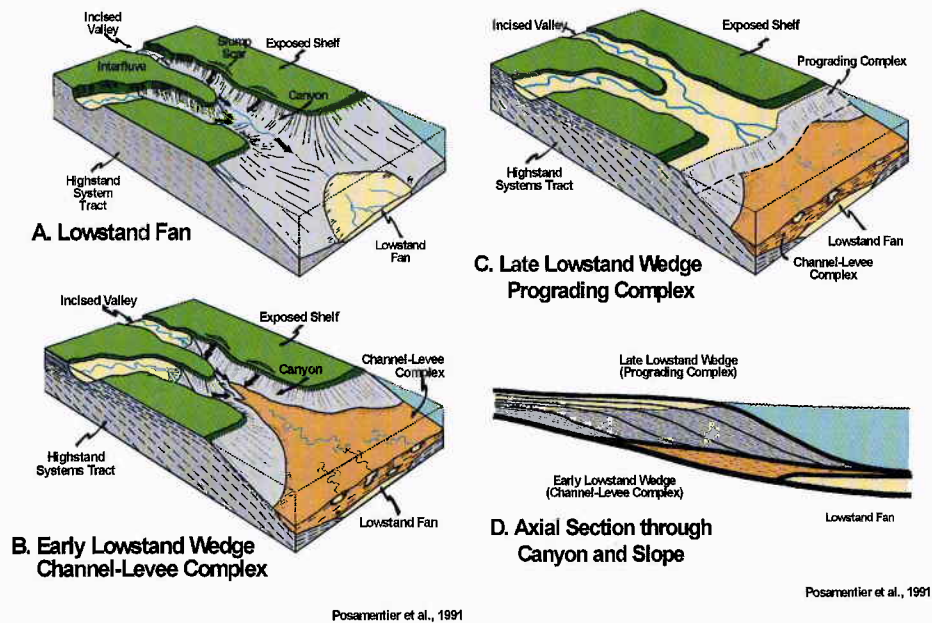


Figure 13. Cartoons showing three stages of development of the lowstand systems tract: (A) Lowstand fans form at lowered sea level. (B) Leveed-channel complex forms at minimum sea level and early turnaround. (C) During subsequent slow rise in sea level, fine-grained sediments prograde into deep water, and feeder channels backfill. (D) The three components of the lowstand systems tract. Modified from Posamentier and others (1991).

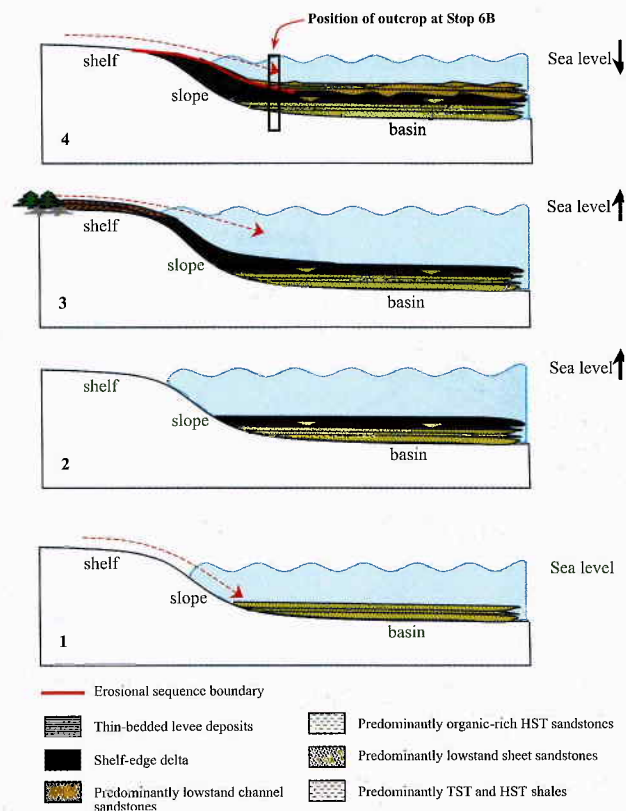


Figure 14. Sequence-stratigraphic interpretation of deposition of outcrop A-2. During stage 1 (lower figure), basin-floor (sheet) sands are deposited in the basin. During stages 2 and 3, sea level rises, and thin beds of sand and shale are deposited. During stage 4, sea level falls, providing a seaward shift in the depositional axis, resulting in an erosional sequence boundary and deposition of more proximal channel sands on top of more basinal sheet sands. Modified from Omatsola (2003).

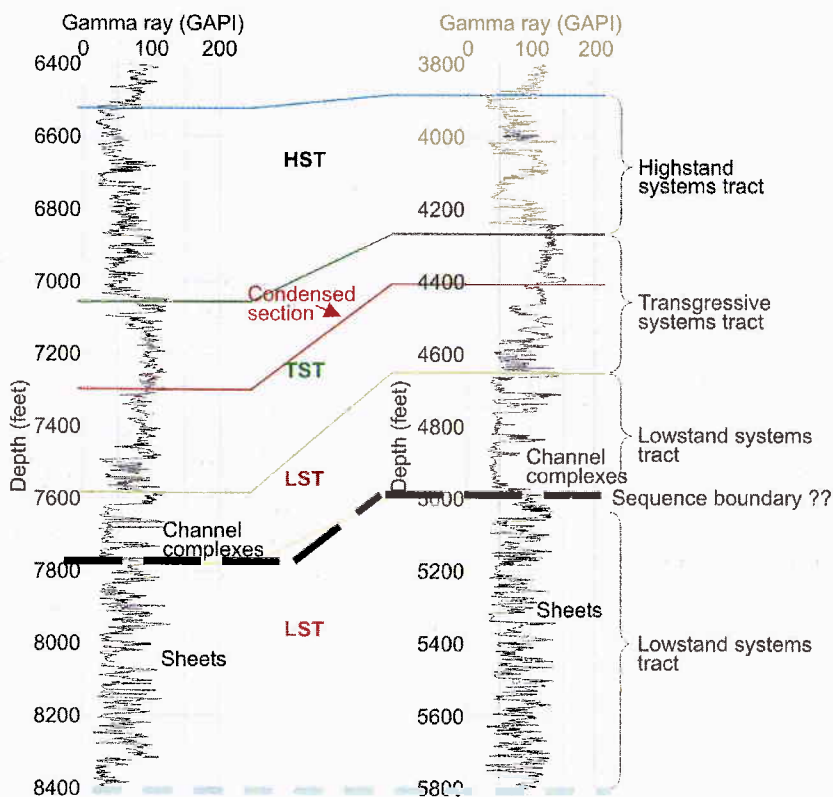


Figure 15. Correlation of two logs from wells ~2 mi apart. Channel- and sheet-sandstone facies are identified in these intervals on the basis of well-log patterns, and a sequence-stratigraphic framework has been developed. A probable sequence boundary is placed at the base of the channel complex, which represents a lowstand systems tract (LST), overlain by a transgressive systems tract (TST), and a highstand systems tract (HST). An interval of interpreted sheet sandstones of an older LST underlies the sequence boundary (modified from Garich, 2004). Note the similarity of the stratigraphy of the 7,600–7,900-ft interval (left well) and the 4,600–5,200-ft interval (right well) to that of outcrop A-3 of Omatsola (2003).

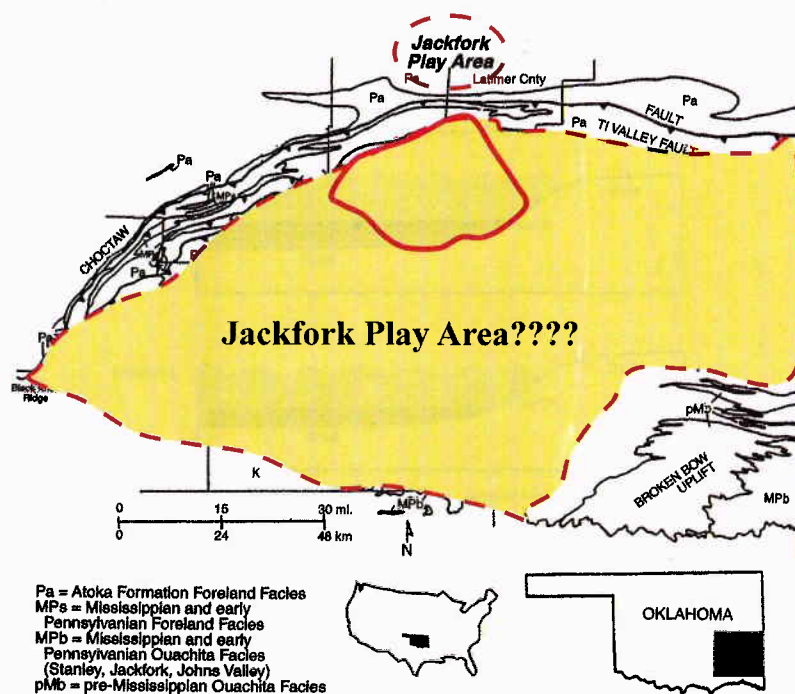


Figure 16. Map showing current and possible Jackfork play areas (yellow) in southeastern Oklahoma.

- Channel sandstones also exhibit diagnostic dipmeter, and somewhat diagnostic gamma-ray, log patterns; these sandstones are prone to be friable to semifriable and to contain matrix porosity;

- Borehole-image logs (as well as whole-diameter core) provide a better means for differentiating sandstone types than conventional well logs;

- With porosity logs, it should be possible to recognize zones of anomalously high matrix porosity, although we have not tested this concept;

- The sheet and channel sandstones can be placed within a sequence-stratigraphic framework using subsurface wells, provided faulted zones are identified and excluded from stratigraphic interpretation.

Thus, development of a local- to regional-scale sequence-stratigraphic framework for the subsurface Jackfork might prove reliable for predicting the occurrence of different reservoir types (matrix vs. fracture porosity) in the subsurface. Therefore, a large area of southeastern Oklahoma may contain subsurface Jackfork sandstones (Fig. 16) that are worth investigating from a combined structural-stratigraphic perspective rather than just from a structural perspective, as is the case now.

REFERENCES CITED

- Briggs, Garrett, 1973, Geology of the eastern part of the Lynn Mountain syncline, Le Flore County, Oklahoma: Oklahoma Geological Survey Circular 75, 34 p.
- Browne, G. H.; and Slatt, R. M., 2002, Outcrop and behind-outcrop characterization of a late Miocene slope fan system, Mt. Messenger Formation, New Zealand: American Association of Petroleum Geologists Bulletin, v. 86, p. 841–862.
- Chapin, M. A.; Davies, P.; Gibson, J. L.; and Pettingill, H. S., 1994, Reservoir architecture of turbidite sheet sandstones in laterally extensive outcrops, Ross Formation, Western Ireland, *in* Weimer, P.; Bouma, A. H.; and Perkins, B. F. (eds.), Submarine fans and turbidite systems: Gulf Coast Section, Society of Economic Paleontologists and Mineralogists (SEPM), 15th Annual Reservoir Conference, p. 53–68.
- Garich, A. M., 2004, Porosity types and relation to deepwater sedimentary facies of subsurface Jackfork Group sandstones, Latimer and Le Flore Counties, Oklahoma: University of Oklahoma unpublished M.S. thesis, 94 p.
- Hansen, S. M.; and Fett, T., 2000, Identification and evaluation of turbidite and other deepwater sands using open hole logs and borehole images, *in* Bouma, A. H.; and Stone, C. G. (eds.), Fine-grained turbidite systems: American Association of Petroleum Geologists Memoir 72 and Society of Sedimentary Geology Special Publication 68, p. 317–337.
- Montgomery, S. L., 1996, Jackfork Group, southeastern Oklahoma: new gas play in the Ouachita overthrust: American Association of Petroleum Geologists Bulletin, v. 80, p. 1695–1709.
- Omatsola, B., 2003, Origin and distribution of friable and cemented sandstones in outcrops of the Pennsylvanian Jackfork Group, southeast Oklahoma: University of Oklahoma unpublished M.S. thesis, 227 p.
- Pauli, D., 1994, Friable submarine channel sandstones in the Jackfork Group, Lynn Mountain Syncline, Pushmataha and Le Flore Counties, Oklahoma, *in* Suneson, N. H.; and Hemish, L. A. (eds.), Geology and resources of the eastern Ouachita Mountains frontal belt and southeastern Arkoma Basin, Oklahoma: Oklahoma Geological Survey Guidebook 29, p. 179–202.
- Posamentier, H. W.; Erskine, R. D.; and Mitchum, R. M., 1991, Models for submarine fan deposition within a sequence stratigraphic framework, *in* Weimer, P.; and Link, M. H. (eds.), Seismic facies and sedimentary processes of submarine fans and turbidite systems: Springer-Verlag, New York, p. 127–136.
- Romero, G. A., 2004, Identification of architectural elements of turbidite deposits, Jackfork Group, Potato Hills, eastern Oklahoma: University of Oklahoma unpublished M.S. thesis, 238 p.
- Ross, C. A.; and Ross, J. R. P., 1988, Late Paleozoic transgressive-regressive deposition, *in* Wilgus, C. K.; Hastings, B. S.; Ross, C. A.; Posamentier, H. W.; VanWagoner, J. K.; and Christopher, J. K. (eds.), Sea-level changes: an integrated approach: Society of Economic Paleontologists and Mineralogists Special Publication 42, p. 227–247.
- Slatt, R. M., 2000, Why outcrop characterization of turbidite systems, *in* Bouma, A. H.; and Stone, C. G. (eds.), Fine-grained turbidite systems: American Association of Petroleum Geologists Memoir 72 and Society for Sedimentary Geology Special Publication 68, p. 181–186.
- Slatt, R. M.; Stone, C. G.; and Weimer, P., 2000, Characterization of slope and basin facies tracts, Jackfork Group, Arkansas, with applications to deepwater (turbidite) reservoir management, *in* Deep water reservoirs of the world: Gulf Coast Section, SEPM (Society for Sedimentary Geology), 20th Annual Reservoir Conference, Houston, p. 940–980.
- Weimer, P.; and Slatt, R. M., 2006, Petroleum systems of deepwater settings: Society of Exploration Geophysicists and European Association of Geoscientists and Engineers, 2004 Distinguished Instructor Short Course Series 7 (pagination by chapter).
- Witton-Barnes, E. M.; Hurley, N. F.; and Slatt, R. M., 2000, Outcrop and subsurface criteria for differentiation of sheet and channel-fill strata, example from the Cretaceous Lewis Shale, Wyoming, *in* Deep water reservoirs of the world: Gulf Coast Section, SEPM (Society for Sedimentary Geology), 20th Annual Reservoir Conference, Houston, p. 1087–1104.

Imaging Thin Morrow and Springer Sandstones with High-Frequency Three-Dimensional Seismic Techniques in the Anadarko Basin

Bob Springman

Dominion Exploration and Production, Inc.
Oklahoma City, Oklahoma

ABSTRACT.—Morrow–Springer sandstones in the Anadarko Basin have been excellent exploration targets for seismic-stratigraphic applications since the mid-1970s. These high-impedance sandstones are detectable and can be better delineated with new high-frequency imaging methods.

The resolution of these Pennsylvanian–Mississippian sandstones has improved significantly in the last 30 years, with an increase in frequency content of the seismic data, as follows:

<i>Date</i>	<i>Frequency</i>	<i>sandstone resolution</i>
1980	60 Hz.	62 ft
1995	90 Hz.	42 ft
2003	160 Hz.	23 ft

With three-dimensional coverage, areal mapping of these sandstones can be enhanced to better define environments of deposition and increase the understanding of potential reservoirs.

INTRODUCTION

The Morrow and Springer sandstones of the Midcontinent Anadarko Basin have been prolific gas-producing reservoirs in stratigraphic or structural-stratigraphic traps. Future reservoirs

will be primarily pure stratigraphic traps (Fig. 1). Owing to the high-risk nature of finding stratigraphic traps without adequate well control, seismic data are necessary to reduce the number of

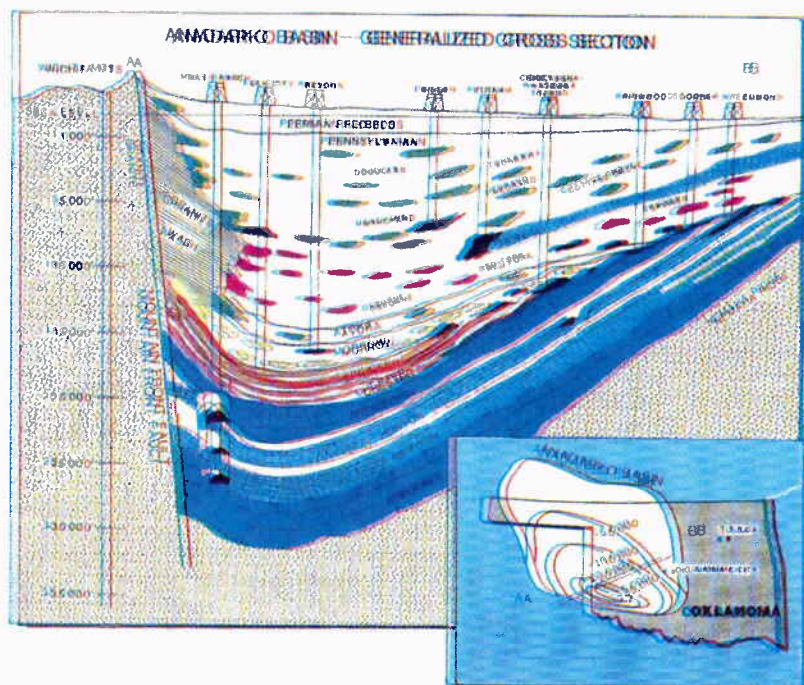


Figure 1. Generalized cross section across the Anadarko Basin, showing future reservoir targets amenable to 3-D seismic prospecting.

dry holes. Three-dimensional (3-D) seismic data are a reliable tool for gross stratigraphic identification of potential sandstone reservoirs.

WAVE DEFINITIONS

Prior to a discussion of geophysical methods as used herein to identify sandstone stratigraphic traps, an understanding of a few terms will be necessary. Figure 2 is a graphical presentation representing the components of a sound wave traveling through the subsurface. The line of sinusoidal propagation from the surface through the subsurface is defined by the word *position*, also referred to as the *zero line*. The amplitude is the strength of the reflected signal, or the distance measurement from the zero line to the maximum apex of the sinusoidal line.

The wavelength is the length of the wave in the direction of propagation from the zero line to the second zero line crossing. Or, every other zero line crossing by the wavelet is one wavelength.

The frequency, as commonly measured in hertz (Hz), is the number of complete cycles the wave makes in 1 second. Now, with the understanding of these few geophysical terms, the resolution of the seismic reflector can be calculated:

Seismic resolution = one-fourth (0.25) wavelength, and

Wavelength = velocity/frequency.

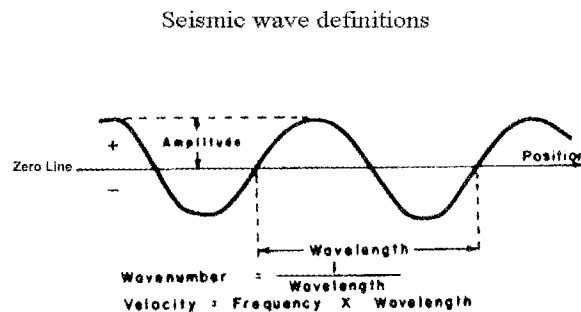
In the 1990s, seismic data in the Anadarko Basin had usable frequencies as high as 90 Hz. The velocity of the Morrow-Springer sandstones typically is 14,000 to 16,000 ft per second (ft/sec). The seismic resolution is:

$$0.25(15,000 \text{ ft/sec})/90 \text{ Hz} = 42 \text{ ft.}$$

With new high-frequency imaging processing as of 2003, frequencies as high as 160 Hz are now achievable. The seismic resolution now is:

$$0.25(15,000 \text{ ft/sec})/160 \text{ Hz} = 23 \text{ ft.}$$

Thin sandstone <25 ft thick that was not resolvable in the 1990s can now be resolved with high-frequency imaging processing.



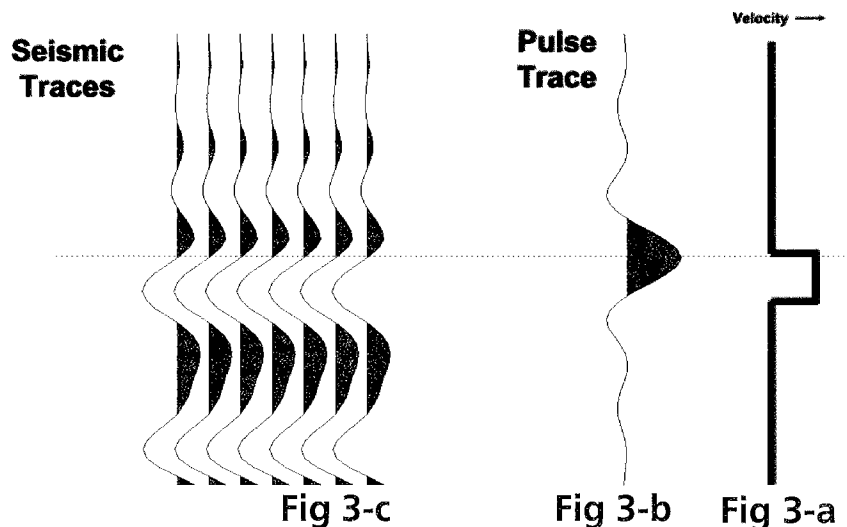
$$\text{Seismic Resolution} = \frac{1}{4} \text{ wavelength} = \frac{1}{4} \text{ velocity/frequency}$$

$$90\text{Hz resolution} = \frac{1}{4} (15,000/90) = 42 \text{ feet}$$

$$160 \text{ Hz resolution} = \frac{1}{4} (15,000/160) = 23 \text{ feet}$$

Figure 2. Graphical representation of sound-wave components traveling through the subsurface.

Figure 3. (A) Simple geologic model with a thin sandstone having a seismic velocity of 15,000 ft per second (fps) encased in "clean" shale having a velocity of 11,000 fps. (B) One-D trace convolved with the geologic model. (C) Synthetic seismogram from a well with the same thin sandstone thickness as the model but encased in shaly limestone with carbonate strata above and beneath, respectively.



With improved data processing in static solutions, velocity analysis, random noise reduction, and high-frequency imaging, the geophysical industry has come a long way since the 1990s. We can now do an excellent job of defining certain types of sandstone beds with a thickness of ~25 ft, but, unfortunately, not everything can be consistently delineated with the new processing methods. There are still constraints that prohibit the ability to accurately define the thickness of sandstone, or even detect it.

Figure 3A is a simple geologic model with a thin sandstone bed having a seismic velocity of 15,000 ft/sec encased in "clean" shale having a seismic velocity of 11,000 ft/sec. Figure 3B is the 1-D pulse trace convolved with the geologic model. The synthetic traces in this paper are log positive polarity (the deflection to the right indicates a velocity increase). Visibly, the synthetic seismic response is exactly one-fourth (0.25) of the wavelength and accurately resolves the simple geologic model. Figure 3C is a synthetic seismogram from a well with the same thin sandstone thickness as the model, only the borehole has numerous shaly-lime streaks directly above the thin sandstone, and a laminated carbonate beneath. With interference from the strata above and beneath the thin sandstone bed, the seismic response has a completely different appearance. Therefore, the interpretation of seismic data will only be as good as the accuracy of the geologic model.

SEISMIC MODELING

From the work of Bob Sheriff (2002), in the case of a high-impedance sandstone (a high-velocity sandstone encased in low-velocity shale), the amplitude can be used as a gross tool to estimate sandstone thickness. Figure 4 is a wedge model showing the response of a high-impedance sandstone from 0 to 1 wavelength. Notice that the amplitude increases sharply from 0 to 0.25 wavelength, at which it reaches maximum amplitude. Thereafter, the amplitude decreases to a point at which the wedge thickness

is about equal to one-half (0.5) wavelength and remains fairly constant with a thickness >0.5 wavelength.

The color attribute of the amplitude spectrum (not shown in this figure) is blue to green for negative low amplitude, yellow for medium amplitude, and red for positive high amplitude. A simple 2-D synthetic model of the Springer Britt sandstone (Fig. 5) illustrates the seismic response from a 25-ft, thin sandstone in the Anadarko Basin convolved with a band-pass wavelet of 150 Hz (~0.25 wavelength). The high-impedance Britt sandstone increases in amplitude as the sandstone increases from 0 to 25 ft thick, and then decreases as the sandstone thins to 0 ft. Notice that the shading attributes are similar to the wedge model in Figure 4. This is considered the type seismic response for the Morrow-Springer sandstones in the Anadarko Basin.

TYPE SYNTHETIC SEISMOGRAMS

To better define these thin sandstones, higher frequency data are necessary. This principle is exemplified in Figure 6 in which two synthetic seismograms are compared. Here, the sonic-log curves (convolved with a low- and high-frequency band-pass wavelet) are displayed side by side. The seismic response of the high-frequency wavelet does not completely define all the high-impedance sandstones owing to constraints mentioned previously, but it does a far better job in defining sandstones than the lower frequency wavelet.

The focus area for Springer sandstone seismic imaging is in parts of Caddo, Custer, and Washita Counties, Oklahoma (Fig. 7). Five synthetic seismograms were selected from across this area to demonstrate the regional seismic response of the Springer Cunningham, Britt, and Boatwright sandstones.

The gross and net thicknesses for the Britt sandstone are spotted at the base of the synthetic seismograms for a reference of the amplitude to the thickness. Also, the cumulative gas production

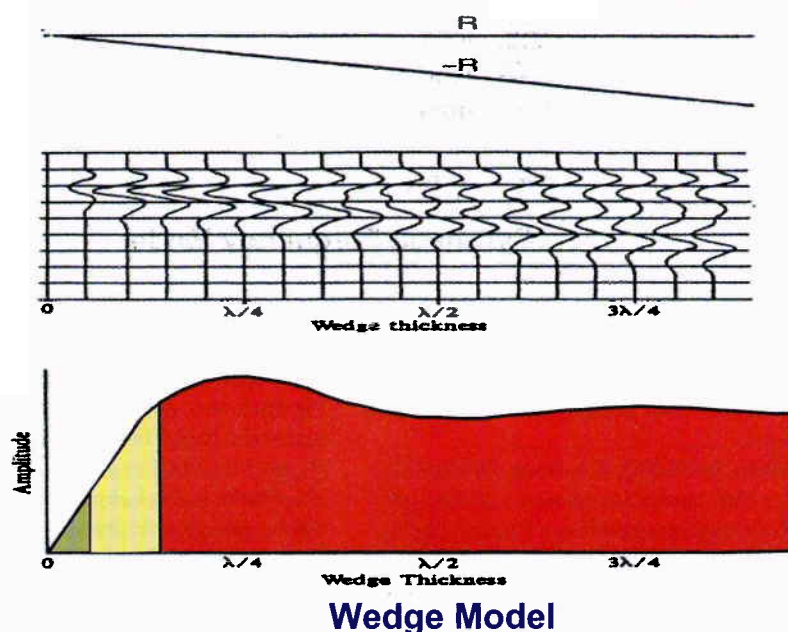


Figure 4. Wedge model showing the response of a high-impedance sandstone from 0 to 1 wavelength.

2-D Seismic Model

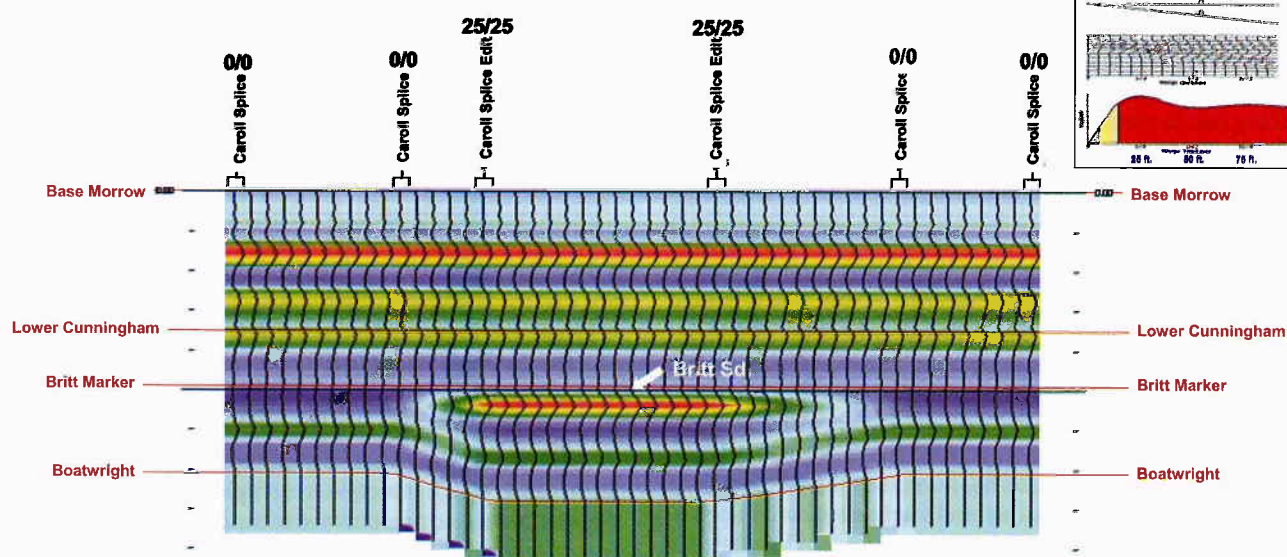


Figure 5. Two-D synthetic model of the Springer Britt sandstone, showing the seismic response from a 25-ft sandstone convolved with a band-pass wavelet of 150 Hz (~0.25 wavelength).

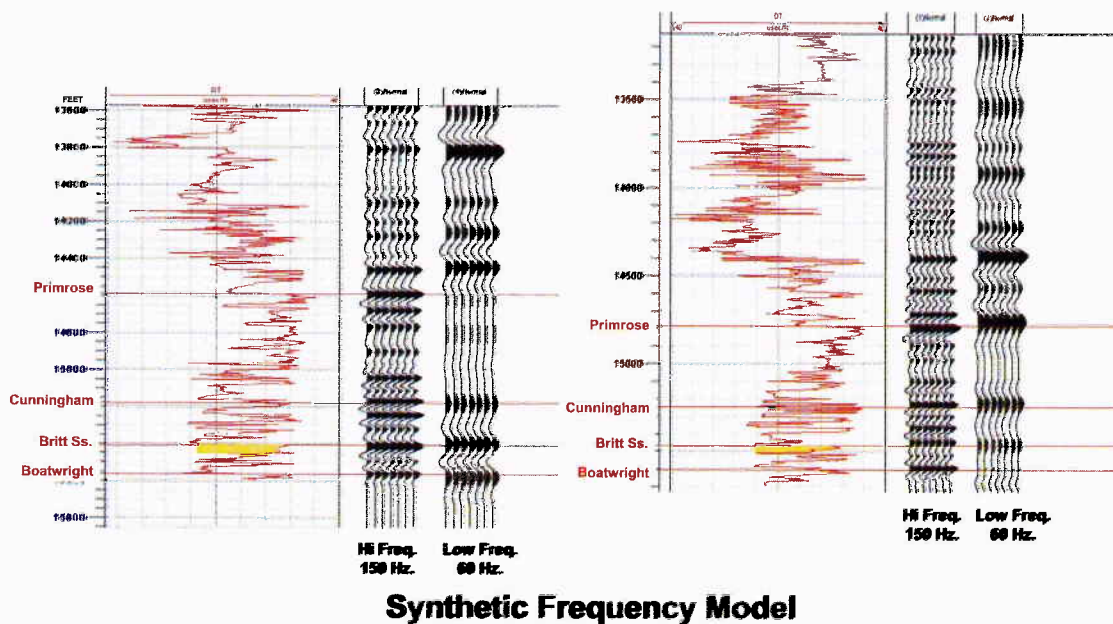


Figure 6. Two synthetic seismograms displaying the sonic-log curves convolved with a low- and high-frequency band-pass wavelet.

and expected ultimate recovery are given at the base of these synthetic seismograms to show the prolific production from these Springer sandstones.

The first synthetic seismogram (Fig. 8) is from the H&P No. 2-18 Tall Bear well. Notice that the Britt sandstone has the highest amplitude. It has a clean shale directly above it and is slightly above tuning (0.25 wavelength) in thickness. This matches the results from the wedge-tuning model for amplitude versus thickness taken from the work of Bob Sheriff (2002) (Fig. 4). The overlying upper Cunningham also has a clean shale interval di-

rectly above it, but the sandstone is much thicker than the tuning thickness, resulting in a lower amplitude in comparison to that of the Britt. Therefore, greater sandstone thickness does not always mean higher amplitude. The Boatwright has the weakest amplitude, as it is below the tuning thickness and does not have clean shale directly above it.

In both the Santa Fe No. 1-33 Larry well (Fig. 9) and the Lear No. 1-17 Frost well (Fig. 10), the Britt sandstone has a lower amplitude response than some of the Cunningham sandstones. Some of the Cunningham sandstones are close to tuning thick-

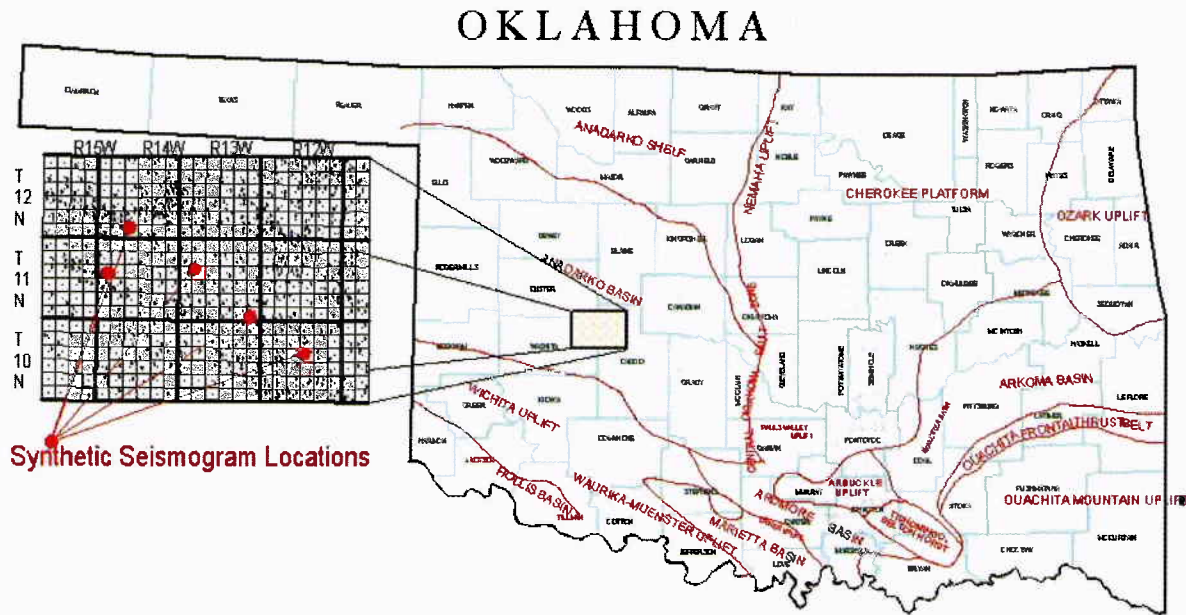


Figure 7. Map showing locations of five synthetic seismograms from the Anadarko Basin that were used to demonstrate the regional response of the Springer Cunningham, Britt, and Boatwright sandstones.

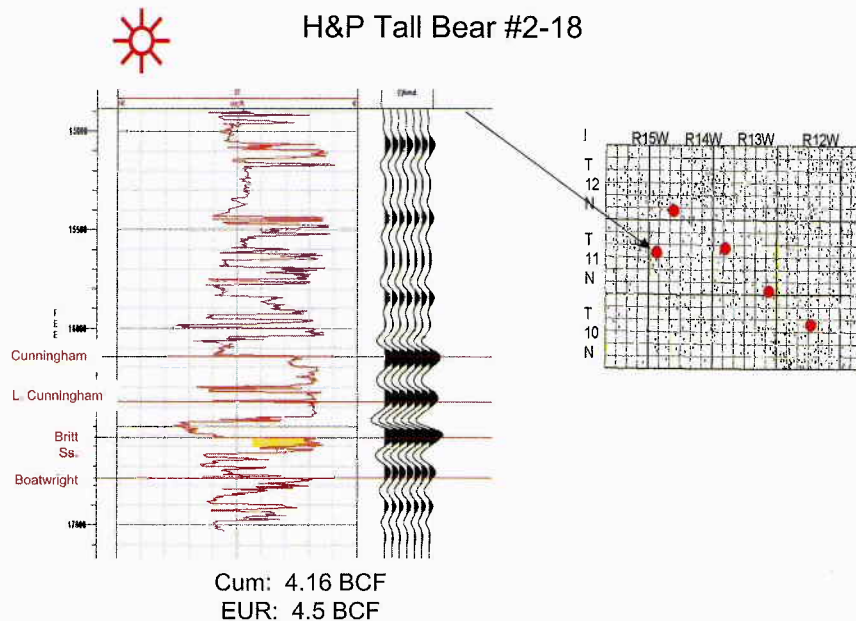


Figure 8. Synthetic seismogram from the H&P No. 2-18 Tall Bear well. *Cum*, cumulative production; *EUR*, estimated ultimate recovery; *BCF*, billion cubic feet.

ness, whereas the Britt sandstone is almost twice the tuning thickness. Again, the greater thickness does not always correspond to the greater amplitude.

In the Lear No. 1-36 Hart well (Fig. 11) the amplitudes of the Britt sandstone and the upper two Cunningham sandstones are similar because the thicknesses are similar. They are both above tuning. The lowest two Cunningham sandstones are much lower in amplitude because they are beneath the tuning thickness.

Springer sandstone in the Lear Petroleum No. 1-15 Patton well (Fig. 12) shows a different amplitude pattern in that the amplitudes of the Britt and lower Cunningham sandstones are

lower than the amplitude of the Boatwright sandstone. The Britt sandstone is below tuning thickness and has a velocity notch in the shale directly above it. The middle Cunningham sandstones are present and close to the tuning thickness, but they are spaced too closely together, creating interference by their side lobes and diminishing their amplitude. In this case the Boatwright sandstone has the highest amplitude, with a thickness close to tuning, and with a clean shale directly above it.

After reviewing the responses of geophysical models and synthetic seismograms, the amplitude information from the tuned seismic data can be helpful in predicting sandstone thickness,

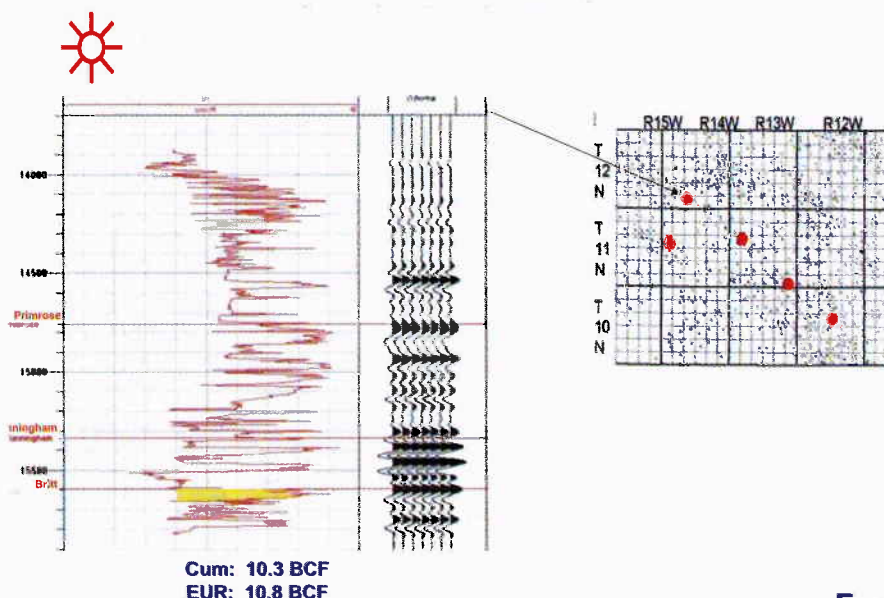
Larry #1-33

Figure 9. Synthetic seismogram from the Santa Fe No. 1-33 Larry well.

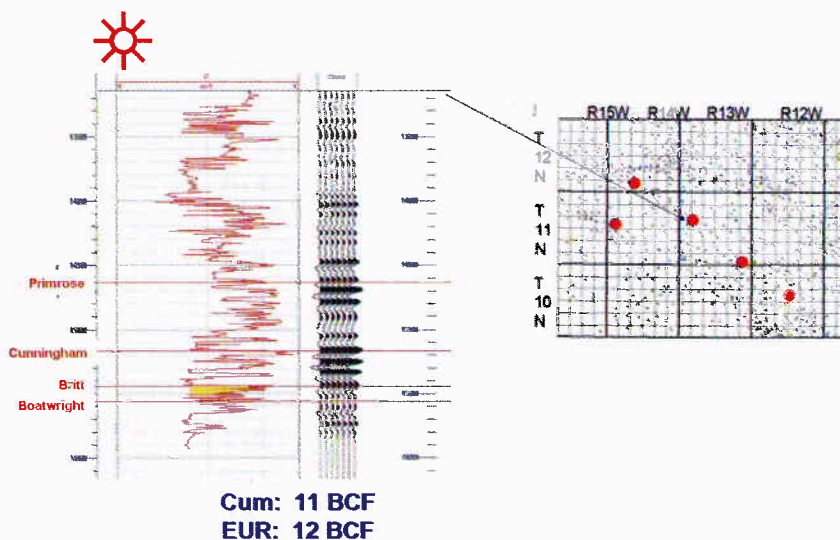
Frost #1-17

Figure 10. Synthetic seismogram from the Lear No. 1-17 Frost well.

given an accurate geologic model and properly recorded and processed seismic data.

Case-History Examples

An extracted line from a 3-D seismic survey with the basic geophysical Britt sandstone model above it (Fig. 13) is an excellent example of the improvement made with high-frequency data acquisition and high-frequency imaging processing. The extracted line from the 3-D volume matches the Britt synthetic model. The high-end frequency in 1995 was ~90 Hz. Since 2003, frequencies as high as 160 Hz are achievable in the Anadarko Basin. Both the stratigraphic and structural information is greatly enhanced. The resolution of the thin beds is almost half the thickness from data processed in 1995. Also, the structural information is improved, with the definition of faults that were not obvious on the lower frequency processing.

The high-seismic-impedance Britt sandstone can now be more confidently interpreted with correlation from the synthetic seismograms. This is demonstrated by the interpretation of two Britt sandstone bars trending northwest to southeast (Fig. 14). The northern bar at the top is an existing field producing from the Britt sandstone. The southern bar at the bottom is a Britt sandstone bar that was newly discovered as a result of interpretations using high-frequency 3-D seismic data. The high-frequency 3-D data constitute an essential tool for continued success in finding limits of existing Springer sandstone fields and new field discoveries.

The 3-D data have proven capabilities in grossly delineating these Springer sandstones, but how accurate are they in measuring the thickness of these sandstones? The theory works well, but the results are not always what the data suggest. Figure 15 are graphs of 17 Springer sandstone results. The bottom graph shows the sequential well numbers (x-axis), decreasing in thick-

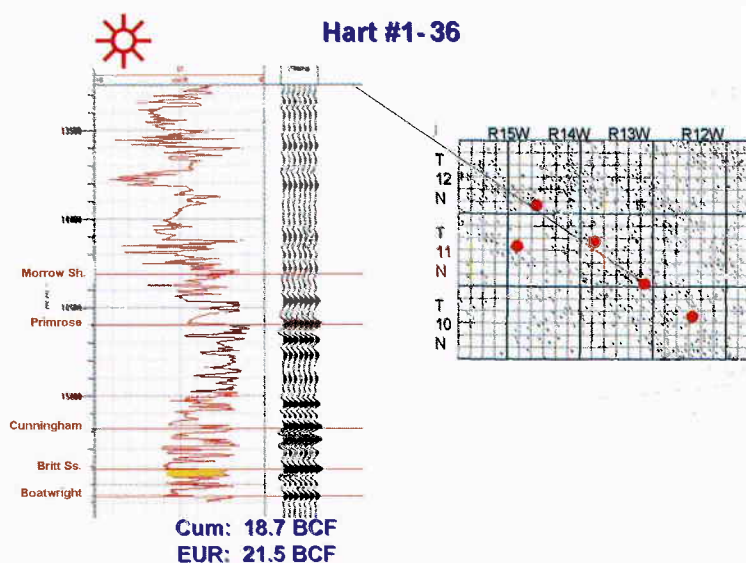
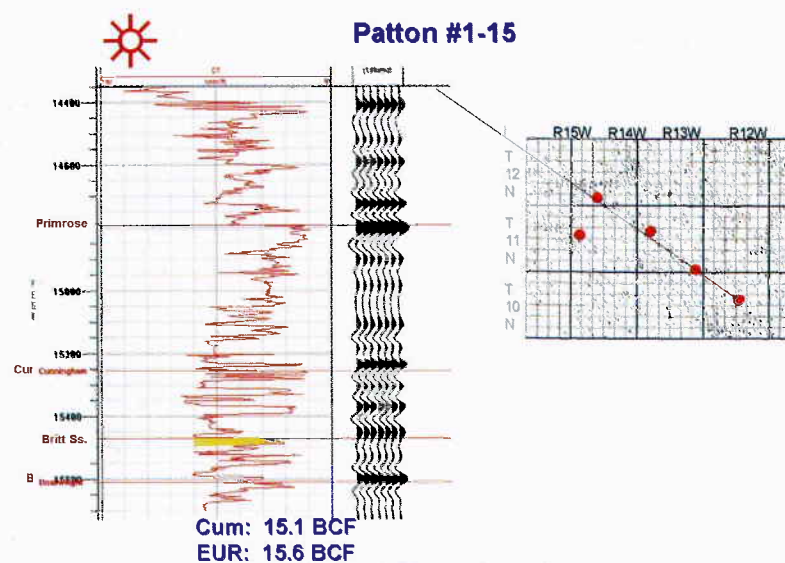


Figure 11. Synthetic seismogram from the Lear No. 1-36 Hart well.

Figure 12. Synthetic seismogram from the Lear No. 1-15 Patton well.



ness from left to right, versus the thickness (y-axis) in feet. The top graph is the same order of well numbers (x-axis) versus the normalized amplitude (y-axis). It appears that the results of thickness versus amplitude are not always consistent.

As mentioned previously in this paper, constraints that affect the amplitude compound the results of the seismic response. Also, of these 17 wells (Fig. 15), only two had bottom-hole surveys. Allowing for deviations of <500 ft, the results of the two graphs (amplitude versus thickness) could match the wedge model more closely. However, to be objective, the surface locations and the bottom-hole locations of all wells are assumed to be the same. We, as an industry, need to better document the bottom-hole locations of wells in order to correlate 3-D seismic results more accurately.

The high-impedance Morrow sandstone in the Texas Panhandle portion of the Anadarko Basin has the same seismic response as Springer sandstones in the previously presented synthetic seismograms. The high-velocity Morrow sandstone, encased in low-velocity shale, makes an excellent reflector when tuned (Fig. 16). The 20-ft, thin Morrow sandstone is below tuning

at 90 Hz (1995 processing) but is much closer to tuning at 130 Hz (2004 processing) with high-frequency imaging.

On the basis of this synthetic model, it was recommended that a 3-D seismic survey be conducted to help identify additional drilling locations for the Morrow Puryear sandstone. After the data were recorded and interpreted, the sonic and gamma-ray logs were correlated with the 3-D seismic data. These data seemed to correlate and fit the model. Sandstone was interpreted along the west edge of the Morrow channel, and an obvious location was chosen 1,200 ft to the east. The extracted line (Fig. 17) indicated that the Morrow channel sandstone was thicker to the east on the basis of the tuning theory and the response of the geophysical model. Unfortunately, the objective reservoir was absent and instead was replaced by limy shale. An unforeseen facies change in the subsurface was not apparent, because both the modeled sandstone and the limy shale have similar velocities.

The Morrow sandstones are very elusive. The same laws and theories of geophysics apply to the Morrow sandstones as well as to the Springer sandstones, but the Morrow geologic model

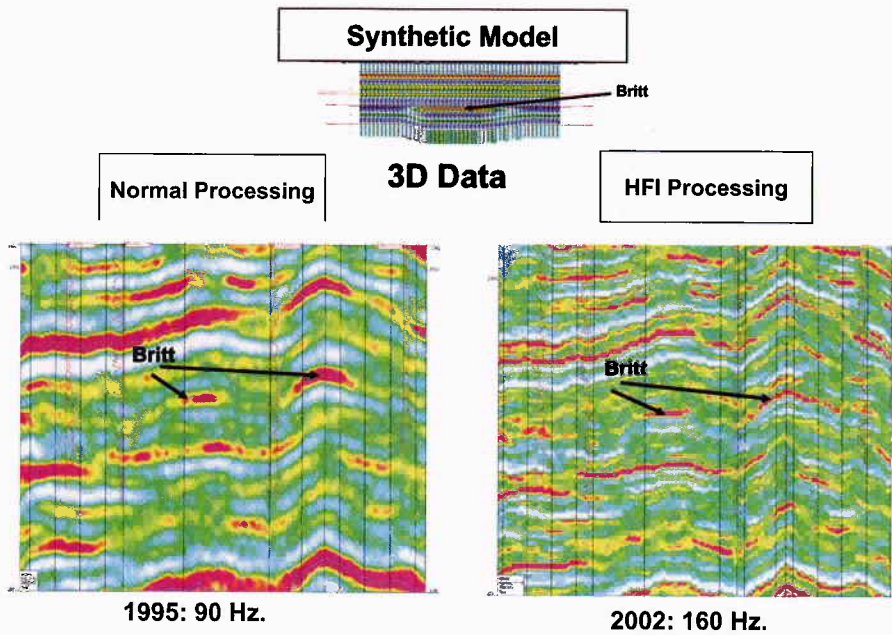


Figure 13. Extracted 3-D seismic line, showing imaging improvement using ~90 Hz (1995) versus ~160 Hz (2002).

Figure 14. Map view showing the interpretation of Springer Britt sandstone bars.

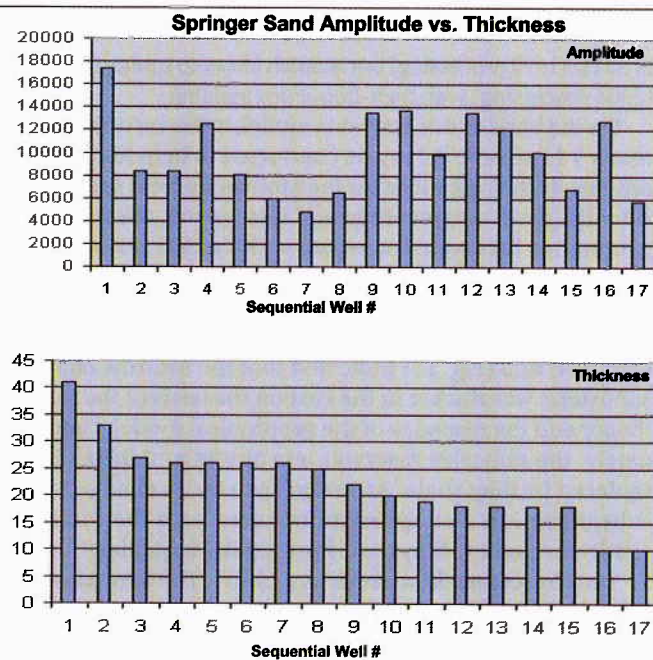
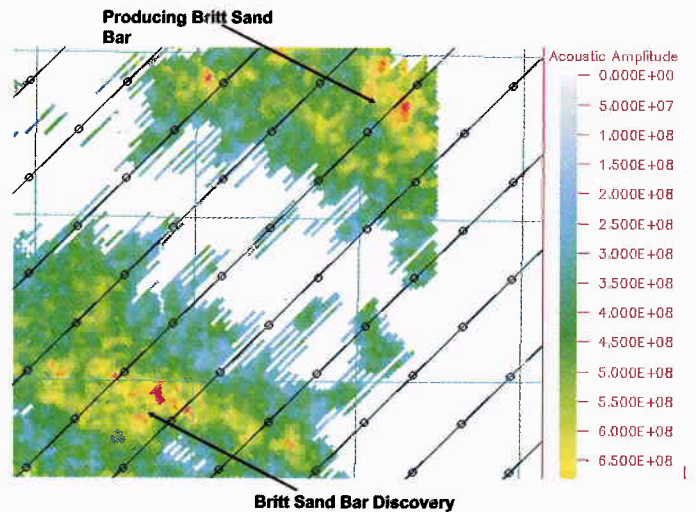


Figure 15. Graphs of 17 wells, showing Springer sandstone thickness versus normalized amplitude.

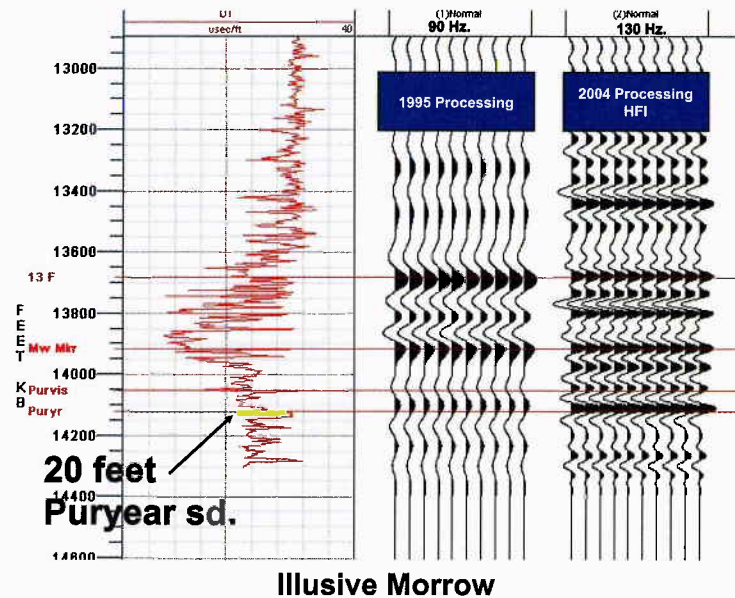


Figure 16. Comparison of synthetic seismograms of a 20-ft sandstone, using 90 Hz versus 130 Hz.

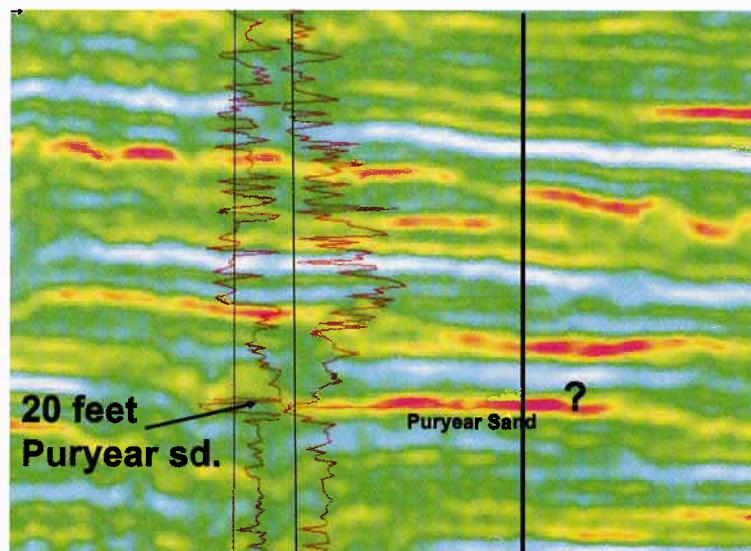


Figure 17. Extracted seismic line indicating an apparent Morrow channel. The anticipated sandstone was not present since it changed facies to a limey shale having a similar velocity.

is much more unpredictable. The interpretation of geophysical data will only be as good as the accuracy of the geologic model. Exploring for Morrow sandstones in the western part of the Anadarko Basin requires a thick-skinned individual capable of absorbing the frustration of limited success owing to the numerous unpredictable facies changes. More research needs to be done on amplitude variation with offset (AVO) to detect possible elastic property changes not evident in the (P-wave) data. High-frequency imaging will still be necessary to better resolve these sandstones pre-AVO.

RECOMMENDATIONS

1. Strive for accuracy in geologic modeling (results will be as accurate as the geologic model).
2. Calibrate your seismic data (set phase).

3. Use real-life models (synthetic seismograms).
4. Stay tuned (resolve the objective).
5. Adequately sample your target (use 3-D data).
6. Eliminate ambiguities (record necessary well logs).

ACKNOWLEDGMENTS

The author acknowledges Ernie Knirk, Mark Thomas, and Richard Easley at Dominion Exploration and Production.

REFERENCE CITED

Sheriff, R. E., 2002, Encyclopedic dictionary of applied geophysics (4th edition): Society of Exploration Geophysicists, Tulsa, 429 p.

Geo-Engineering Modeling of Morrow/Atoka Incised-Valley-Fill Deposits Using Web-Based Freeware

W. Lynn Watney, Saibal Bhattacharya, Alan Byrnes,
John Doveton, and John Victorine

Kansas Geological Survey
Lawrence, Kansas

ABSTRACT.—Atokan- and Morrowan-age incised-valley-fill (IVF) estuarine sandstones in the Hugoton Embayment produce >21% of the oil in Kansas. Improved exploitation of remaining reserves is dependent on building robust geo-engineering reservoir models with limited data, and doing this in a cost-effective, user-friendly, and efficient manner. A geomodel was constructed for an Atokan-age IVF sandstone reservoir in the Minneola Field complex, using free web-based software called GEMINI (Geo-Engineering Modeling through INternet Informatics; www.kgs.ku.edu/GEMINI). The geomodel represents the quantification of reservoir properties (e.g., porosity, permeability, fluid saturations) of rocks deposited in a simple tripartite estuary-mouth, inner-estuary, and alluvial-plain environment, including sand bars and small-scale tidal-dominated deltaic deposits with sources from small tributaries bordering a larger trunk valley.

The mapping of petrophysically distinct hydrocarbon pay (economically producible intervals) in the IVF involved determination of optimal cutoffs for gamma ray (shale fraction), porosity, and water saturation to define the productive reservoir. The application of cutoffs resulted in a refined understanding not only of the continuity and overall geometry of the sandstone reservoir but also of improved modeling of production from wells. The cumulative lease-production map covaries closely with that of estimated volumes of initial hydrocarbon reserves in place. Also, the calculated field-recovery factor is characteristic of a solution-gas-drive reservoir, indicating an average primary recovery. The geomodel helps explain the limited success of water injection initiated late in the production life of the field and indicates limited communication of injector zones with the producing zones.

INTRODUCTION

The Minneola Field complex has been studied over the last decade in various investigations (Kruger, 1996, 1998; Clark, 1987, 1995; Youle, 1992). The reservoir is an incised-valley-fill (IVF) sandstone deposited in a tributary system of incised valleys that drained westward along the eastern margin of the Hugoton Embayment (Fig. 1) (Clark, 1987). Whereas some authors have assigned the reservoir age as Morrowan, these strata were correlated with mid-shelf marine carbonates that have been dated with fusulinids as late Atokan (Youle and others, 1994).

The focus of this study is Norcan East Field, Clark County, Kansas, and within the Minneola Field complex. This field has produced nearly 420,000 barrels of oil (BO) and 2.6 billion standard cubic ft of gas (BCFG) (Fig. 2) as of 2000. Norcan Field was discovered in September 1980 with the drilling of the Murfin Drilling Company No. 1-8 Norton well in sec. 8, T. 30 S., R. 25 W. This well flowed 157 barrels of oil per day (BOPD) and 120 thousand cubic ft of gas per day (MCFGPD). Development of Norcan East Field began in 1983, with wells in this field producing between 38 and 164 BOPD and with most wells producing associated gas. Until 1994, Norcan East Field produced under solution-gas drive with negligible water production. To counter declining reservoir pressure, a small

water-injection program was initiated in 1994 in the Minneola Unit in western Norcan East Field.

Drill-stem-test (DST) analyses show that wells completed in the early half of 1983 averaged an initial reservoir pressure of 1,555 pounds per square inch (psi), whereas those completed in 1985 averaged 817 psi. By June 1993, production from the Minneola Unit had dropped to 26 BOPD. The rapid decline in reservoir pressure as the field produced without a pressure-maintenance program resulted in reduced production rates, leading to unitization of the Minneola Unit (western part of the field) to initiate water injection. Results of the water-injection program included limited incremental oil recovery, particularly post-1997 (Fig. 2) in some leases; premature breakthrough in several leases; and no response in others. Wells in the western part of the field produced oil and gas, while those in the eastern part produced mainly gas, suggesting the possibility of compartmentalization, which was not previously modeled (Fig. 3). Currently, pressure and production have declined to marginal levels, causing the geomodel to be reevaluated for improved recovery using various enhanced-recovery schemes including different waterflood designs and tertiary recovery from carbon dioxide (CO₂) miscible flooding. Carbon dioxide flooding is currently being considered for sandstone reservoirs in southwestern Kansas

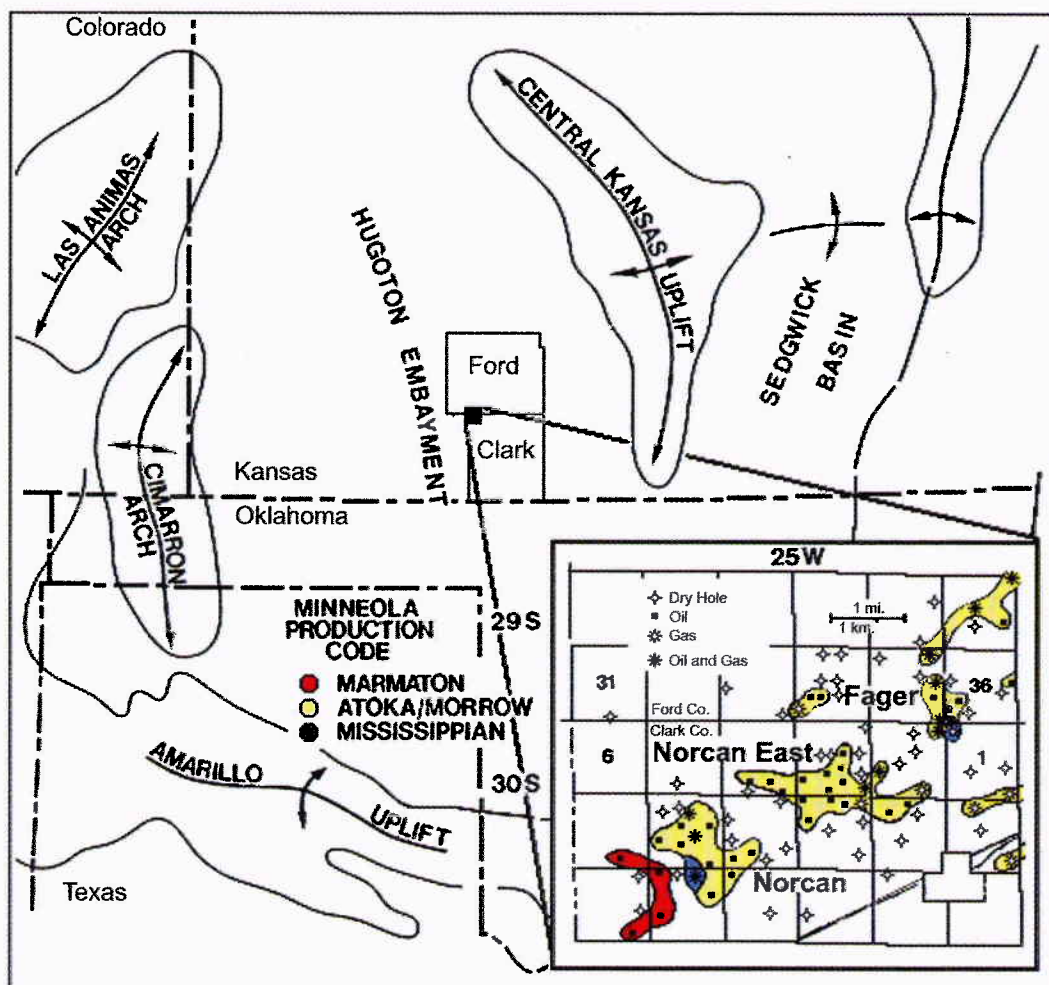


Figure 1. Map of the west-central Midcontinent, showing the Minneola Field complex (Kruger, 1996).

owing to the availability of CO₂ from a local pipeline and/or from new ethanol plants being planned in western Kansas. Higher crude-oil and natural-gas prices further justify studies to develop refined quantitative geomodels of enhanced recovery from mature oil and gas reservoirs.

This paper reviews the work performed on the Minneola Unit with the objective to (1) demonstrate the integration of core and log petrophysics, lithofacies, and stratigraphic analysis to refine reservoir geometry in the Minneola Unit; (2) illustrate how the improved geomodel better explains reservoir performance; and (3) show the efficiency, versatility, and potential for remote collaborative geomodel development using the web-based modeling software GEMINI (Geo-Engineering Modeling through INternet INformatics), which was funded by the U.S. Department of Energy under Cooperative Agreement No. DE-FC26-00BC15310 between 2000 and 2003. Details of the design and operation of GEMINI are described in Victorine and others (2005). The data and analyses used in the Minneola project which are presented in this paper can be reviewed and regenerated in a non-editing mode via the GEMINI website, www.kgs.ku.edu/GEMINI, once a user is identified and allowed access. If editing capability is granted,

users can participate in the analysis wherever they might be located.

GEOLOGIC BACKGROUND

The Minneola Field comprises a tributary portion of an IVF system containing sediments deposited in a simple tripartite estuary-mouth, inner-estuary, and alluvial-plain environment. Sandstone facies that constitute the IVF system include bars and small-scale, tidal-dominated deltaic deposits with sources from small tributaries bordering a larger trunk valley. Incision resulted from an apparent subregional topographic break formed during the Late Mississippian and Early Pennsylvanian Periods along the eastern edge of the Hugoton Embayment. Incision corresponds closely with the subcrop of the Upper Mississippian Ste. Genevieve Limestone. Erosional knickpoints were initially formed that eventually developed into incised valleys along topographic breaks during a prolonged subaerial-exposure event that occurred between the Late Mississippian and Early Pennsylvanian. The Minneola Field complex resides along the wall of the valley system that developed a series of hydrocarbon accumulations formed in reservoirs along the same northwest-southeast-trending

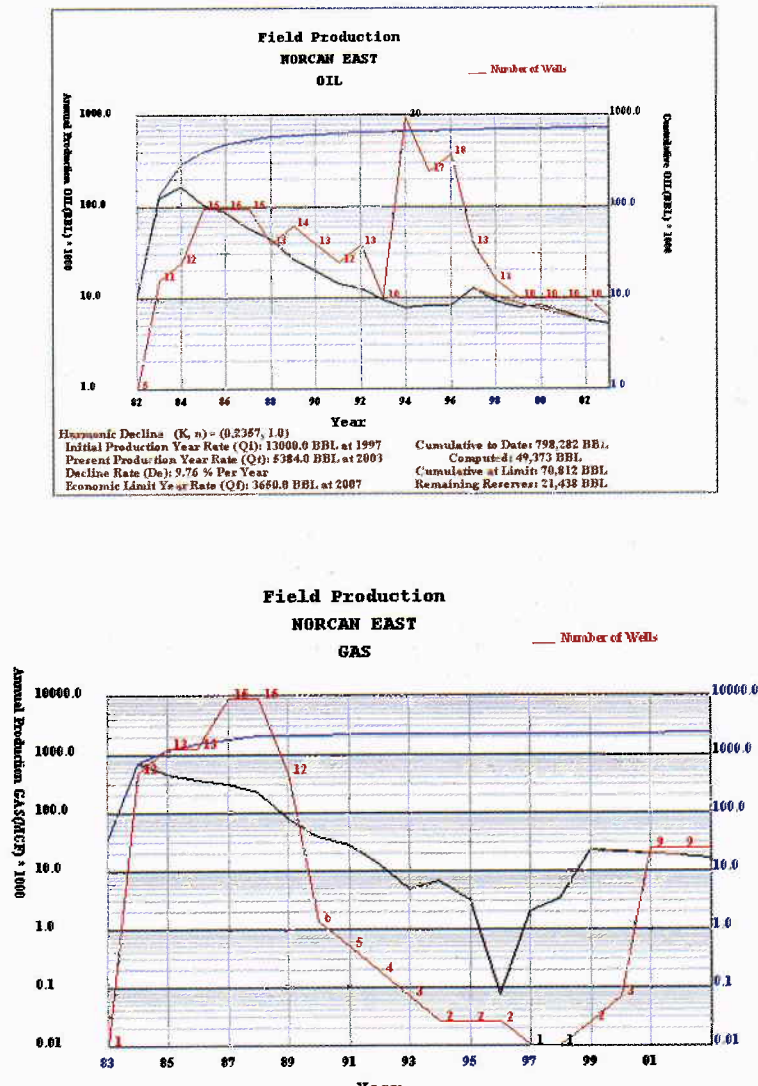


Figure 2. Oil and gas production plots of greater Norcan East Field. Plots are generated on-the-fly from www.ksg.ku.edu, using the latest data available on the server. Plots are generated as a Java applet with the web-based production data, a stand-alone application of GEMINI. Total production is for an area beyond the confines of the study area; thus the higher cumulative oil production.

subcrop of the Ste. Genevieve Limestone. Early Atokan strata overlapped the western edge of the Central Kansas Uplift during a long-term sea-level rise in the Pennsylvanian. The sequences within the IVF at Norcan East Field are believed to represent the updip limit of the marine seaway in early Atokan time (Fig. 4).

Pronounced 4th-order (of 235–400 k.y. duration) fluctuations in sea level during the Pennsylvanian resulted in development of unconformity-bounded depositional sequences that average 10–20 m in thickness and are distributed extensively over the upper Midcontinent region (Heckel, 1994; Watney and others, 1995) (Fig. 4). These sequences are clearly defined on well logs, including those used in this study, as shown in a cored well in Figure 5. Regional correlation across the eastern edge of the Hugoton Embayment in western Kansas by Youle (1992) and Youle and others (1994) illustrates

progressive lateral changes in lithofacies composition of each sequence, ranging from (1) lower-shelf, sediment-starved, high-gamma-ray shales and thin carbonates to (2) a thick, carbonate-dominated succession developed along the mid-shelf, and (3) proximal, upper-shelf estuarine deposits confined to filling incised valleys (Fig. 4). IVFs were bordered by upland settings and slightly higher elevations, and they were capped predominantly by thin paleosols (Fig. 4).

Marine shorelines during the Atokan were driven by glacio-eustasy and were shifted progressively higher onto the margins of the Hugoton Embayment throughout much of the Pennsylvanian. Marine depositional cycles I, J, and K (Youle, 1992) apparently reached near their maximum extent in the Minneola Field complex, with each successive cycle (within this sequence set) reaching farther landward. These paleo-shorelines, trending NW–SE, were correlated by Youle (1992).

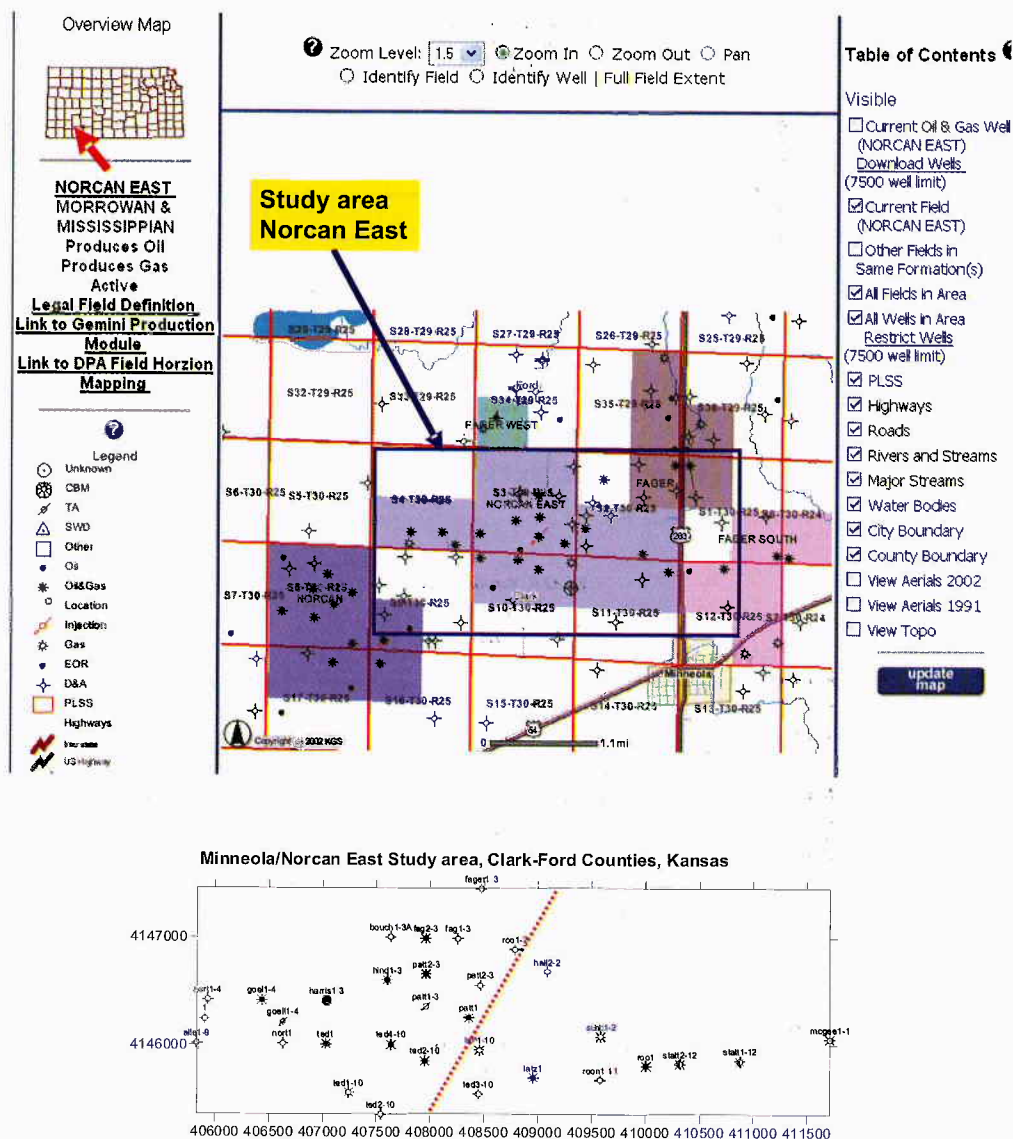


Figure 3. (A) Map of Norcan East Field, shown in ARC-IMS map-server graphic, showing mapped area included in part B. (B) Mapped area of study, showing locations of 32 wells. Database included 32 LAS (log ASCII standard) files, two cores, test results, and associated lease production. Map also serves as a location map for the No. 2-12 Statton well shown in Figure 11.

Youle and others (1994) demonstrated that comparable cycles and shifting shoreline conditions occurred in nearby Lexington Field (also in Clark County) and Stewart Field (in Finney County) (Montgomery, 1996). Both fields have significant production from sandstone reservoirs. Other valley-infill sandstones may be found along this regional play. This current study provides insight into these other genetically similar reservoirs.

ROCK DATA

The log-core plot (Fig. 5) from the No. 1-3 Patton well, in the central part of Norcan East Field (Fig. 3), provides a good stratigraphic context for correlation of core data to well logs. Values of porosity and permeability derived from depth-cor-

rected core analysis are shown alongside the log curves in this GEMINI display. The illustration is annotated with stratigraphic divisions, including the top and base of the limited Atoka section at this shelf location. The well lies within an IVF and contains three depositional sequences, labeled here S3, S2, and S1, from the bottom up. Nearby upland areas outside the valley are missing the lower S3 and S2 sequences, presumably owing to lack of deposition beyond their respective marine shorelines. These depositional sequences are stratigraphically delimited by correlative marine flooding surfaces that passed through the estuary during abrupt rises in sea level. The flooding surface separating the S2 and overlying S1 sequences is evident in a core from the No. 2-12 Statton well. The estuarine reservoir sandstone in S2 is sharply overlain



Figure 5. Log profile and core description of the No. 1-3 Patton well, annotated with boundaries and labels of depositional sequences S1, S2, and S3. S2 sandstone is subdivided into lower "a" and upper "b" flow units separated by a nonporous interval. The lower, slightly coarser sandstone layer is also more permeable. A flaser-bedded silt-sand-shale interval separates the two flow units. Flow unit "a" is perforated for water injection. Well-log profile, including perforations and core analyses, generated as Java Applet by GEMINI.

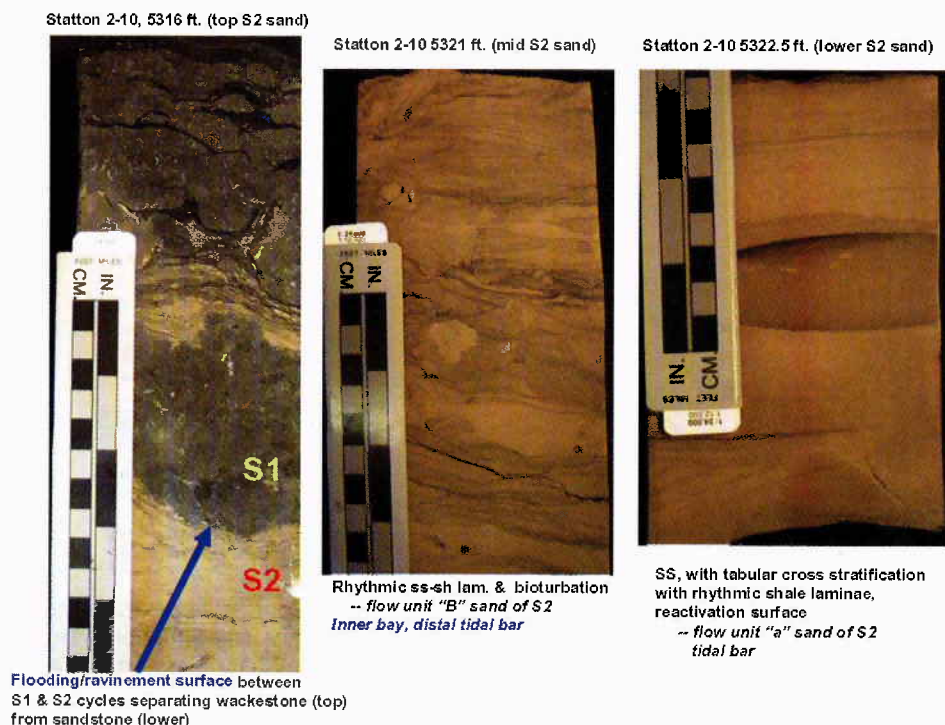


Figure 6. Core photographs showing (A) upper sequence boundary of the S2 sequence, separating a lower sandstone bed from an overlying wackestone; (B) heterolithic sandstone member, identified here as flow unit "b" of the S2 sandstone; (C) better sorted, fine-grained lower flow unit "a" of the S2 sandstone. GEMINI manages core-analysis data and images.

by open-marine carbonate of sequence S1 (Figs. 5, 6). On the basis of the cutoff parameters identified for pay, the upper S1 and S3 sequences that bound S2 do not contain reservoir intervals. Layer S1 is predominantly nonporous limestone, and the lower S3 sequence is nonreservoir shaly sandstone.

The perforated interval in all wells is confined to the S2 sandstone, delimited in Figure 5 by the small dots along the depth column. It contains clean, fine-grained, porous and permeable sandstone.

Regional sequences identified as I, J, and K by Youle (1992) appear to correlate with the S1, S2, and S3 sequences, respectively. The basal sequence, S3, is discontinuous and restricted to the lower parts of the valley, whereas the middle sequence, S2, containing the main reservoir sandstone, occupies both the lower and higher areas of the valley system (Fig. 5). The uppermost cycle, S1, comprises mainly subtidal marine limestone and extends throughout and beyond the IVF. The limestone was deposited as the result of backstepping (landward shift) of marine lithofacies to topographically higher areas on the shelf, lying farther to the east. The carbonate and shale strata overlying the sandstone serve as effective seals for trapping hydrocarbons.

Four cores, including two in the study area, contain variable amounts of very fine to fine grained sandstones, ranging from clean, well sorted to poorly sorted, and shaly sandstone with variable amounts of clay laminae, producing a heterolithic lithofacies (Fig. 6). The cores invariably are dominated by estuarine sediments in the IVF, representing accumulation

in a quiet, low-energy inner bay to an energetic tidal bar. A thin section of a laminated, very fine grained sandstone (Fig. 7A) illustrates a gradation from fine, poorly sorted to very fine, clean and well sorted quartz sandstone alternating with clay laminae. Together, these variations in strata are characteristic of tidal laminations (tidal rhythmites).

The S3 sequence overlies the unconformity at the base of the Pennsylvanian and rests on the Ste. Genevieve Limestone of Late Mississippian age (Fig. 5). The initial S3 deposit consists of shale having similar log properties to shale in the lower part of the overlying S2 section. Core analysis reveals that the basal part of the S2 sequence consists of marine inner-bay-fill shale. This core shows that the uppermost part of the S2 sequence contains silty to shaly, very fine grained sandstone. The sharp upper contact between the S2 and a thin marine-shale bed in the lower part of the S1 interval defines an unconformable surface that is indicative of rapid transgression and flooding. Most of the strata directly above this thin shale consist of Atokan limestone. In Norcan East Field, the S2 sequence is capped by reservoir sandstone.

The S2 and S1 sequences were cored in wells several miles west of the study area (No. 1-8 Wears and No. 1 Harris) and consist mostly of carbonate rock. This indicates a greater marine influence in the west (basinward) side of the incised-valley system. Interestingly, small, apparently in situ caliche clasts are developed within the sandstone in sequence S2, as seen in core from the No. 1-3 Patton well in Norcan East Field, suggesting that this sequence ended with subaerial exposure

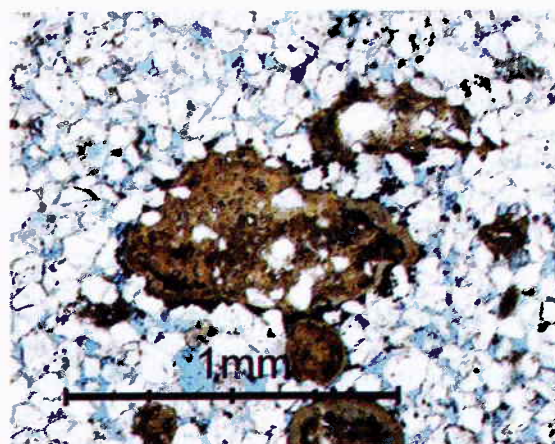
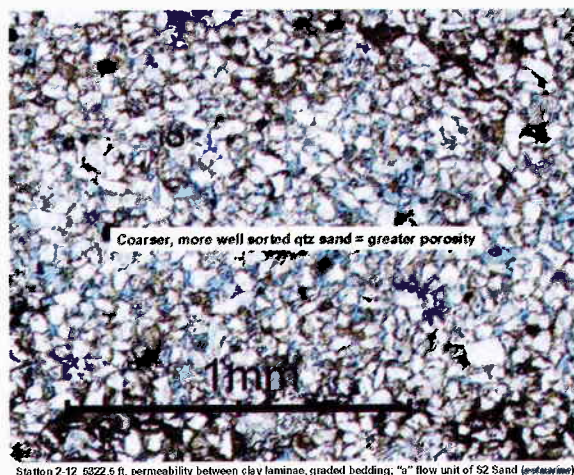


Figure 7. Thin-section photomicrographs of the upper "b" and lower "a" flow units in the S2 sandstone. (A) No. 2-12 Statton, 5,322.5 ft; permeability between clay laminae, graded bedding; "a" flow unit of S2 sand (estuarine). (B) No. 1-3 Patton, 5,321.8 ft; caliche, probably in situ; dispersed pyrite seen as small black grains; lower part of "b" sand (early subaerial exposure).

and possible paleosol development. Evidence for both sub-aerial exposure and paleosol development was apparently removed during ravinement except for what is preserved below that surface in the sandstone (Fig. 7B). Subaerial-exposure surfaces that bound this regionally correlated 4th-order sequence are consistent with the high shelf location near or at the site of landward limits of the sequence (Fig. 4).

The common transgressive-regressive lithofacies succession in the reservoir-bearing sequence within the incised valley consists of, from bottom to top: bay-fill shale; distal tidal-bar sandstone; and heterolithic, intertidal, central-bay, mixed heterolithic and flaser-bedded shale-siltstone-sandstone-carbonate; this succession is capped by fluvial-dominated, bay-mouth-bar to tidal-bar sandstone. Depositional conditions and resultant lithofacies appear to vary, depending on their original local elevations and positions in the valley and their proximity to the sediment source and the mouth of the valley (as inferred from mapping, described in a later section).

The development of a geomodel results from integration of the stratigraphy, lithofacies, petrophysics, and engineering. The process is iterative in that the early classifications may need to be refined as their importance and impact are realized. Reservoir conformance and continuity are quantitatively derived from core and log petrophysics, but analysis and significance are accomplished in the context of the geology and engineering data. Further, the assignment of flow units evolves as petrophysical data are integrated with wireline-log and production/pressure data within the context of the geologic model. The ease with which the central software, such as GEMINI, handles integration and provides updates of iterative solutions is critical to successful geomodel development.

CORE AND LOG PETROPHYSICS

Reservoir quality can be defined as a combination of good porosity, permeability, sandstone continuity, and conformance. Log and core analyses provide data for delineation of

reservoir properties and net pay, where net pay can be defined as the economically producible reservoir rock. These IVF sandstones are defined using the log and core petrophysical well data and are mapped in the context of the stratigraphic and lithofacies models.

To predict permeability within the sandstone for all well locations, a relationship among measured permeabilities, porosities, and degrees of shaliness was developed. The general relationship between permeability and porosity for the Norcan East Minneola Morrow Unit is similar to the relationship exhibited by other Morrow channel sandstones (Byrnes and others, 2001). Although a previous study of Morrowan sandstone (Bhattacharya and others, 2002) has shown relationships between permeability and porosity as a function of lithofacies, a simpler predictive relationship for permeability was developed. This was necessary because lithofacies details were not available for many wells in the Minneola Unit, and several penetrated only channel sandstone. A measure for shaliness was obtained from the correlation of shaliness in core with API gamma-ray units on logs. Permeability increases with both increasing porosity and decreasing shaliness. Also evident is the fact that cleaner sandstones do not invariably exhibit the highest porosity values. This may be due to greater quartz cementation or poorer sorting. Permeability can be predicted within a factor of 3.4 using the following relation:

$$k_{ik} = 10^{(0.134f - 0.03 \text{ GR} + 0.138)},$$

where (k_{ik}) is the in situ Klinkenberg permeability in millidarcies (md), GR is the gamma-ray value from logs, and (f) is the in situ porosity (percentage). The standard error of prediction for this equation is a factor of 3.4 (e.g., a predicted permeability of 1 md might be 3.4 md or 0.3 md). Three sets of gamma-ray ranges also correspond to a natural grouping of lithofacies as follows:

GR ≤ 30 API:	fine sandstone,
30 > GR < 40 API:	very fine sandstone,
GR ≥ 40 API:	mixed clay, silt, and sandstone.

For prediction of reservoir permeability, the three classes of shaliness were utilized in predictive equations. Each sandstone interval was assigned to one of the three classes on the basis of the average interval gamma-ray value and the permeability calculated using the appropriate equation for that class as determined by linear-regression analysis for each class:

$$\begin{aligned} \text{GR} \leq 30: & \quad k_{ik} = 10^{(0.140f - 0.558)}, \\ 30 < \text{GR} < 40: & \quad k_{ik} = 10^{(0.137f - 0.924)}, \\ \text{GR} \geq 40: & \quad k_{ik} = 10^{(0.121f - 1.069)}. \end{aligned}$$

Both the No. 1-3 Patton and the No. 2-12 Statton encountered a fining-upward sequence that also correlates with increasing gamma-ray values upward. Because permeability decreases with increasing shaliness, the lower intervals in these wells exhibit higher permeability. The division of the Minneola reservoir into three layers is consistent with subdivision of the fining-upward sequence. Using the predicted permeabilities for each of the three layers at each well location, gridcell permeability values were assigned. Values for the surrounding gridcells in the simulation model were assigned values on the basis of mapping interpolation.

In general, for each class increase in shaliness (higher shale fraction, V_{sh}) in sandstones in the Norcan East Field, permeability decreases by a factor of 5.6 for any given porosity value.

It is imperative that the correlation of core and log depths be well defined for appropriate use of the equations presented. A potential issue in some reservoir models can arise from sudden shifts in calculated permeability at similar porosities owing to log-derived gamma-ray value at the corresponding depth falling within a different gamma-ray category (shown along with the previously stated equations). Where necessary, this can be avoided by using the multivariate equation shown, or alternately, nonlinear neural net models. However, limited sample size, as is often the case, and non-unique solutions may limit the applicability of such a technique. A free-gas correction of density porosity was determined from log analysis and applied to wells on the east side of the field that contain gas. Also, the measured matrix density for the cored sandstones, 2.647 g/cm³, was used to compute log-derived porosity.

A spreadsheet-based, pattern-recognition plot, called *Super-Pickett analysis* (log f vs. log R_t [true formation resistivity]) with points connected by depth with contours of water saturation (S_w), bulk-volume water (BVW), and permeability (Doveton and others, 2000), visually aids in the identification of hydrocarbon pay (Fig. 8). Intervals that have significant hydrocarbon saturation, and therefore tend to produce with little or no water, plot as tight clusters or closely positioned trends of points on the Super Pickett plot. Similarly, wet porous zones and transition zones can be identified by their signature of cutting across saturation contours toward the water line ($S_w = 100\%$). Excel-based Super Pickett analysis also allows sensitivity testing of variables. In Norcan East Field, the reservoir lies significantly above the oil- and gas-water contacts; thus the hydrocarbon pay appears as a tight cluster (circled) on the Super Pickett plot (Fig. 8). Points within the circle represent the depth interval that was perforated within subzone "a" in the lower part of the S2 sandstone (Fig. 5). In the No. 1-3 Patton well, water is injected into subzone "a." Another cluster offset from the "a" cluster on the crossplot corresponds to a separate, upper subzone "b," of the S2 sandstone. Core data indicate that the lower "a" zone is cleaner and more porous and permeable than the upper "b" zone, which is finer grained and exhibits lower permeability (Fig. 5).

CONTINUITY AND PAY CUTOFFS

Core from the No. 1-3 Patton well shows a thin, heterolithic shaly interval that separates the "a" and "b" subzones. The nonporous and impermeable shaly interval, albeit thin, possibly acts as a barrier to vertical fluid movement, dividing the "a" and "b" subzones into two separate flow units. The correlation of these subunits to nearby wells indicates that the lower "a" zone is absent at different places (Fig. 9) in the field. Wells lacking the "a" flow unit also did not exhibit water breakthrough, consistent with the thin shaly zone acting as a barrier to fluid movement. A consequence of this shale-bed architecture is that perforations isolated in one flow unit where two are present may not provide sweep or recovery

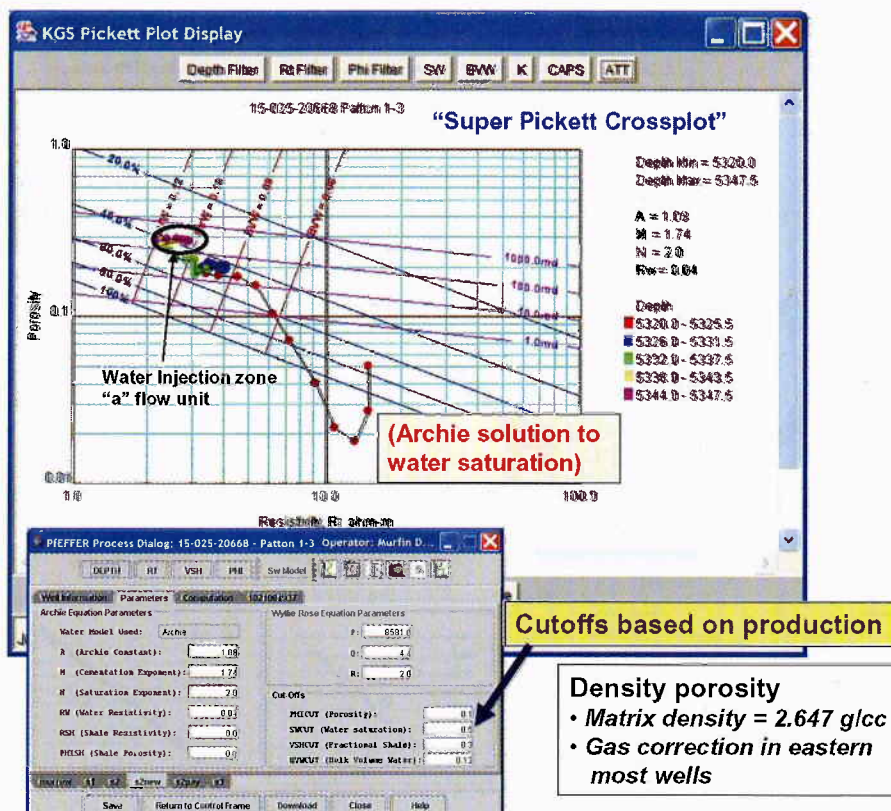


Figure 8. Super-Pickett porosity-resistivity crossplot of the S2 sandstone interval in the No. 1-3 Patton well. Crossplot illustrates contours for water saturation, bulk-volume water, and permeability. Points are connected by depth, so trends can be followed. Cluster of points circled indicates location of flow unit "a," which is the interval that is perforated. Dialog box from GEMINI is also included, providing cutoff values used to derive pay within the S2 sandstone.

of oil and gas in the adjacent interval. Although the No. 1-3 Patton injector well is located in an excellent structurally low position for a bottom-water drive, the waterflood was not effective in reaching significant parts of the reservoir owing in part to the lack of continuity and isolation of the flow units (Fig. 10A).

Hydrocarbon pay is defined in this study as the net reservoir thickness that passes cutoffs derived from log analysis, including f , S_w , and V_{sh} . Cutoff values for defining pay were calibrated by comparing values for these petrophysical parameters for perforated intervals with fluid history and test data from the well. Because most production in the Norcan East Field is attributed to single-well leases, and perforations are mostly limited to one interval, production history is highly useful for gauging pay defined from core and log analysis. Cutoff values for productive intervals were $V_{sh} < 30\%$, $f > 12\%$, and $S_w < 50\%$. Archie equation parameters as measured from core were found to be $A = 1.8$, $M = 1.74$, $N = 2$, and $R_w = 0.04$, and were used to calculate porosity and initial water saturation from wireline logs. These parameters are defined as A , tortuosity; M , cementation exponent; N , saturation exponent; and R_w , resistivity of formation water. Hydrocarbon-porosity-feet at each well in the study area were calculated using:

$$\text{Hydrocarbon-porosity-feet} = (1 - S_w) \cdot f \cdot h,$$

where h is the net pay thickness (in feet) that passes the cutoff parameters at each well, and porosity (f) and hydrocarbon saturation ($1 - S_w$) are expressed as fractions. Having the ability to revisit the petrophysical relationships and revise cutoffs is necessarily an iterative process. Moreover, because this is a multidisciplinary project, interactions between team members were facilitated by real-time web-based interactions through GEMINI, which expedited decision making.

MAPPING

A map of the top of the S2 sandstone in Norcan East Field delineates a current-day structural low at the center of the field. The east side of the field is generally higher than the west side (Fig. 10A). A comparison of the structure map with an isopach map of the Atoka Stage (Fig. 10B) clearly shows the correspondence of the structural low with the axis of a thick Atoka section, inferring that the area of thickening is the location of the main incised valley. The deepest parts of the valley form an L-shaped pattern from the southeast to the northeast before draining through the southwest side of the mapped area (see arrows in Fig. 10B).

A comparison of the gross and net pay for the S2 sandstone suggests that discontinuous pay is characteristic of this reservoir and that the Norcan East Field produces from two

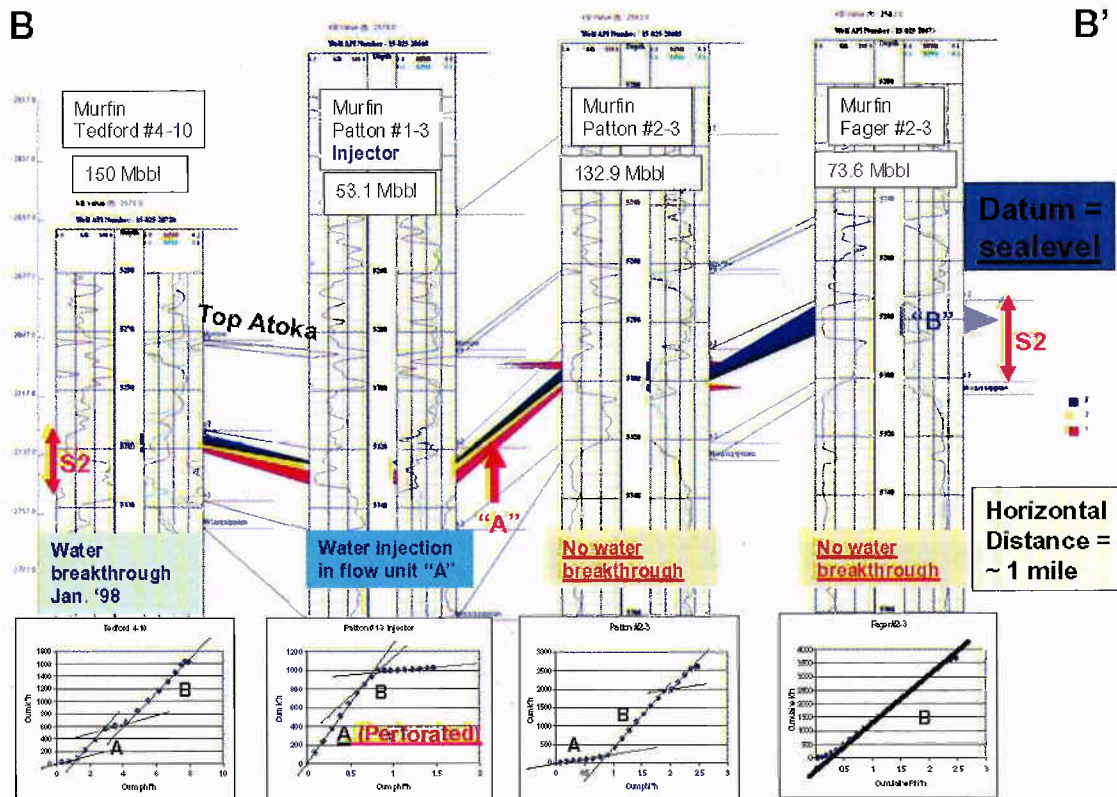


Figure 9. South-to-north structural cross section B-B' generated by GEMINI, showing Atoka interval and S2 sandstone flow units "a" (colored in red) and "b" (colored blue) in well logs on either side of the cored injector well, No. 1-3 Patton. Although unit "a" is present at the Patton well, in a structurally low position and within the main part of the valley, it does not extend to the higher areas. Line of section shown in Figure 10A. Yellow layer is nonpermeable.

separate compartments. The separation between the western and eastern volumes is shown on the maps in Figure 11 by the diagonal dotted line. As noted, the pay is also subdivided into separate flow units "a" and "b" on the western lobe, though this is not shown in the aggregate thickness maps. The No. 1-3 Patton well was drilled near the eastern edge of the western lobe of pay.

Volumetrically calculated hydrocarbon-porosity-feet are mapped in Figure 12A, and cumulative production is mapped in Figure 12B. Similar patterns in these two maps are consistent with production from different reservoir bodies. The best reservoir quality lies in two areas: (1) the northwest corner outside of the main valley and, in contrast, (2) the southeastern corner, closely coinciding with the axis of the valley. Better volumetrics occur where average V_{sh} for the S2 sandstone is lower, suggesting less shaly and possibly coarser grained sandstone. Better reservoir quality on the northern side of the western lobe, and higher average (calculated) permeability present in the northern part of this lobe, support the contention that the source of the sandstone originated from that corner rather than from the main fairway of the valley. This lobe may represent a bayhead delta, which came from a tributary entering the larger valley system along the northern edge, or a large tidal bar created by stronger currents that resided along that edge of the valley, in proximity to a local sediment source.

The source of the southeastern lobe of sand appears to have originated from the southeast on the basis of better reservoir properties to the southeast, with the sandstone following the axis of the deeper valley. The lithofacies, as indicated from cores, is indicative of fluvial channel sand modified by marine and tidal energies. The sandstone reservoir is lobate in form and limited in extent. A stillstand in sea level at this location when the valley system was partly submerged possibly led to these accumulations of sand. Clark (1987) describes regional, northwest-trending barrier bars that cross the area and that are consistent with possible stillstands in sea level.

PROVENANCE AND SEQUENCE STRATIGRAPHY

Atoka quartz sandstone closely resembles the sandy matrix of the underlying Mississippian Ste. Genevieve Limestone into which the incised valley developed. The sea-level stillstand may also have been responsible for sand accumulation through local erosion, transport, and deposition of sediment derived from the weathered Mississippian limestone. This limited sand supply and accumulation framework in this IVF suggests a local sand supply, rather than having been part of a large throughgoing tributary-fluvial drainage system. Also, the western part of the S2 sequence in Norcan East Field grades westward from sandstone to limestone and indicates a rapid loss of clastics rather than a throughgoing estuarine system. The marine-shelf deposits extend beyond a relatively local area of turbidity. The

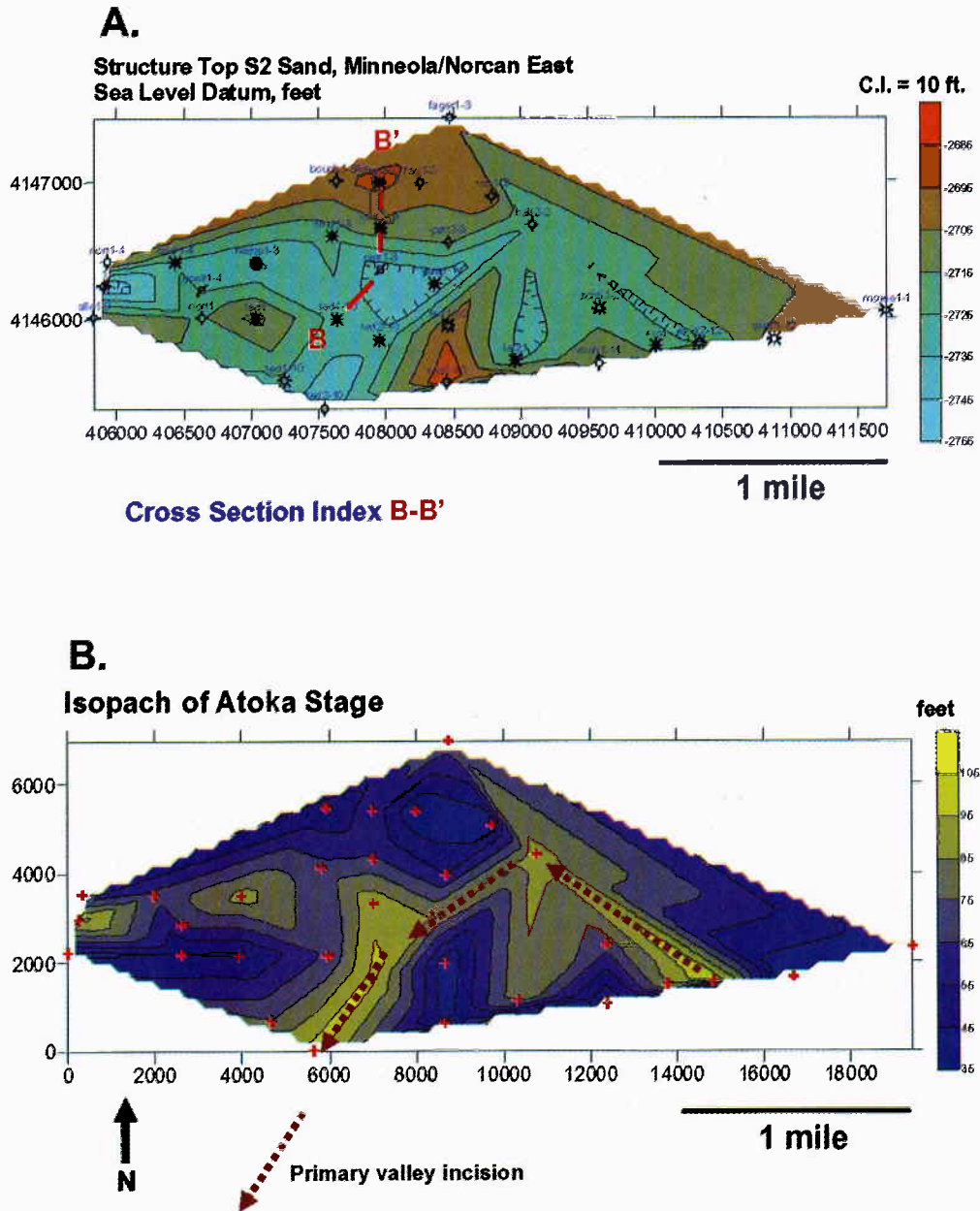


Figure 10. (A) Structure map depicting the top of the S2 sandstone in Norcan East Field. Structural cross section B-B_ shown in Figure 9. (B) Isopach map of the Atoka Stage in Norcan East Field.

reservoir studied here is, therefore, unlike the large, extensive, and throughgoing Morrow IVF systems.

The division of the S2 sandstone whereby a thin, shaly, heterolithic unit is sandwiched between two estuarine sandstones is widespread in the field, particularly in the lower reaches of the depositional valley. This condition indicates some degree of regional control, namely fluctuating sea level: a fall, a rise, and finally a fall that ends the sequence. This fluctuation may represent a high-frequency sea-level cycle (5th order, ~100 k.y. duration), which led to high-frequency cycles in many other Pennsylvanian reservoirs, both carbonate and clastic (Watney and others, 1995). In the case of Norcan East Field, the thin heterolithic unit provides an apparent barrier

to flow and separates two flow units, thus affecting secondary recovery. This level of stratigraphic resolution is important, particularly when designing enhanced-recovery projects.

The same type of regional stratigraphic division is observed in the Atoka sandstone reservoir in the 5-mi-long Stewart Field in Finney County, Kansas. Stewart Field lies about 60 mi northwest of the Minneola complex and resides on the same subcrop of the Upper Mississippian Ste. Genevieve Limestone. In this field, in contrast to Norcan East Field, thick productive sandstone was deposited during all three phases of the succession over most of the field (Youle, 1992; Montgomery, 1996). Oil recovery in Stewart Field is >350,000 barrels per well, whereas that in Norcan East Field is apparently

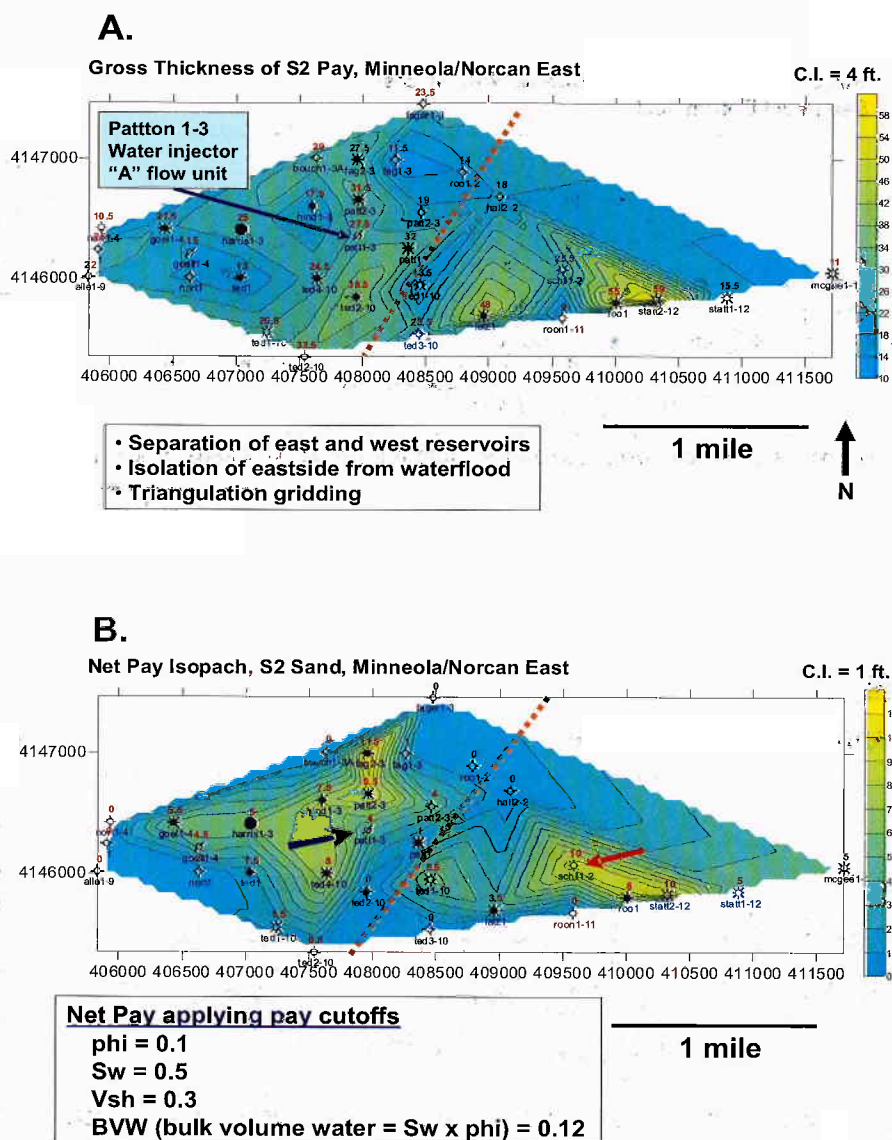


Figure 11. Map showing gross (A) and net (B) pay sandstone, in feet, for the S2 sequence in Norcan East Field. Pay is defined as the interval that passes petrophysical cutoffs (see listing above), using the Archie water-saturation equation and the coefficients $A = 1.8$, $M = 1.74$, $N = 2$, with $R_w = 0.04$. Dotted line separates eastern and western lobes of pay. Arrow on left identifies the No. 1-3 Patton well; arrow on right identifies the No. 2-12 Statton well. GEMINI log analysis used to compute net pay and build database from which mapping was done. A , tortuosity; M , cementation exponent; N , saturation exponent; R_w , resistivity of formation water; V_{sh} , shale fraction; BVW , bulk-volume water.

<89,000 barrels per well. This large variation in oil recovery is due not only to reservoir size but also to reservoir quality and continuity. Stewart Field is now undergoing a highly successful waterflood and may be a candidate for carbon dioxide injection in the future.

The increased sandstone content at Stewart Field is probably due to greater and sustained sediment supply during the turnaround sea-level cycle associated with this depositional sequence. It also indicates that the IVF system at Stewart Field was part of a larger drainage system. However, the basinward equivalent to the sandstone is again carbonate, suggesting no through-going clastic depositional system, at least during the critical event associated with this reservoir development (Youle, 1992).

The depositional sequences in Stewart and Norcan East Fields may be equivalent. Both locations appear to reside along depositional strike (Youle, 1992). Sea level history appears to have produced a common contemporaneous sandstones, albeit with variations in sediment supply and sand content. The resulting reservoirs may be analogous in distribution, internal properties, and sequence development, and thus justify comparison as reservoir analogs. However, these two fields show different levels of hydrocarbon production. Similarly, other Ato-ka sandstone reservoirs along the east side of the Hugoton Embayment offer opportunities for stratigraphic and petrophysical characterization for comparative studies. Slight variations in depositional setting and sediment supply probably resulted in

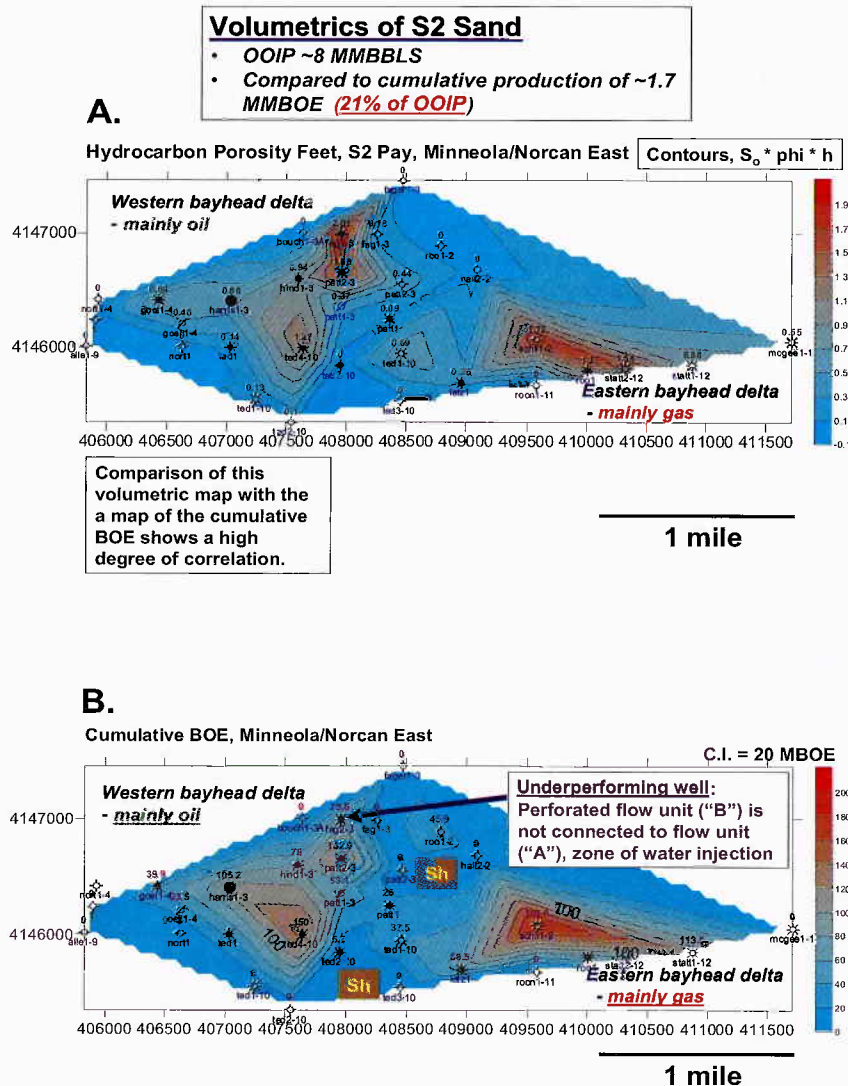


Figure 12. (A) Map of the original hydrocarbon pore volume, using well-log cutoffs for pay. Two lobes of high volume are delimited. OOIP, original oil in place. (B) Map of cumulative barrels of oil equivalent (BOE), showing the same high-volume lobes as in A. Relatively low cumulative production in the No. 2-3 Fager well, on the northern edge of the western lobe, coincides with a high hydrocarbon pore volume. Thus, underproduction is suggested. Injection zone is not present in the No. 2-3 Fager, which might explain the underperforming well. Computations and database for volumetric calculations were handled by GEMINI.

variations in reservoir quality in similar ways to those observed at Norcan East and Stewart Fields.

SUMMARY AND CONCLUSIONS

1. Early Atokan sandstone reservoirs in Norcan East Field were deposited in an east-west-trending incised valley that was part of a drainage system developed along the eastern flank of the Hugoton Embayment. The oil- and gas-producing reservoir resides within an unconformity-bounded depositional sequence that can be regionally correlated along the eastern edge of the Hugoton Embayment. The sandstone is characteristically limited in lateral extent and embedded with a stack of silty and shaly sandstone and shale, making characterization and correlation difficult.

2. Flooding surfaces most clearly delineated the depositional sequences, because subaerial-exposure surfaces appear to have been removed by marine erosion during flooding (ravinement). Once the natural sedimentary architecture was delineated, core and log petrophysical analyses were used to define intervals of effective hydrocarbon pay. This process led to delineation and correlation of flow units. These flow units are not laterally continuous and explain the lack of water breakthrough in offsetting wells. Comparison of volumetric and cumulative mapping, using barrels-of-oil equivalent, show strong spatial correlation in calculated volume and production, suggesting that cutoffs applied to delineate the pay are acceptable at this level. Field-scale reservoir-simulation studies are necessary to verify these cutoffs and flow

units. Two distinct and poorly or unconnected lobes of pay help explain the predominance of gas production on the east side versus both oil and gas on the west.

3. Mapping indicates proximal and distal orientation of these lobes. The western lobe apparently originated from the north edge of the valley, possibly as a large tidal bar or a tidally dominated bay-head delta, where the source may have been side tributary drainage. In contrast, the eastern lobe lies in the deepest part of the valley, where sediment accumulated as a tidal bar. Sedimentary textures from core provide evidence of a strong tidal current, which is consistent with an estuarine environment of deposition.

4. The supply of sandstone apparently was limited to nearby weathering of the sandy limestones exposed along adjacent uplands and from local drainage. Therefore, the continuity and conformance of sandstone are restricted. Whereas primary hydrocarbon recovery from this reservoir was characteristic of a solution-gas drive, waterflooding had limited success owing to the lack of continuity of sandstone flow units. In contrast, a nearby Atoka sandstone reservoir at Stewart Field in Finney County has much higher lateral and vertical continuity, which is attributed to a greater supply of sandstone having filled the valley. As expected, waterflooding in Stewart Field is highly successful.

5. Integrated characterizations of complex sandstone reservoirs that require the interaction of a multidisciplinary team are facilitated by use of web applications such as GEMINI, as demonstrated in this project, in which core and log petrophysics are combined with volumetric and production analysis to refine reservoir characterization.

ACKNOWLEDGMENTS

Appreciation is extended to the support of GEMINI development by the U.S. Department of Energy and to companies who participated in the evaluation of the software and its applications: Anadarko Petroleum Corporation, BP, Conoco-Phillips, Mull Drilling Company, Murfin Drilling Company, Lario Oil and Gas Company, and Pioneer Resources Company.

REFERENCES CITED

- Bhattacharya, S.; Byrnes, A. P.; Gerlach, P.; and Olea, R., 2002, Reservoir characterization to inexpensively evaluate the exploitation potential of a small Morrow incised valley-fill field: Kansas Geological Survey Open-File Report 2002-9, www.kgs.ku.edu/PRS/Poster/2002/2002-9/index.html (accessed Jan. 2006).
- Clark, S. L., 1987, Seismic stratigraphy of early Pennsylvanian Morrowan sandstones, Minneola Complex, Ford and Clark Counties, Kansas: *American Association of Petroleum Geologists Bulletin*, v. 71, p. 1329–1341.
- , 1995, Minneola Complex, Ford and Clark Counties, Kansas, in Anderson, N. L.; and Hedke, D. E. (eds.), *Geophysical atlas of selected oil and gas fields in Kansas*: Kansas Geological Survey Bulletin 237, p. 95–98.
- Doveton, J. H.; Watney, W. L.; and Guy, W. J., 2000, Integrated analysis of reservoir petrofacies in platform carbonates of Kansas: techniques and case studies, in Johnson, K. S. (ed.), *Platform carbonates in the southern Midcontinent*, 1996 symposium: Oklahoma Geological Survey Circular 101, p. 223–225.
- Heckel, P. H., 1994, Evaluation of evidence for glacial-eustatic control over marine Pennsylvanian cyclothems in North America and consideration of possible tectonic effects, in Dennison, J. M.; and Ettensohn, F. R. (eds.), *Tectonic and eustatic controls on sedimentary cycles*: Society of Economic Paleontologists and Mineralogists, *Concepts in Sedimentology and Paleontology* no. 4, p. 65–87.
- Kruger, J. M., 1996, Seismic modeling in the Minneola Complex, Ford and Clark Counties, Kansas: differentiating thin-bedded Morrow sandstones from shale in lower Pennsylvanian channel fill: Kansas Geological Survey Open-File Report 96-50, www.kgs.ku.edu/PRS/publication/OFR96_50/index.html.
- , 1998, High-resolution seismic survey of the Minneola complex, southwest Kansas, 1998 final report: Kansas Geological Survey Open-File Report 98-44, 85 pages. Available online: http://www.kgs.ku.edu/PRS/publication/OFR98_44/f2index.html.
- Montgomery, S. L., 1996, Stewart field, Finney County, Kansas: seismic definition and thin channel reservoirs: *American Association of Petroleum Geologists Bulletin*, v. 80, p. 1833–1844.
- Victorine, J.; Watney, W. L.; and Bhattacharya, S., 2005, Use of XML and Java for collaborative petroleum reservoir modeling on the Internet: *Computers and Geosciences*, v. 31, no. 9, p. 1151–1164.
- Watney, W. L.; French, J. A.; Doveton, J. H.; Youle, J. C.; and Guy, W. J., 1995, Cycle hierarchy and genetic stratigraphy of Middle and Upper Pennsylvanian strata in the upper Mid-Continent, in Hyne, N. (ed.), *Sequence stratigraphy in the Mid-continent*: Tulsa Geological Society Special Publication 3, p. 141–192.
- Youle, J. C., 1992, Sequence stratigraphy of the Lower Middle Pennsylvanian and distribution of selected sandstones, eastern Hugoton embayment, southwestern Kansas: University of Kansas unpublished M.S. thesis, 202 p. (also available as Kansas Geological Survey Open-File Report 92-55).
- Youle, J. C.; Watney, W. L.; and Lambert, L. L., 1994, Stratal hierarchy and sequence stratigraphy; Middle Pennsylvanian, southwestern Kansas, U.S.A., in Klein, G. D. (ed.), *Pangea: paleoclimate, tectonics, and sedimentation during accretion, zenith, and breakup of a supercontinent*: Geological Society of America Special Paper 288, p. 267–285.

Hunting for Overlooked Pay in Midcontinent Carbonates

Edward A. Beaumont

Independent Geologist
Tulsa, Oklahoma

Dan J. Hartmann

Independent Geologist
Fredericksburg, Texas

ABSTRACT.—The mystery of evaluating pay and predicting performance of complex carbonate reservoirs can be mitigated by integrating log, core, test, and pressure data into a petrophysical reservoir model. A diagnostic process is required to identify the dots, and then to connect them using appropriate models for pore type and water-saturation (S_w) distribution. The process includes:

- Asking appropriate questions of the data and geology;
- Documenting relevant pore-geometry models applicable to carbonates;
- Defining flow units on the basis of intervals of uniform gamma-ray, porosity, and resistivity values;
- Integrating the data and the models;
- Relating the results of data and model integration to performance history.

The process is best illustrated by examining case histories from Midcontinent carbonate reservoirs such as the Hunton or the Kansas City–Lansing. Here are some of the key questions important to the diagnostic process:

1. What is valid determination of formation-water resistivity (R_w) for the project?
2. Are core data available to document the relevant pore types responsible for hidden pay, and how do we use these data?
3. How many flow units define the zone of interest, and what is their net thickness?
4. What is the best transform for converting porosity and true formation resistivity (R_t) to S_w ?
5. Does the S_w -depth profile (by flow units) reflect variation in pore type?
6. What is the amount of net feet of pay by pore type?
7. Where, oh where, is the aquifer?

This diagnostic process, in the context of the geological and engineering constraints of the carbonate-reservoir system, can be utilized to predict the hidden pay candidates and predict their performance. Recognizing that subtle hydrocarbon accumulations exist as part of a continuous system yields several basic carbonate-reservoir models that optimize the application of data available from a wellbore.

Springer Gas-Play Development—Anadarko Basin

Tim O. Brown

Drillinginfo, Inc.
Austin, Texas

Robert A. Northcutt

Consulting Geologist
Oklahoma City, Oklahoma

ABSTRACT.—Gas production from Springer reservoirs is a significant contributor to Oklahoma gas production. The Springer gas play of the Anadarko Basin extends from the southeastern corner of Grady County, Oklahoma, northwestward to Texas County in the Oklahoma Panhandle. First discovered in 1946 at Chitwood Field in Garvin County, Oklahoma, Springer gas reservoirs were slow to be developed and were generally found in structural traps on the periphery of the Anadarko Basin. Springer gas exploration markedly increased in the 1970s with greater demand for natural gas, rising gas prices, greater availability of pipelines, and the lessening of federal restrictions on natural gas. Currently, increased density drilling is the dominant activity in the play, with >80 gas wells completed in the past 2 years at depths generally in the 10,000–20,000-ft range; four wells were >20,000 ft deep.

A sandstone facies of the Springer dominates the main part of the basin. A carbonate facies of two members of the Springer occurs to the northwest, from Major County into the Panhandle. The play is limited on the north by the truncation of Springer rocks, and on the south by the frontal thrust belt of the Wichita Uplift. A better understanding of the stratigraphic-trapping character of the Springer reservoirs encouraged more development, resulting in Springer gas production throughout the Anadarko Basin.

The Springer rocks are mostly Late Mississippian in age, although the uppermost part is thought to be transitional to earliest Pennsylvanian. The productive Springer sandstones, informally named in the subsurface, are the Cunningham, Britt, Boatwright, Goodwin, and Goddard, in descending order. The depositional environment for the Springer sandstones was primarily offshore bars, trending from southeast to northwest. Some evidence of submarine channels is present in the Britt sandstone near the updip truncation of the Springer.

More than 125 fields in the Anadarko Basin currently produce gas from the various Springer members. The larger of these, such as Cement Field, the Eakley-Weatherford Trend, Verden Field, and the Watonga-Chickasha Trend, have produced significant volumes of gas as a result of the Springer gas play.

Controls on Porosity Origin, Preservation, Reduction, and Restoration in Two Types of Morrow Reservoirs in Western Oklahoma

Bruce N. Carpenter

Log Experts
Edmond, Oklahoma

ABSTRACT.—Several regional and many individual well studies of Morrow data were made by the staff of Target Reservoir Analysis (now a division of Stim-Lab, Duncan, Oklahoma). Studies were concentrated in areas where cores and modern logs were available. Cores were examined using petrographic and scanning electron microscopes and X-ray diffraction. Cores were described in detail, and hundreds of thin sections and core plugs were analyzed. These data were integrated with drilling, log, completion, and production data to understand the Morrow reservoirs and to evaluate stimulation and production results.

Two distinct types of Morrow reservoirs were recognized: the “Panhandle” quartz-rich sandstones of northwestern Oklahoma, and the deep, chert-rich conglomerates along the Anadarko Basin axis. Original porosity in the quartz-rich sandstones was intergranular, with preservation dependent upon early grain-coating clays. Very little original porosity survived during burial in the upper Morrow chert-rich conglomerates. Reservoir porosity is controlled by enough permeability remaining after burial to allow later access of acid waters.

In the quartz-rich sandstones, early clay coats on the quartz grains inhibited porosity-reducing quartz overgrowths. Carbonate cements could still fill the porosity and reduce compaction during burial. Later dissolution of carbonate cements restored much of the porosity. Dissolution of non-quartz matrix added to the porosity. Most of the effective reservoir porosity resulted from this dissolution process. Little porosity remained where permeability was reduced to the extent that acid waters could not access carbonate cements and matrix material. Although the clay coats have little volume, they typically have very high surface areas. These clay surfaces are electrically conductive and bind formation water, reducing resistivity values in the presence of hydrocarbons.

In the chert-rich conglomerates, clays also appear to control reservoir porosity. Early clay coats and quartz overgrowths play a relatively minor role. However, early carbonate cements and compaction may have first reduced porosity to near zero, but if acid waters can later access them after burial, porosity can be restored by dissolution—even at great depths. Access of acid waters can be limited by pore-filling clays and compaction.

Dissolution can occur both to the cements and within chert pebbles. The resulting dissolution porosity varies widely in pore-throat size. Small pore throats can limit the hydrocarbon charge, and the remaining water-filled porosity can reduce formation resistivity to the point of looking wet. However, this water is usually bound by capillary forces unless it is released by acid or fracture stimulation.

In the stimulation of quartz-rich sandstones, one must consider iron-rich chlorite and fragile illite clays. Thus, iron-sequestering and clay-stabilizing agents should be used. Stimulation of the chert-rich conglomerates should be designed to enhance the paths followed by the dissolving waters. Some of these paths are small fractures around the chert pebbles, which can close with depletion of reservoir pressure. After preconditioning to remove carbonate cements, a mixture of hydrofluoric and hydrochloric acids was highly effective. Repeated treatments during production life are recommended.

Morrowan to Early Atokan Structural Evolution of the Frontal Ouachitas and Arkoma Basin, Southeastern Oklahoma

**Ibrahim Çemen, James Puckette, Rodney Feller,
Steve Hadaway, and Ata Sagnak**

Oklahoma State University
Stillwater, Oklahoma

ABSTRACT.—The south-dipping Choctaw thrust fault is the leading-edge thrust between the highly folded and faulted Mississippian to Pennsylvanian rocks of the Frontal Ouachitas and the mildly folded Pennsylvanian rocks of the Arkoma Basin. The high strains on the hanging wall of the Choctaw Fault partitions into low strains in the Arkoma Basin along the Frontal Ouachitas–Arkoma Basin transition zone. The south-to-north and west-to-east strain partitioning is accomplished primarily by a triangle zone and an associated duplex structure. The triangle zone is flanked by the Choctaw Fault to the south and the Carbon Fault to the north in the area of the Wilburton Gas Field.

The Morrowan to lower Atokan Wapanucka/Spiro Formation is present between the Choctaw and Woodford detachments. The Woodford detachment makes a ramp and continues in the Morrowan Springer shale in the Arkoma Basin. The duplex structure lies between the Springer detachment (the floor thrust) and the lower Atoka detachment (the roof thrust). This duplex structure continues northward, displacing the Red Oak sandstone, before reaching a shallower depth and forming the Carbon Fault as a north-dipping backthrust below the San Bois Syncline through a zero-displacement point.

We have conducted a comprehensive pressure–depth–gradient study in the Wilburton Gas Field and surrounding areas. We have found that in the duplex structure, the Spiro reservoirs that were brought to structurally higher positions by the thrust faults generally exhibit higher pressure–depth gradients. Thus, thrust faults in the Wilburton area must have been formed after the Spiro sandstone reservoirs were charged. Therefore, we suggest that the thrust faulting in the Wilburton Gas Field and surrounding areas was post–early Atokan and most probably middle Atokan in age.

Logging-Tool-Deployment Methods that Ensure Acquisition of Accurate Log Data through Morrow and Springer Strata

Mark W. Houpe

Weatherford International
Oklahoma City, Oklahoma

ABSTRACT.—Various techniques have evolved, and are currently in use, for logging horizontal or highly deviated wells, problem holes, or traditional vertical wells. Safe, efficient methods are now available to attain a cost-effective means of gaining valuable open-hole data while providing operators maximum flexibility in designing and optimizing well completions.

These techniques include the use of a compact tool string for data acquisition. Various methods can be used to log problem or complex holes without compromising data quality. The flexibility inherent in the design and implementation of these techniques affords the operator control over pressure problems, borehole-condition problems, wellbore-stability issues, and geometric problems.

These results allow efficient distribution of the log data to the operators and their partners, as well as manipulation of the data for quick evaluation.

Cromwell Sandstone Sequence Stratigraphy and Porosity Development in Kinta Field, Haskell County, Oklahoma

Bryant Reasnor

ChevronTexaco
Midland, Texas

Dennis Kerr

University of Tulsa
Tulsa, Oklahoma

ABSTRACT.—The Cromwell sandstone (Morrowan) is a prolific gas-producing reservoir in Kinta Field and elsewhere in the Arkoma Basin. However, the predictability of Cromwell reservoirs has been elusive, according to remarks in the published literature. This study uses well logs from four townships in western Kinta Field and includes two cores, which were used to calibrate well-log response. The identification and correlation of sequence-stratigraphic elements provide new insights to the prediction of porosity development in the Cromwell.

Cromwell sandstones are regarded as mostly being deposits of offshore sand ridges during an overall increase in accommodation. Five retrogradational parasequence sets are identified; two to seven parasequences are associated with each set. In addition, two 4th-order sequence boundaries are developed within the Cromwell lithostratigraphic unit. Typically, the highest pore-foot values are developed in the upper parasequences of a set. In addition, it appears that pre-Cromwell topographic relief influenced the vertical stacking of reservoir-quality sandstones.

The Concept of Intermittent Structure and Its Influence on Morrow–Springer Deposition

Kurt Rottmann

Independent Geologist
Oklahoma City, Oklahoma

ABSTRACT.—Structural movement occurred at various times throughout the Paleozoic. Those structural events were generally related to the tectonic forces responsible for the formation and development of the Anadarko and Arkoma Basins. One interesting aspect of the structural history is that often a localized area may have been the recipient of several structural events, which created an area of apparent persistent or intermittent structural movement. For the explorationist, the knowledge of this concept can be a useful tool for evaluating the potential presence of deeper structure in an area devoid of deeper well control.

Isopach irregularities—such as local unconformities, facies changes, onlap or offlap beds, and anomalous thick- or thin-bed isopach intervals—suggest structural influence during deposition. The purpose of this study is to demonstrate the possibility that areas where these isopach irregularities are present, which reflect penecontemporaneous structural influence, could also be areas of earlier structural movement that resulted in potentially deeper hydrocarbon entrapment, as the following four examples show.

First, in the Arkoma Basin, a regional unconformity within the Jefferson–Cromwell sequence of Morrowan age coincides with a deeper post-Ordovician arch feature. Second, a facies change within Springieran strata from shaly limestone to an organic biofacies coincides with Silurian, Devonian, and Mississippian structural movement. Third, an area of Springieran and Morrowan isopach thins coincides with deeper Hunton production. Fourth, an area of Cherokeean marine bars coincides with deeper production, which is dependent upon structural closure.

Regional Sequence Stratigraphy and Depositional Environments of the Lower Pennsylvanian in Southwest Kansas

Galo A. Salcedo and Timothy R. Carr

Kansas Geological Survey
Lawrence, Kansas

ABSTRACT.—Lower Pennsylvanian Morrow sandstones in southwestern Kansas have produced hydrocarbons for >60 years but are still attractive targets for exploration and development. The Morrow succession was deposited across the Hugoton Embayment, a shelf extension of the Anadarko Basin, above a pre-Pennsylvanian regional unconformity.

On the basis of core analysis and wireline logs, 12 lithofacies/petrofacies were identified and grouped in open-marine siliciclastic assemblage, open-marine carbonate assemblage, marginal-marine assemblage, and fluvial and paleosol. A regional sequence-stratigraphic framework was established for the Morrow of southwestern Kansas as a series of five depositional sequences. Four out of five of these Morrow sequences are associated with large incised valleys (IV-1, IV-2, IV-3, and IV-5). Incised valleys are oriented NW–SE, extend for 100 to 270 km, and range in width from 30 to 50 km. Each incised valley is infilled with 24 to 84 m of sediments. Depositional systems of older incised valleys (IV-1 and IV-2) are composed of fluvial, estuarine, and marine-shoreface facies; younger incised valleys (IV-3 and IV-5) are predominantly estuarine. In the northeastern part of the study area, within sequence 4, a carbonate buildup characterized by shoaling-upward parasequences of open-marine subtidal, minor shale, and paleosol facies is present. The carbonate buildup is up to 33 m thick and covers an area 45 km wide and 260 km long. In the southwestern corner of the study area, relatively small incised valleys are present in all five Morrow sequences. These incised valleys are related to the pre-Pennsylvanian Keys Dome.

Each Morrow sequence migrated an average of 25 km northeastward (landward), reflecting a globally transgressive, eustatically controlled pattern. Pre-Pennsylvanian faulting seems to have controlled eastern margins of incised valleys and sequences during Morrow time in southwestern Kansas.

Overview of Postle Field, a Morrow CO₂ Flood, Texas County, Oklahoma

John Southwell

Celero Energy
Midland, Texas

ABSTRACT.—Since discovery by Republic Gas in 1958, Postle Field has produced >110 million barrels of oil (MMBO) from upper Morrow sandstone. Located in the northwest corner of the Oklahoma Panhandle, the field is characterized by coarse clastic sediments shed from proximal pre-Pennsylvanian emergent highlands. Typical reservoir facies within well-sorted channel fill have average porosities of 16% and permeabilities of >100 millidarcies (md). Deposition is characterized by channels and sediment that have infilled preexisting paleotopographic lows. Three distinct sand units are present within the upper Morrow sequence. The field was unitized for waterflooding in the mid-1960s, when peak production of >25 thousand barrels of oil per day (MBOPD) occurred. Recovery factors from primary and secondary recovery are on the order of 40%. CO₂ injection was implemented in stages over selected areas of the field from 1995 to the present on an 80-acre five-spot pattern. The field is currently producing ~4,000 BOPD from ~80 wells, with CO₂ injection of ~50 million cubic ft per day. Future plans are to expand the CO₂ flood into the remaining waterflood units.

Examples of Trapping Mechanisms in the Cromwell Sandstone (Morrowan), Hughes County, Oklahoma

Maxwell J. Tilford

Tilford Pinson Exploration, LLC
Edmond, Oklahoma

ABSTRACT.—Hughes County, in eastern Oklahoma, lies on the boundary between the Seminole Platform on the west and the shelf of the Arkoma Basin on the east. Production in the western part of the county is typically oil, while production to the east, along the mid-Pennsylvanian hinge line of the Arkoma Basin, is predominantly gas. The most prolific producing zone in Hughes County historically has been the Cromwell sandstone, Morrowan in age.

The subsurface usage of the term *Cromwell* encompasses several stratigraphic units, including the Union Valley limestone and sandstone, and the Cromwell and Jefferson sandstones. In general, the Cromwell sandstone is characterized by high porosity and permeability in a marine-bar depositional environment, although these favorable reservoir conditions are commonly lacking in the southeastern part of the county as the Arkoma Basin is approached.

A gradation of various types of oil- and gas-trapping mechanisms occurs for the Cromwell in Hughes County, ranging from simple one-well anticlinal traps and fault traps, to pure stratigraphic traps, to complex fault-bounded structures exhibiting abrupt stratigraphic changes within the known productive area. Reservoir-drive mechanisms are variable, ranging from a strong, active water drive to gas-expansion and gas-solution drives. Well logs, structure and isopach maps, and seismic sections are important resources to aid in gaining an understanding of the mechanics of oil and gas entrapment in the Cromwell sandstone in selected fields. Modern-day analysis of older producing areas can yield valuable insights into how traps formed through time. An understanding of the geologic conditions necessary to entrap oil and gas through study of producing analogs is paramount in the deliberate search for the subtle trap.

Deep-Gas-Well Stimulation of the Springer in the Anadarko Basin

Steve Wolhart

Pinnacle Technologies
Houston, Texas

ABSTRACT.—Pinnacle Technologies recently conducted a study on hydraulic fracturing of deep gas wells for the U.S. Department of Energy (DOE). The study consisted of an assessment of current and projected U.S. deep-gas drilling activity; a review of rock mechanics and fracture growth in deep, high-pressure/temperature wells, and studies of a few wells in selected areas. The DOE's Deep Trek Program is targeted at improving the economics of drilling and completing deep gas wells. The challenges of drilling and completing such wells are significant. Relatively few deep wells (>15,000 ft true vertical depth) are drilled annually. Of the estimated 29,000 wells (oil, gas, and dry holes) drilled in the United States in 2002, ~300 were deep wells. Deep drilling has risen since then and is expected to reach ~600 wells in 2005 and stay at that level through 2007. The Midcontinent, along with South Texas, is one of the leading areas of deep-gas-well drilling. Targeted deep formations in the Midcontinent include the Springer, Morrow, Bromide, Arbuckle, and Granite Wash.

The study included a review of rock mechanics and hydraulic fracture growth in deep reservoirs. As expected, this shows that fracture stimulation is more challenging in deep environments. Fracture propagation does not depend on depth per se but is impacted by the change in stresses and how that impacts failure along natural rock discontinuities. Poor near-wellbore conditions stemming from drilling problems, low effective stress (overpressured formations), and/or high deviatoric stress can lead to complex fracture growth. There can also be compaction and collapse as pore pressure depletes. Major contributors to fracture complexity are rock discontinuities, natural fractures, and faults. A clear example of this was seen in a well completed in the Bossier sand of East Texas. Microseismic mapping was performed for two treatment stages in one well. The mapping showed that the hydraulic fracturing was fairly well contained near the wellbore. However, a previously unmapped fault encountered not far from the wellbore allowed the fracture to move upward into another zone and actually back toward the wellbore.

Key to the project were case studies developed for several formations in the Midcontinent: the Bossier sand in East Texas, the Lobo sand in South Texas, and a Wyoming deep gas reservoir. Results from one of the Midcontinent wells is included here. Pinnacle worked with data provided by Marathon for the No. 1-16 Emma Bia well in Caddo County, Oklahoma. This well was completed in the Boatright and Cunningham intervals of the Springer Formation. These zones are found at 15,000 to 17,000 ft in this well and have pore pressures of 10,000 to 12,000 psi (0.65 to 0.73 psi/ft). The permeability is estimated to range from 0.01 to 0.1 md. Fracture engineering and modeling was performed for two of the four stages pumped in this well. The stimulation treatments are pumped using borate cross-linked fluids with proppant volumes ranging from 40,000 to 100,000 lb. A review of the treating-pressure data gives some indication of complexity in the near-wellbore region. Analysis indicates that fracturing designs might be conservative with relatively low proppant concentrations to avoid screenouts. There may be an opportunity to increase job size and improve well performance.